INTERDEPENDENCE BETWEEN SEGREGATION AND FLOW PROPERTIES OF BULK SOLIDS

A thesis submitted in fulfilment of

the requirement for the award of the degree of

DOCTOR OF PHILOSOPHY

Submitted by

RACHIT PODDAR

Registration No.: 901908008

THAPAR INSTITUTE
OF ENGINEERING & TECHNOLOGY
(Deemed to be University)

MECHANICAL ENGINEERING DEPARTMENT
THAPAR INSTITUTE OF ENGINEERING AND TECHNOLOGY
PATIALA – 147004, PUNJAB, INDIA

NOVEMBER 2024

THESIS CERTIFICATION

I, Rachit Poddar, declare that the work presented in this thesis report entitled, **"INTERDEPENDENCE BETWEEN SEGREGATION AND FLOW PROPERTIES OF BULK SOLIDS"** submitted in fulfilment of requiremen for the award of degree of Doctor of Philiosophy in Mechanical Engineering Department, Thapar Institute of Engineering and Technology, Patiala, is an authentic record of my work carried out under the supervision of Dr. S . S. Mallick (Professor, Mechanical Engineering Department, Thapar Institute of Engineering and Technology, Patiala), and Dr. Kundan Lal (Assistant Professor, Mechanical Engineering Department, Thapar Institute of Engineering and Technology, Patiala) from August 2019 to November 2024. The matter presented in this thesis has not been submtted either in part or full to any other Unversity or Institute for the award of any other degree.

8th Nov, 2024

Rachit Poddar
Registration No.: 901908008

Date: November 08, 2024

It is certified that the above statement made by the student is correct to the best of my knowledge and belief.

Dr. S. S. Mallick, Ph.D. Supervisor
Professor,
Mechanical Engg. Department,
Thapar Institute of Engineering and
Technology, Patiala
Date: 08-11-2024

Dr. Kundan Lal, Ph.D. Supervisor
Assistant Professor,
Mechanical Engg. Department,
Thapar Institute of Engineering and
Technology, Patiala
Date: 08-11-2024

This thesis is dedicated to my parents, sister, wife and son for their love, support, and patience.

ACKNOWLEDGEMENT

I am grateful for this achievement to Dr. S. S. Mallick, my research mentor, who welcomed me as a PhD student and provided me with guidance, connections and support. This accomplishment would not have been possible without his involvement and daily encouragement throughout my work. Working with him allowed me to overcome challenges and acquire a wealth of knowledge. His unwavering commitment to excellence, enthusiasm, courage and conviction always motivated me to strive for my best. Thanks to his support and endorsement, this thesis has become my possession. He has taught me that "goodness cannot be ignored or denied in human beings," which I will carry throughout my life. I am deeply grateful to him for all of this. I will remain indebted to him forever.

I would like to express my deepest gratitude to Dr. Kundan Lal for his invaluable guidance and firm support throughout my PhD journey. His insightful feedback and encouragement have been instrumental in shaping my research and academic growth. Many thanks to my lab colleagues, Mr. Gourav Saluja, Mr. Chandan Kishore, Mr. Partha Mukherjee, Mr. Jashandeep Singh and Mr. Karan Chhabra.

I would like to thank the most important people in my life, my parents, my sister, my wife and my son, for believing in me, allowing me to pursue my passions unhindered and giving me unconditional love and support. I appreciate the loving and supportive environment you provided me throughout my journey toward my Ph.D. Without your support and guidance, I would not be where I am today. With all the unconditional care, suffering, and sacrifices you have given me, I would like to express my deepest gratitude to all of you. This success is our joint effort. I will never be able to repay for all the kindness you people have shown me.

I thank the Thapar Institute of Engineering and Technology, Patiala, for providing me with a great atmosphere in which to learn and perform my research. I greatly appreciate and acknowledge the support received from the Mechanical Engineering Department.

Finally, I thank the Almighty for giving me the strength and patience all these years to stand proud today.

ABSTRACT

This thesis presents the results of an ongoing investigation into the characteristics of segregation, which is critical for ensuring product homogeneity and process reliability. Additionally, moisture content certainly affects the segregation behaviour of powders, which may degrade the product quality and cause lot rejection. Therefore, understanding the segregation characteristics affected by changes in moisture content plays a vital role in achieving the desired goals in powder handling industries. In this research, a deeper understanding of powder segregation and flow behaviour was achieved by addressing a critical gap in the literature for Geldart Group A to B borderline powders, providing practical insights and predictive tools applicable to real-world scenarios. A key contribution is the introduction of a novel dimensionless parameter, the modified dimensionless cohesion number, which improves the prediction of segregation in complex powder fluidising systems. High-accuracy models were developed by incorporating important factors such as moisture, cohesion, flow function, and particle properties. Notably, the research also established clear empirical relationships between moisture levels and segregation behaviour, an area with minimal prior modelling despite its industrial significance. By highlighting the role of moisture management in maintaining product uniformity and preventing lot rejection, this work supports higher safety and quality standards. These models were validated across a diverse set of powders, including fly ash, pharmaceuticals, detergents, and semolina, demonstrating strong generalisability. The study further explores segregation challenges in pneumatic conveying systems. A 75:25 blend ratio of coarse-to-fine ash was found optimal for dense phase flow. Criteria based on the bulk powder Froude number (<10) and coarse-to-fine ratio (>10) were proposed for reliable conveying. By highlighting the role of moisture management in maintaining product uniformity and preventing lot rejection, this work supports higher safety and quality standards.

Based on the comprehension testing that includes the sifting segregation test, fluidisation test, particle and flow properties testing on various powders such as 6 different fly ash, sand, three different brands of detergent and semolina, the model for sifting and fluidisation segregation index has developed based on particle, flow and powder bed properties. The developed models can be used as a design tool based on particle, flow, and powder bed properties, which may assist in controlling the segregation issues by considering the required changes in designing and operating parameters. A study which aims at modelling the sifting and fluidisation segregation index for Geldart group A to B borderline materials, for which very little research has been carried out till date.

In a separate set of experiments, physical and flow property tests were carried out on 8 pharmaceutical powders. The results obtained from heap analysis and shear cell testing have been compared. A relationship to represent the static angle of repose has been developed using a bulk powder-based Froude number and fine size. The experimental results and predictions for a range of bulk properties have shown that the values of static angle of repose decrease with an increase in the value of bulk powder Froude number, increase in particle shape factor and decrease in the median to fine ratio. Out of all the dimensionless parameter groupings, the particle shape factor strongly influences the static angle of repose, as indicated by its larger absolute value of the exponent in the power function format relationship.

Sifting and fluidisation segregation characteristics were determined for 6 different fly ash samples (particle size 'd(50)' ranging from 68 to 141 μm) using standard testers. The results have shown that the coarser particles have a greater tendency to sifting segregation, and the finer powders respond more to fluidisation segregation. The angle of repose for the fine ash and coarse ash were 55° and 38°, respectively, which indicated poor to good flowability conditions. The flow function test shows that all the samples were in an easy-flowing to a free-flowing zone. The angle of repose and material flow function have provided a good correlation with the sifting segregation index. In contrast, cohesion between particles, the ratio of free terminal velocities and diameters for coarse to fine particles have shown a good fit with fluidisation segregation indices. For both sifting and fluidisation segregation, the model correlation values are 0.91 and 0.94, indicating the predicted results are a good fit to the experimental data.

Experiments were carried out using sand, three different brands of detergent and semolina powders. Additionally, data from six fly ash samples were taken for the purpose of modelling. While comparing the powder characteristics in the first and last samples in sifting segregation and top and bottom samples in fluidisation segregation, considerable differences in the bulk properties were found, indicating the occurrence of segregation in the case of Geldart group A to B borderline powders. A new model has been developed for the sifting segregation index using flow function, course-to-fine ratio, and shape factor, which resulted in 97% prediction accuracy. A novel dimensionless cohesion number has been developed as a ratio of inter-particle cohesion to the dynamic pressure of air along; this number has been used with minimum fluidisation velocity to model the fluidisation segregation index. The model has shown an 86 % fit to the experimental data.

Another study aims to model the sifting and fluidisation segregation index for powders from Geldart group A to B borderline while considering the change in moisture content. Five different powders, such as sand, three different brands of detergent, and semolina powders, have been utilised for physical and flow properties and segregation tests at three different moisture content levels. The results revealed that with an increase in moisture content, there is a decrease in the value of the sifting and fluidisation segregation index. A new model has been developed for the change in sifting segregation index w.r.t change in moisture content based on flow function, course-to-fine ratio, and shape factor, providing a good fit of 91 % accuracy with the experimental data. By using the minimum fluidisation velocity of the particle and a novel dimensionless cohesion term, a model was developed for the change in fluidisation segregation index that showed an 85 % fit with the experimental data. In the initial study, the model presented in Chapter 4 was best described by the parameter "Median to Fine ratio (d50/d10)." To encompass the entire range of a powder, the parameter "Coarse to Fine ratio (d90/d10)" was found to be more relevant for the models discussed in Chapters 5 to 8.

Finally, the difficulty of handling segregated powder samples having narrower particle size distribution compared to wider size distribution has been illustrated for a pneumatic conveying system. Based on a pilot plant study of conveying 10 blends of ash, 75% coarse ash and 25% fine ash provided the optimal blend for dense phase conveying. A new bulk powder Froude number term (based on loose poured bulk density) and coarse-to-fine ratio have been used to represent reliable conveying criteria. For reliable dense-phase conveying, the ash mixture should have a bulk powder Froude number < 10 and a coarse-to-fine ratio > 10.

The significance of this study improves scientific understanding and predictive ability for segregation characteristics of Geldart group A and B borderline powders by integrating particle properties, flow characteristics, and moisture effects into highly accurate models. The introduction of novel parameters, including the modified dimensionless cohesion number and bulk powder Froude number, provides robust, generalisable tools applicable across diverse industrial contexts such as fly ash, pharmaceuticals, detergents, construction, and food powders. The validated models deliver practical design and operational criteria to reduce segregation, maintain product uniformity, reduce lot rejection, and ensure reliable pneumatic conveying, thereby improving process reliability and overall quality standards.

TABLE OF CONTENTS

LIST OF FIGURES

LIST OF TABLES

NOMENCLATURE

List of symbols

C	Cohesion, kPa
MFR	Median to fine ratio (d_{50}/d_{10})
CI	Compressibility index, %
C_i	Cohesive index
d(10)	The particle size at the cumulative percentage of 10%, µm
d(50)	The particle size at the cumulative percentage of 50%, µm
d(90)	The particle size at the cumulative percentage of 90%, µm
d_{90}/d_{10}	Ratio of particle size (d_{90}) to particle size (d_{10})
1/ffc	Material flow function
Ar	Archimedes number
Coh*	Modified cohesion number
$w_{fo,lb}$	Terminal settling velocity based on bulk powder, m/s
Fr_{lb}	Bulk powder Froude number (based on loose poured bulk density)
S-AOR	Static angle of repose, °
D-AOR	Dynamic angle of repose, °
S or SF	Shape factor
HR	Hausner ratio (ρ_t/ρ_{lb})
t/h	Material conveying rate, tonnes/hour
V_o	initial volume, ml
ρ	Air density, kg/m³
V	Superficial air velocity, m/s
wfo_{10}	Particle settling velocity for particle size (d_{10})
wfo_{90}	Particle settling velocity for particle size (d_{90})
wfo_{90}/wfo_{10}	Difference of particle size-based settling velocity, i.e., the ratio of particle settling velocity for particle size (d_{90}) to particle settling velocity for particle size (d_{10})
B	Constant
C_1	Constant used in fluidization correlations
C_2	Constant used in fluidization correlations
d	Volume surface mean diameter, m

d_{vi}	Mean of two successive passing and retaining sieve sizes, m
g	Acceleration due to gravity, m/s^2
K	Constant used in Coltters and Rivas equation
M_v	Dimensionless number, $(\rho_p - \rho)/\rho$
Re_{mf}	Reynolds number at incipient fluidisation
u_t	Particle terminal velocity, m/s
x_i	Weight/volume fraction of a given particle size
C_F	Mass content (in %) in the first batch at particle size range, *k*.
C_L	Mass content (in %) in the last batch at particle size range, *k*.
C_T	Mass content (in %) in the top batch at particle size range, *k*.
C_B	Mass content (in %) in the bottom batch at particle size range, *k*.
Cv	Mass content (in %) in the virgin sample at particle size range, *k*.
$\bar{I}_S$	Mean segregation Index
n	No. of the particle size range, *k*.
$\bar{I}_{SS}$	Mean sifting segregation index
$\bar{I}_{FS}$	Mean fluidisation segregation index
$I_{SS(k)}$	Sifting segregation index of the particle size range, *k*.
Greek symbols	
ρ_{lb}	Loose-poured bulk density (kg/m^3)
ρ_p	Particle density (kg/m^3)
ρ_t	Tapped bulk density (kg/m^3)
τ	Pre-shear stress, kPa
σ	Consolidation stress, kPa
φ	Angle of friction, °
μ	Dynamic viscosity of air, Pa.s
Subscripts	
mf	Minimum fluidization
v	Volume
i	Count
p	Particle
av	Average
sb	Solids bed
0	Initial

Abbreviations

ASTM	American Society for Testing and Materials
PFT	Powder flow tester
CI	Compressibility index
SEM	Scanning electron microscopy
ESP	Electrostatic precipitator
I.D.	Inner diameter

CHAPTER 1

Introduction and Objectives

1.1 Introduction

Bulk powders are handled in many industries, such as pharmaceutical, food processing, power, cement, chemical, petrochemical, detergent, and paint, either as raw materials or finished products (Zinatlou et al., 2024; Vikram et al., 2021; Kritika et al., 2022; McGlinchey, 2023). The typical bulk handling processes involve belt conveying, pneumatic conveying, screw feeding, flow through hoppers and silos etc. Segregation is the separation of components within a particulate mixture due to variations in its particle size, density and shape during powder handling. Thus, whenever there is a difference in the particle properties like shape, size and density amongst a powder sample, there would be a natural tendency of segregation. Segregation is undesirable in all cases where it is required that a mixture of powder should maintain its uniformity. The different observed segregation mechanisms, as reported, are the sifting mechanism, percolation mechanism and influence of air resistance (Ghosal et al., 2015; Heartwin et al., 2020).

Whenever particles from bulk materials glide over the inclined surface or the heap of itself, tiny particles can adjust themselves into the small voids, thus not moving far compared to the large particles. These large particles trundle or slip downhill from top to bottom of the heap—this act of phenomenon is called sifting segregation (Engblom et al., 2012; Gray et al., 2005). When the mixture of bulk materials (consisting of fine and coarse particles) in a container is jiggled or vibrates up and down, the smaller particles move against the gravitational force and collect at the lower layer. In contrast, granular material percolates and takes a new place towards the upper layer. This process of deformation of particles and relative motion between them is also known as percolation segregation. Due to the imposition of the external vibration on a powder bed, generally, small particles pass through the voids of the coarse particles. The mechanism due to which fine collection at the bottom and coarse remains from the top to the middle layers is commonly referred as sieving segregation (Hogg, 2009; Ireland et al., 2016; Mondal et al., 2022).

When granular materials are conveyed through a chute, like from a conveyor into a silo, their movement is influenced by factors like particle size, shape, and the chute's angle, leading to varied trajectories. During these trajectories, fine particles travel less horizontal distance component than coarse ones due to air resistance. Because of this, the segregation of particles (fine and coarse) may be likely to happen – known as trajectory segregation (Schulze, 2008). Trajectory segregation has been utilised to explain the effect of aerodynamic drag, which is higher with fine particles compared

to the coarse or bigger particles projected from the chute exit into a silo. The projection of different fine and coarse streams would certainly lead to separation of particles in the silo (Hogg, 2009).

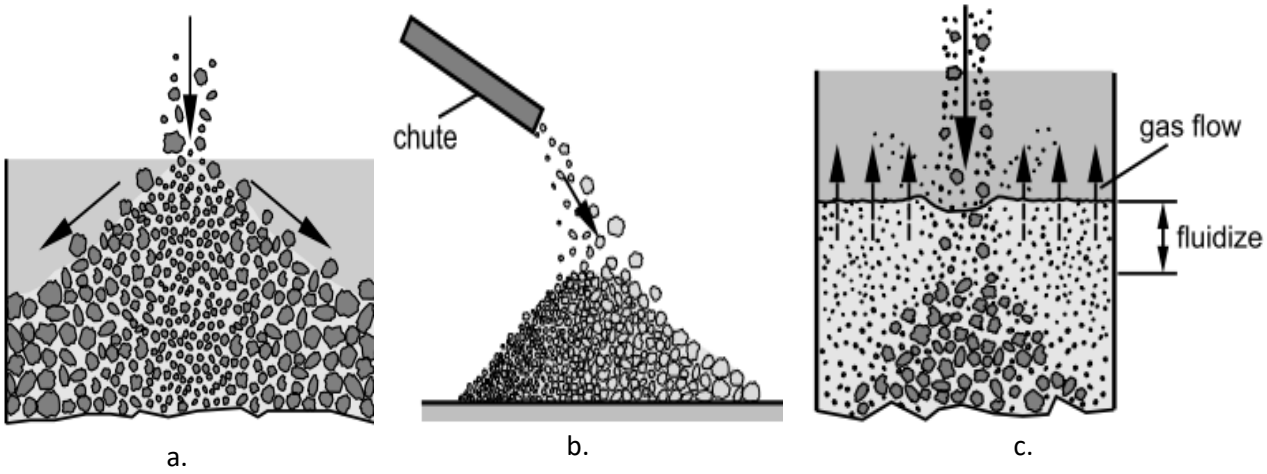

Figure 1.1: Segregation mechanism: a) Shifting; b) Trajectory; c) Fluidisation (Schulze, 2008)

In a silo, if bulk material is allowed to fall freely under gravity, i.e., without any conveying medium of the air stream, the stream of particles entraps the air stream through itself. After escaping the air from the stream of particles, particles drop or settle down on the top surface of filled bulk material. Additionally, suppose small particles go into the layer of bulk material with entrapped air. In that case, the airstream starts to flow upward with fine particles and the coarse remains lower. It makes the upper layer of fine particles in fluidised form, causing fluidisation (also known as air current) segregation (Tang et al., 2004; Schulze, 2008; Parmar et al., 2013). Air-induced segregation is defined as the action of separation of fines from the rest of the powder due to the interaction of fines with the opposite airflow current (Deng et al., 2010).

For sieving segregation to occur, mean particle size lies in the range of 70 to 200 µm. Segregation starts to decrease by particle size, typically below 500 µm, because of the dominating effect of different interparticle forces such as van de Waals, electrostatic, etc., compared to the gravitation force. Wider particle size distribution amongst the bulk powder is more prone to segregate (Tang et al., 2004). Generally, the binary or multicomponent mixture consists of a wide particle distribution, which may act as an influencing parameter for segregation (Devriendt et al., 2013). Those powders having different shapes (for example, large particles having spherical shapes, but small particles are irregular) are more accessible to separate than those with similar-shaped particles (for example, both small and large particles are spherical). The reason for this could be: (1) non-uniform particles can

lodge into the void space between them, and (2) the void space becomes greater between the non-uniform particles as compared to the spherical-shaped particles (Tang et al., 2004). Spherical particles are more prone to segregate than irregular particles of the same size. Due to the high rolling tendency of spherical particles over a heap or slant height relating to cumulative changes in particle density, causing segregation, which might be due to potential energy considerations. However, the effects are generally less dominant than those having different in sizes. The reason could be partially because of the small density differences found in bulk powder in which a ratio of 5:1 is assumed to be large, while a ratio of 1000:1 is considered a common size range (Hogg, 2009). Segregation in bulk solids can happen because of differences in particle density (Schulze, 2008), but it is ambiguous to say that it can considered as a reliable model in describing the powder flow (Devriendt et al., 2013). If the movement of individual particles can be restricted, then cohesion can diminish the intensity of segregation. However, the interparticle cohesion is generally considered in bulk powder with fine particles having a size below 20 μm. Because of liquid or moisture content, the cohesion generally extends with a wider particle size range than that due to fine components and may lead to diminished segregation (Hogg, 2009). The bulk powders that are not free-flowing in nature due to fine particles or moisture content are dominated by particle-to-particle adhesion, which restricts the free movement of particles and, thus, arrests the segregation (Schulze, 2008).

For sifting segregation to take place, particles must roll down or slide against each other. However, the inter-particle adhesion and cohesion effects would try to prevent such relative movement between the particles. The powder must have strong inter-particle mobility and should be free-flowing for sifting segregation to occur. Segregation would be suppressed by cohesive, fibrous, or rough-textured particles because of their difficulty to flow (Li et al., 2016; Oka et al., 2016). In the case of fluidisation segregation, air drag on a single particle must be substantial compared to the inter-particle forces for the powder to fluidise properly. Particles will remain stuck together with each other till the air flow rate becomes exceedingly significant and turbulent if cohesive forces are significant relative to air drag. Thus, cohesion would be one of the important parameters, but certainly not the only parameter, for fluidising segregation to occur. Since cohesion is one of the flowability parameters of powders, so fluidising segregation can be thought of as indirectly linked to powder flow properties.

Powder flowability is believed to be influenced by the existence of fines in powder samples. The flowability of bulk powder having the same median size decreases with an increasing presence of fines (Schulze, 2008). The decrease in flowability of fine particle sizes is because of higher surface area per unit mass of powder. Higher surface area is exposed for cohesive forces, in actual, and

frictional forces to arrest the free flow (Li et al., 2016). In case of particle size greater than 500 µm, the rough-shaped particles show better flowability compared to the sharp and irregular particles. The fibrous particles (like crushed biomass) often create flow issues when experiencing high stress (Schulze, 2008). The flowability of powders depends on the shape and size distribution of particles (Salameh et al., 2016). The packing density of a binary mixture strongly affects the frictional properties such as frictional angle (Kojima et al., 2012). A definite roughness can hamper the particle-to-particle tactic as smooth particles can do so that the coarse particles may reveal additional complimentary flow performance (Schulze, 2008). The larger the value of the flowability index, the better a bulk solid flow and the smaller its cohesion value (Kojima et al., 2012). The liquid bridge can be formed between the gap of dry bulk material if a small quantity of dilute liquid is added because of the surface tension, which leads to negative capillary pressure. This increases particle bonding and may decrease the flowability (Schulze, 2008). Moisture affects the flowability of Avicel PH102 by increasing the interparticle bonds. Control of R.H. during flowability evaluation is difficult for Avicel PH102 and formulations containing it (Sun, 2016). In the following table (Table 1.1), different methods and apparatus are provided for measuring the flowability of powder:

Table 1.1: Different arrangements for measurement of powder flowability

Funnel	Bulk materials are served into a funnel by changing opening diameters. The minimum opening size at which flow happens and the flowability can be determined by evaluating the time required to discharge the powder sample taken through the minimum opening size. Some discharge aids (e.g., the stirrer can be used to dodge flow blocks with cohesive bulk materials. The lesser the time, the superior the rating of flowability (Schulze, 2008).	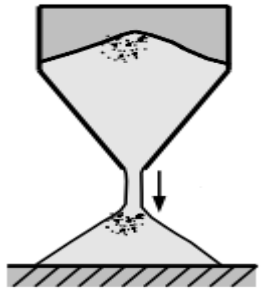 **Figure 1.2:** Funnel (Schulze, 2008)
Angle of repose	Repose angle is the heap in the conical shape of the loose, un-compacted bulk solid. By pouring the powder sample into the funnel, the heap is formed on the bottom support. Rotating a drum consisting of powder samples along the horizontal axis provides the dynamic repose angle. Depending on the drum rotating speed (in rpm) and bulk properties of the powder, one can experience different slope profiles. The higher value of the dynamic repose angle suggests poor flowability and vice versa (Schulze, 2008).	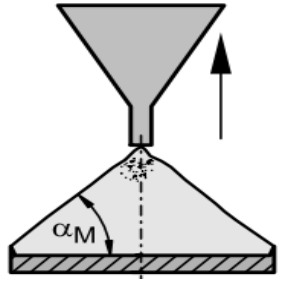 **Figure 1.3:** Measurement of angle of repose (Schulze, 2008)

Imse test	The powder sample is poured into a funnel that is placed over a sieve and raised slowly. A measure of flowability is the mass left on the sieve, i.e., the smaller the left mass, the better the flowability of bulk material is there (Schulze, 2008).	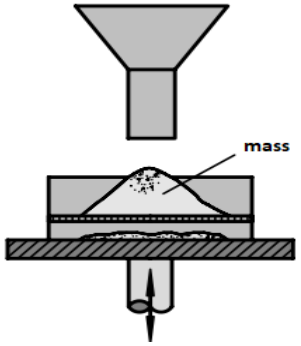 **Figure 1.4:** Principle of the Imse test (Schulze, 2008)
Carr flowability index	This test setup consists of different tests to measure the flow behaviour, which are explained below: • Angle of repose can be calculated by pouring the powder into a funnel and forming the heap on a flat and circular support. • To evaluate the affordability index or angle of fall, the circular support is provided with the shock five times by falling the weight, and the slope angle is measured. • The angle of the spatula is measured from the angle made by the slope of powder that formed on a spatula that is lifted from a heap of powder (Schulze, 2008).	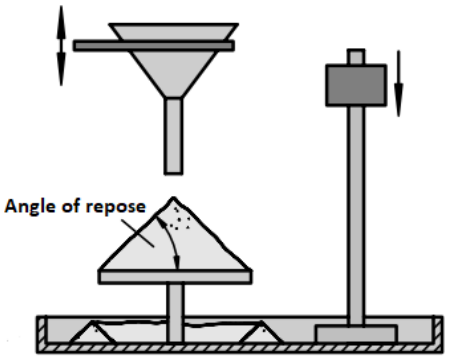 **Figure 1.5:** Principle of the Carr flowability index (Schulze, 2008)

Stirrer	A vertical stirrer is provided with some angular speed and allowed to stir the powder sample into a container. The torque is calculated as a function of time or angular speed, used to represent the flowability of bulk powder (Schulze, 2008).	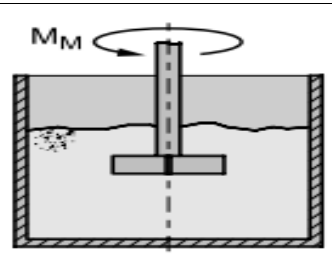 **Figure 1.6:** Stirrer (Schulze, 2008)
Compressibility test	A powder sample confined in a container is compressed with axial loading, which increases the bulk density of the powder sample. The flow behaviour of the powder sample under a certain stress value can be evaluated. By increasing the consolidation stress, the flowability of the powder sample comes down. Generally, compressibility can be determined by two properties: bulk and tapped densities (Schulze, 2008).	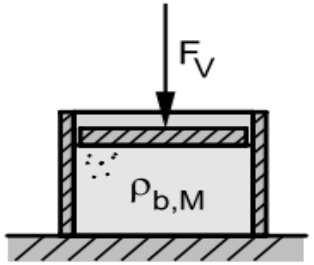 **Figure 1.7:** Principle of a compressibility test (Schulze, 2008)
Flowability test	A powder sample confined in a container was consolidated with axial loading on the top plate while the stirrer remained immersed in the powder sample. After that, the plate is raised, the stirrer starts to turn slowly, and torque is measured. The flowability of the powder sample is measured from the torque value (Schulze, 2008).	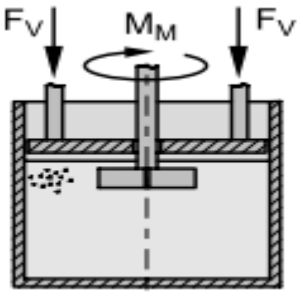 **Figure 1.8:** Flowability test (Schulze, 2008)

Penetration test	The bulk powder is compressed perpendicularly. Then force is applied to the powder sample through a lid placed on the powder sample. By applying a certain amount of vertical force, the failure happens along the curved slip lines. The strength of bulk powder is calculated from the force applied up to the point of failure (Schulze, 2008).	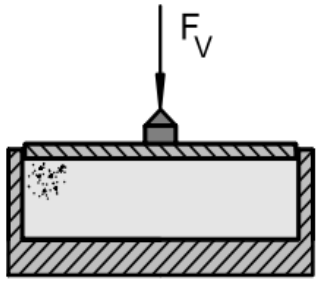 **Figure 1.9:** Penetration test (Schulze, 2008)
Uniaxial compression test	In case the container surface or wall is frictionless, then test results in a partial measurable report about flowability and time consolidation for cohesive bulk materials with a trend for smaller strength values because of the consolidation procedure "uniaxial compaction". In contrast, the consolidation stress may strongly decrease downwards if the walls are not friction-free, which leads to a severe underestimation of the strength. Additionally, the strength determined depends on the angle of wall friction (Schulze, 2008).	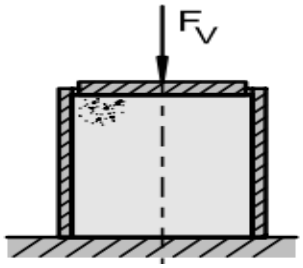 **Figure 1.10:** Uniaxial compression test (Schulze, 2008)
Monoaxial shear test	This test method is the same as the above-mentioned uniaxial compression test. The powder sample is consolidated with axial loading. The unconfined failure strength is determined from the force measured at the point of failure (Schulze, 2008).	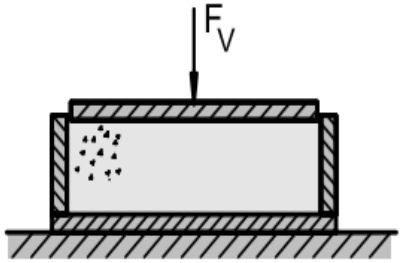

		Figure 1.11: Principle of the monoaxial shear test (Schulze, 2008)
Uniaxial tensile strength test	A powder sample is compressed with an undersized plate in the downward direction. The plate is coated with an adhesive to adhere the particles to that plate, representing the failure that has happened within the powder sample. The tensile strength of powder is determined from the change of the maximum force measured at failure and the weight of the plate with the adhering bulk powder (Schulze, 2008).	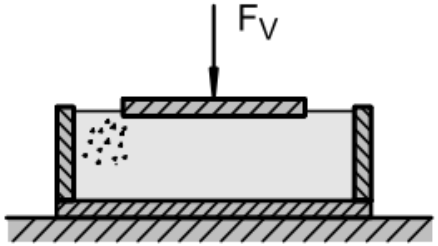 **Figure 1.12:** Principle of uniaxial tensile strength test (Schulze, 2008)
Jenike shear tester	The base of the shear cell is made to be fixed on which a shear ring is placed. Then, it is filled with a bulk powder sample and covered with a shear lid and thus, the specimen powder sample is applied with a normal force. The upper part of the shear cell, i.e., the shear ring and lid, moved horizontally to shear the powder sample. For this purpose, the bracket in the shear lid is used that moves around with a speed of 1 mm/min. the bracket pin is connected to a load cell that provides the value of shear force (Schulze, 2008).	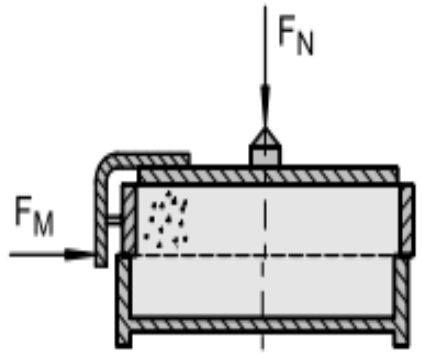 **Figure 1.13:** Shear cell of the Jenike shear tester (Schulze, 2008)

Torsional shear tester	A powder sample is confined in a cylindrical-shaped shear cell. Then, the powder sample is compressed with axial loading along with a rotation of the top lid relative to the shear cell, and thus, shearing of the powder sample happens, and torque is measured. The shear stress acting in the powder sample is determined by the value of torque (Schulze, 2008).	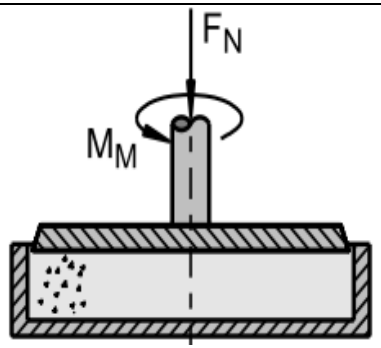 **Figure 1.14:** Shear cell of a torsional shear tester (Schulze, 2008)
Ring shear tester	This test method is similar to the above-mentioned torsional tester, with the only difference being that the powder sample is poured in an annular trough. The axial load is applied through the grooved lid, and the lower trough rotates relative to the top lid. The shear stress acting in the powder sample is determined by the value of torque (Schulze, 2008).	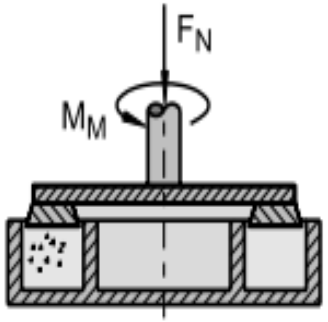 **Figure 1.15:** Shear cell of a ring shear tester (Schulze, 2008)

To minimise the potential of segregation, some common methods are enhancement of material properties while manufacturing, the right choice of device parameters, and appropriate control of material handling environmental situations. The enhancement of material properties minimises the extent of segregation patterns. To minimise size segregation, narrowing down the size distribution can be opted for a costly process. Granulation or agglomeration is two techniques to narrow the size distribution. Segregation can also be minimised when the absolute size of particles is decreased below 100 μm, which can enhance the flowability issues. Non-uniform particles should be ignored to minimise the segregation due to the shape. It is likely to evaluate a suitable balance between the size ratio and density ratio to minimise the density effect. By increasing the moisture content, the free flow of powder can be arrested, which can lead to avoiding segregation (Tang et al., 2004). In some cases, the addition of moisture can help in better flowability, which acts as a lubrication effect between the particles (Mehos, 1971).

To reduce shifting segregation, some techniques exist: prevent forming heap, decrease the size of a heap, and lesser free-fall during loading of the silo. Different types of distributors and inserts can be employed to reduce the size of the heap or avoid the heap formed, which can lead to segregation due to the rolling effect. Figure 1.16 shows different inserts and distributors, which are powdered and non-powered based (Tang et al., 2004). Sifting segregation is more prone with the funnel flow hopper, which can be diminished by keeping the level of powder in the hopper at its high capacity or at full level by regular loading and unloading the bulk powder, which may act as a standpipe (Mehos, 1971).

Several inserts are shown in Figure 1.17 that can be utilised to diminish segregation while unloading a silo or bin and are explained below. The conical insert sited in a funnel flow hopper can arrest segregation and extend the flow profile but is not able to alter the funnel flow to mass flow. A bullet-type insert is able to alter a funnel flow hopper to a mass flow hopper. A cone-in-cone insert can translate the funnel flow hopper, with a hopper angle equal to twice the mass flow, into the mass flow without having the drawback of the bullet-type insert (Tang et al., 2004). The tendency of a powder to be segregated often depends on the parameters of handling, such as the unloading rate. By increasing the unloading rate, the particles have less time to segregate and, thus, reduce segregation (Mehos, 1971).

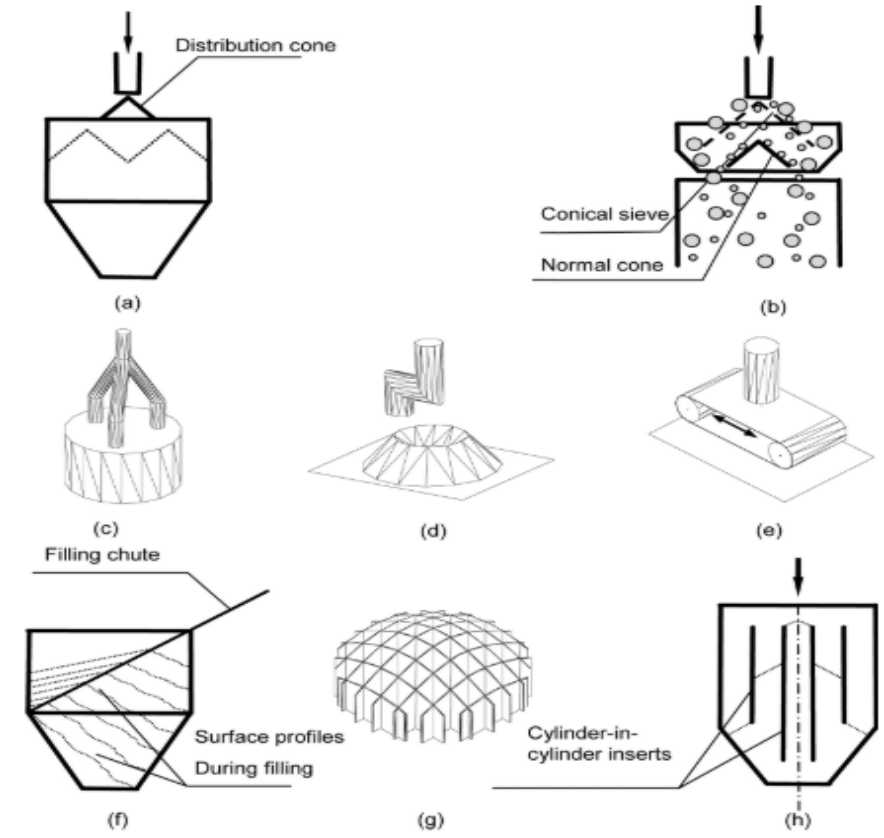

Figure 1.16: Techniques or tools for minimising segregation during filling: (a) conical distributor, (b) conical sieve distributor, (c) branch pipe distributor, (d) rotating tube distributor, (e) movable belt distributor, (f) filling chute, (g) egg-box insert (h) cylinder-in-cylinder insert (Tang et al., 2004)

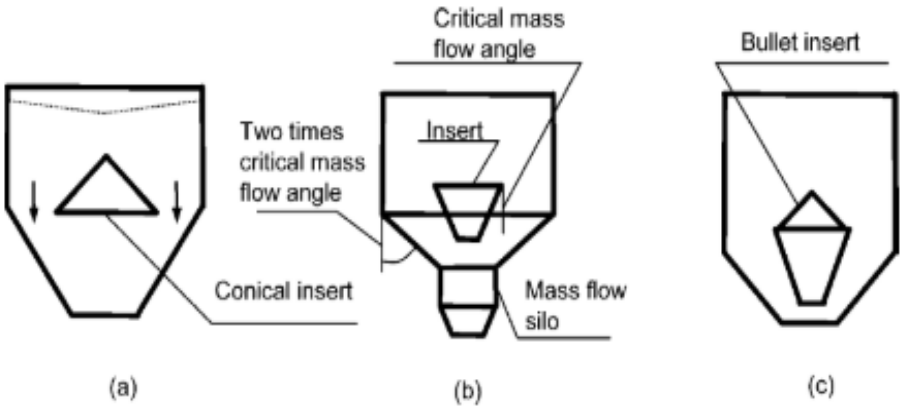

Figure 1.17: Techniques or tools for minimising segregation while discharging; (a) conical insert, (b) cone-in-cone insert, and (c) bullet insert (Tang et al., 2004)

A dense phase pneumatic conveying with less feeding air in the pipeline may suppress the segregation. During the conveying of fine particles into a hopper or bin, it is advisable to use the tangential entry of the powder rather than from the top or at 90˚. This may lead to some sought of side-to-side segregation and minimise the chance of top-to-bottom segregation, which is more challenging. During mechanical conveying through the conveying belts, the bulk powder can be segregated in a side-to-side way. Generally, conveyor belts or other means of mechanical conveyors operate at low speeds and under control conditions; the in-line chance of segregation happening cannot be significant (Tang et al., 2004). In order to reduce the segregation due to the effect of fluidisation, a long pipe can drop in the layers of bulk powder or introduce the powder stream directly towards the silo wall. The effect of air entrainment can be eliminated up to a certain extent by having the option of a proper vent system (Mehos, 1971).

A good mixer can be attained by utilising a submerged-impeller type of mixer instead of a tumbler mixer while using a bulk powder that is more prone to segregate. Of the three mixing mechanisms, i.e., diffusive, shear, and convective mechanisms, the convective mechanism is most likely to minimise segregation while mixing is in progress (Tang et al., 2004). It is observed that the mixtures exiting the continuous blender (refer to Figure 1.18) are more consistent compared to the state of consistency accomplished at the end of a batch blending process (Oka et al., 2016).

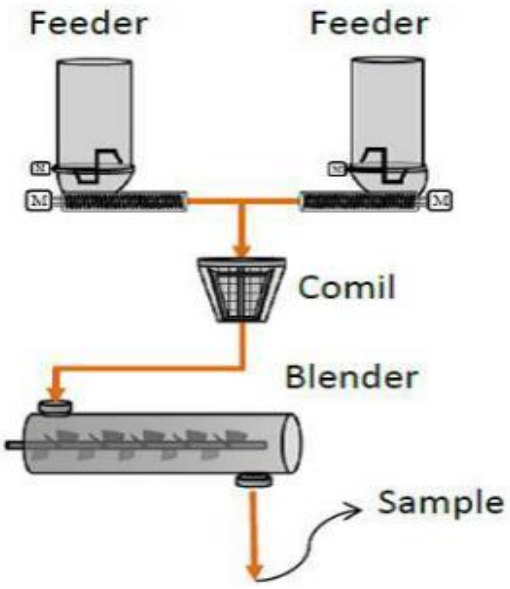

Figure 1.18: Schematic of the continued blending setup (Oka et al., 2016)

Based on the review of the literature and industrial feedback, the following research gaps are found:

- Only limited research has been reported for the segregation of powders in the range of 50 to 1000 µm, which typically comes in the Geldart A and B (Geldart, 1973) regime, with emphasis on Geldart A to B borderline materials in terms of assessing segregation tendencies, indexing the same, and relating powder flow properties with segregation tendencies.
- Minimal attempts have been made to date in connecting powder segregation to flow properties.
- Only limited work has been carried out in relating the physical characteristics of powders to their segregation properties.
- Only limited work has been carried out in modelling changes in segregation tendencies with the addition of moisture.

1.2 Objectives

The subsequent objectives have been recognised under the research work entitled "Interdependence between Segregation and Flow Properties of Bulk Solids".

1. To develop segregation testers based on the sifting and fluidisation mechanism of segregation.
2. To carry out segregation, flow properties and characterisation tests for Geldart A and B type powders (such as pharmaceutical, food and detergent powders) with emphasis on Geldart A to B borderline material.
3. To develop appropriate models for powders describing the interdependence between segregation and flow properties.
4. To evaluate segregation characteristics under different humidity/moisture conditions.

1.3 Thesis outline

Chapter-wise distribution of the contents of the thesis is as follows:

Chapter 1 Outlines the importance of predicting the powder segregation characteristics for Group A to B powders and lists thesis objectives

Chapter 2	Provides literature on the mechanism of segregation, the effect of particle properties on segregation and quantification of segregation
Chapter 3	Includes a description of test facility development that carries out segregation, flow properties, and characterisation tests
Chapter 4	Links the particle properties data to powder flow properties for powders
Chapter 5	Links the particle, flow, and fluid properties data to segregation characteristics for the different Geldart A and B-type powders
Chapter 6	Develop a validated model for sifting segregation based on particle and flow properties. Asses the existing models for minimum fluidisation velocity for single/multi-component particles and develop a new validated model, including a modified cohesion number for fluidisation segregation.
Chapter 7	Assess the flow properties and segregation characteristics of Geldart A and B-type powders under different moisture content
Chapter 8	Potential difficulties in conveying of segregated powders
Chapter 9	Includes conclusion and future scope of work

References

Amagliani, L., J.O. Regan, A.L. Kelly, and J.A.O. Mahony. 2016. Physical and Flow Properties of Rice Protein Powders. *Journal of Food Engineering* 190: 1–9.

ASTM International, D 6941, Standard practice for measuring fluidization segregation tendencies of powders, *ASTM International*, West Conshohocken, PA, 2012.

ASTM International, D6940, Standard practice for measuring shifting segregation tendencies of bulk solids, *ASTM International*, West Conshohocken, PA, 2010.

Chávez Montes, B.E., J.M. Martínez-Alejo, H. Lozano-Perez, J.C. Gumy, D. Zemlyanov, and M.T. Carvajal. 2019. A Surface Characterization Platform Approach to Study Flowability of Food Powders. *Powder Technology* 357 (December): 269–280.

Devriendt, L., C. Gatumel, and H. Berthiaux. 2013. Experimental Evidence of Mixture Segregation by Particle Size Distribution. *Particulate Science and Technology* 31, no. 6 (November 2): 653–657.

Deng, T., K.A. Paul, M.S.A. Bradley, L. Immins, C. Preston, J.F. Scott, and E.H. Welfare. 2010. Investigations on Air Induced Segregation of Pharmaceutical Powders and Effect of Material Flow Functions. *Powder Technology* 203, no. 2 (November): 354–358.

Engblom, N., H. Saxén, R. Zevenhoven, H. Nylander, and G.G. Enstad. 2012. Segregation of Construction Materials in Silos. Part 2: Identification of Relevant Segregation Mechanisms. *Particulate Science and Technology* 30, no. 2 (March): 161–178.

Emery, E., J. Oliver, T. Pugsley, J. Sharma, and J. Zhou. 2009. Flowability of Moist Pharmaceutical Powders. *Powder Technology* 189, no. 3: 409–415.

Kritika, D., V. Karde, A. Jauhari, S.C Bhattacharyya, C. Ghoroi. 2022. Flow Improvement of Fine Oxidizer Using Nano-Additives. *Advanced Powder Technology* 33(8), 103711.

Fathollahi, S., E. Faulhammer, B.J. Glasser, and J.G. Khinast. 2020. Impact of Powder Composition on Processing-Relevant Properties of Pharmaceutical Materials: An Experimental Study. *Advanced Powder Technology* 31, no. 7: 2991–3003.

Faqih, A.N., A.W. Alexander, F.J. Muzzio, and M.S. Tomassone. 2007. A Method for Predicting Hopper Flow Characteristics of Pharmaceutical Powders. *Chemical Engineering Science* 62, no. 5 (March): 1536–1542.

Ghosal, D., S. Sengupta, J. K. Basu. 2015. Characterization of alumina and H-ZSM-5 zeolite and comparison of their performance by toluene methylation reaction with ceramic foam as catalyst support, *Current Catalysis* 4, no. 2, 111-124(14).

Gray, J.M.N.T., A.R Thornton. 2005. A theory for particle size segregation in shallow granular free-surface flows. In Proceedings of the Royal Society *A: Mathematical, Physical and Engineering Sciences* 461, Issue 2057, 1447–1473.

Geldart, D. 1973. Types of Gas Fluidization. *Powder Technology* 7: 285–292.

G. Mehos, Storage and flow of bulk solids, 1971

Heartwin, P., H. Mitra, M. E. Franklin, C. Ghoroi, R. Prabin, K. Ambrose, S. Battula. 2020. Physicochemical, Thermal, and Flow Properties of Ice Cream Powder as Influenced by Moisture Content. *Journal of Food Processing and Preservation*, 45(2), 35-48.

Hart, A. 2015. Effect of Particle Size on Detergent Powders Flowability and Tabletability. *Journal of Chemical Engineering & Process Technology* 06, no. 01: 1–4.

Hart, A., C.-Y. Wu. 2011. The Impact of Dry Granulation on Detergent Powder Properties, *in: Particulate Materials: Synthesis, Characterisation, Processing and Modelling*, pp. 102–110.

Huang, Q., H. Zhang, and J. Zhu. 2010. Flow Properties of Fine Powders in Powder Coating. *Particuology* 8, no. 1 (February): 19–27.

Hogg, R. 2009. Mixing and Segregation in Powders: Evaluation, Mechanisms and Processes. *KONA Powder and Particle Journal* 27: 3–17.

Ireland, E., K. Pitt, R. Smith. 2016. A review of pulsed flow fluidisation; the effects of intermittent gas flow on fluidised gas–solid bed behaviour, *Powder Technology* 292, 108-121.

Ji, J., J. Fitzpatrick, K. Cronin, M.A. Fenelon, and S. Miao. 2017. The effects of fluidised bed and high shear mixer granulation processes on water adsorption and flow properties of milk protein isolate powder. *Journal of Food Engineering*. 192: 19–27.

Kojima, T., and J.A. Elliott. 2012. Incipient Flow Properties of Two-Component Fine Powder Systems and Their Relationships with Bulk Density and Particle Contacts. *Powder Technology* 228: 359–370.

Li, R., Y.H. Roos, and S. Miao. 2016(a). In Fluence of Pre-Crystallisation and Water Plasticization on Flow Properties of Lactose / WPI Solids Systems. *Powder Technology* 294: 365–372.

Li, R., Y.H. Roos, and S. Miao. 2016(b). The Effect of Water Plasticization and Lactose Content on Flow Properties of Dairy Model Solids. *Journal of Food Engineering* 170: 50–57.

Liu, L.X., I. Marziano, A.C. Bentham, J.D. Litster, E.T.White, and T. Howes. 2008. Effect of Particle Properties on the Flowability of Ibuprofen Powders. *International Journal of Pharmaceutics* 362, no. 1–2 (October): 109–117.

McGlinchey D, (ed.). 2023. Simulations in Bulk Solids Handling: Applications of DEM and other Methods. *Wiley*. UK.

Mondal, S., K Aikat, G Halder. 2022. Sorptive uptake of Ranitidine hydrochloride by Parthenium hysterophorus based chemically treated N-biochar in static bed continuous flow system. *Surfaces and Interfaces* 8, p. 100071.

Oka, S., A. Sahay, W. Meng, and F. Muzzio. 2016. Diminished Segregation in Continuous Powder Mixing. *Powder Technology* 309 (March): 79–88.

Opaliński, I., M. Chutkowski, and A. Hassanpour. 2016. Rheology of Moist Food Powders as Affected by Moisture Content. *Powder Technology* 294 (June): 315–322.

Parmar, R., S. K. Majumder. 2013. Microbubble generation and microbubble-aided transport process intensification—A state-of-the-art report. *Chemical Engineering and Processing: Process Intensification* 64, 79–97.

Sun, C.C. 2016. Quantifying Effects of Moisture Content on Flow Properties of Microcrystalline Cellulose Using a Ring Shear Tester. *Powder Technology* 289: 104–108.

Salameh, C., J. Scher, J. Petit, C. Gaiani, C. Hosri, and S. Banon. 2016. Physico-Chemical and Rheological Properties of Lebanese Kishk Powder, a Dried Fermented Milk-Cereal Mixture. *Powder Technology* 292: 307–313.

Schulze, D. 2008. Powders and Bulk Solids. Chemie Ingenieur Technik 82, no. 4 (April): 553–554.

Shah, K.R., S.I. Farag Badawy, M.M. Szemraj, D.B. Gray, and M.A. Hussain. 2007. Assessment of Segregation Potential of Powder Blends. *Pharmaceutical Development and Technology* 12, no. 5 (January 7): 457–462.

Traina, K., R. Cloots, S. Bontempi, G. Lumay, N. Vandewalle, and F. Boschini. 2013. Flow Abilities of Powders and Granular Materials Evidenced from Dynamical Tap Density Measurement. *Powder Technology* 235 (February): 842–852.

Tang, P., and V.M. Puri. 2004. Methods for Minimizing Segregation: A Review. *Particulate Science and Technology* 22, no. 4 (October): 321–337.

Teunou, E., and J.J. Fitzpatrick. 2000. Effect of Storage Time and Consolidation on Food Powder Flowability. *Journal of Food Engineering* 43: 97–101.

Vikram, K., C. Ghoroi. 2021. Humidity-Induced Interparticle Friction and Its Mitigation in Fine Powder Flow. *Particulate Science and Technology* 40 (5), 598–608.

Vasilenko, A., B.J. Glasser, and F.J. Muzzio. 2011. Shear and Flow Behavior of Pharmaceutical Blends — Method Comparison Study. *Powder Technology* 208, no. 3: 628–636.

Wang, Y., R.D. Snee, W. Meng, and F.J. Muzzio. 2016. Predicting Flow Behavior of Pharmaceutical Blends Using Shear Cell Methodology: A Quality by Design Approach. *Powder Technology* 294: 22–29.

Zinatlou, S., D. Sofia, C. Hare, D. Barletta, M. Poletto. 2024. Experimental characterisation of the spreading of polymeric powders in powder bed fusion additive manufacturing process at changing temperature conditions, *Advanced Powder Technology* 35,104412.

CHAPTER 2

Literature Review

2.1 Introduction

Bulk powders have various types of applications, such as in paint, pharmaceutical, chemical, detergent, food, power, mining, construction industries etc. This means that issues in handling such bulk powders are quite important, given the demand for such bulk powders in the market, Rosato et al., 2020. Segregation or de-mixing is one of the significant problems in flowing a bulk powder as it occurs due to similar characteristics such as shape, size, and density when particles accumulate at a particular location within a bulk powder due to forces such as gravity, vibration, and/or shear. Segregation can be a big challenge when dealing with powders from their manufacturing up to the final product, which can impede the quality standards of the finished product by affecting its homogeneity, which may lead to the rejection of the lot. The API content may vary from batch to batch, which may lead to the failure of a high-value batch in the pharmaceutical industry, Prescott et al., 2001, because it does not comply with the USP requirements for uniformity of content, U.S. Pharmacopeia, 2011.

2.2 Segregation mechanisms

Segregation is a multi-component phenomenon where there may be one or several causes of segregation. There are some segregation mechanisms, such as trajectory, rolling, displacement, percolation, sieving, air current, fluidisation, agglomeration, concentration-driven displacement, push-away, impact/bouncing, embedding, and angle of repose (McGlinchey, 1998; Mosby et al., 1996; De Silva et al., 2000). Carson et al., 1986; and Johanson, 1996, have reduced them into five major mechanisms, which are trajectory, sifting, fluidisation, air current, and angle of repose. Trajectory segregation generally occurs in large particles at the time of free-fall or when their rolling or moving velocity is comparatively high during the flow through the heap or chute. Sieving segregation patterns generally tend to occur in situations when fines pass over the void spaces created by coarse particles due to exterior energy inputs such as vibration and/or shear motion. Fluidisation segregation occurs when fine particles get a chance to be fluidised during a free fall from the top of a silo while loading. As per the particle size, Tang et al., 2004, classified the segregation into four mechanisms: trajectory (Geldart A to B group), sieving (Geldart A group), fluidisation (Geldart C to A group), and agglomeration segregation (Geldart C to A group), shown in Figure 2.1.

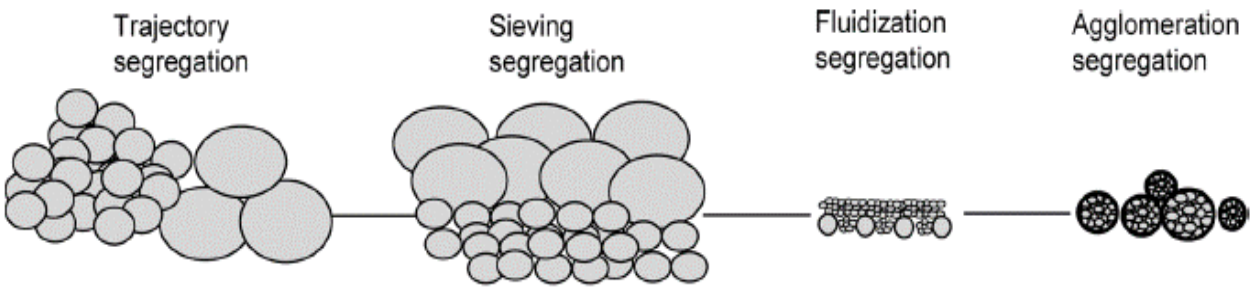

Figure 2.1: Schematic of primary segregation mechanisms (Tang et al., 2004)

For Geldart group A to B borderline powders, the most common segregation mechanisms were found to be sifting, fluidisation, trajectory, and differences in angle of repose.

Sifting (sieving or percolating)

As the powder is filled into a bin, a powder heap will form, and the particles slide and/or roll down the surface of the heap during powder loading. The probability of getting caught by a large cavity on the surface is higher for smaller particles than for larger ones. Thus, the particles that are smaller in size accumulate at the top position of the heap, and larger particles roll down on the slant height by overcoming the obstacle or irregularities from top to bottom of the heap, forming a structure similar to a Christmas tree (Garcia et al., 2015), as shown in Figure 2.2.

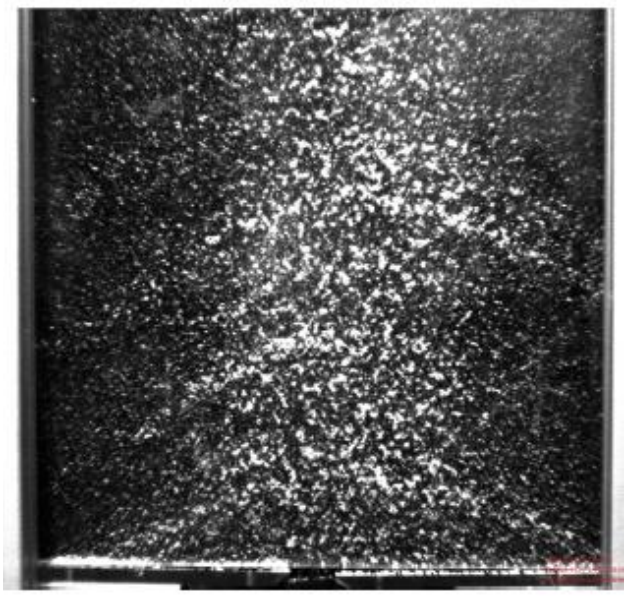

Figure 2.2: Differently coloured particles formed a Christmas tree filling the silo (Garcia et al., 2015)

Meanwhile, during the sliding and rolling action of the smaller particles in bulk powder, they may percolate into the void spaces created by the larger particles. Embedding is a process in which, upon hitting the free-flow surface of the bulk solid, heavier particles break up the surface layer and get embedded into that. In the phenomenon of sliding, rolling, percolating, and embedding, the heap surface can behave like a sieve. Hence, this phenomenon is commonly known as sifting. Sifting can be found in the following situations: a fairly large size difference of the particle, an adequately greater average diameter of pores, a free-flowing nature to flow through pores or a lack of cohesion and existence of motion between the particles (Fan et al., 2017). Narendran et al., 2019, observed that the major mechanism of segregation of kidney beans and soybeans within a blend of wheat, canola, soybean, and red kidney beans is embedding and sliding that occurred during the loading process of the wheat mixture, hence producing sifting segregation.

The industrial manufacturing process of dry mineral-based construction materials includes an innocuous mixture of raw materials according to specified proportions while maintaining well-mixed products. The critical processing stage, according to segregation, is short-term storage in silos before packing. Segregation reveals a process in which a concentration increase of fine particles near the end of a full discharge. At the end of complete discharge, fines content is increased since in filling, powders are not uniformly distributed across the cross-section of the silo and discharge through funnel flow. The areas at the vicinity of the walls of the silo appear as fine-rich region in the late discharge batches. This causes non-uniform particle distribution because of mechanisms of fluidisation and air-current segregation. Such segregation is not present if the material is distributed uniformly, which indicates that percolation or sifting has not taken place, although it has a character of discharge during emptying by way of funnel flow. Engblom et al., 2012(a), investigated the size segregation of binary and ternary powder mixtures in a silo of 0.5 m^3, as well as in commercial construction products in silos of 20 m^3 and 70 m^3 sizes and found an identical segregation pattern, i.e., fine is accumulated at the walls of the silo during filling.

Garcia et al., 2015, reported that the region of fine particle exhaustion is wider in the case of flat-bottom silo-type discharge with a belt conveyor (Figure 2.3), and the parabolic shape is more pronounced compared to free discharge. The interface zone is steeper when a belt conveyor is utilised as a discharge device compared to the discharge without a belt conveyor. Therefore, in this region, the velocity component in the horizontal direction is lower. Because of this effect, the large particles those have the same velocity as the finer particles and are mixed in the vertical direction. A second interface is observable in the discharge where both components are mixed (Figure 2.3(c), (d)).

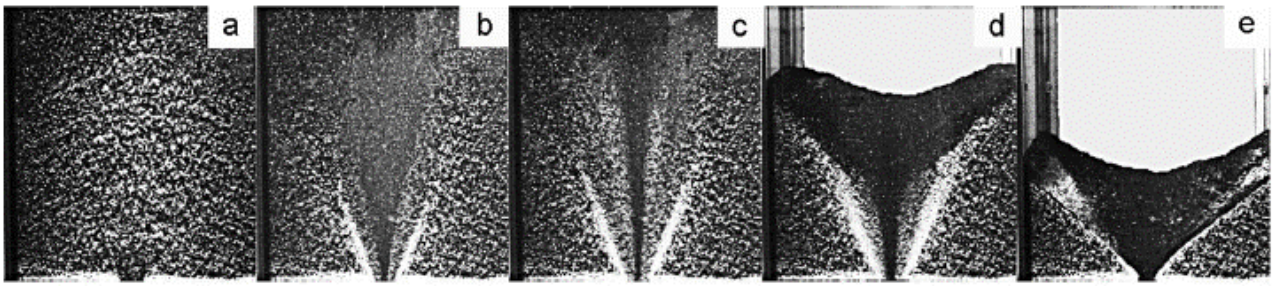

Figure 2.3: Pattern formation due to segregation profiles while unloading of a silo with a flat bottom and belt conveyor w.r.t. time: a) at starting, b) after 30 s, c) after 60 s, d) after 120 s, and e) after 180 s (Garcia et al., 2015)

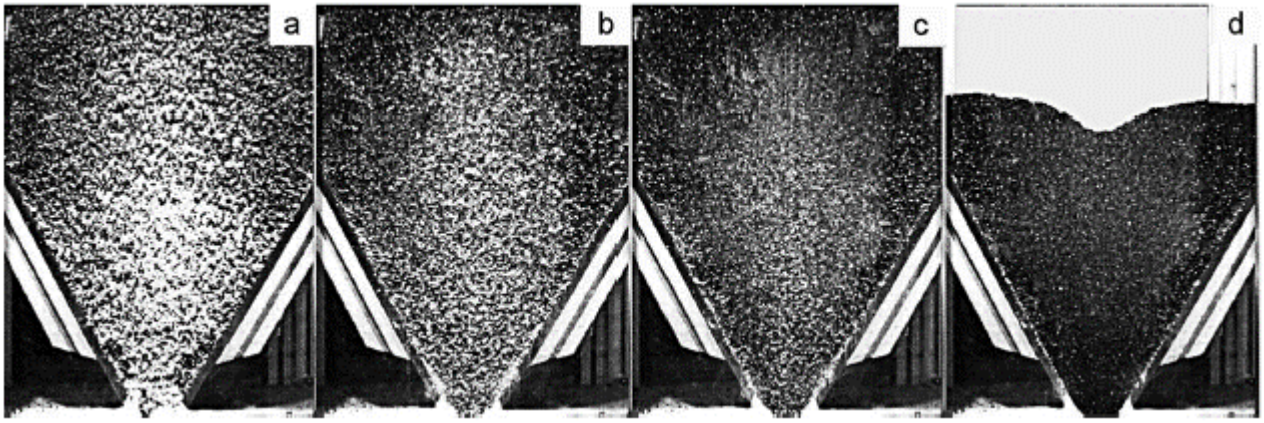

Figure 2.4: Pattern formation due to segregation profiles while unloading of a silo with a hopper angle of 30˚ w.r.t. time: a) at starting, b) after 2 s, c) after 5 s, and d) after 10 s (Garcia et al., 2015)

No different zones are observed to be present under mass flow pattern, i.e., for 30° hopper and free discharge (Figure 2.4). The entire bulk is in motion, and the velocity gradients are not adequate enough for the percolation of fines, so no fine depletion is noticed.

Fluidisation segregation

If the mixture is fine, the trapped air in the interstitial voids can be enough to make the material in a fluidised state. When a big particle is embedded into this layer, its energy makes big particles penetrate this fluidised layer and segregate fine and coarse particles from top to bottom. It also requires a supply of air. Any material would separate due to the differences in particle properties, provided the handling system can induce some stimulus that increases that particular mode of separation. For instance, the variation in surface friction leads to an angle of repose segregation, but

this arises only if the piles are built up during a process. Air-induced segregation is influenced by the height of the free-fall and powder flow rate, which may change the entrained gas content in bulk powder. This is more significant with a higher value of free-fall. This means that any potentially feasible segregation test setup must be able to vary feed and pile formation conditions. Many segregation testers inject some arbitrary amount of gas, which is quite often greater than the amount likely to be found in a real gravity feed process and measure the segregation potential of fines to coarse on this basis. Such a segregation method has limited capability of predicting the true extent of segregation. For a segregation method to be worthwhile, one should consider a handling process that is least affected by the external stimulus or prove some feasible solution to control the external stimulus to allow for matching process operations. For instance, the test method should subject the material to the same or similar condition as the actual system. Engblom et al., 2012(b) observed that the free fall of the particles depends upon their material. By increasing the free fall height, the fine content is concentrated in the vicinity of the silo wall. By considering a low free fall height below 0.5 m in all silos, fines content accumulated at the point of filling due to the sieving and rolling effect.

Large size differences of particles in the blends tested may be the cause of the high chance of air-induced segregation, coupled with assuming the bulk powder is free to flow. This might even improve the powder flow failure function, limited to the degree that would not introduce problems with the flow in the process, and consequently make segregation less susceptible because of greater internal stresses in the particle resulting from the elutriation by air through a stronger agglomeration. Deng et al., 2010, examined the outcomes of the flowability tests, where both blends are 'free-flowing' materials. API 1 has higher segregation compared to both API 2 and API 3. It would be concluded that the segregation observed in these two trial blends is largely due to API 1 because its particle size is significantly higher than all the other components of the blend, thus making the particle size difference much higher.

Vertical chute transport is widely applied in pharmaceutical manufacturing for powder and powder mix transportation; however, this also promotes segregation. The different constituents of a powder mixture, such as API or excipient, may segregate based on their size. Therefore, the properties of the finished product depend upon the size of its constituting particles, including the property of compressibility, rate of dissolution, and uniformity of the content. Jakli et al., 2015, experimentally investigated the extent of segregation of single-particle pharmaceutical powder based on particle size. Single-particle pharmaceutical powders were allowed to fall into a vertical chute consisting of two tubes and with a closed bottom. The different powder samples were collected at different powder bed

heights for particle-size distribution analysis. The experiments led to particle size-based segregation of all the materials investigated, and the segregation level were found to be material-specific. Part of the observed segregation phenomena could be rationalised using the flow behaviour of free-falling powder and the properties of the bulk of the powder. One more interesting result was the segregation degree of smaller D(0.1) sized particles in less cohesive and, therefore, more freely-flowing materials that can be related to the application of the vertical chute system with a closed bottom being airtight. There is a size threshold below which particles concentrate toward the top of the sediment and above which particles focus at the bottom of the sediment.

Trajectory segregation

There may be different air drag experienced by coarse and fine particles while loading into a silo. Thus, trajectory segregation caused the different trajectories of particles. Trajectory segregation may be induced when particles drop from a loading outlet or are jetted out from the auger or conveyor to the pile of bulk powder. The air drag increases with the decrease in particle diameter, and the drag coefficient also increases. The larger the surface area, the greater the drag coefficient for a particle. Particles with different diameters and surface areas, therefore, have different trajectories. With the decrease in particle size and sphericity, the ratio of air resistance to gravity force is increased considerably in the gravity field. The particle having lesser particle size, typically below 100 µm, the particle shape has minimal impact on this ratio. By reducing the particle size to less than 10 µm, the gravitational pull also comes down, and hence, the ratio of air resistance to gravity force would be high. Particles less than 1 µm will have a falling velocity of less than 0.08 mm/s (Schulze, 2008). The falling velocity of particles with 10 and 25 µm diameters is approximately 8 and 51 mm/s (Schulze, 2008), respectively. Particles less than 100 µm diameter will be suspended in air, and air currents will strongly affect them. Powder sediments can be highly segregated following a drop of 0.3-0.6 m (Theimer, 1973).

Angle of repose differences

The elevation potential renders the top of a heap to be in a fluidising state. These can flow as a result of the effects of different angles of repose, impacts or pushes by other particles, and movement of other particles. Associated segregation angles of repose occur whenever particles have a smaller angle

of repose that ends up flowing over particles whose angle of repose is larger. A powder pile will create a shear region amongst the powder-flowing layers that slide on the slant height, and the stagnant region will form the pile. The repose angle may be significantly influenced by little change in the moisture content of the powder, the geometry of the silo and particle properties such as shape and size. Lumay et al., 2012, found that for particle diameters less than 50 µm, the cohesion of dry particles is substantial. The seed kernels' diameters are larger than 50 µm. For this reason, grain kernels can flow in non-free water conditions on the surfaces of kernels when the angle of a grain pile exceeds its repose angle. The particles roll or slide on the surface of the grain heap because of the different repose angles. The repose angles of grains are within 24˚- 44˚ except maize grain at high moisture content (Jian et al., 2019). Flow is possible when the repose angle is below 41˚-45˚, and poor flowability can occur with a repose angle between 46˚ and 65˚ (Lumay et al., 2012).

2.3 Segregation measurement

As far as the literature is concerned, there is some evidence of different types of devices or testers or apparatus researchers have used to measure the extent of segregation.

Sifting (rolling) segregation measurement

Using the basic idea of heap formation, segregation can be quantified. The set-up of Devriendt et al., 2013, comprised of well-mixed powders that are poured through a funnel in a heap into the segregation box that is 3 cm in width, 68 cm in length, and 49 cm in height. The powder that filled the funnel was always confined to the outlet funnel tube at the top. In this way, the flow in the funnel is mass flow, and segregation will not occur until the heap starts to build. On both sides of the box, there were 48 numbers of holes on each side, each spaced at identical distances. Once the heap has begun to build, the holes would be stopped to prevent powder from escaping into the test box. After constituting the heap, plugs were withdrawn, and small copper tubes of the order of holes were packed orthogonally to the box so as to define samples of about 3 g. All the copper tubes remained with the setup because the powder was aspirated into it during sampling. They investigate the segregation of three types of Ammonium perchlorate as well as two types of Polymeric resin. On similar lines of cell formation, another experiment employed four Hele-Shaw cells superimposed to prepare a flow cascade. Dimensions here are 100 mm with respect to width and the thickness is 15mm. The mass,

m, of one granulated type and the mass, M, of the other one constitute the well-mixed mixture. Pouring this mixture into the top cell, the first aperture is opened, and the mixture flows into the first cell. During the flow of the mixture, the different components may separate from each other due to segregation. The top portion of the heap accumulates with a mass (pm) of the first type and a mass ((1-p) M) of the second one. The dimensionless parameter (p) is the measure of heterogeneity induced by segregation. The value p = 1/2 is the measure of homogeneity. Additionally, p > 1/2 if m and M correspond to the mass of small and large particles, respectively. The bottom of the pile contains, respectively, a mass (1-p) m of the first sort and a mass p M of the second one. When opening the aperture that lies at the bottom of the first cell, grains of the top part of the heap fall into the second cell. The concentration ratio of grains remaining in the first cell is expressed by $x_1 = (1\text{-}p)\, x_0/p$. Similar calculations result in that the concentration ratio, which enters the second and last cell, reads as $x_2 = x_0$, $x_3 = p^2/(1-p)^2 x_0$. The model then makes an assumption that this segregation probability p does not depend on both species' concentrations. Lumay et al., 2013, carried out this procedure of testing, and Figure 2.5 shows the experimental setup, including all steps of the measurement cascade.

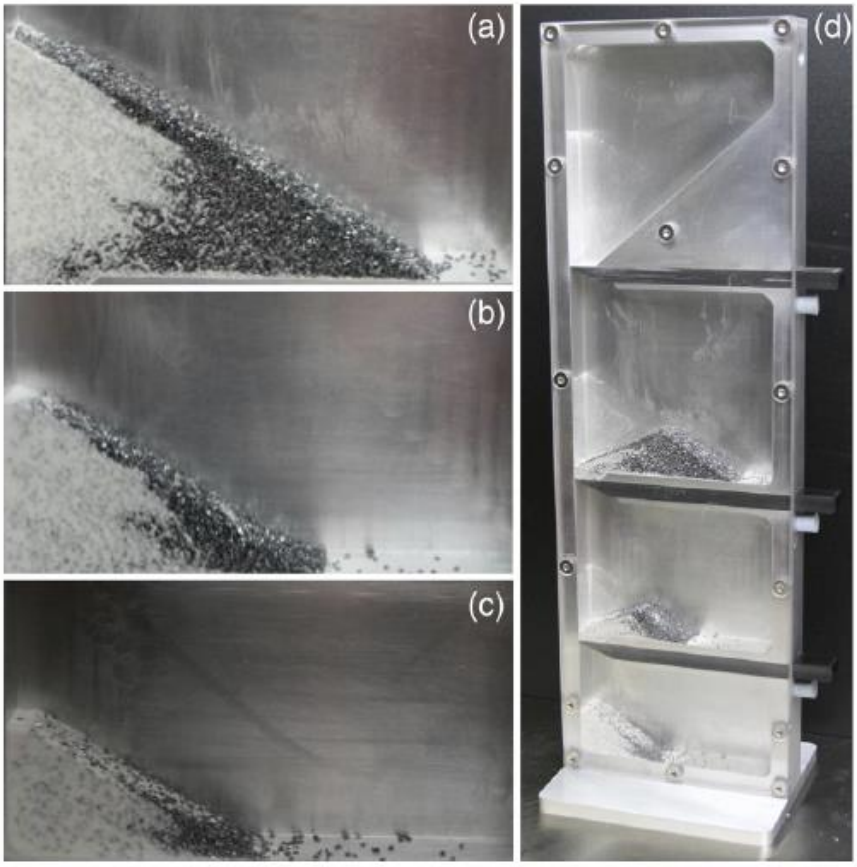

Figure 2.5: (a) Mixture after the flow in the first cell, (b) One-half of the initial mixture in the second cell, (c) One-quarter of the initial mixture in the last cell. (d) Cells after a cascade of flows (Lumay et al., 2013)

Based on the heap formation concept, a tester to determine the extent of rolling segregation consists of a cubic mixer and an inclining plane. The equipment is around 800 mm in height and is mounted on the bench. The particles can be about 3 mm in diameter and can accommodate a sample size of about 600 mL. The well-mixed powder sample is loaded into the top section of the tester. The falling of powder into the one-sided plane section formed a heap, and thus, segregation happened. During the test, the separation plates form six equal-sized sections on the inclined plane, with section 1 positioned at the top and section 6 placed at the bottom. These separated portions can then be sorted as per the materials, enabling an analysis that calculates the percentage of material it constitutes in that mixture. Combarros et al., 2014, Deng et al., 2021(b), and Deng et al., 2023, have used a similar segregation tester, as shown in Figure 2.6.

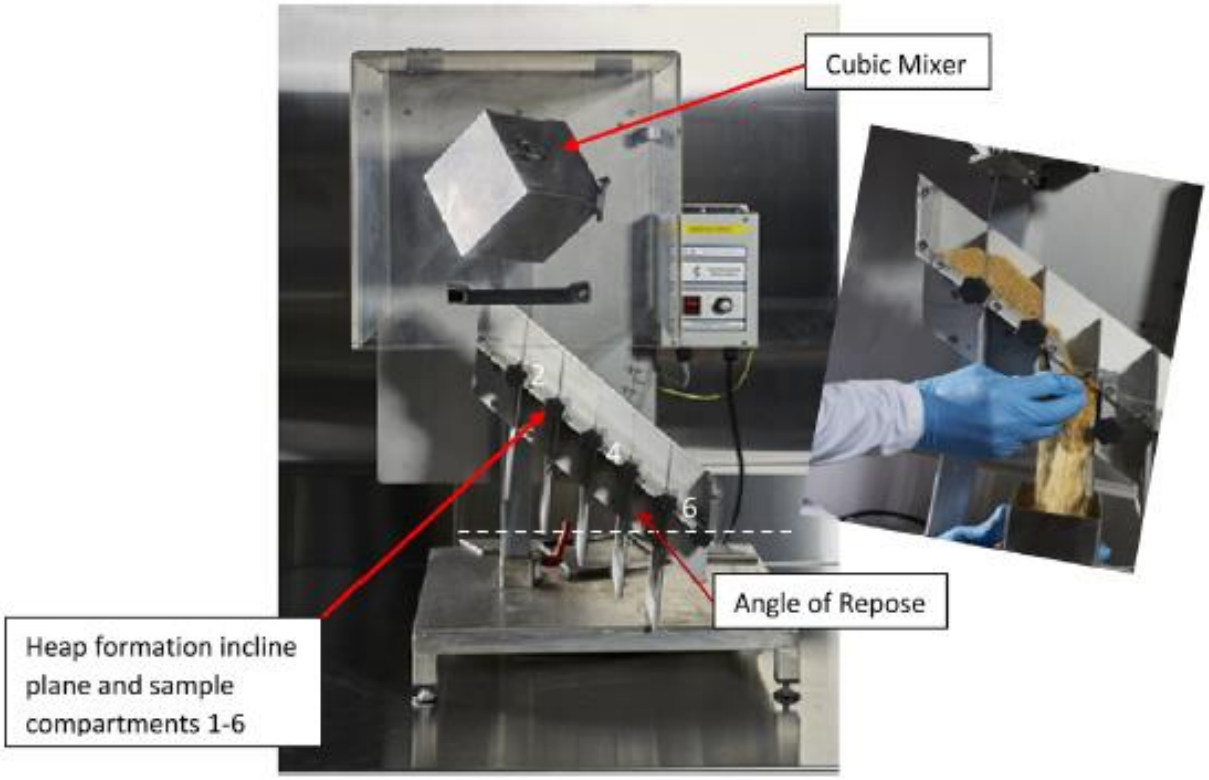

Figure 2.6: Test setup to determine the rolling segregation (Deng et al., 2023)

According to the ASTM D6940-12 testing method, the powder flows through the mass flow hopper when the discharge valve is opened and allowed to fall into a funnel flow hopper. The mass flow that occurred can be visualised through the transparent mass flow hopper. In the lower hopper, the powder sample experienced the funnel flow when the discharge value was opened of the lower hopper. According to the sifting mechanism, segregation intensity could be determined by carrying the tests

as per ASTM D6940-12 sifting segregation procedure that requires 1±0.1 L of blended material in the upper hopper top gate to be closed upon filling. Once the upper hopper is filled, the upper gate is opened, and then the lower hopper is filled. When the lower hopper was filled, the bottom gate was closed. The samples were collected from the lower hopper in a discontinuous manner. Normally, 18 to 24 samples of about 40 mL were collected and indexed on the basis of the particle size distribution. Marucci et al., 2018, used the sifting segregation tester as presented in Figure 2.7 according to the ASTM D6940-12 standard for the different blends of MCC, and the number of samples obtained was between 13 to 24 at the end. He et al., 2013, also employed the bench scale sifting segregation tester for the segregation tendency of pharmaceutical powers.

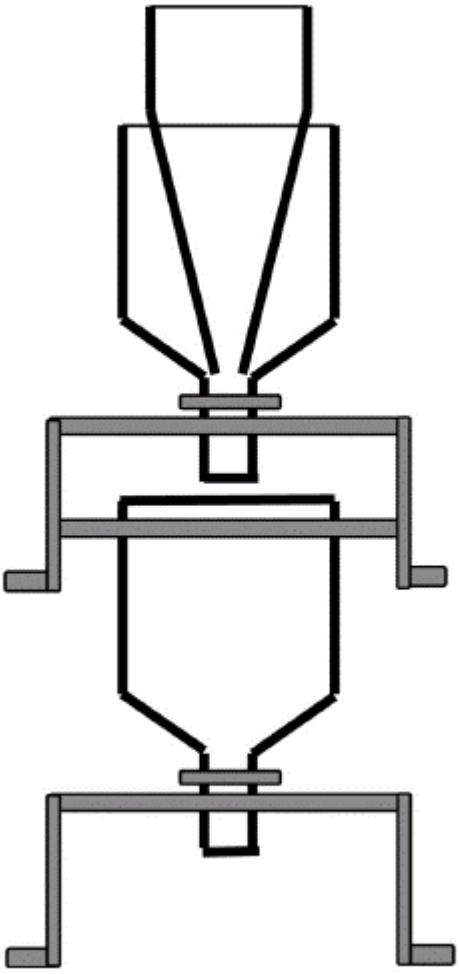

Figure 2.7: Schematic of sifting segregation tester (Marucci et al., 2018)

Fluidisation segregation measurement

Vertical chutes are simple and commonly used in industries that handle the flow of granular materials using gravity-driven methods. The final dosage forms are transported between the different phases of the process via these vertical chutes in the pharmaceutical sector, usually from a hopper to the processing machine, such as tabletting. The experimental setup consisted of two transparent borosilicate glass tubes, having a wall thickness of 5 mm, with an inner diameter of 70 mm and a length of 80 mm, arranged vertically one above the other, separated in the middle by a knife valve, and stainless steel. It carried the powder container, an 800 mm high cylindrical vessel topped with a vent to the atmosphere, and at the bottom had a 1200 mm vertical drop chute. The knife valve was spring-loaded and contained a trigger device for quick release of the powder bed from the container holding the powder. The bottom of the chute was covered by the sampling valve designed particularly with an airtight closure of the chute during powder fall. The sliding plate formed a central core of 10.5 mm of this valve and had on either side two openings with a diameter of 70 mm: when the sliding plate was in the central position, it would act as the closing valve of the chute. Two different holes on both sides of the middle location allow layer-by-layer extraction of the powders from the chute. The height of each layer was formed of 10.5 mm height. The samples were collected from the chute by sliding the value in a way of to and fro motion. By keeping the slide plate towards the right-hand side, a hole below the left-hand side faced the chute, and powder filled the cavity. While shifting the plate on the left-hand side, the powder sample was collected in the container. Concurrently, the right hole was filled with powder. The volume of each powder sample was about 39 ml. Jakli et al., 2015, used a laboratory-scaled model to investigate the segregation characteristics of various pharmaceutical powers, as shown in Figure 2.8.

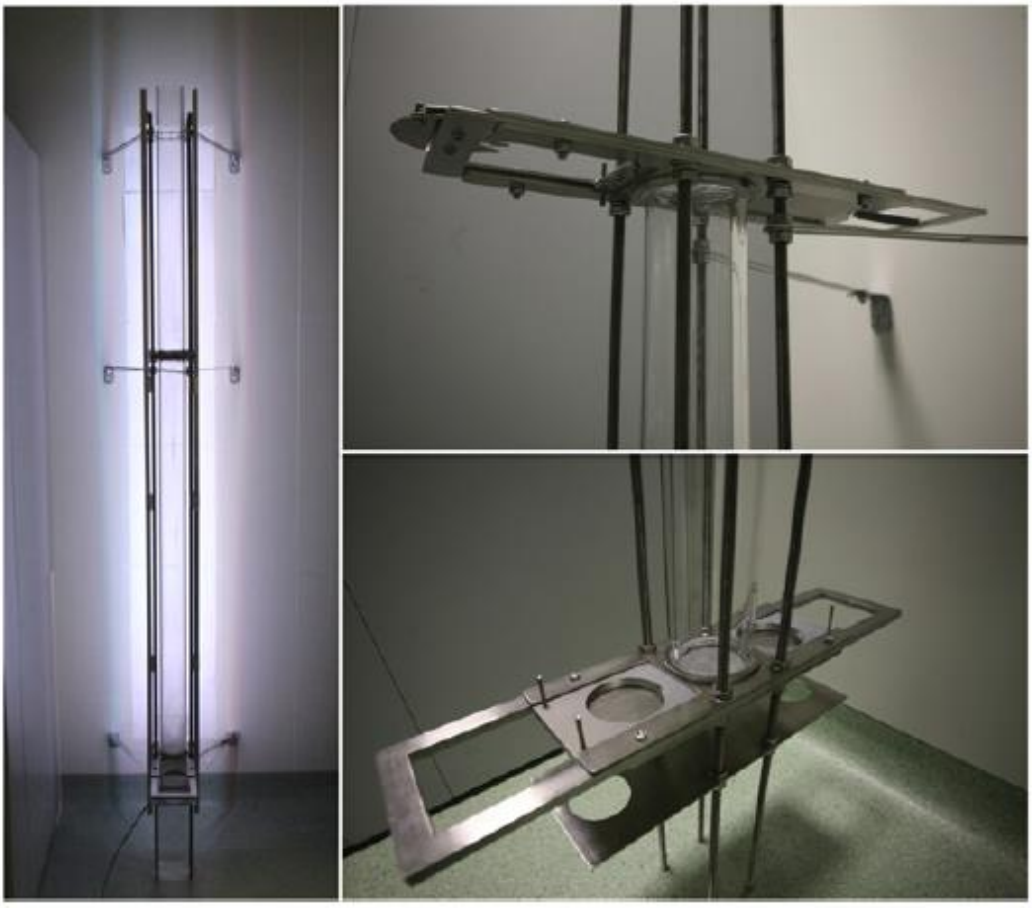

Figure 2.8: Laboratory scaled model of the vertical chute (Jakli et al., 2015)

By ASTM D6941-05, the segregation intensity was obtained according to the segregation mechanism of fluidisation. This test method requires that the powder is put at a specified height of the powder in the apparatus, such that the bed of powder get enough space for getting the powder fluidised. Fluidised states of the different flow rates with time intervals are created by making a pressurised blow of air from the bottom. The test sequence was planned as follows: ramp up to high flow rate: 30 s; maintain high: 30 s; ramp down to low flow rate: 30 s; maintain low 120 s, ramp back to zero: 30 s. High flow rates were determined in the step of pre-test to be in all tested blends 20%. Low flow rates were decided in the pre-test run also and depended on what test material was used that varied between 7-10%. Once the airflow was cut off, the powder within the test chamber was separated into three samples from the bottom, centre, and top of the column. Samples were analysed based on particle size distribution or other powder properties. He et al., 2013 and Deng et al., 2010, employed the fluidisation segregation test setup illustrated in Figure 2.9 to measure the intensity of segregation of pharmaceutical blends that result from fluidisation or air-induced mechanism.

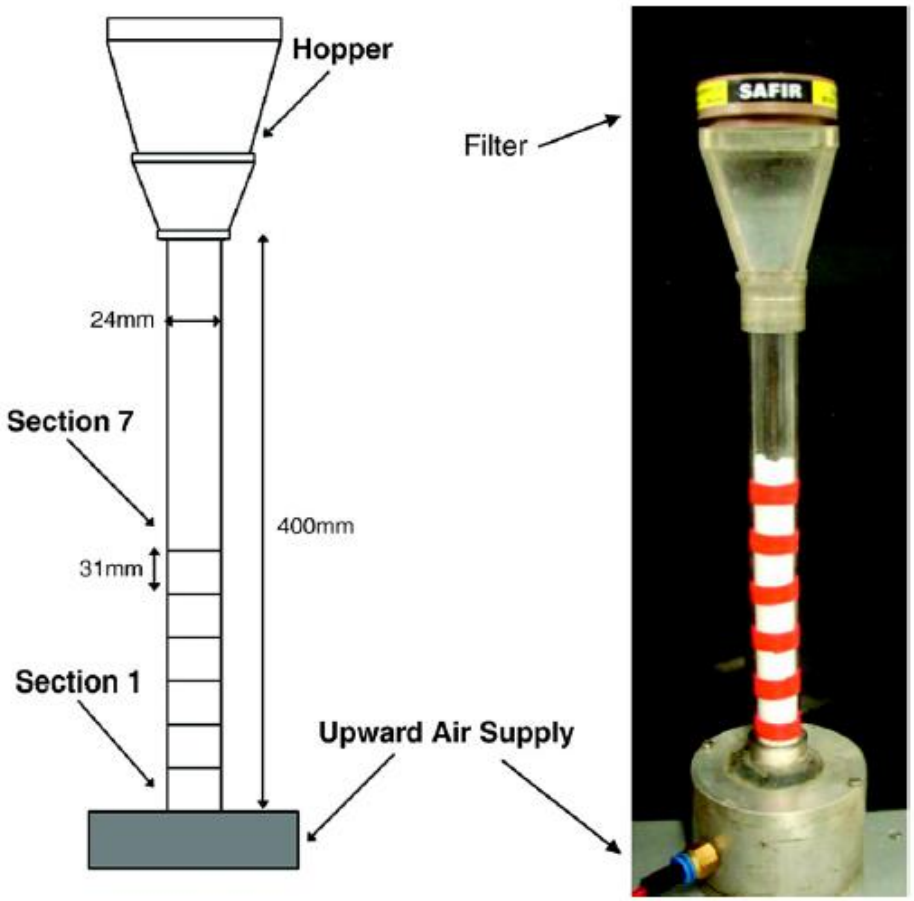

Figure 2.9: Laboratory-scaled model of the fluidisation or air-induced segregation (Deng et al., 2010)

Percolation segregation measurement

From the percolation mechanism, the PSSC-II consisted of five main parts: shear box, drive system, sieving system, measurement system, and frame. The shear box was rectangular in shape with dimensions 150 (length)_63 (width)_100 (height) mm, consisting of four walls, pivot pins, and latex seals. The sieving system, as well as the bottom of the shear box, helped to effectively separate the percolated and sieved fines that tend to collect at the lower part of the mixture; the drive system had adequate power and motion for meeting the kinetic energy requirement of the test material-loaded shear box. The measurement system comprised four load cells mounted in a row, 28 mm apart from each other. A small podium of size 13 x 13 mm^2 was devoted to different load cells. Therefore, fine particles are able to collect into these podiums, which is about 3.4 % of the total screen area. The segregation of fine content by mass measured by each load cell could, therefore, be considered an approximate point measurement. In the case of four sampling points, i.e. four load cells, it was

positioned along the centre of the shear box. Tang et al., 2005; Tang et al., 2008; and Jha et al., 2009, have successfully used this PSSC-II, as demonstrated in Figure 2.10, to find the character of percolation segregation for binary mixtures of fertilisers like potash and urea.

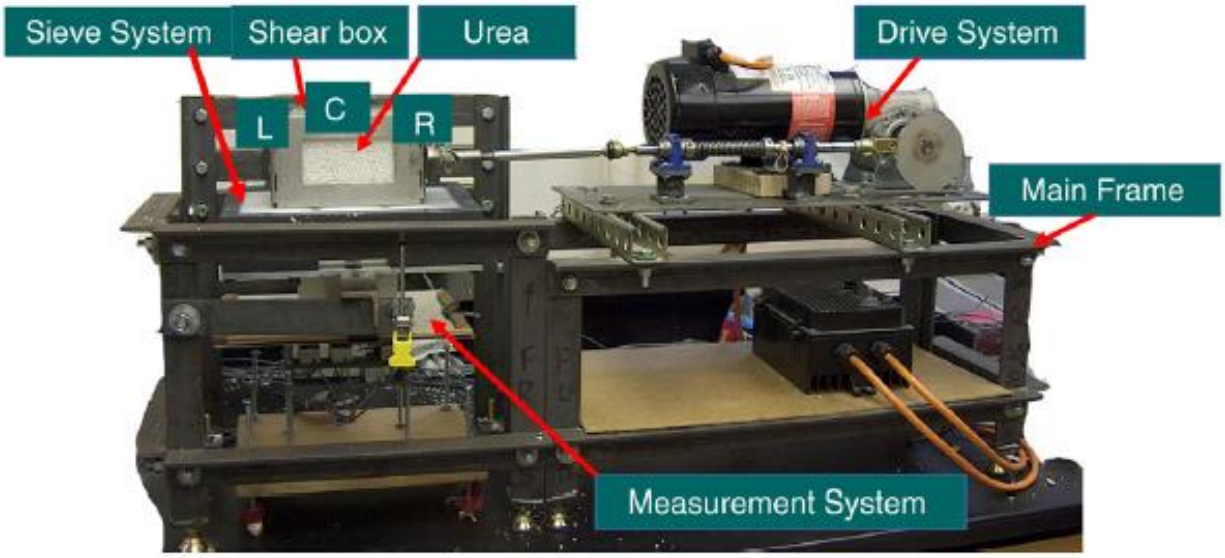

Figure 2.10: Test setup of primary segregation shear cell (PSSC-II) (Jha et al., 2009)

2.4 Segregation in bulk solids

Table 2.1 lists the previous attempts for the measurement of segregation in bulk solids. The table includes a brief description of the setup/test facility used for experimentally quantifying the segregation by characterising or indexing the level of segregation with fine and coarse material.

Table 2.1: Different types of powders with size, setup/testers and methods to quantify segregation

Reference	**Powder type with particle size**	**Setup/test facility used**	**Quantify/index the degree of segregation**
Engblom et al., 2012(a)	Sand has a coarse particle size ranging from 0.5–1.2 mm, limestone has a medium particle size ranging from 0.032–0.71 mm, and cement has a fine particle size of 0.063 mm.	Silo-small scale ($0.5m^3$), intermediate ($20m^3$) and large ($70m^3$) scale	Approx. 100 g of sample was collected, and sieved the fine content (below 0.125 mm) in %-wt. were calculated by taking samples from radial positions at different levels while loading and unloading. The flow pattern was evaluated by tracing the particles.
Devriendt et al., 2013	Three types of ammonium perchlorate (average particle size 215.4, 215.6 and 196.2 µm) and two polymeric resins (average particle size 160.1 and 190.7 µm)	The test setup consisted of a total of forty-eight holes made in a box with equal spacing. During experiments, the holes were closed to avoid spilling of powders. After heap formation, the holes were allowed to insert the copper tubes to take the samples of approximately a weight of three grams.	A total of 23 samples have been taken for their differences in the particle size distribution below 100 µm. To evaluate the segregation index, the COV (coefficient of variation) has been considered. With a low value of COV, there is less segregation in a heap and vice-versa. Laser diffraction was used for PSD.

Shinohara et al., 2002	Glass beads having particle size range from 0.174, 0.358, 0.507, 0.784 and 1.66 mm.	A two-dimensional rectangular vessel (0.75 x 0.5 x 0.03 m^3) was used for segregation experiments. The acrylic as a material is used to make it transparent. From the front side of the vessel, the distribution of mass in the horizontal direction was evaluated through 25 tapping points which were 0.01 m equally apart from each other. To evaluate the concentration of each component, the samples were sieved.	Segregation indices were defined to characterise the change in the degree of separation within a heap. This degree of separation as a curve is plotted on the x-axis, which intersects to the width of the segregation zone. The point of a tangent to this curve at the intersection defines the degree of segregation.
Fry et al., 2020	Cellets have particle sizes ranging from 0.2 to 1.4 mm.	The experimental apparatus consists of a funnel flow hopper over a belt feeder. Particles are then fed into a rectangular box (30 x 10.2 x 3.8 cm^3) to form a powder heap. The angle at the base is adjusted in such a way that it matches the repose angle of the powder being tested. Then, the power heap was divided longitudinally into nine equal segments with the metal cards. Further, the samples are sieved for their	The coefficient of segregation (S) was determined based on the concentration profiles in conjunction with the diffusion-segregation model.

		differences in terms of particle size distribution.	
Engblom et al., 2012(b)	The powder consists of two types of different sand, two types of limestone powder and a portland cement (ranging in size from 0.063 to 4 mm). The particles below 125 µm considered fine particles for quantifying the segregation.	The tendency of segregation in a powder mixture was experimentally investigated by utilising the cylindrical-shaped silo of 0.4 m^3 capacity. For loading the silo, a different hopper was used with a manually operated valve.	The samples were taken from the top-most layers of the heap with different radial positions and filling levels to evaluate the distribution of material. Tracing particles were utilised to observe the flow patterns. The samples were also taken while unloading the silo, which was further sieved.
Deng et al., 2010	Three types of API (average particle size 220.1, 94.4 and 36.9 µm) and three excipients, microcrystalline cellulose grade 1 & 2, sodium starch glycolate and magnesium stearate, having median sizes of 116.3, 53.3, 45, and 6.3 µm, respectively.	A fluidisation segregation test rig was utilised to evaluate segregation in the two different mixtures. The rig has a top hopper for sample powder to load into the test chamber, a vertical cylindrical column made from acrylic. The air was supplied into the test chamber through the air distributor.	For both the blends, after the air elutriation or fluidisation testing, it was found to be varied in terms of particle size distribution. Fine particles collect in the top layers, while coarse particles collect at the bottom of the chamber. The particle size distribution further confirmed that segregation had occurred due to the effect of air-elutriation.

He et al., 2013	Four types of Aspirin (average particle size 343, 9.9, 21 and 157.5 µm) and Lactose (Fast Flo 316) and MCC (Avicel PH 200) (average particle size 103.4 and 172.4 µm, respectively)	A Piccola tablet press was employed with a specially designed hopper that helped segregation to occur at the industrial-scale level. The intensity of segregation was evaluated by utilising the lab-scaled sifting and fluidisation segregation test setup as per the ASTM standards D 6940 and D6941, respectively. The level of API content in the segregated samples was analysed by using the NIR method.	The intensity of segregation was evaluated by utilising the lab-scaled sifting and fluidisation segregation test setup as per the ASTM standards D 6940 and D6941, respectively.
Jaklič et al., 2015	Different pharmaceutical powders were tested, such as Lactose monohydrate, spray-dried lactose, Avicel PH 102, Avicel PH 200, Paracetamol, dicalcium phosphate anhydrous and hypromellose. Particle size distribution confirmed that the medium particle size varied from 80 to 300 µm.	A vertical chute consists of two tubes made of borosilicate glass tubes (thickness of 5 mm and diameter of 70 mm) placed one above the other with an operating valve made apart from each other. The powder was filled up to the level of 800 mm high, and the bottom was designed like a chute having a free fall of 1200 mm.	The single-particle pharmaceutical powder was allowed to make a free fall in a vertical chute with one side open and the other closed. Then, the powder samples were taken from different heights to evaluate the difference in particle size distribution. The segregation index was determined by having the ratio of fine to coarse particle property.

Hastie et al., 2015	The powder mix of of pulverised coal and crushed nickel ore was used, having median particle sizes of 51.7 and 20.5 µm, respectively.	A mass flow hopper was selected to experience the mass flow to arrest the segregation. With the help of a manually operated valve, the powder sample was collected in the form of a powder heap into 200 Lts. drum, which was further slotted with the copper tubes to collect the samples from the centre to the periphery of the heap.	The collected samples were analysed for the bulk properties like the loose-poured bulk, instantaneous tapped bulk and settled tapped bulk densities to compare against previously generated calibration curves. Further, they were utilised to solve the equations to determine the content of nickel ore present in each sample, thus predicting the segregation occurring from the feed bin.
Oka et al., 2016	Samples of Avicel PH-10, Copper Sulphate, Sugar, Poppy and Mustard seeds were utilised with average particle sizes 57.5, 287.7, 355.7, 1023 and 1302.5 µm, respectively.	The degree of segregation of the powder samples was evaluated by measuring the level of de-mixing of a powder when exposed to repetitive mass flow in a sifting segregation tester. After the completion of 10 cycles, the material was uploaded from the hopper. The 10 different samples were further analysed.	The relative standard deviation or coefficient of variability of the 10 different samples was evaluated and considered as the segregation index as the intensity of segregation. The tests were repeated thricely, and an average value was taken.
Marucci et al., 2018	Microcrystalline cellulose (MCC) particles were utilised: MCC-127, MCC-263, MCC-305 and MCC-507	A lab-scaled sifting segregation tester, as per ASTM standard D6940, was utilised as the experimental setup.	The degree of segregation was calculated by evaluating the standard deviation in normalised mass fraction,

	grade with particle mean diameters 161, 307, 444 and 661 µm, respectively.		the ratio of coarse-to-fine, and the mass ratio of samples having lower and higher fine content.
Břenková et al., 2006	API, microcrystalline cellulose such as avicel PH101 and avicel PH102, and anhydrous lactose.	At the lab scale, a standard well-mixed powder was tested in a segregation cell to determine the degree of segregation of separated particles. The segregation cell consisted of a tube of S. S. made with a length of 250 mm and a diameter of 25 mm.	The vibration was imposed on the segregation cell, which consisted of a powder mixture, in order to evaluate the tendency of the powder mixture to be segregated. Several sets of experiments were explored in terms of orientation and direction of vibration that were used to promote different segregation mechanisms.
Deng et al., 2021(a)	Different 8 blends were formed from the grades of calcium carbonate, having average particle sizes 3.3, 4, 10, 26.7, 82.3, 131.1, 367.9 and 898.1 µm, respectively.	A lab-scale rolling segregation tester was employed to test the intensity of segregation based on the heap formation on an inclined platform at the angle equal to the repose angle of the powder being tested.	The segregation index was evaluated by comparing between the segregated samples obtained after the test and the virgin sample.

2.5 Indexing and modelling segregation

As per the literature, the segregation index was evaluated based on the standard deviation, variances or coefficient of variance of the components segregated in a bulk powder, which represents the intensity of variation in the components of segregated samples compared to the components in the virgin powder sample. The purpose of this segregation index was to assess the intensity of segregation of a powder mixture, and the different indexes used by the researchers are as follows:

Segregation index

Using a QPM segregation tester, Deng et al., 2023, measured segregation intensity in heap formation and introduced a segregation index ($P_{s(i)}$) based on volumetric concentration changes of fines.

$$P_{s(i)} = \frac{C_i - C_{o(i)}}{C_{o(i)}} \tag{2.1}$$

Where $C_i, and\ C_{o(i)}$ are the mass concentration of fines after segregation and in virgin samples at the size *i*, respectively. Another segregation index suggested by Deng et al., 2023, to quantify segregation intensity, calculated based on the difference in volumetric concentrations of fines before and after segregation at specified particle sizes.

$$SI_{s(i)} = \frac{\Delta C_i\ (segregated\ between\ locations\ in\ a\ size\ fraction) x\ 100\ \%}{C_i\ (virgin\ in\ the\ size\ fraction)} \tag{2.2}$$

where ΔC_i is the difference of the volumetric concentrations of the particle in the size fraction *i* between two locations after segregation. C_i is the concentration at *d(50)* of the virgin material.

In order to minimise the sampling errors before and during segregation tests, the segregation index used by Deng et al., 2021(b), is defined as a ratio of the concentration difference of the fines between segregated samples at different locations on a surface segregation tester and the average of the concentrations at the particle size, *k*, as:

$$I_{S(k)} = 2\left(\frac{C_B - C_T}{C_B + C_T}\right)_k \tag{2.3}$$

where C_B and C_T denote the mass content (in %) of the bottom or last sample and top or first batch, respectively, in the particle size range of 'k'.

To quantify the segregation of mixed particles, Chen et al., 2022, defined the degree of segregation (DOS) to describe the segregation. The DOS calculation is as follows:

$$DOS = \frac{1}{\bar{a}^2 n} \sum_{i=1}^{n} (a_i - \bar{a}^2)^2 \quad (2.4)$$

Where, $\bar{a}$, is the ratio of the target to the total particle number, a_i, is the ratio of the number of target particles to the total number of particles at sample *i*, and n is the number of samples. The range of DOS is 0 -1, and 0 represents the particles being fully mixed, while 1 represents complete segregation.

The other most common index used as the Lacey index (Lacey, 1943), utilised by Combarros et al., 2014 is as follows:

$$M_L = \frac{S_0^2 - S^2}{S_0^2 - \sigma_r^2} \quad (2.5)$$

Where $S_0^2, S^2 and\ \sigma_r^2$ are the unmixed state variance, sample variance and mixed state variance, respectively. The index takes values between 0 and 1, 0 being a completely segregated state and 1 being a randomly mixed state.

2.6 Segregation modelling

In the literature, there is hardly any evidence has been found where researchers have given empirical formulas for predicting the segregation index. In a recent work by Deng et al., 2021(b), a total of 8 blends were prepared from several grades of calcium carbonate based on different particle size and their adhesions. The intensity of segregation was evaluated by comparing the different components of the segregated samples to the components of the virgin samples. Particle size distribution as the particle property was considered to compare the components between segregated and virgin samples to evaluate the segregation index. Then segregation tests were performed on the same blends.

Differences between them indicate segregation did occur. The empirical formula proposed from the particle size ratio $Rs=D_{90}/D_{10}$ and the particle median size D_{50} can be written as:

$$P_s = k\, D_{50}^{m} \left(\frac{D_{90}}{D_{10}}\right)^{n} \tag{2.6}$$

The *k*, *m*, and *n* in the above are constant for the material tested. The empirical parameters for the powders taken are determined as k = 0.0045, m = 0.15 and n = 0.4393. The forecast of P_s is compared to the experiment results, which showed a good agreement with R^2 of about 0.964 (refer to Figure 2.11).

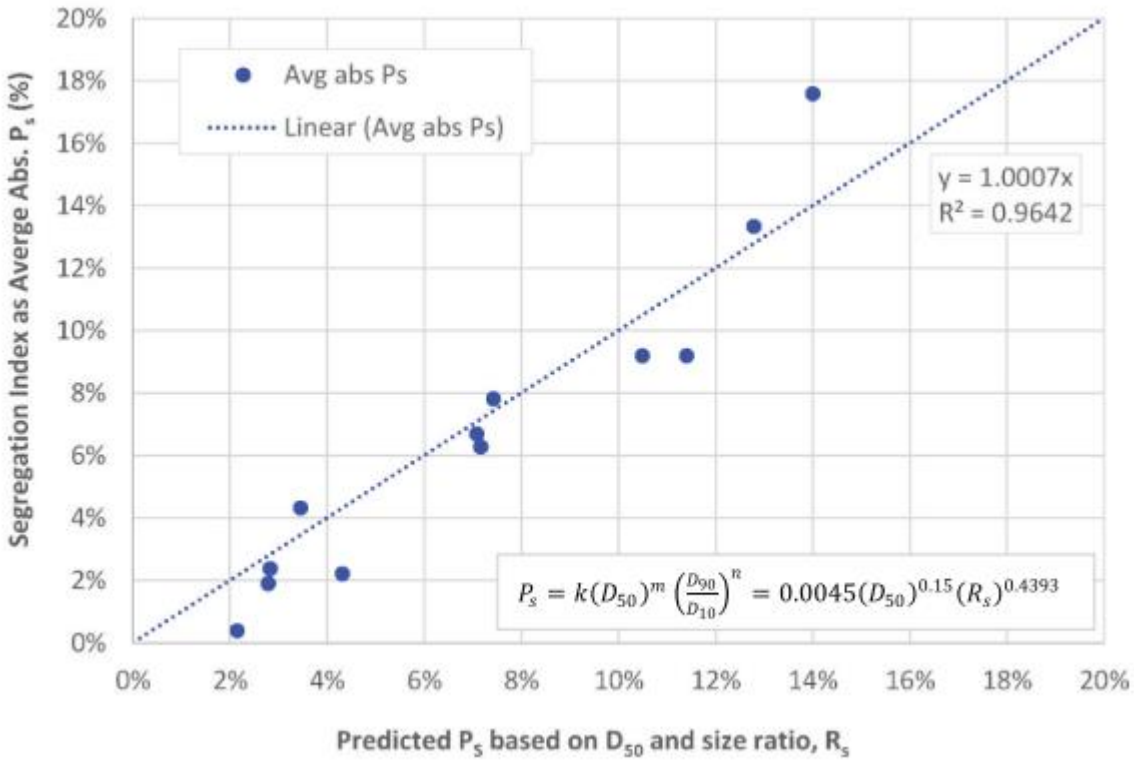

Figure 2.11: Comparison between the empirical model to experimental data (Deng et al., 2021(b))

Based on experimental results with binary and ternary mixtures aside from commercial construction materials, silos of varying scale exhibit segregation of powder mixtures, as Engblom et al. in 2012(b), have found from their observations. Based on these experimental correlations, they used models to predict the fine particle concentration at the walls of the silo, or the type and order of magnitude for horizontal segregation by comparison with the fines content in the silo centre, resulting from filling by free fall and the mass of segregated material withdrawn at the end of complete discharge. Figure 2.12 shows the model is in good agreement with experimental data (R^2 = 0.90), which indicates that

the concentration of fine particles at the silo walls increases with increasing: a) mass fraction of fine particles, b) particle size ratio (coarse/fine), c) particle solid density ratio (coarse/fine), d) ratio for free fall distance and silo diameter and, e) ratio for silo diameter and inlet diameter. In Figure 2.13, the segregation model at discharge is typically in agreement with experiments (R^2 = 0.70), and segregation at the end of fully completed silo discharge depends almost entirely on material distribution caused by filling. The surprisingly small effect on the flow pattern, either funnel or mass flow, at the end of emptying segregation shows that though not correcting entirely, mass flow design does correct the initial side-to-side segregation at the silo outlet.

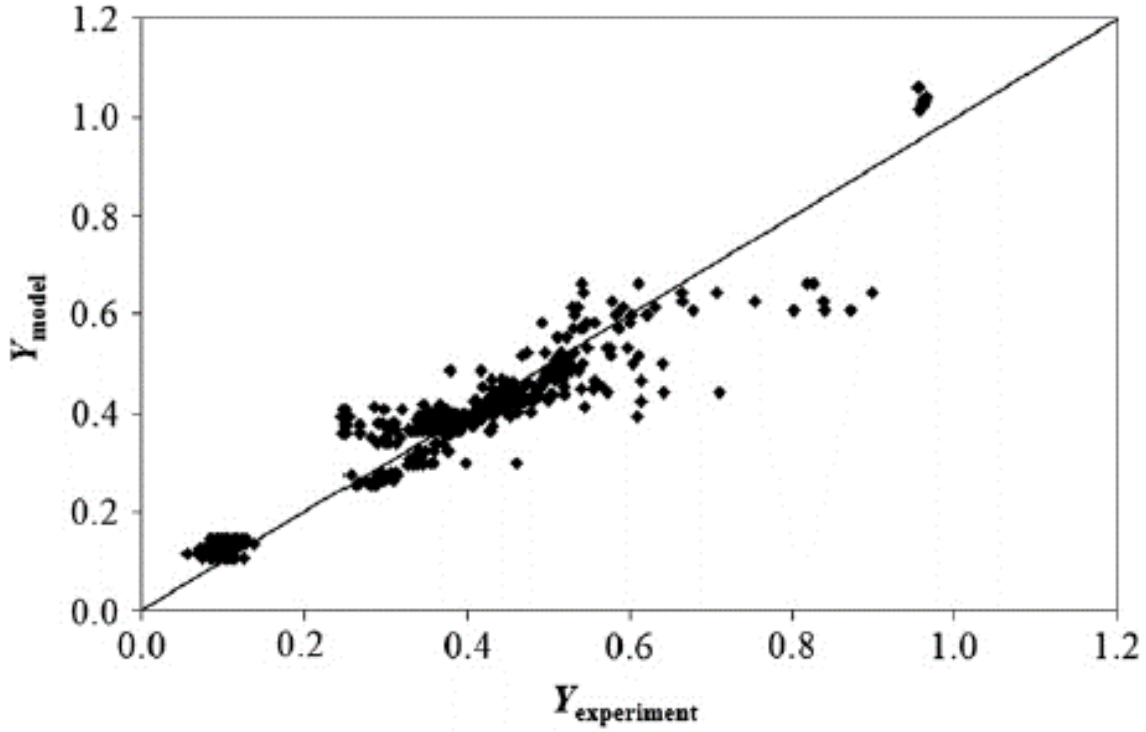

Figure 2.12: Fines content at the silo wall (Y) predicted by the filling model versus experiment data, R^2 = 0.90 (Engblom et al., 2012(b))

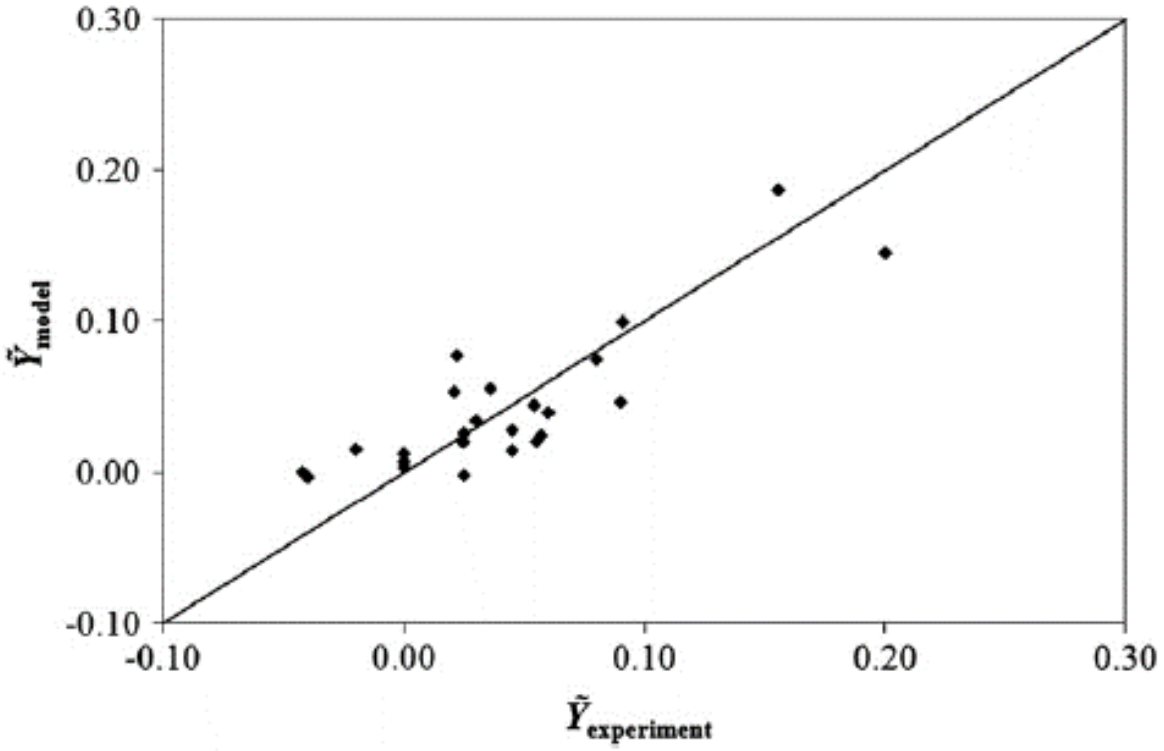

Figure 2.13: Mass of the segregated mixture at the end of discharge predicted by model versus experiment data, $R^2 = 0.70$ (Engblom et al., 2012(b))

Complete remixing is not achieved because the flow velocity is higher near the outlet than in outer areas where the silo fill levels are lower or at least less massive (i.e., towards the end of the complete draining of the silo). Still, the character of the flow out of the silo does affect how the silo contents discharge and mass flow can actually reduce segregation because the latter part of the silo contents that withdraw have to fall a shorter distance for the free fall.

2.7 Miscellaneous review

Other than above mentioned, miscellaneous review has been carried out, which is presented below:

Tai et al., 2010, performed research on the density segregation in a two-dimensional vibrated granular bed. In this work, fluctuating velocity distributions were measured via image processing technology and using a particle tracking method. Fluctuating velocity distributions were anisotropic due to the bulk convection motion formed in the larger filling layers of the bed. The mechanism of density segregation in a two-dimensional vibrated granular bed was explored using different packing ratios and filling layers of mixtures of stainless steel and glass beads. As the packing ratio of stainless-steel

beads increases, the heavier stainless-steel beads tend to migrate towards the bottom region of the bed while the lighter glass ones towards the surface of the bed due to the fact that granular temperature is lower at the bottom region and higher at the surface. Hence, the role of granular temperature in the density segregation is tremendous for the lower filling layers. The higher the filling layers in the mixtures, the bulk convection motion shall be the dominant mechanism driving segregation, and the possibility exists that the vibrated granular bed of bulk convection motion influences the density segregation. With the increased packing ratios of the stainless-steel beads of the stainless steel–glass mixtures, the larger stainless-steel beads will migrate toward the convention centre, and the region of dense grain at the bottom is enlarged with the bulk convection motion.

Ward et al., 2011, investigated the segregation by utilizing a tilted and rotating cylindrical drum having the granular mixture of an isopycnic, a nearly bi-disperse granular mixture of particles. The different experiments were carried out to evaluate the differences in segregation quality, i.e., the fine content relative to the total powder sample (by volume), the angle of tilt, and the drum rotating speed, which was varied for different tests. Avalanching and void filling are two phenomena that lead to segregation but have relative influence. Here, the relative influences were adjusted by changing the angle of tilt. The parameters are still being determined in a form to develop segregation with an operation similar to a dish granulator for the smaller particles to the bottom of the drum. Experiments were carried out using different glass beads having particle sizes ranging from 180 to 850 μm, and the glass drum at the range of rotation rates of about 0.25 and 1 Hz, with the range tilt angle ranging from 35° to 65°. The flowing system is captured from both the side-on and overhead views after the system has stabilised into a configuration. Using a geometric analysis of the stable shape, images were utilised to determine the apparent volume of the smaller beads and the total volume of the mixture by measuring their breadth as they formed a single segregated band. The equality of the tilt angle (α) and bottom-wall contact angle (β) was a key premise of the investigation. While the measured and apparent quantities of the segregated volume were not acceptable, the comparison between the calculated value and the measure of total granular volume was. It was observed that the maximum values of the tilt angle and Froude number resulted in the movement of the smaller particles to the bottom of the drum.

Asahi et al., 2018, investigated the effects of the physical properties of the particles, specifically size, shape, and density, on the segregation behaviour of constituents in a commercial powder mixture of detergent. It was established that the sieve cut size of BP and TAED particles in the size range 355–425 μm is the optimal criterion for fully mixed EP granules with mode particle size distribution for

the ternary system. Instead of the complete particle size distribution of BP and TAED, the application of this size to the ternary mixture might reduce the SI of EP granules from 1.36 to 0.67. The reduction of segregation of EP granules due to coating of EP granules is explored. From the flowability test results, it was found that 2.5 wt% PEG was sufficient to bring the segregation level down without impairing the flowability of the mixture itself and the EP granules as well. It has been observed that fine powder of BP and TAED get deposited on EP-coated granules giving some sort of roughness and which will likely affect less mobility of the granule since interlocking at each ternary mixture surface intensifies. The SI of EP granules drops from 1.36 to 0.69 using the proposed optimum coating percentage in the ternary mixture with full particle size distribution of the components.

Barik et al., 2023, have studied mass flow rate, average velocity profiles, and segregation with experiments and by doing DEM analysis. DEM studies were verified with the outcomes of experimental studies. Based on this, the studies were further extended to simulate the behaviour of the mixing of real-world pharmaceutical powders in terms of binary and ternary mixes. The mass flow rate of MCC spheres becomes less with the incrementing size of the particle. Using the orifice diameter as a constant, the more the particle sizes, the lesser the observed flow rate. In the case of a mixture, mass flow rate increases with an increased percentage of fines. Initially, in the beginning of the discharge, the average velocity of fines is more than coarser fractions. After that, the average velocity of the coarser particle remains higher up to the end of the discharge. The DEM study showed that segregation occurs in the case of mixtures, and fines are released faster in the initial phases of the considered flat bottom silo. The size difference is more, and the quantity of fines is less, and then the segregation effect happens to be more. Segregation intensity was found to be higher in the binary mixtures than in the ternary mixtures.

Through experimentation and modeling, Chen et al. (2022) investigated the segregation behavior of rice husks and brown rice mixtures, concentrating on the effects of inclined chute angle, mixture particle flowing distance, and particle layer height. Analyzing the particle flow velocity, the segregation process, the particle flow structure, and the evolution process reveals the segregation mechanism. The following are the key findings. In the inclined chute flow, the binary mixture of brown rice and rice husks will naturally separate. As the inclined chute angle increases, the degree of segregation (DOS) decreases. The DOS initially rises when the inclined chute angle is 30°, but it eventually tends to remain constant with the increase of the mixture particles' flowing distance. The DOS first rises and then gradually falls when the inclined chute angle is between 35° and 45°. The more pronounced the decline in DOS, the greater the inclined chute angle. As the particle flowing

distance increased, the DOS clearly revealed a jump in higher particle flow layers. In higher particle flow layers, the concentration of rice husk reaches 100% when the chute angle is 30°. The leap of DOS is more noticeable when the inclined chute angle is less. Jumping in the lower particle flow layers is not seen in the DOS. There were still a lot of rice husks, but the brown rice collected in the bottom layer. The primary method of separating the brown rice mixture from the rice husks in inclination chute flow is kinetic sieving. However, the variation in surface density and roughness is what causes the "kinetic sieving." Rice husks are less fluid than brown rice because of their low density and high surface roughness. Thus, the difference in the likelihood of filling lower voids results from that. The kinetic sieving of particle size difference and "kinetic sieving" are not the same thing.

Garcia et al., 2015, have compared the magnitude of segregation in a silo; experimental results are matched to those from DEM simulations; the concentration is determined during silo discharge as a deterministic influence of segregation during silo filling. Because the fine particles percolate and the coarser particles roll along inclined surfaces, more fine particles are discovered in the center and bottom of a silo after it has been filled gravimetrically. The concentration ultimately discovered at the outlet is influenced by the way the silo is released. A remix at the silo outlet is produced whenever mass flow is present in a silo up to an extent where most of the segregation gets reduced. In the presence of funnel flow, fine particles are discharged first and then the coarser ones. The mechanism of percolation during the discharging of the silo can be seen in the experiments performed. This percolation happens in the mobile zone of the silo, and a relative motion of particles occurs here. Thus, depletion of fines develops in the centre of the silo and its concentration increases in the top portion of the stagnant zone. Moreover, using the belt conveyor partly remixing the segregation is reduced during discharge. The segregation study shall take into account the overall system, including filling and discharging types. A segregation study was performed with DEM, and this led to a slight underprediction of the segregation after filling as a result of the simplifications that were considered for the simulation to be run. On the one hand, a less segregated estate resulted from the filling procedure's assumption of a homogenous composition at the outset. However, the percolation rate is reduced when monodisperse materials are used in place of particle size distribution and when particle form is ignored, resulting in a smaller void ratio. Consequently, DEM simulations can only accurately investigate segregation if particles are simulated under the actual settings. Even if the concentration profile is still within the experiment's precision, this underprediction after filling is rather noticeable as the silo is being emptied.

Hadi et al., 2024, determined the predominant DEM parameters governing multi-component segregation during various flow scenarios and the initial configurations of the mixture. For this purpose, we worked on a pellets-sinter mixture; at different steps, the quantification of segregation is given, applying blast furnace processes as investigated case: post-hopper discharge (KPI 1), post-chute flow (KPI 2), and in static heap (KPI 3). We also extended the scope of the investigation to evaluate the effect of some parameters, including sinter particle geometry, initial layering mode, and pellet-sinter mass ratio on KPIs. The results showed that the interaction parameters related to particle geometry have a more significant effect on segregation after hopper discharge (KPI 1). The particle-particle interaction parameters seem to be negligible for KPI 1. Moreover, within the scope of this study, no considerable segregation occurs on the chute itself. In the heap, segregation in the radial direction is much higher than it is in the vertical and circumferential directions. For radial segregation, meaning KPI 3, the particle-geometry interaction will be significant for some configurations, while the particle-particle interaction will be large for others. The DEM parameters are sensitive to the hopper filling configuration for both dominant parameters and degree of segregation. This shifts the bottom-most particle from pellets to sinter. That makes L1 shift to L2. As a result of that, the sinter-geometry parameters become more significant. The radial segregation in the heap also reduced by the shifting.

Liao et al., 2020, studied the dynamic properties, especially the density segregation behaviour in a granular matter composed of fine powder in negligible concentration mixed into a material undergoing a rotational drum. Techniques in velocity measurement, granular temperature, and segregation index have been attained by employing image processing techniques in tandem with the help of particle tracking. This result has shown that the slightly fine powder added to the granular matter is actually responsible for granular dynamics and density segregation behaviour. The velocity and granular temperature will increase with an increase of content from fine powder due to a lubrication effect between two particles and particles. The velocity, as well as granular temperature, increases with an increase in rotation speed. Because of the lubrication effect between particles, fine powder content enhances its steady-state segregation index gradually. It has been shown that by adding a low concentration of fine powder with granular matter, the granular temperature and density segregation of the granular matter can also be improved.

2.8 Conclusion

The literature review showed that the majority of the work on segregation focuses on Geldart B and D-type powders (refer to Table 2.1 for the type of powder and its particle size), which are coarse particles and have demonstrated segregation tendencies. A relatively small amount of effort has been directed to study the effect of segregation in the case of fine powder (Geldart group A powders) (Tang et al., 2004; Schulze, 2008). There is very little evidence available in the literature which has focused on the segregation behaviour of the existing work of Geldart A or B borderline. Therefore, further studies are required on the segregation behaviour of Geldart A to B borderline materials. While most of the work has been carried out to understand the segregation mechanism and to measure and index the extent of segregation, very little work has been carried out in modelling the segregation index in terms of particle and bulk properties. Therefore, effort has to be put into developing models which can reliably predict the segregation index. The existing work on segregation uses dry particles, or at least the amount of moisture has not been quoted. It seems that the effect of moisture on the segregation behaviour of powders has not been adequately studied. Therefore, there is a need to study the effect of moisture on the segregation behaviour of powder.

References

Asachi, M., A. Hassanpour, M. Ghadiri, A. Bayly. 2018. Experimental Evaluation of the Effect of Particle Properties on the Segregation of Ternary Powder Mixtures. *Powder Technology* 336, 240–254.

ASTM Standard, D6941-12. 2012. Standard Practice for Measuring Fluidization Segregation Tendencies of Powders, West Conshohocken, PA, USA: *ASTM International* (www.astm.org).

ASTM Standard, D6940-10. 2010. Standard Practice for Measuring Sifting Segregation Tendencies of Bulk Solids, West Conshohocken, PA, USA: *ASTM International* (www.astm.org).

Barik, S.K., V.N. Lad, I. Sreedhar, C.M. Patel. 2023. Investigation of Mass Discharge Rate, Velocity, and Segregation Behaviour of Microcrystalline Cellulose Powder from a Copley Flow Tester. *Powder Technology* 417, 118234.

Břenková, L., Z. Bělohlav, P. Durdil, H. Eliášová, J. Hanika, P. Řápek, V. Tomášek, and P. Zámostný. 2006. Particles Segregation in Pharmaceutical Mixtures for Direct Tablets Compression. *In CHISA 2006 - 17th International Congress of Chemical and Process Engineering*.

Chen, P., F. Jia, Y. Han, X. Meng, A. Li, Y. Chu, H. Zhao. 2022. Study on the Segregation of Brown Rice and Rice Husks Mixture in Inclined Chute Flow. *Powder Technology* 404, 117393.

Combarros, M., H.J. Feise, H. Zetzener, and A. Kwade. 2014. Segregation of Particulate Solids: Experiments and DEM Simulations. *Particuology* 12: 25–32.

Carson, J. W., T. A. Royal, D. J. Goodwill. 1986. Understanding and eliminating particle segregation problems. *Bulk Solids Handling* 6(1), 139–144.

Deng, T., L.M. Sousa, V. Garg, and M.S.A. Bradley. 2023. Segregation of Formulated Powders in Direct Compression Process and Evaluations by Small Bench-Scale Testers. *International Journal of Pharmaceutics* 647, 123544.

Deng, T., V. Garg, H. Salehi, and M.S.A. Bradley. 2021(a). An Experimental Study on Free-Surface Rolling Segregation and Correlations with Angle of Repose and Particle Sphericity. *Powder Technology* 379: 307–320.

Deng, T., V. Garg, H. Salehi, M.S.A. Bradley. 2021(b). Correlations between Segregation Intensity and Material Properties Such as Particle Sizes and Adhesions and Novel Methods for Assessment. *Powder Technology* 387, 215–226.

Devriendt, L., C. Gatumel, H. Berthiaux. 2013. Experimental Evidence of Mixture Segregation by Particle Size Distribution. *Particulate Science and Technology* 31, no. 6, 653–657.

Deng, T., K.A. Paul, M.S.A. Bradley, L. Immins, C. Preston, J.F. Scott, E.H. Welfare. 2010. Investigations on Air Induced Segregation of Pharmaceutical Powders and Effect of Material Flow Functions. *Powder Technology* 203, no. 2, 354–358.

De Silva, S., A. Dyroy, G. G. Enstad. 2000. Segregation mechanisms and their quantification using segregation testers. *In IUTAM Symposium on Segregation in Granular Flows*.

Engblom, N., H. Saxén, R. Zevenhoven, H. Nylander, G.G. Enstad. 2012(a). Segregation of Construction Materials in Silos. Part 2: Identification of Relevant Segregation Mechanisms. *Particulate Science and Technology* 30, no. 2, 161–178.

Engblom, N., H. Saxén, R. Zevenhoven, H. Nylander, G.G. Enstad. 2012(b). Segregation of Powder Mixtures at Filling and Complete Discharge of Silos. *Powder Technology* 215–216, 104–116.

Fry, A.M., V. Vidyapati, J.P. Hecht, P.B. Umbanhowar, J.M. Ottino, and R.M. Lueptow. 2020. Measuring Segregation Characteristics of Industrially Relevant Granular Mixtures: Part II – Experimental Application and Validation. *Powder Technology* 368, no. 1 (May): 278–285.

Fan, Y., K. V Jacob, B. Freireich, R.M. Lueptow. 2017. Segregation of Granular Materials in Bounded Heap Flow: A Review. *Powder Technology* 312, 67–88.

Garcia, M. C., H.J. Feise, S. Strege, A. Kwade. 2015. Segregation in Heaps and Silos: Comparison between Experiment, Simulation and Continuum Model. *Powder Technology* 293, 26–36.

General chapter., b905. 2011. Uniformity of dosage units in *United States Pharmacopoeia* (USP34)/National Formulary (NF29)

Hadi, A., H. Shi, Y. Pang, D. Schott. 2024. Identification of Dominant DEM Parameters for Multi-Component Segregation during Heap Formation, Hopper Discharge and Chute Flow. *Powder Technology* 444, 119985.

Hastie, D.B. 2015. On the Difficulties of Sampling Bulk Powder Blends in Determining Segregation Propensity — A Case Study. *Powder Technology* 286 (December): 164–171.

He, X., X. Han, N. Ladyzhynsky, R. Deanne. 2013. Assessing Powder Segregation Potential by near Infrared (NIR) Spectroscopy and Correlating Segregation Tendency to Tabletting Performance. *Powder Technology* 236, 85–99.

Jian, F., S. Yavari, R.B. Narendran, D.S. Jayas. 2019. Physical properties of hemp seeds: clean and containing dockages. *Applied Engineering in Agriculture* 34(6):1017-1026.

Jaklič, M., K. Kočevar, S. Srčič, R. Dreu. 2015. Particle Size-Based Segregation of Pharmaceutical Powders in a Vertical Chute with a Closed Bottom: An Experimental Evaluation. *Powder Technology* 278, 171–180.

Jha, A.K., and V.M. Puri. 2009. Percolation Segregation of Binary Mixtures under Periodic Movement. *Powder Technology* 195, no. 2, 73–82

Johanson, J. R. 1996. Predicting segregation of bimodal particle mixtures using the flow properties of bulk solids. *Pharmaceutical Technology Europe* 8(1), 38–44.

Liao, C.C., S.F. Ou, S.L. Chen, Y.R. Chen. 2020. Influences of Fine Powder on Dynamic Properties and Density Segregation in a Rotating Drum. *Advanced Powder Technology* 31, 1702–1707.

Lumay, G., F. Boschini, R. Cloots, N. Vandewalle. 2013. Cascade of Granular Flows for Characterizing Segregation. *Powder Technology* 234, 32–36.

Lumay, G., F. Boschini, K. Traina, S. Bontempi, J.-C. Remy, R. Cloots, N. Vandewalle. 2012. Measuring the Flowing Properties of Powders and Grains. *Powder Technology* 224, 19–27.

Lacey, P.M.C. 1943. The mixing of solid particles, *Transactions of the Institution of Chemical Engineers* 21, 53–59.

Marucci, M., B. Al-saaigh, C. Boissier, M. Wahlgren, H. Wikström. 2018. Sifting Segregation of Ideal Blends in a Two-Hopper Tester: Segregation profiles and Segregation Magnitudes. *Powder Technology* 331, 60–67.

McGlinchey, D. 1998. Assessment of segregation in industrial processes. *Journal of Powder Bulk Solids Technology* 22: 54–56.

Mosby, J., S. R. de Silva, G. G. Enstad. 1996. Segregation of particulate materials— Mechanisms and testers. *KONA Powder* Part. 14: 31–42.

Narendran, R.B., F. Jian, D.S. Jayas, P.G. Fields, N.D.G. White. 2019. Segregation of canola, kidney bean, and soybean in wheat bulks during bin loading. *Powder Technology* 344, 307-313.

Oka, S., A. Sahay, W. Meng, and F. Muzzio. 2016. Diminished Segregation in Continuous Powder Mixing. *Powder Technology* 309 (March): 79–88.

Prescott, J.K., T.P., Garcia. 2001. A solid dosage and blend uniformity troubleshooting diagram, *Pharmaceutical Technology*, 68–87.

Rosato, A., C. Windows-Yule. 2020. Segregation in Vibrated Granular Systems.

Shinohara, K., and B. Golman. 2002. Segregation Indices of Multi-Sized Particle Mixtures during the Filling of a Two-Dimensional Hopper. Advanced Powder Technology 13, no. 1: 93–107.

Schulze, D. 2008. Powders and Bulk Solids. *Chemie Ingenieur Technik* 82, no. 4, 553–554.

Tai, C.H., S.S. Hsiau, C.A. Kruelle. 2010. Density Segregation in a Vertically Vibrated Granular Bed. *Powder Technology* 204, no. 2–3, 255–262.

Tang, P., V.M. Puri. 2008. Segregation Quantification of Two-Component Particulate Mixtures: Effect of Particle Size, Density, Shape, and Surface Texture. *Particulate Science and Technology* 25, no. 6, 571–588.

Tang, P., V.M. Puri. 2005. An Innovative Device for Quantification of Percolation and Sieving Segregation Patterns–Single Component and Multiple Size Fractions. *Particulate Science and Technology* 23, no. 4, 335–350.

Tang, P., V. M. Puri. 2004. Methods for Minimizing Segregation: A Review. *Particulate Science and Technology* 22, no. 4, 321–337.

Theimer, O.F. 1973. Cause and prevention of dust explosions in grain elevators and flour mills. *Powder Technology* 8 (3-4), 137-147.

Ward, T., W. Hourigan. 2011. Granular Segregation in a Tilted-Rotating Drum. *Powder Technology* 215–216, 227–234.

CHAPTER 3

Experimental Work

3.1 Introduction

Segregation occurs when powders have different shapes, sizes, and densities, which may hamper the quality of the final product. Due to the differences in the particle and bulk properties (in terms of size, shape, bulk density etc.), it is possible to have content inhomogeneity of powder during the discharge from silo/hopper because of sifting segregation (Marucci et al. 2018; Hogg 2009; Engblom et al. 2012 (a)). The non-uniform distribution of fines and coarse particles inside large silos, with fine particles settling over a layer of coarse particles (Engblom et al. 2012 (a); Schulze 2008; Engblom et al. 2012 (b)), cause segregation due to air interaction, known as fluidisation segregation (Tang et al. 2004). To explore the segregation characteristics of particles, a bench-scale fluidisation segregation tester (ASTM Standard D 6941, 2012) and a sifting segregation tester (ASTM Standard D6940, 2010) were used (Marucci et al. 2018; Ketterhagen et al. 2007; Oka et al. 2017; Shah et al. 2007; Deng et al. 2010). In addition to these, particle and flow properties are also explored, utilising the different test setups in this study.

3.2 Details of the developed segregation test facilities

Sifting segregation testing

A segregation tester on a laboratory scale, utilising the sifting mechanism and according to ASTM standard D6940, 2010, was fabricated at the Powder Flow Laboratory within Thapar Institute of Engineering and Technology. Figure 3.1 depicts the complete construction divided into two sub-assemblies: funnel and mass flow hoppers, sliding valves for initiating/stopping powder flow, guide cylinders, and a sample cup for gathering small samples during testing. Borosilicate (grade 3.0) glass was predominantly chosen for the tester assembly to facilitate observing powder flow patterns. The top assembly comprises of an inner/mass flow hopper (steep conical shape) nested within an outer/funnel flow hopper (less steep), connected with a slide valve and guide cylinder for powder outflow. The bottom assembly is positioned to align well with the top assembly, consisting of a funnel flow hopper, slide valve, and guide cylinder. A sample cup at the base collected different samples from the guide cylinder. Approximately one litre of well-mixed powder sample was placed in the inner hopper of the top assembly with the slide valve closed. Subsequently, the same powder sample was allowed to descend from the top to the bottom assembly (into the funnel flow hopper) by opening

the slide valve. Once the bottom assembly's funnel flow hopper was filled, 16-18 samples were collected by opening the slide valve via the guide cylinder, each sample comprising of 58 ml in volume. The initial and final samples collected (part of the 1 L volume powder initially taken in the instrument, as per the ASTM Standard, D6940-2010) were designated as the "first batch" and the "last batch," respectively. During the test for each powder, observations were made regarding the mass flow (first-in-first-out) and the funnel flow pattern (first-in-last-out) of the powder sample from the top and bottom hopper assembly, respectively. The first and last batches of segregated and virgin samples were used to calculate the sifting segregation index due to variations in their bulk properties. All experiments were conducted in triplicate. The virgin sample is meant by the fresh sample on an "as received basis". Fineness was the characteristic evaluated for analysis within a specific sample.

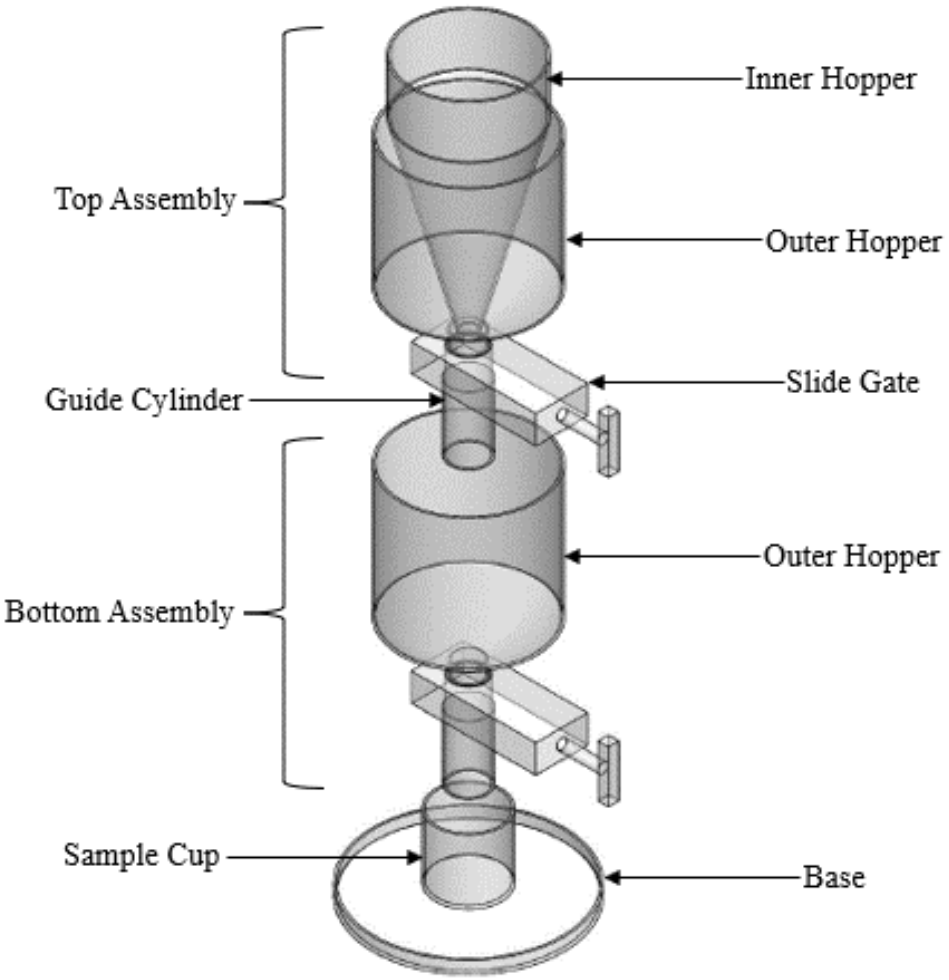

Figure 3.1: Sifting segregation tester as per ASTM Standard, D6940-2010

Fluidisation segregation testing

The behaviour of particle's segregating due to air interaction, known as fluidisation segregation, was assessed using a laboratory-scale tester developed at the Powder Flow Laboratory of Thapar Institute of Engineering and Technology, following ASTM standard D6941, 2012. Borosilicate glass was selected to provide clear visuals of the bubbling and fluidisation state of the powder sample inside the tester during the experiment. The entire fluidisation tester assembly (refer to Figure 3.2) is divided into three chambers: the expansion chamber, the test chamber, and the air chamber. The top expansion chamber includes a filter to prevent the loss of fines during testing and a hopper to introduce the powder sample into the test chamber. The middle test chamber consists of three cylinders (top, middle, and bottom) stacked and sealed during the experiment. Upon completion of the experiment, the test chamber is disassembled to collect the segregated powder samples from the three cylinders. At the bottom, the air chamber comprises of an air distributor (a sintered SS disc with 5 µm filtration) to distribute air into the test chamber. The test chamber was carefully filled to a level of 170 mm with powder sample and then covered with a filter, according to the ASTM standard D6941, 2012. Air is supplied from the air chamber into the test chamber at a recommended pressure of 150 to 200 kPa. Pilot experiments were conducted beforehand to determine the high and low flow rates for each powder, which were then used in the actual experiments as follows:

- After filling the test chamber, the airflow rate was gradually increased from zero to a high value over 30 seconds to reach the fluidisation state of the powder sample. The fluidised state was then maintained for 30 seconds.
- The airflow rate was then slowly decreased to a low rate over 30 seconds to reach the bubbling state and was maintained at this state for 120 seconds.
- The airflow rate was slowly reduced to zero over 30 seconds by stopping the air supply.

It took a few minutes for the fines to settle in the test chamber, after which the three cylinders were unsealed and separated to analyse the segregated samples. The top and bottom segregated samples and the virgin samples were used to calculate the fluidisation segregation index. All experiments were conducted in triplicate. The primary characteristic tested was fineness, expressed as the mass or volume percentage of powders within a specific sample. Comparative studies of the powder characteristics between the segregated samples (top and bottom cylinders) were carried out to emphasise the expected variations between these locations.

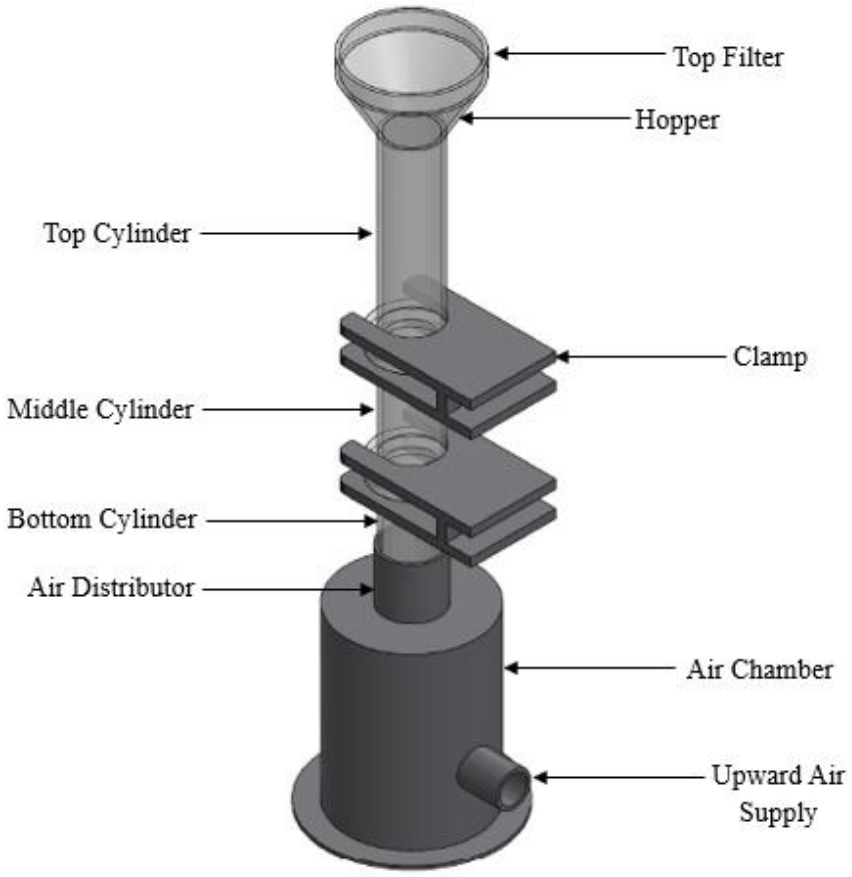

Figure 3.2: Fluidisation segregation tester as per ASTM Standard, D6941-2012

3.3 Powder characterisation tests

The following powder characterisation tests were carried out.

Particle size distribution

Particle size distribution was analysed using a Malvern Mastersizer 3000. This instrument has a particle size measurement range of 0.2 μm to 2000 μm and utilises both a red laser and a blue laser. It employs forward angle detection and side angle scatter detection to determine the large particle size distribution. The powders were fed into the dry dispersion unit using a scirocco feeder, and the particle size distribution was measured at a dispersion pressure of 1.5 bar g. The size (in μm) is represented by three values: d(10), in which 10% of the sample's mass is comprised of smaller particles; d(50), the median particle diameter, meaning 50% of the sample's mass is comprised of

smaller particles and d(90), in which 90% of the sample's mass is comprised of smaller particles. All tests were carried out in triplicate. The course-to-fine is the ratio of d(90) to d(10), representing the wide distribution of particle size.

Particle shape

Particle shape and surface texture for each powder were obtained using scanning electron microscope images (Model-JSM-6510LV by JEOL, USA) by visual observation (Janssen et al. 2021; Rowe et al. 2006). Before the actual measurements, samples were placed on carbon tapes under an argon atmosphere for sputtering deposition with a gold layer of thickness of 4 nm. All tests were carried out in triplicate.

Loose poured and tapped bulk densities

Loose poured bulk (ρ_{lb}) and tapped density (ρ_t) were measured as per the ASTM standard (ASTM D7481, 2010). Firstly, the powder was poured gently into a 100 ml graduated cylinder for loose pour bulk density without compression. After measuring the initial volume (V_o), tapping was done 1250 times (Hastie, 2015). It was found that after 1250 no. of tapping, there was no further volume reduction of the bulk powder. The density of the particles (ρ_p) was calculated using the liquid displacement method (ASTMC693, 1993) or gas pycnometer. The following formulae calculated the Hausner ratio and compressibility index. All tests were carried out in triplicate. Several researchers have used these numbers as an initial estimate of powder flowability (Traina et al. 2013; Garg et al. 2018; Saker et al. 2019; Marchetti et al. 2021).

$$\text{Hausner ratio (HR)} = \rho_t / \rho_{lb} \quad (3.1)$$

$$\text{Compressibility index (CI)} = 100[1 - \rho_{lb} / \rho_t] \quad (3.2)$$

Samples conditioning for different moisture content

A powder sample with a saturated moisture content was conditioned using the microclimate method (Juarez-Enriquez et al., 2017). This method placed a powder sample in a conditioning compartment

with a high relative humidity. In this paper, the maximum moisture content is meant to be the maximum absorbed moisture in a saturated moisture condition in laboratory conditions. Approximately 150-200 grams of the powder sample was evenly spread over a tray and placed in the conditioning compartment for 1-2 days until it reached its maximum moisture content. The powder sample was regularly mixed throughout the conditioning process to ensure that each layer was exposed to moisture. The moisture content absorbed by the powder sample was determined by measuring the weight loss after oven drying, following the ASTM standard D2216, 2019. A fresh powder sample was used for further conditioning using the oven drying method, with zero and average moisture content (Kalman et al., 2021; Lamešić et al., 2022). All tests were carried out in triplicate.

3.4 Powder flow property tests

Annular shear testing

Powder flow tester-PFT (Brookfield, USA), working based on Jenike's methodology (refer to Figure 3.3), was employed to measure the flow parameters of powder samples. As per the procedure (Ding et al. 2012, Berry et al. 2015, Jenike, 1964; ASTM D6128, 2010), after sieving (through 850 microns), the powder sample was filled into a sample trough (PFT-400: 6") on an annular shear cell and enclosed with a top lid (PFT-500: 6", 304 S.S. vane profiled) as shown in Figure 3.3; subsequently, the consolidation stress over the sample powder was gradually increased. The sample trough was rotated at one revolution per hour to shear the sample powder. The applied normal stresses were in the range of 0.2 to 4.8 kPa. For the wall friction test, the applied normal stresses ranged from 0.4 to 4.8 kPa using the top lid (PFT-507: 6", 304 S.S. flat surface profiled). All tests were carried out in triplicate. In order to determine the powder flow properties, various researchers have also utilised Powder Flow Tester (PFT) (Leung et al., 2016; Garg et al., 2018; Lupo et al., 2019 and Garg et al., 2022).

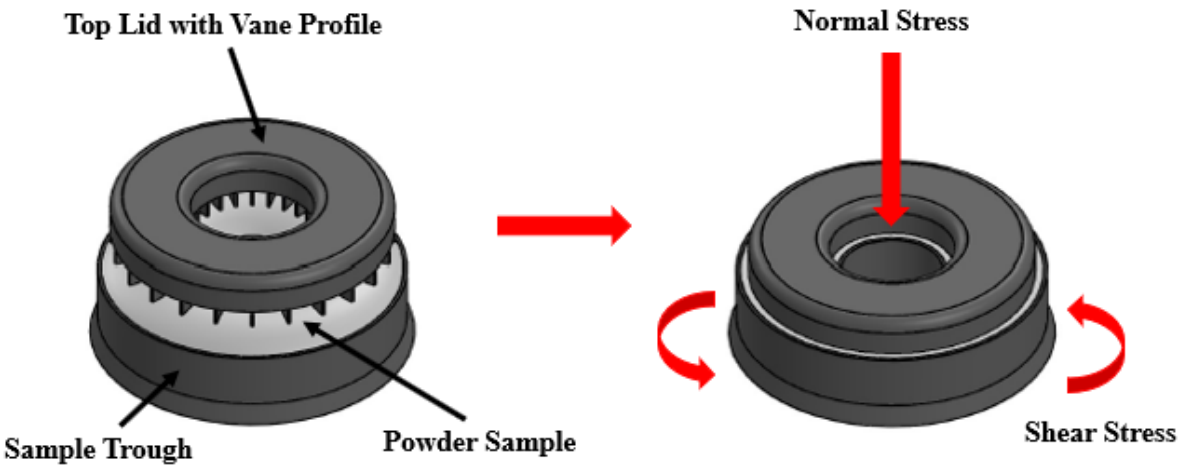

Figure 3.3: Schematic view of the annular shear cell testing procedure

Static angle of repose

The GranuHeap instrument of Granutools, Belgium, was used to measure the static angle of repose. A powder sample of 100 ml was slightly poured into an initialisation tube placed on a cylindrical support with a diameter of 40 mm. After filling, the initialisation tube was set to lift with a constant upward velocity of 5 mm/s. As the powder had flown out from the tube, it made a heap on the cylindrical support. Further, the base of the cylindrical support began to rotate around its axis with a constant velocity of 1 rpm, allowing diverse heap elevations to different heap orientations. The measurement model of 16 pictures/11.25˚ was selected for this study. The image of the powder heap was taken with a CCD camera by using GranuHeap software. A machine-built algorithm was used to evaluate the location of the powder/air interface through image analysis for each shape of the heap. The static angle of repose (S-AoR) is the angle made by the image of the isosceles triangle with the base. S-AoR values were obtained for different heap orientations, and an average value was subsequently calculated. All tests were carried out in triplicate. An empirical relation (European pharmacopoeia 7.0 2010) has been reproduced in Table 3.1 involving static repose angle, the Hausner ratio and compressibility index with powder flow character ranging from ‘excellent’ to ‘very, very poor’. In addition to this parameter, the cohesive index term is a standard term associated with the GranuHeap instrument. The value of cohesive index is determined by the integrated software of the GranuHeap instrument by analysing the deviation between the actual powder's heap formed (blue in colour) and the isosceles triangle-shaped heap (red in colour) with the help of GranHeap software.

Table 3.1: Powder flowability guideline (European pharmacopoeia 7.0, 2010)

Flow character	**Static angle of repose (˚)**	**Hausner ratio (HR)**	**Compressibility index (%)**	**Cohesive index (C_i): as per the user guide of the GranuHeap instrument**
Excellent	25-30	1.00-1.11	1-10	< 0.2
Good	31-35	1.12-1.18	11-15	0.3-0.5
Fair	36-40	1.19-1.25	16-20	0.6-0.8
Passable	41-45	1.26-1.34	21-25	0.9-1.2
Poor	46-55	1.35-1.45	26-31	1.3-1.7
Very poor	56-65	1.46-1.59	32-37	1.8-2.4
Very, very poor	>66	>1.60	>38	>2.5

References

ASTM Standard, D2216-19. 2019. Standard Test Methods for Laboratory Determination of Water (Moisture) Content of Soil and Rock by Mass, West Conshohocken, PA, USA: ASTM International (www.astm.org).

ASTM Standard, C618. 2015. Standard specification for coal fly ash and raw or calcined natural pozzolona for use in concrete, West Conshohocken, PA, USA: ASTM International (www.astm.org).

ASTM Standard, D6941. 2012. Standard Practice for Measuring Fluidization Segregation Tendencies of Powders, West Conshohocken, PA, USA: ASTM International (www.astm.org).

ASTM Standard, D6128. 2010. Standard Test Method for Shear Testing of Bulk Solids Using the Jenike Shear Cell, West Conshohocken, PA, USA: ASTM International (www.astm.org).

ASTM Standard, D6940. 2010. Standard Practice for Measuring Sifting Segregation Tendencies of Bulk Solids, West Conshohocken, PA, USA: ASTM International (www.astm.org).

ASTM Standard, D7481. 2010. Standard Test Methods for Determining Loose and Tapped Bulk Densities of Powders Using a Graduated Cylinder, West Conshohocken, PA, USA: ASTM International (www.astm.org).

ASTM Standard, C693. 1993, Standard Test Method for Density of Glass by Buoyancy, West Conshohocken, PA, USA: ASTM International (www.astm.org).

Boschini, F., V. Delaval, K. Traina, N. Vandewalle, and G. Lumay. 2015. Linking Flowability and Granulometry of Lactose Powders. *International Journal of Pharmaceutics* 494, no. 1 (October): 312–320.

Berry, R.J., Bradley, M.S.A. and McGregor, R.G., 2015. Brookfield powder flow tester–Results of round robin tests with CRM-116 limestone powder. *Proceedings of the Institution of Mechanical Engineers, Part E: Journal of Process Mechanical Engineering*, *229*(3), pp.215-230.

Deng, T., K.A. Paul, M.S.A. Bradley, L. Immins, C. Preston, J.F. Scott, and E.H. Welfare. 2010. Investigations on Air-Induced Segregation of Pharmaceutical Powders and Effect of Material Flow Functions. Powder Technology 203, no. 2 (November): 354–358.

Ding, X.J., Liu, L.L. and Bradley, M.S., 2012. New instrument PFT for powder flow researching. Trans Tech Publications Ltd. In *Advanced Materials Research* (Vol. 508, pp. 141-145).

Engblom, N., H. Saxén, R. Zevenhoven, H. Nylander, and G.G. Enstad. 2012 (a). Segregation of Powder Mixtures at Filling and Complete Discharge of Silos. *Powder Technology* 215–216 (January): 104–116.

Engblom, N., H. Saxén, R. Zevenhoven, H. Nylander, and G.G. Enstad. 2012 (b). Effects of Process Parameters and Hopper Angle on Segregation of Cohesive Ternary Powder Mixtures in a Small-Scale Cylindrical Silo. *Advanced Powder Technology* 23, no. 5 (September): 566–579.

European pharmacopoeia 7.0, Chapter 2.9.36.: Powder flow, 2010, p. 308.

Garg, V., Deng, T. and Bradley, M.S., 2022. A new method for assessing powder flowability based on physical properties and cohesiveness of particles using a small quantity of samples. *Powder Technology*, *395*, pp.708-719.

Garg, V., Mallick, S.S., García-Trinanes, P. and Berry, R.J., 2018. An investigation into the flowability of fine powders used in pharmaceutical industries. Powder Technology, 336, pp.375-382.

Hastie, D.B. 2015. On the Difficulties of Sampling Bulk Powder Blends in Determining Segregation Propensity — A Case Study. *Powder Technology* 286 (December): 164–171.

Hogg, R. 2009. Mixing and Segregation in Powders: Evaluation, Mechanisms and Processes. *KONA Powder and Particle Journal* 27: 3–17.

Janssen, P.H.M., S. Depaifve, A. Neveu, F. Francqui, and B.H.J. Dickhoff. 2021. Impact of Powder Properties on the Rheological Behavior of Excipients. *Pharmaceutics* 13, no. 8 (August 4): 1198.

Juarez-Enriquez, E., G.I. Olivas, P.B. Zamudio-Flores, E. Ortega-Rivas, S. Perez-Vega, and D.R. Sepulveda. 2017. Effect of Water Content on the Flowability of Hygroscopic Powders. *Journal of Food Engineering* 205: 12–17.

Kalman, H., and D. Portnikov. 2021. Analyzing Bulk Density and Void Fraction: B. Effect of Moisture Content and Compression Pressure. *Powder Technology* 381 (March): 285–297.

Ketterhagen, W.R., J.S. Curtis, C.R. Wassgren, A. Kong, P.J. Narayan, and B.C. Hancock. 2007. Granular Segregation in Discharging Cylindrical Hoppers: A Discrete Element and Experimental Study. *Chemical Engineering Science* 62, no. 22 (November): 6423–6439.

Lamešić, D., B. Grilc, R. Roškar, S. Kolokytha, J. Hofmann, A. Malekos, R. Kaufmann, and O. Planinšek. 2022. Spherical Agglomerates of Lactose Reduce Segregation in Powder Blends and Improve Uniformity of Tablet Content at High Drug Loads. *AAPS PharmSciTech* 23, no. 1 (January 10): 17.

Lupo, M., Schütz, D., Riedl, E., Barletta, D. and Poletto, M., 2019. Assessment of a powder rheometer equipped with a cylindrical impeller for the measurement of powder flow properties at low consolidation. Powder Technology, 357, pp.281-290.

Leung, L.Y., Mao, C., Chen, L.P. and Yang, C.Y., 2016. Precision of pharmaceutical powder flow measurement using ring shear tester: High variability is inherent to powders with low cohesion. *Powder Technology*, *301*, pp.920-926.

Marchetti, L., and C. Hulme-Smith. 2021. Flowability of steel and tool steel powders: A comparison between testing methods. Powder Technology 384 (May):402–13.

Marucci, M., B. Al-saaigh, C. Boissier, M. Wahlgren, and H. Wikström. 2018. Sifting Segregation of Ideal Blends in a Two-Hopper Tester : Segregation pro Files and Segregation Magnitudes. *Powder Technology* 331: 60–67.

Oka, S., A. Sahay, W. Meng, and F. Muzzio. 2017. Diminished Segregation in Continuous Powder Mixing. *Powder Technology* 309 (March): 79–88.

Rowe, R.C., P.J. Sheskey, and S.C. Owen. 2006. *Handbook of Pharmaceutical Excipients*. *Pharmaceutical Press and American Pharmacists Association*.

Saker, A., M.-G. Cares-Pacheco, P. Marchal, and V. Falk. 2019. Powders Flowability Assessment in Granular Compaction: What about the Consistency of Hausner Ratio? *Powder Technology* 354 (September): 52–63.

Schulze, D. 2010. Powders and Bulk Solids. *Chemie Ingenieur Technik* 82, no. 4 (April): 553–554.

Shah, K.R., S.I. Farag Badawy, M.M. Szemraj, D.B. Gray, and M.A. Hussain. 2007. Assessment of Segregation Potential of Powder Blends. *Pharmaceutical Development and Technology* 12, no. 5 (January 7): 457–462.

Traina, K., R. Cloots, S. Bontempi, G. Lumay, N. Vandewalle, and F. Boschini. 2013. Flow Abilities of Powders and Granular Materials Evidenced from Dynamical Tap Density Measurement. *Powder Technology* 235 (February): 842–852.

Yablokova, G., M. Speirs, J. Van Humbeeck, J.-P. Kruth, J. Schrooten, R. Cloots, F. Boschini, G. Lumay, and J. Luyten. 2015. Rheological Behavior of β-Ti and NiTi Powders Produced by Atomization for SLM Production of Open Porous Orthopedic Implants. *Powder Technology* 283 (October): 199–209.

CHAPTER 4

Powder Flow Properties

4.1 Introduction

It has been considered that powder flow properties would be influencing the segregation phenomenon. This chapter has been dedicated to powder flow properties, which would be further used in subsequent sections of this thesis. Accurate prediction of powder flow properties is of paramount importance in most of the powder processing and handling plants, especially it is critical for the pharmaceutical industry because of its precise quality control requirement (Chávez et al. 2019; Ghadiri et al. 2020; Baserinia et al. 2022). In a pharmaceutical formulation plant, if the powder blend is highly cohesive, poor flowability can be a bottleneck resulting in non-uniform powder flow, arching and rat-holing at the hopper discharge (Boschini et al. 2015; Baserinia et al. 2022). On the contrary, if the blend is excessively free-flowing, non-homogeneity in blend constituents may be triggered due to the enhanced segregation characteristics induced in powders helped by the ease of particle rearrangement (Shah et al. 2007; Fathollahi et al. 2020; Janssen et al. 2021). In other words, either of the extremes (i.e. too cohesive or too free-flowing) is detrimental to the formulation process (Ghadiri et al. 2020; Shi et al. 2020; Tan et al. 2021) and may cause lot rejection. Therefore, it is important to predict the flow properties of powders that would be subjected to the formulation process in the pharmaceutical industry to avoid potential bottlenecks, downtime and quality control issues at a later stage. In order to predict the flow properties of cohesive powders, the static angle of repose (S-AoR) is considered to be an important indicator (European pharmacopoeia 7.0 2010; Yu et al. 2011; Lumay et al. 2012; Barjat et al. 2020). Testing static angle of repose is fast and does not require a high level of expertise for testing, data analysis and interpretation. Moreover, it requires only a limited amount of powder sample. However, this testing method does involve stress to be applied on powders; also, it is unsuitable for predicting the time consolidation effects (Schulze 2008; Marchetti et al. 2021; Francia et al. 2021). On the contrary, the classical Jenike test procedure for shear cell testing requires comprehensive testing (which may be better representing the actual powder flow conditions), a much longer time, a larger amount of powder samples (arranging this can be difficult for hazardous and/or costly powders), high level of technical skills to carry out the tests and a strong understanding/knowledge of powder flow in analysing the data and for predicting the results. However, testing is carried out under different consolidation stresses, and the effect of loss of powder flowability w.r.t time consolidation can be assessed (Schulze 2008; Jager et al. 2015; Leung et al. 2016). Thus, while the shear cell testing offers procedural comprehensiveness, the static angle of repose method has the advantage of practical convenience suiting a wider range of industrial circumstances. Under such situations, it is important to carry out a comprehensive study comparing the results of both these processes, i.e., between the static angle of repose and the shear cell method.

The first objective of this study is to investigate into the apparent similarities (or otherwise) between the results obtained from both of these test procedures. Results related to powder flow behaviour in terms of static angle of repose obtained from the GranuHeap instrument (by Granutools, Belgium) and powder flow function and cohesion obtained from Powder Flow Tester- PFT (by Brookfield, USA) have been compared using several pharmaceutical powders. A subset of this objective is also to study the relationship between the static angle of repose and cohesive index (a term associated with the GranuHeap instrument) if there is any. The other objective of this study is to investigate into the linkage of particle and bulk properties of powders to their static angle of repose.

4.2 Experimental data

In Table 4.1, particle shape and size distribution are presented for each powder sample. Median size (d_{50}) is the particle size at the cumulative percentage of 50%, whereas d_{10} and d_{90} are the particle size at the cumulative percentage of 10% and 90%, respectively. The heap images (showing the static angle of repose) are provided in Figure 4.1, consist of the actual powder's heap formed (blue in colour) on a base and the isosceles triangle-shaped heap formed by Granuheap software (red in colour) and overlapping of actual powder's heap with the isosceles triangle-shaped heap marked as black in colour. To obtain reproducible results, a controlled rotation of the base enables the generation of various heap projections corresponding to different orientations of the heap. A custom image recognition algorithm identifies the position of the powder-air interface. The software then processes the isosceles triangle-shaped heap to calculate the static angle of repose, which is the angle formed between one of the slanted sides and the base of the isosceles triangle in the projected image of the powder heap. The repose angle is calculated for each image, representing each heap orientation, and an average value is subsequently computed. Scanning Electron Microscopy (SEM) images have been provided in Figure 4.2. Table 4.1 includes a comprehensive list of powder properties. It can be seen from Table 4.1 and the SEM images that there is a wide variation of particle shapes ranging from granular to needle-shaped to irregular shaped with shape factor (ratio of smallest to largest dimension), S, ranging from 0.40 to 0.88 with the Starch particles showing some degree of roundness. The Microcrystalline Cellulose and Croscarmellose Sodium powder samples show fibre-shaped structures, whereas Starch particles show relatively spherical shapes. Powder samples of Lactose Monohydrate and Mannitol show relatively large/sharp particles with tomahawk and needle edge/shape, respectively. The Crospovidone XL-10 and Magnesium stearate samples have a relatively large amount of fines with a granular form and smooth shape granules,

respectively. In contrast, Sodium Carbonate Anhydrous has a granular and irregular shape with few fines.

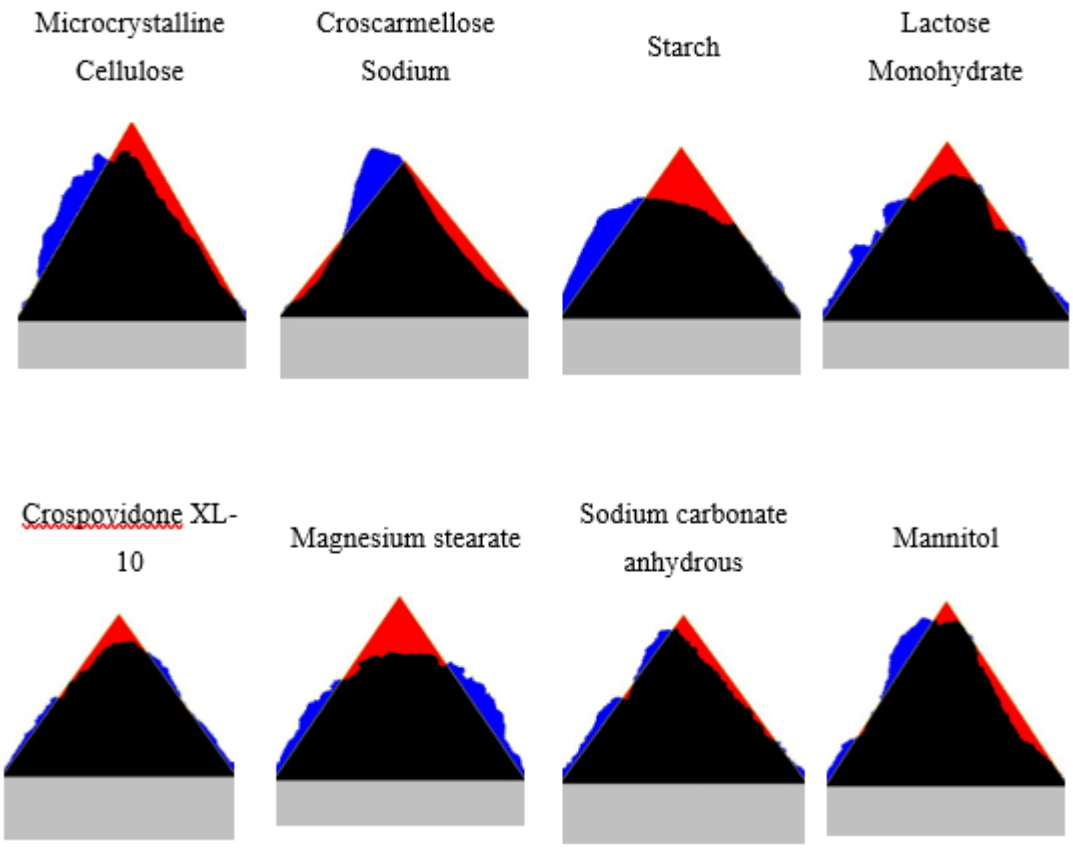

Figure 4.1: Heap images of powders

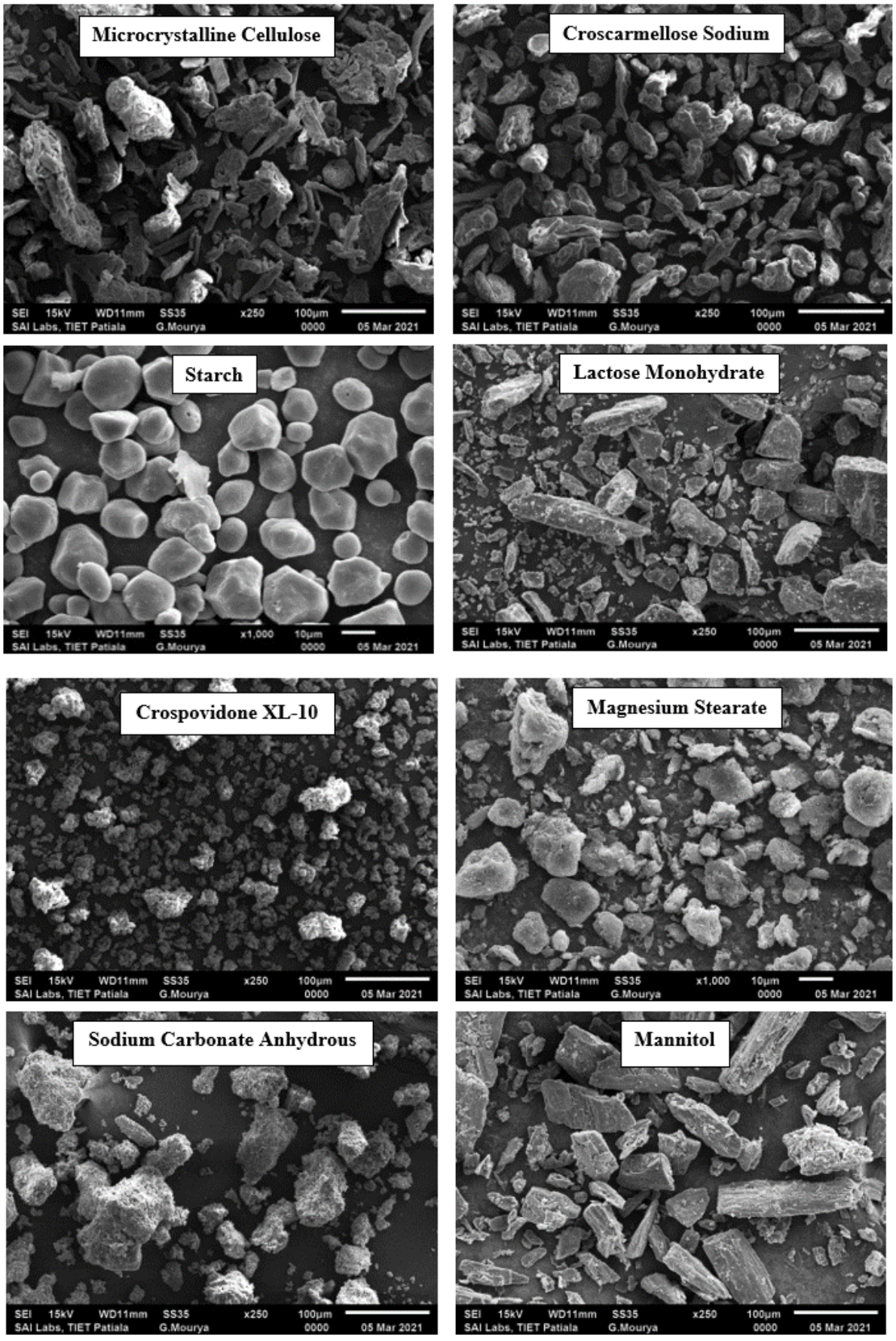

Figure 4.2: SEM images of powders

Table 4.1: Physical properties of powders (from Geldart group C)

Powder	**d_{10}**	**d_{50}**	**d_{90}**	**d_{90} / d_{10}**	**S**	**Particle shape**	**ρ_{lb}**	**ρ_t**	**HR**	**CI**	**C_i**	**S-AoR**	**Powder flow as per (European pharmacopoeia 7.0)**
	µm	**µm**	**µm**				**kg/m^3**	**kg/m^3**		**%**		**(º)**	
Microcrystalline cellulose (MCC)	16	57	126	7.88	0.40	Fibre	397	611	1.54	35	3.44	66.1	Very, very poor
Croscarmellose Sodium (CCS)	20	42	75	3.75	0.49	Fibre	515	778	1.51	34	2.68	57.1	Very poor
Starch (ST)	9	31	60	6.66	0.88	Spherical/regular	480	680	1.41	29	4.1	58.3	Very poor
Lactose monohydrate (LT)	12	51	107	8.92	0.63	Tomahawk/fine	517	808	1.56	36	2.31	65.4	Very poor
Crospovidone XL-10 (CPD)	8	23	62	7.75	0.81	Granular/fine	275	393	1.43	30	0.85	56.5	Very poor
Magnesium stearate (MS)	2	5	17	8.5	0.73	Smooth shaped granule	279	506	1.82	45	4.27	66.3	Very, very poor
Sodium carbonate anhydrous (SCA)	14	78	179	12.79	0.64	Granular/fine	517	922.8	1.78	44	1.35	58.6	Very poor
Mannitol (MT)	12	63	218	18.16	0.45	Needle edge/shape	487	716.6	1.47	32	1.15	66.2	Very, very poor

4.3 Static angle of repose and cohesive index

Figure 4.3 shows the plots between the static angle of repose and cohesive index. It may be intuitive to think that cohesive index and static angle of repose would follow the same trend, i.e. higher cohesive index would lead to higher values of static angle of repose. However, the results show that the cohesive index and static angle of repose do not follow the same trend; the static angle of repose values tend to follow a fluctuating pattern about a mean value in a range where the cohesive index has steadily increased.

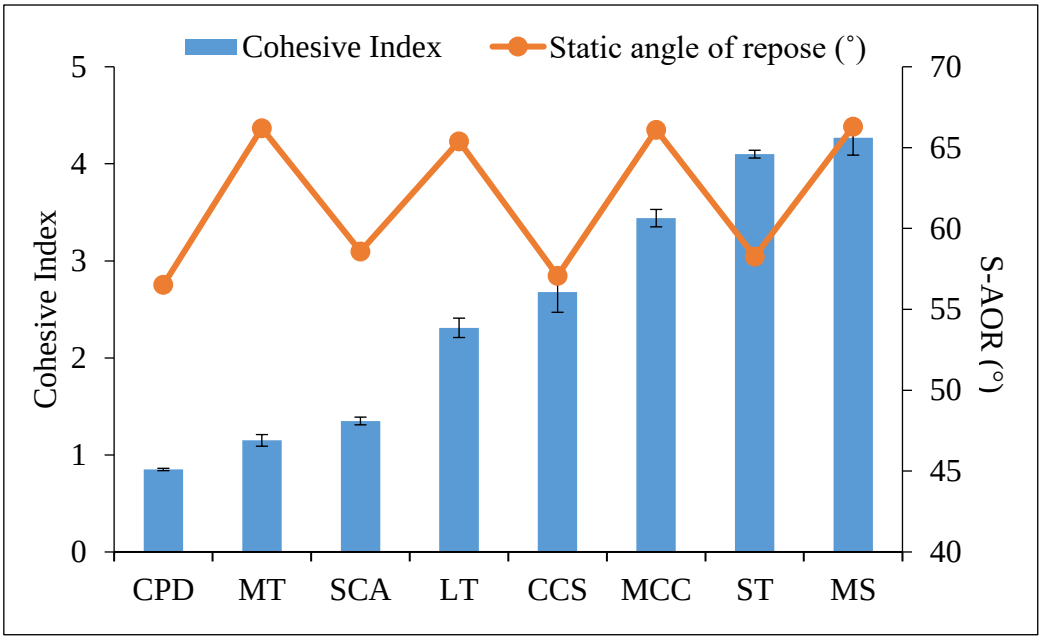

Figure 4.3: Static angle of repose versus cohesive index

4.4 Cohesion

The experimental data obtained from the Powder Flow Tester (PFT) are provided in Figure 4.4. For powder to flow, consolidation stress is a crucial parameter (Schulze 2008). The powder flow tester carried out the yield locus test for several normal consolidated stresses at various pre-shear stresses. The following equation (4.1) represents the ideal Coulomb criteria at given pre-shear stress (τ) as a function of given consolidation stress (σ) and angle of friction (ϕ) with (c) as cohesion value:

$$\tau = \sigma (\tan\phi) + c \qquad (4.1)$$

In the shear stress versus normal stress plot, the value of cohesion (c) in equation (4.1) is the point where the yield locus bisects the axis of shear stress when normal stress is zero. The effective yield locus within the same plot is the straight line starting from the origin and tangent to the Mohr circle for steady-state flow. The angle made by the effective yield locus with a horizontal axis (normal stress) is known as the effective angle of internal friction (ϕ_e), which is the ratio of σ_2/σ_1 (Schulze 2008), where σ_1 and σ_2 are major and minor principal consolidation stresses, respectively. The PFT software used a linear regression model to fit the data using equation (4.1) for an individual set of yield locus values. The approximate pre-shear stress values (operating range of PFT) for each excipient powder sample were 0.49, 0.87, 1.53, 2.72 and 4.83 kPa. The effective angle of internal friction (ϕ_e), flow function coefficient (ff_c), major principal consolidation stress (σ_1), unconfined yield strength (σ_c) and cohesion (c) for each powder were calculated by drawing the tangent using Mohr's circles through every yield locus.

The flow function coefficient (ff_c) is defined as the ratio of major principal consolidation stress (σ_1) to unconfined failure strength (σ_c). This ff_c was utilised to compare the powder flowability of different pharmaceutical powder samples. As per Jenike's methodology of flow behaviour (Schulze 2008), Figure 4.4 is divided into five regimes/zones of flow behaviour: non-flowing (ff_c value less than 1), very cohesive (ff_c lies between 1 and 2), cohesive (ff_c lies between 2 and 4), easy flowing (ff_c lies between 4 and 10) and free-flowing (ff_c value greater than 10).

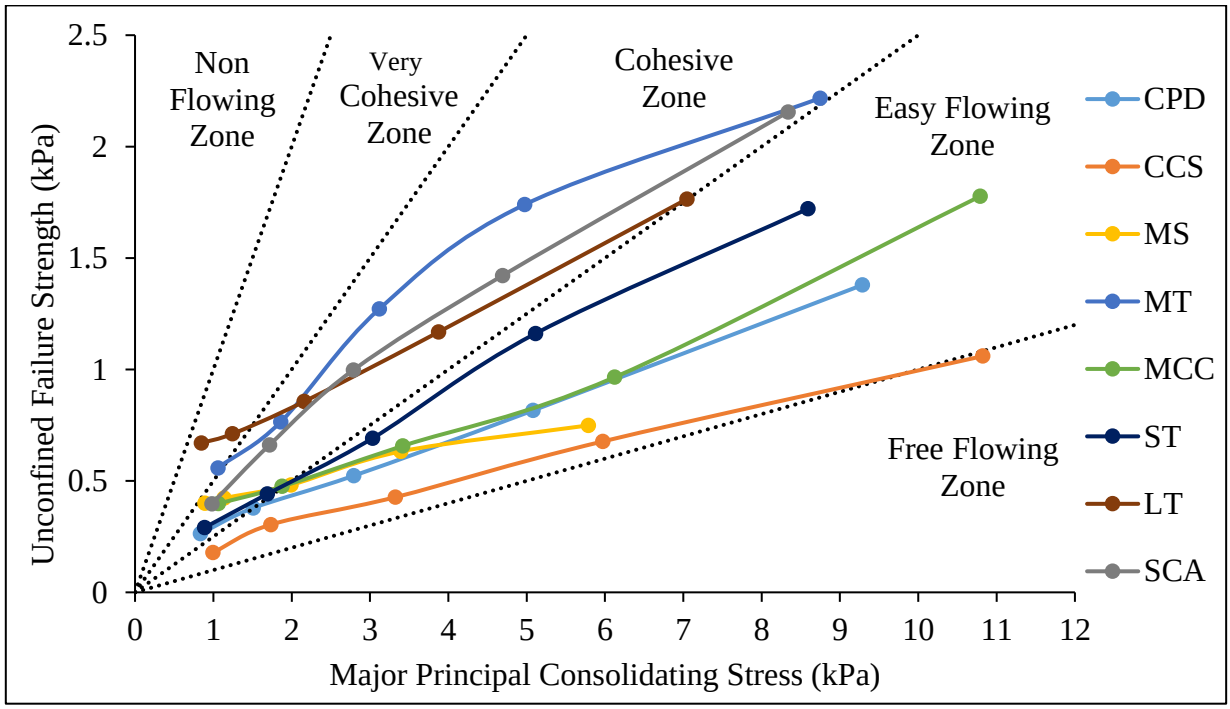

Figure 4.4: Flow function curve for powders

Table 4.2 provides a comparison of the flowability associated with the static angle of repose of each powder, as outlined in the European Pharmacopoeia 7.0, with the regime/zone in the flow function curve (refer to Figure 4.4). There is a noticeable difference between the flowability indicated by the static angle of repose and the regime or zone in the flow function curve, which reflects the flow characteristics of the powders under no stress versus with consolidating stress. In practical terms, the actual condition is characterised by the consolidating stress during the flow of a powder. Additional details can be found in Chapter 3.

Table 4.2: Comparison of the static angle of repose, cohesion, flow function curve and European Pharmacopoeia 7.0

Powder	**Static angle of repose (°)**	**Cohesion (kPa)**	**Regime/zone in flow function curve**	**As per European Pharmacopoeia 7.0 (w.r.t static angle of repose)**
Microcrystalline cellulose (MCC)	66.1	0.103	Cohesive to easy flowing	Very, very poor
Croscarmellose Sodium (CCS)	57.1	0.047	Easy flowing to free-flowing	Very poor
Starch (ST)	58.3	0.09	Cohesive to easy flowing	Very poor
Lactose monohydrate (LT)	65.4	0.246	Very cohesive to cohesive	Very poor
Crospovidone XL-10 (CPD)	56.5	0.08	Cohesive to easy flowing	Very poor
Magnesium stearate (MS)	66.3	0.225	Cohesive to easy flowing	Very, very poor
Sodium carbonate anhydrous (SCA)	58.6	0.114	Cohesive	Very poor
Mannitol (MT)	66.2	0.155	Very cohesive to cohesive	Very, very poor

After obtaining the cohesion (c) values, the same has been plotted against the 'cohesive index' and subsequently with the static angle of repose. The results are provided in Figures 4.5 and 4.6, respectively.

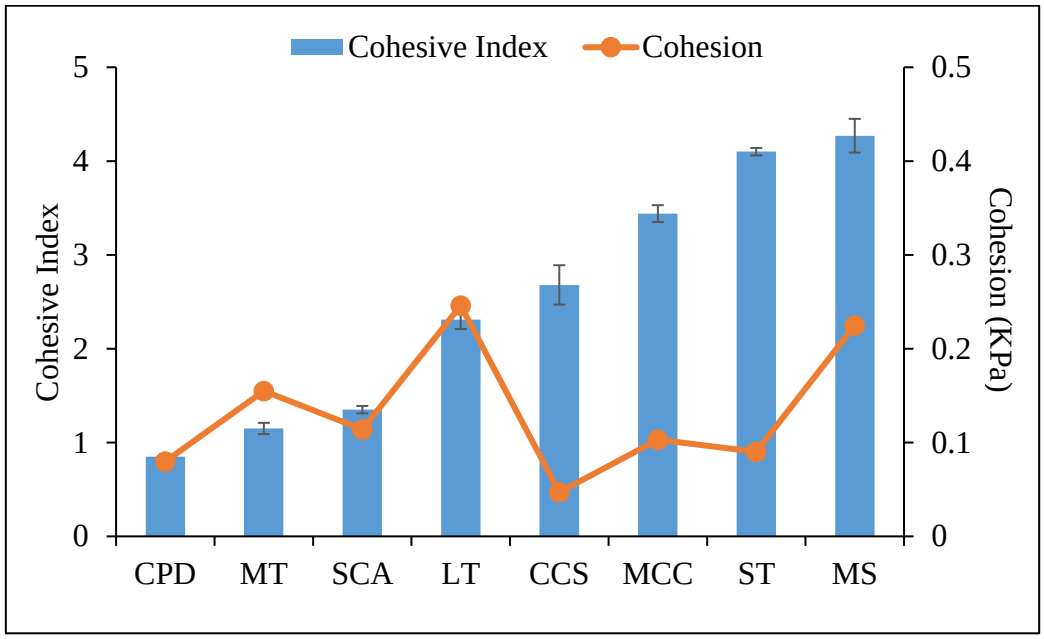

Figure 4.5: Cohesion versus cohesive index

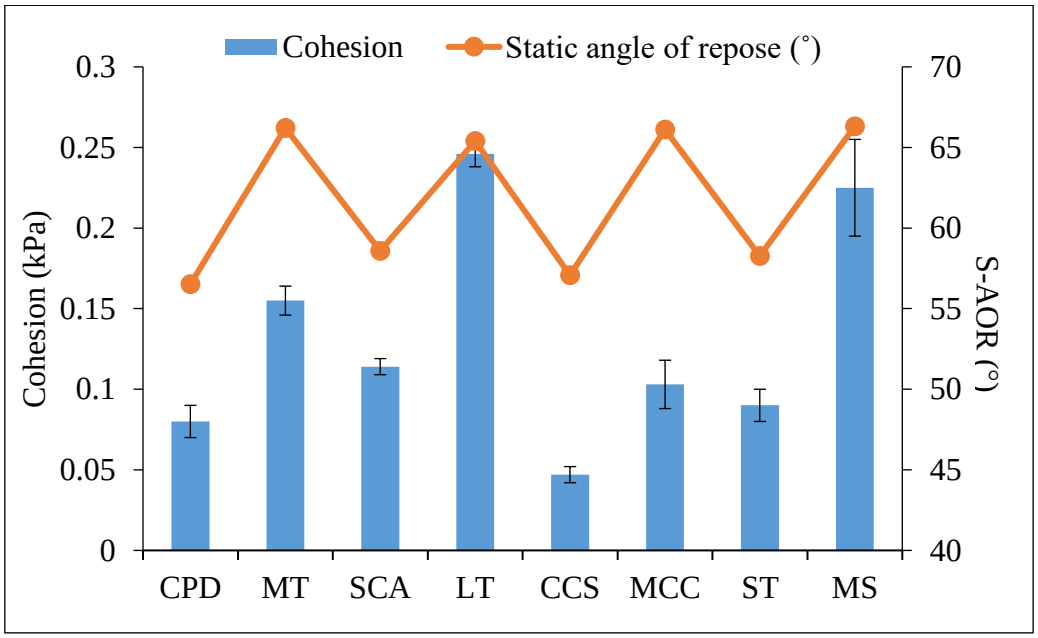

Figure 4.6: Static angle of repose versus cohesion

It can be seen from Figure 4.5 that the cohesive index and cohesion do not follow the same trend. Microcrystalline Cellulose, Croscarmellose Sodium and Starch exhibit low cohesion values, while these particles have higher values of cohesion index. Comparatively, the relationship between

cohesion and static repose angle seems stronger in Figure 4.6. Except for the case of Lactose monohydrate and Magnesium Stearate, an increase in cohesion value is significantly associated with an increase in the static angle of repose. This indicates that the cohesive index is not significantly relevant in this study and does not correlate well with the terms cohesion and static angle of repose.

4.5 Model for the static angle of repose

In order to identify powder parameters responsible for determining the static angle of repose, regression analysis was carried out with the method of some of the least square values using several parameters and/or parameter groupings to find the non-linear relationship into a form of simpler linear model, which is easier to evaluate using direct and standard techniques. A logarithmic transformation can easily transform a highly skewed variable into a more normalised dataset. Error probabilities may also be skewed negatively when modelling variables with non-linear connections (Kissell et al. 2017). Kalman (2021) has developed a model for coarser particles, but very limited work has been carried out for finer powders. From principal component analysis, it was found that a bulk powder-based Froude number (based on loose poured bulk density) (Kalman 2020; Saluja et al. 2023; Poddar et al. 2024), shape factor and median-to-fine ratio provided a good strength of correlation. However, the Hausner ratio and the compressibility index do not demonstrate any significant relationship. The resulting relationship is provided below.

$$\text{S-AoR} = 46.13\,(Fr_b)^{-0.037}\,(S)^{-0.19}\,(MFR)^{0.094} \quad (4.2)$$

where, $Fr_b = w_{fo,b}/\sqrt{(gd_{10})}$ (4.3)

$w_{fo,b}$ = Particle terminal velocity $= 9.81(d_{10})^2\rho_{lb}/(18\mu)$ (4.4)

S = Shape factor

MFR = Median to fine ratio = d_{50}/d_{10}

The Froude number is a dimensionless parameter representing the ratio of the inertia force on an element of fluid to the weight of the fluid element (i.e. the inertial force divided by gravitational force) (Mallick and Wypych 2009; Klinzing et al. 2010; Mallick 2010; Mallick et al. 2011). In the literature, Klinzing et al. 2010, and Mallick 2010, discussed the minimum transport boundary using the Froude number. The analysis inherently incorporates geometric scaling effects, producing consistent trends across different pipeline sizes and improving the reliability of design and operational predictions. Equation (4.3) represents a bulk powder-based Froude number (Fr_b), a

dimensionless quantity used to characterise the flow conditions of particles, which is based on particle terminal velocity in equation (4.4). Particle terminal velocity refers to the velocity at which individual particles fall through a fluid under the influence of gravity, reaching a constant velocity (terminal velocity) when the forces of gravity, buoyancy, and drag balance out. The velocity of a particle relative to a gas is definitely influenced by the air resistance of the particle. The ratio of air resistance to gravity force increases strongly with decreasing particle size. Thus, the steady-state terminal velocity of particles in the gravity field decreases significantly with decreasing particle size. This effect plays an important role even for particle sizes of 50 to 100 μm, but becomes significant at particle sizes below 10 μm. Thus, small particles suspended in a gas cannot move with noticeable velocities relative to the gas and can be easily carried away by a gas stream. In this chapter, the particle terminal velocity is defined based on loose poured bulk density (instead of the conventional method of using particle density) (Saluja et al. 2023; Poddar et al. 2024). This is because, for fine powders (especially which are dominated by cohesion), the existence of a 'free' particle is unlikely in a solid-solid environment comprising of fine powders. In such a scenario, particles are considered to be a bulk powder system and approaching a continuum instead of maintaining their identity as individual particles. Also, the presence of fines tends to play a dominant role in the bulk behaviour of powders. Therefore, d_{10} has been considered to be a more relevant parameter instead of the otherwise average or median size (d_{50}). Overall, Fr_b can be considered to be a size-normalised gravitational force which helps the particles to roll over and/or slide down along the surface of a heap under the influence of gravity. Higher the value of Fr_b, the less would the value of the static angle of repose due to the higher normalised inertia of sliding down of particles along the surface of the heap.

On the contrary, a smaller value of Fr_b would indicate particles would get stuck on the surface of the heap due to their smaller size (smaller getting interlocked between larger particles already present on the surface of the heap) and/or lower bulk density, unable to provide adequate gravity force to overcome the frictional resistance of the heap surface. Thus, a smaller value of Fr_b would result in powder getting ‘piled up’, or a steep heap is being formed, i.e., a higher value of static angle of repose. It can be seen in equation (4.3) that the exponent of Fr_b is negative, i.e. smaller value of Fr_b would increase the value of the static angle of repose. This is in agreement with the physical significance of Fr_b w.r.t static angle of repose.

Intuitively, it can be thought that spherical particles would tend to roll over the surface of a heap easier than irregular or more needle-shaped particles. Thus, higher the value of the shape factor, i.e.

more closer the particles are to spheres as far as shape is concerned and better would be the sliding down tendency of particles along the heap surface, thus forming a flatter heap with the reduced static angle of repose. Therefore, the negative exponent of shape factor (S) in equation (4.3), i.e. an increase in the value of the static angle of repose with more needle-shaped particles, is in agreement with the physical understanding. A wider size distribution indicates a larger value of the median to fine ratio (i.e. MFR). A large amount of mixed-sized particles (due to higher MFR) would enable the fine particles to get stuck between the larger/median particles on the surface of the heap. Thus, the finer powders would not be able to slide down the surface of the heap (as the fines get entrapped on the heap surface); as a result, powder mass would get accumulated on the face of the heap, causing an increase in the value of the static angle of repose. Therefore, the positive exponent value of MFR in equation (4.3), i.e., an increase in the value of the static angle of repose with an increase in the median to fine ratio, is in agreement with the physical understanding. Figure 4.7 shows the predicted versus experimental result for the static angle of repose.

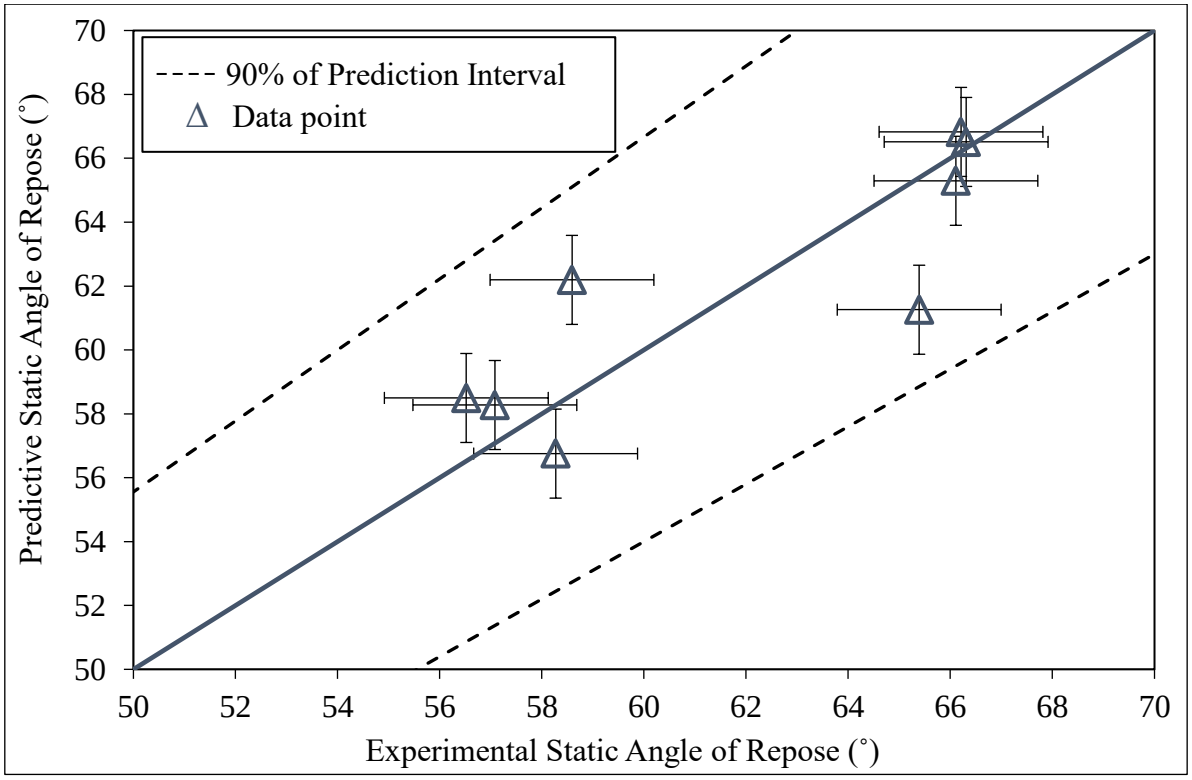

Figure 4.7: Predicted versus experimental static angle of repose

In order to further investigate into the parametric influence of Fr_b, S and MFR over a wider range of values, a series of predictions have been carried out using equation (4.3) by holding one of the parameters as constant. The results are provided in Figure 4.8 and Figure 4.9.

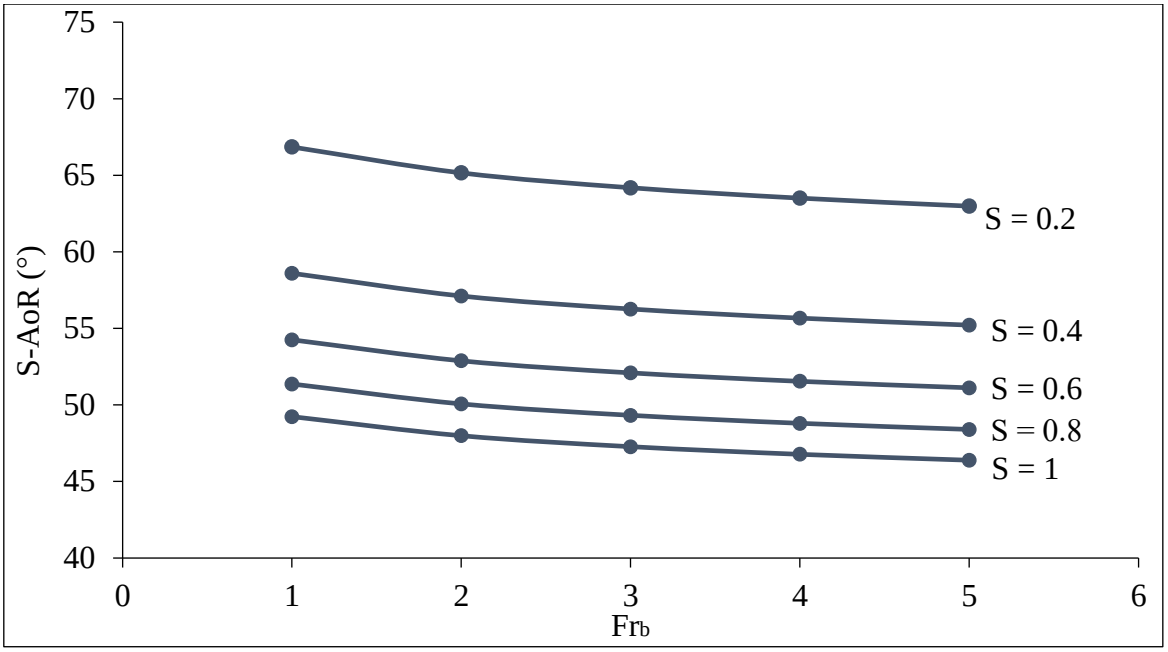

Figure 4.8: Predicted contours of the static angle of repose for different shape factors and MFR =2

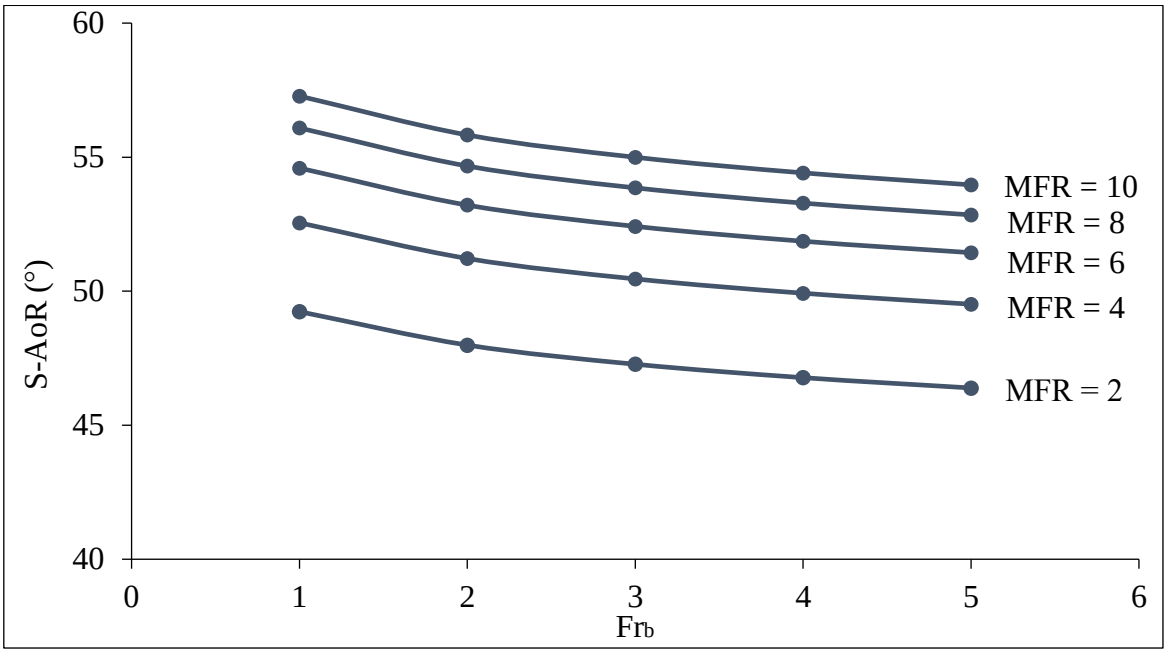

Figure 4.9: Predicted contours of the static angle of repose for MFR values and for the spherical shape

In Figure 4.8, static angle of repose values for have been plotted for different shape factors (S = 0.2 to 1, where S = 1 represents spherical particles) and MFR = 2. The results show that with an increase in the value of Fr_b, the static angle of repose decreases. The gradient of increase of static angle of repose values w.r.t decrease in Fr_b is steeper at lower Fr_b values. With an increase in shape factor, S

(i.e. particle shape tending to be spherical), the static angle of repose values decrease. There is a sharp drop in the values of the static angle of repose as the shape factor increases from 0.2 to 0.4. Subsequently, the relative improvement w.r.t increase in particle shape factor decreases (although the value of static angle of repose continues to decrease with an in shape factor). The practical implication of this trend is that to get a substantial gain in powder flowability (indicated by a reduced value of static angle of repose), the powder's shape does not have to be made a perfect sphere. If the shape is improved (i.e., the value of the shape factor increases) from needle shape to somewhat irregular shape (may not be a perfect sphere), flowability would be a substantial gain.

Similarly, if in any installation the powders are too fine and that is considered to be causing a loss of flowability (i.e. higher value of static angle of repose caused by a reduced value of Fr_b), improvement of flowability may be achieved by a slight increase in particle size; too much increment in particle size with a hope to obtain a linear rise in the value of flowability would be irrelevant (and not effective) as the slopes of the static angle of repose curves tend to get flatten out with an increase in the value of Fr_b (caused by an increase in particle size). Similarly, referring to Figure 4.9, a decrease in the median to fine ratio value would tend to improve the flowability by decreasing the static angle of repose. However, the gain tends to subside with the reduction of MFR values. Figures 4.8 and 4.9 show that there is a scope for techno-economic optimisation for selecting the most suitable combination of particle shape, size and bulk density towards achieving the desired flowability. The results also show that in a powder handling process, especially if the powders are fragile or there are chances of considerable powder attrition resulting in powder shape and size change, the powder flowability is likely to alter along the process.

4.6 Conclusion

Physical and flow property test data of 8 pharmaceutical powder samples have shown that the static angle of repose is not strictly correlated to the cohesive index; comparatively, cohesion stress values seem to have a more stronger relationship with the static angle of repose. A relationship to represent the static angle of repose has been developed using a bulk powder Froude number based on loose poured bulk density and fine size (d_{10}). The proposed model has been tested and validated at an appropriate rate of powder properties. The experimental results for eight pharmaceutical powders have shown that the value of the static angle of repose decreases with an increase in the modified particle Froude number, an increase in particle shape factor and a decrease in the median to fine

ratio. Out of all the dimensionless parameter groupings, the particle shape factor seems to have the strongest influence on the static angle of repose, as indicated by its larger absolute exponent value. Based on the trends provided for the static angle of repose values with respect to modified particle Froude number, particle shape, and median to fine ratio can act as a techno-economic optimisation tool in the process of particle processing/synthesis while ensuring the requisite flowability. The proposed model is valid for Geldart group C powders having a median particle size range of 5 to 80 μm and loose poured bulk density range of 275 to 525 kg/m^3. Further work will include carrying out similar experiments with a much wider range of powders with an aim to generate a more versatile relationship.

References

ASTM D7481. 2010. Standard Test Methods for Determining Loose and Tapped Bulk Densities of Powders Using a Graduated Cylinder, ASTM International, West Conshohocken, PA.

Baserinia, R., K. Brockbank, and R. Dattani. 2022. Correlating Polyamide Powder Flowability to Mechanical Properties of Parts Fabricated by Additive Manufacturing. *Powder Technology* 398: 117147.

Barjat, H., S., T. Chitu, N. Dawson, A. Farshchi, A. Ferreira, J. Gamble, et al. 2020. Demonstration of the Feasibility of Predicting the Flow of Pharmaceutically Relevant Powders from Particle and Bulk Physical Properties. *Journal of Pharmaceutical Innovation* 16: 181–196.

Beakawi Al-Hashemi, H.M., and O.S. Baghabra Al-Amoudi. 2018. A Review on the Angle of Repose of Granular Materials. *Powder Technology* 330: 397–417.

Boschini, F., V. Delaval, K. Traina, N. Vandewalle, and G. Lumay. 2015. Linking Flowability and Granulometry of Lactose Powders. *International Journal of Pharmaceutics* 494, no. 1 (October): 312–320.

Chávez Montes, B.E., J.M. Martínez-Alejo, H. Lozano-Perez, J.C. Gumy, D. Zemlyanov, and M.T. Carvajal. 2019. A Surface Characterization Platform Approach to Study Flowability of Food Powders. *Powder Technology* 357 (December): 269–280.

European pharmacopoeia 7.0, Chapter 2.9.36.: Powder flow, 2010, p. 308.

Francia, V., L.A.A. Yahia, R. Ocone, and A. Ozel. 2021. From Quasi-Static to Intermediate Regimes in Shear Cell Devices: Theory and Characterisation. *KONA Powder and Particle Journal* 38, no. September: 3–25.

Fathollahi, S., E. Faulhammer, B.J. Glasser, and J.G. Khinast. 2020. Impact of Powder Composition on Processing-Relevant Properties of Pharmaceutical Materials : An Experimental Study. *Advanced Powder Technology* 31, no. 7: 2991–3003.

Ghadiri, M., M. Pasha, W. Nan, C. Hare, V. Vivacqua, U. Zafar, S. Nezamabadi, A. Lopez, M. Pasha, and S. Nadimi. 2020. Cohesive Powder Flow: Trends and Challenges in Characterisation and Analysis. *KONA Powder and Particle Journal* 37, no. October: 3–18.

Hastie, D.B. 2015. On the Difficulties of Sampling Bulk Powder Blends in Determining Segregation Propensity — A Case Study. *Powder Technology* 286 (December): 164–171.

Janssen, P.H.M., S. Depaifve, A. Neveu, F. Francqui, and B.H.J. Dickhoff. 2021. Impact of Powder Properties on the Rheological Behavior of Excipients. *Pharmaceutics* 13, no. 8 (August 4): 1198.

Jager, P.D., T. Bramante, and P.E. Luner. 2015. Assessment of Pharmaceutical Powder Flowability Using Shear Cell-Based Methods and Application of Jenike's Methodology. *Journal of Pharmaceutical Sciences* 104, no. 11: 3804–3813.

Kalman, H. 2021. Effect of Moisture Content on Flowability: Angle of Repose, Tilting Angle, and Hausner Ratio. *Powder Technology* 393: 582–596.

Kalman, H. 2020. Role of Reynolds and Archimedes Numbers in Particle-Fluid Flows. Reviews in Chemical Engineering 38, no. 2 (February 23): 149–165.

Kissell, R., and J. Poserina. 2017. Regression Models. In *Optimal Sports Math, Statistics, and Fantasy*, 39–67. Elsevier.

Klinzing, G.E., F. Rizk, R. Marcus, and L.S. Leung. 2010. Pneumatic Conveying of Solids. Vol. 8. Particle Technology Series. Dordrecht: Springer Netherlands.

Leung, L.Y., C. Mao, L.P. Chen, and C.Y. Yang. 2016. Precision of Pharmaceutical Powder Flow Measurement Using Ring Shear Tester: High Variability Is Inherent to Powders with Low Cohesion. *Powder Technology* 301: 920–926.

Lumay, G., F. Boschini, K. Traina, S. Bontempi, J.-C. Remy, R. Cloots, and N. Vandewalle. 2012. Measuring the Flowing Properties of Powders and Grains. *Powder Technology* 224 (July): 19–27.

Marchetti, L., and C. Hulme-Smith. 2021. Flowability of Steel and Tool Steel Powders: A Comparison between Testing Methods. *Powder Technology* 384 (May): 402–413.

Mallick, S. S., P. W. Wypych. 2009. Minimum transport boundaries for pneumatic conveying of powders. Powder Technology, 194, 181–186.

Mallick, S. S. 2010. Modelling dense-phase pneumatic conveying of powders. University of Wollongong (Doctoral dissertation).

Mallick, S. S., P.W. Wypych, R. Pan. 2011. Minimum transport boundaries for dense-phase pneumatic conveying of powders. In the proceedings of Bulk Solids India Mumbai.

Mehos, G., 1971. Storage and flow of bulk solids.

Poddar, R., S.S. Mallick, and K. Lal. 2024. Reliable Pneumatic Transport of Coarse Ash in Dense-Phase by Optimally Mixing with Fine Ash. Powder Technology 442, no. May (June): 119876.

Rowe, R.C., P.J. Sheskey, and S.C. Owen. 2006. *Handbook of Pharmaceutical Excipients*. *Pharmaceutical Press and American Pharmacists Association*.

Saluja, G., S.S. Mallick, and S. Karmakar. 2023. Modeling Minimum Transport Boundary for Pneumatic Conveying of Powders. Particulate Science and Technology 1–9.

Stavrou, A.G., C. Hare, A. Hassanpour, and C.Y. Wu. 2020. Investigation of Powder Flowability at Low Stresses: Influence of Particle Size and Size Distribution. *Powder Technology* 364: 98–114.

Shi, H., G. Lumay, and S. Luding. 2020. Stretching the Limits of Dynamic and Quasi-Static Flow Testing on Cohesive Limestone Powders. *Powder Technology* 367 (May): 183–191.

Sun, C.C. 2016. Quantifying Effects of Moisture Content on Flow Properties of Microcrystalline Cellulose Using a Ring Shear Tester. *Powder Technology* 289: 104–108.

Schulze, D. 2008. Powders and Bulk Solids. *Chemie Ingenieur Technik* 82, no. 4 (April): 553–554.

Shah, K.R., S.I. Farag Badawy, M.M. Szemraj, D.B. Gray, and M.A. Hussain. 2007. Assessment of Segregation Potential of Powder Blends. *Pharmaceutical Development and Technology* 12, no. 5 (January 7): 457–462.

Tan, Y., J. Zhang, X. Li, Y. Xu, and C.Y. Wu. 2021. Comprehensive Evaluation of Powder Flowability for Additive Manufacturing Using Principal Component Analysis. *Powder Technology* 393: 154–164.

Tinke, A.P., R. Govoreanu, I. Weuts, K. Vanhoutte, and D. De Smaele. 2009. A Review of Underlying Fundamentals in a Wet Dispersion Size Analysis of Powders. *Powder Technology* 196, no. 2: 102–114.

Wang, C., Z. Wang, A. Friedrich, and C.C. Sun. 2022. Effect of Deaeration on Processability of Poorly Flowing Powders by Roller Compaction. *International Journal of Pharmaceutics* 621, no. January: 121803.

Ward, T., and W. Hourigan. 2012. Granular Segregation in a Tilted-Rotating Drum. *Powder Technology* 215–216: 227–234.

Yablokova, G., M. Speirs, J. Van Humbeeck, J.-P. Kruth, J. Schrooten, R. Cloots, F. Boschini, G. Lumay, and J. Luyten. 2015. Rheological Behavior of β-Ti and NiTi Powders Produced by Atomization for SLM Production of Open Porous Orthopedic Implants. *Powder Technology* 283 (October): 199–209.

Yu, W., K. Muteki, L. Zhang, and G. Kim. 2011. Prediction of Bulk Powder Flow Performance Using Comprehensive Particle Size and Particle Shape Distributions. *Journal of Pharmaceutical Sciences* 10, no. 1: 284–293.

CHAPTER 5

Spherical-Shaped Geldart Group A to B Borderline Powders

5.1 Introduction

This chapter provides an account of the initial work carried out in this thesis towards modelling sifting and fluidising segregation. It was considered that a prudent approach would be to start with particles that are mostly spherical (this chapter), and subsequently, models could be generated for non-spherical particles (next chapter). Fly ash has been chosen as a material for study in this chapter, fly ash being spherical. The other reason being, fly ash is a bulk solids which has a large significance in India, Indian power stations being most coal based and Indian ash having high ash content (typically 35-45%). Moreover, fly ash is a rather problematic material to be handled due to its Group A to B borderline characteristics (Wattimena et al., 2017; Wang et al., 2022; Cho et al., 1999; Xing et al., 2019). Globally, coal-fired thermal power plants generate about 500 million tonnes of coal fly ash annually, making it one of the largest producers of industrial waste products (Xing et al., 2019; Miller, 2005). Coal fly ash is defined (ASTM standard C618, 2015) as the finely dispersed by-product substance produced after burning the crushed or pulverised coal and carried by flue gases. Coal fly ash is generally separated from the flue gas flow and collected in the electrostatic precipitator (ESP) hoppers, economiser hoppers and air-preheater/duct hoppers. A pneumatic conveying system transfers the fly ash from each hopper to fly ash silos for storage and further utilisation (Stange, 1985 (a); Stange, 1985 (b)). Significant progress has been made in recent years to effectively use coal ash in construction industries by replacing a part of cement due to its pozzolanic properties (Fernández Jiménez et al., 2003; Kazys et al., 2021; Wattimena et al., 2017; Lanzerstorfer, 2018). Coal fly ash mainly comprises spherical particles ranging from less than 1 μm to 600 μm (Kazys et al., 2021; Snellings et al., 2021). The chemical composition and physical characteristics of fly ash may vary significantly for different power plants and even within the same power plant, depending on the field of ESP from where the ash has been collected (Antoni et al., 2017; Kiattikomol et al., 2001). This is due to the variations in the source of coal, milling characteristics and performance of the electrostatic precipitator field. Due to the differences in the particle and bulk properties (in terms of size, shape, bulk density etc.), it is possible to have content inhomogeneity of fly ash during the discharge from silo/hopper because of sifting segregation (Marucci et al., 2018; Hogg, 2009; Engblom et al., 2012 (a)). Sifting segregation is typically associated with flow through hoppers, where the smaller particles tend to built-up in the centre region of the heap, and bigger particles shift to the bottom of the heap of the bulk solids (Ketterhagen et al., 2007; Marucci et al., 2018). As a result, during discharge from the hopper, the finer particles flow out first, followed by the bigger particles (Shah et al., 2007; Schulze, 2008). This would result in content inhomogeneity of bulk solids being discharged from the hopper. Loading fly ash in silos is typically done using pneumatic conveying pipelines terminating

at the top of the silo, from where the ash particles drop towards the bottom of the silo. Due to the differences in terminal settling velocities, coarse and/or heavy particles (i.e. particles typically with larger free terminal settling velocities ranging from 100 to 300 mm/s) settle down faster. In contrast, the finer particles (with lower terminal settling velocities below 50 mm/s) will remain suspended in the air and require a long time to settle. This would cause non-uniform distribution of fines and coarse particles inside large silos, with fine particles settling over a layer of coarse particles (Engblom et al., 2012 (a); Schulze 2008; Engblom et al., 2012 (d)). This is known as fluidisation segregation (Tang et al., 2004). It must be highlighted that the difference in settling duration, the extent of inhomogeneity and the resulting segregation would be more magnified in the case of large/tall silos due to their height (Engblom et al., 2012 (a); Engblom et al., 2012 (c)). In case there is a horizontal entry of particles to the silo, the different trajectories experienced by coarse and fine particles caused by the differences in their kinetic inertia and air resistance acting on them would cause the coarser particles to travel more compared to the fines, thus causing segregation of the bulk to be coarse and fine powder zones (Schulze, 2008; Tang et al., 2004). Another type of air-induced segregation can occur due to the supply of fluidisation air to silos or hoppers to ensure the powders are in the required flowability state and reduce the chances of flow blockages (arching/rat-holing). It is a common practice to provide a fluidisation pad at the bottom of industrial hoppers and silos (Alkassar et al., 2021; Schulze, 2008). Such type of air supply, especially if excessive, can potentially affect a substantial amount of particle movement. Fine particles can get relatively more entrained than coarser particles. Also, the fine particles will take longer to settle down than the coarser particles (Schulze, 2008; Gernon et al., 2012). As a result, the coarser particles are likely to get settled at the bottom and on top of it, the fine powders will get settled, therefore creating segregated layers of coarse and fine powders (Jaklič et al., 2015; Schulze, 2008). To explore the segregation tendency of particles, a bench-scale fluidisation segregation tester (ASTM Standard D 6941, 2012) and a sifting segregation tester (ASTM Standard D6940, 2010) are often used (Marucci et al., 2018; Ketterhagen et al., 2007; Oka et al., 2017; Shah et al., 2007; Deng et al., 2010). Very few studies have reported the combined impact of segregation mechanisms (i.e., sifting and fluidisation) by which segregation occurs (He et al., 2013) using ASTM standard test setups. Study of segregation behaviour for coarse particles (Geldart Group B or D) (Devriendt et al., 2013; Shinohara et al., 2002; Fry et al., 2020; Oka et al., 2017; Tang et al., 2005; Jha et al., 2008; Tang et al., 2007; Jha et al., 2010; Jha et al., 2011) have generally gained more attention and compared to that for the fines (Geldart Group A) (Deng et al., 2010; Engblom et al., 2012 (b); Engblom et al., 2012 (d); Engblom et al., 2012 (a); He et al., 2013; Hastie, 2015; Jaklič et al., 2015) as the fines are known to be more cohesive, thus naturally inhibiting relative displacement between the particles (and thus suppressing segregation tendencies). This study

investigates into the segregation characteristics of powders which are in borderline between the Geldart Group A to B materials. These powders (typically varying in the 75 to 125 μm range) can often be unpredictable flow behaviour (Devriendt et al., 2013; Shinohara et al., 2002; Fry et al., 2020; Oka et al., 2017; Tang et al., 2005; Jha et al., 2008; Tang et al., 2007; Jha et al., 2010; Jha et al., 2011; Deng et al., 2010; Engblom et al., 2012 (b); Engblom et al., 2012 (d); Engblom et al., 2012 (a); He et al., 2013; Hastie, 2015; Jaklič et al., 2015). A new model has been developed for the segregation of powder linking the same with their flow properties of powders (Geldart Group A to B materials). In the understanding of the author, very limited experimental data for segregation characteristics of powders are available in this size range (Geldart Group A to B borderline) and there seems to be no other available model linking powder segregation to its flow properties.

5.2 Physical and flow properties of fly ash

Figure 5.1 shows the SEM image of fly ash samples 'A' to 'F'. It can be seen from the SEM images in Figure 5.1 that most of the fly ash samples have provided similar and spherical shapes (with a small presence of irregular shaped particles). In the current study, fine ash refers to an ash sample with a median size of less than 100 μm, and coarse ash refers to that having a median size equal to and above 100 μm. Table 5.1 provides results for the physical properties of the powder samples. Results show median sizes, loose poured bulk densities, and particle densities have varied from 68 to 141 μm, 648 to 1096 kg/m^3 and 1523 to 1761 kg/m^3, respectively. Particle size and loose poured bulk densities have varied by factors of 2.07 and 1.69, respectively, which were considered to be considerable to demonstrate differences in segregation characteristics. Also, whereas sample 'A' (finest ash) has a coarse-to-fine ratio of 12.53, the same for sample F (the coarsest ash) is 4.81. The angle of repose for the fine ash (sample A) and coarse ash (sample F) were 55° and 38°, respectively. Figure 5.2 shows the images for the angle of repose that consists of the actual powder heap formed (blue in colour) on a base and the isosceles triangle-shaped heap formed by software (red in colour). The angle of repose is the angle of sides with the base of an isosceles triangle in the projected image of the powder heap. It can also be seen that the ash samples with more fines provide larger values of angle of repose and non-uniform heap, possibly indicating poor flowability and higher cohesion.

Table 5.1: Physical properties of fly ash samples

Fly ash sample	**Particle size (μm)**			d_{90}/d_{10}	ρ_{lb} (kg/m^3)	ρ_p (kg/m^3)	**Geldart group**	**AOR (˚)**
	d_{10}	d_{50}	d_{90}					
A	15	68	188	12.53	744	1761	A borderline	55
B	29	85	231	7.97	1096	1750	A borderline	51
C	35	97	254	7.26	648	1605	A borderline	47
D	32	102	254	7.94	853	1653	A borderline	46
E	38	105	268	7.05	643	1523	A borderline	46
F	57	141	274	4.81	860	1575	A borderline	38

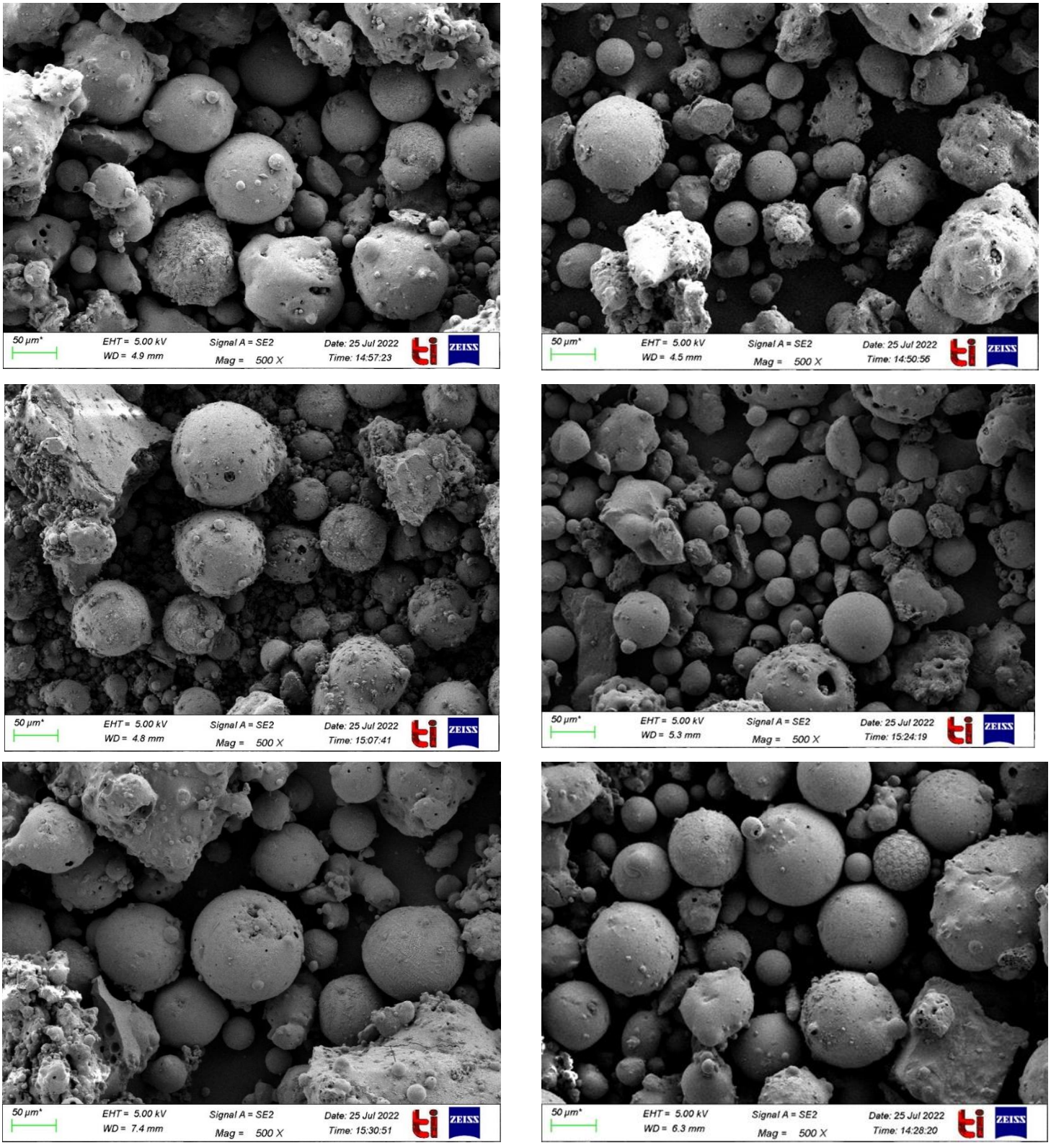

Figure 5.1: SEM images of fly ash samples

(The top and the left image is of sample A; the bottom and the right image is of sample F)

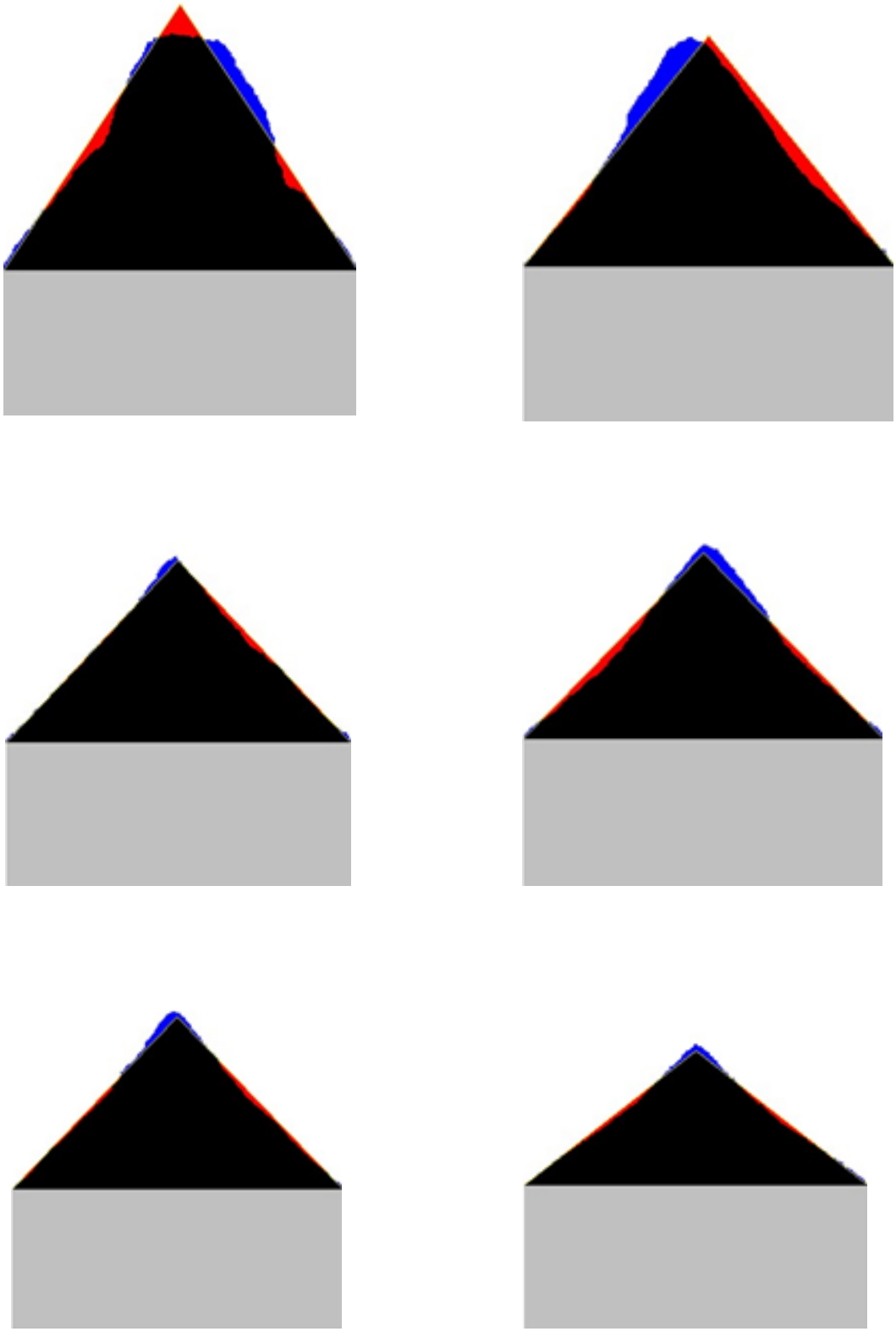

Figure 5.2: Heap images of fly ash samples

(The top and the left image is of sample A; the bottom and the right image is of sample F)

Figures 5.3 and 5.4 show the flow function and cohesion values for the six fly ash samples. All the samples were found to be in an easy-flowing to a free-flowing zone. With the increase in particle size, the powders generally have shown to be getting more free-flowing with reduced cohesion. With an increase in particle size, the specific surface area of each particle tends to decrease. This reduction means there are fewer surface interactions for the particles, resulting in reduced friction and enhanced flowability. As a result, gravity forces become more dominant over particle-particle and particle-wall forces such as electrostatic, air drag, capillary forces from surface tension, mechanical, van de Waals forces, wall friction, etc. (Tang et al., 2004). Cohesion values increase in a linear trend with increasing stress for all samples, indicating enhanced interaction between particles under load. Cohesion is a measure of the internal forces that hold the particles together, important for assessing stability under compression. Larger particle sizes generally exhibit lower cohesion due to reduced contact points and effective surface area. As particle size affects the interlocking of particles under stress, larger particle sizes reduce the cohesive forces acting between them.

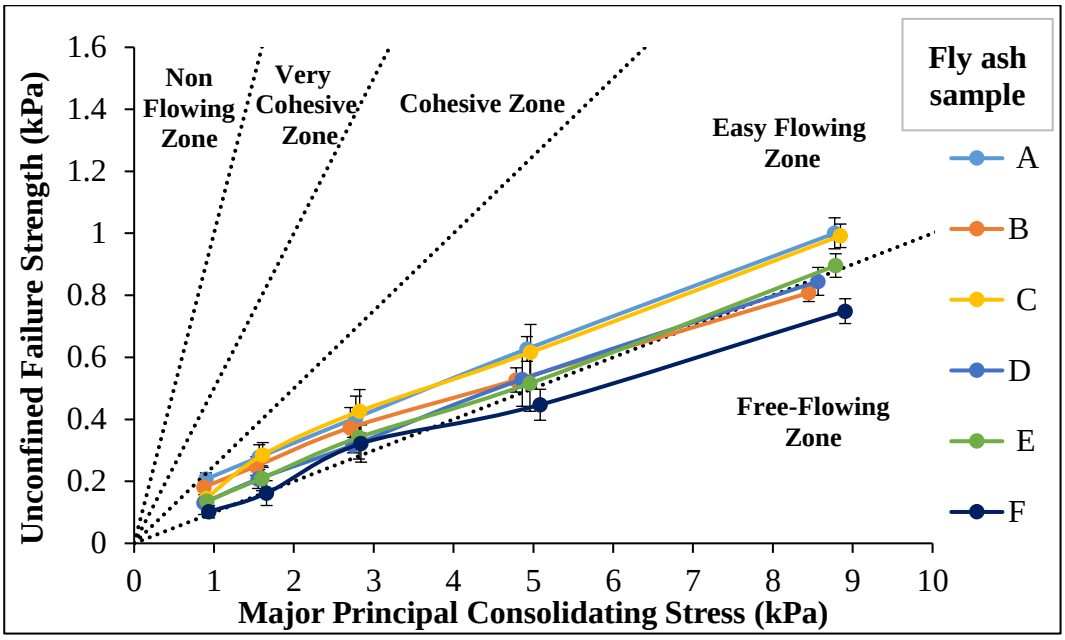

Figure 5.3: Flow function curve for fly ash samples

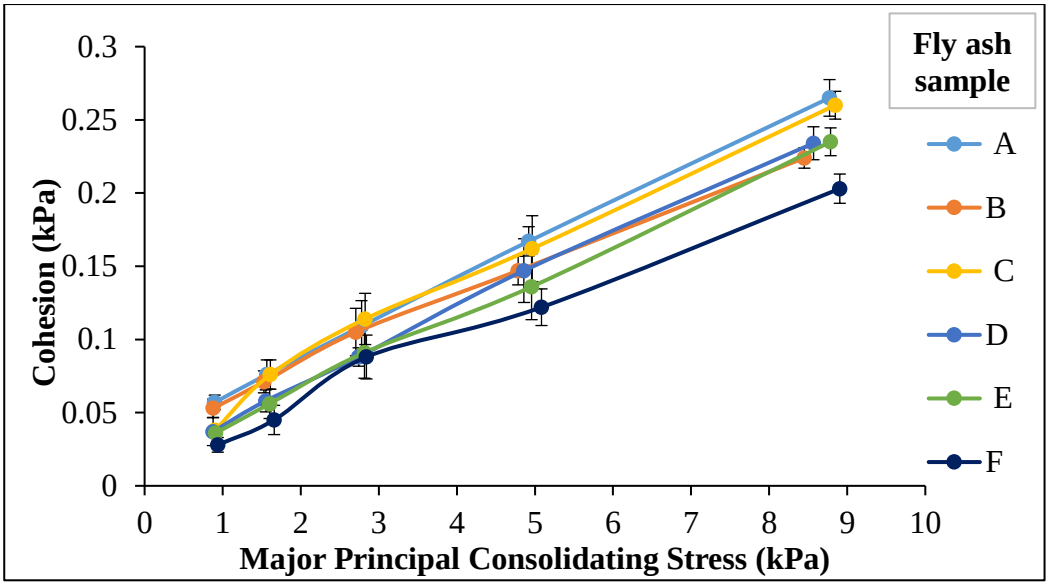

Figure 5.4: Cohesion values for fly ash samples

5.3 Assessment of segregation behaviour

A segregation index is a dimensionless number that indicates the degree of content inhomogeneity between separated samples in comparison to a homogenous powder sample (Deng et al., 2021; Oka et al., 2017). Researchers have developed various indices based on the ratio of the last to the first segregated sample's fine mass fraction (Marucci et al., 2018), the standard deviation of the normalised fine mass fraction (Ketterhagen et al., 2007), the relative standard deviation (Oka et al., 2017; Shah et al., 2007), the potency range (Shah et al., 2007), and a chemical characteristic of the segregated samples (Deng et al., 2010; He et al., 2013) to assess the segregation tendencies of bulk solids. In this study, the segregation index is based on the first (or top) and last (or bottom) batches retrieved after the segregation tests (as explained in the experimental section). Figures 5.5 and 5.6 show the comparison of the fineness of ash samples and their loose poured bulk densities between the first and last batch in case of sifting segregation. The results show that the first batches for all the fly ash samples (A to F) have a higher percentage of fines than the last batches. Also, it can be seen that the first batch samples are heavier (represented by higher loose poured bulk density values) than the last batch. This further confirms the occurrence of sifting segregation due to which the fines have descended down to occupy the spaces between the coarse particles. These results indicate that in practical hopper flow cases (occurring under gravity), on opening the discharge valve at the bottom of the hopper, the first lot of bulk powders would have more fines (but will be heavy) as compared to the last lot of bulk powders which would be more coarser (but lighter). Such segregated powder

layers (caused by sifting segregation) could result in differences in subsequent powder handling characteristics.

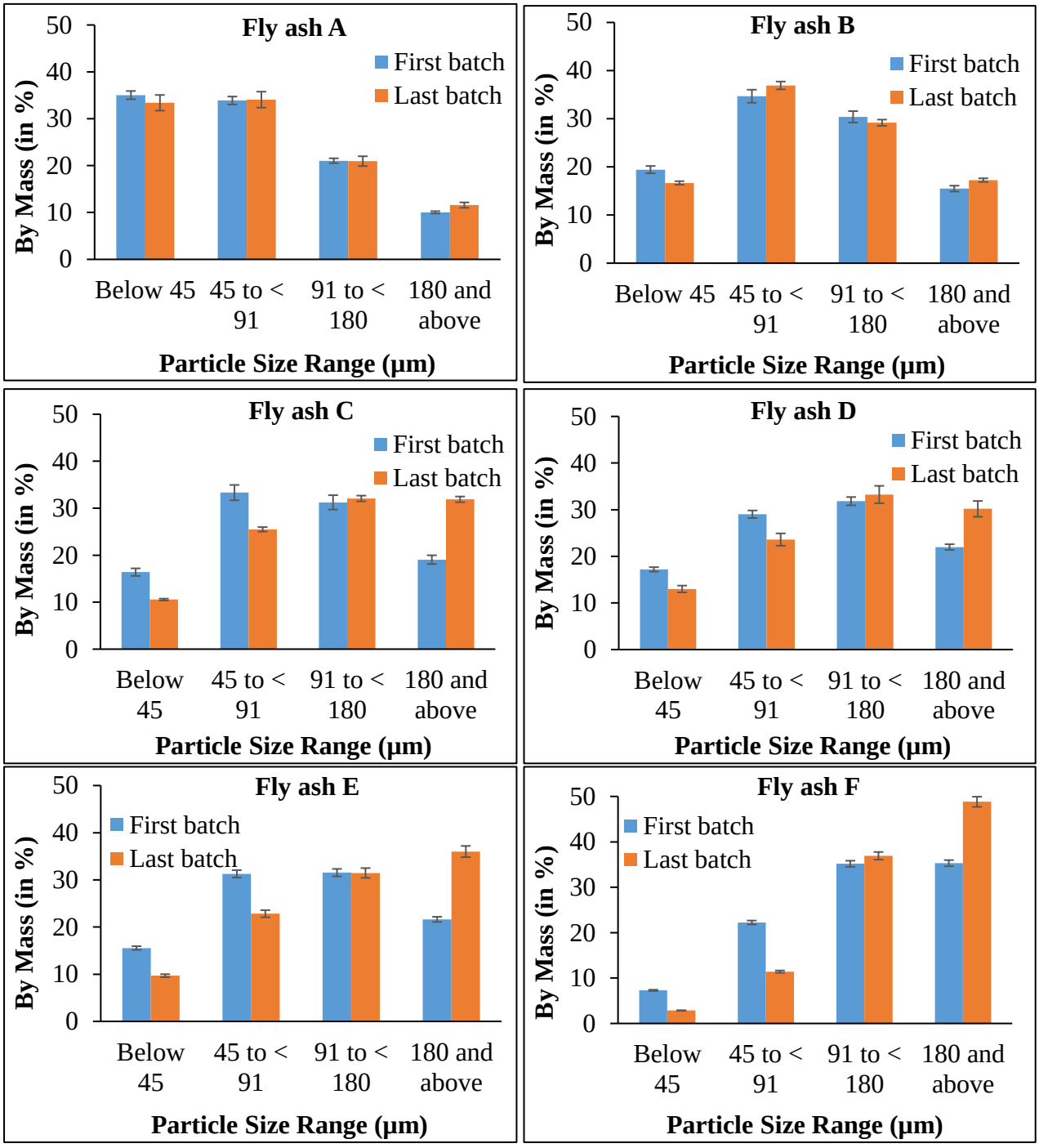

Figure 5.5: Comparison of fineness of fly ash sample between first and last batch (sifting segregation)

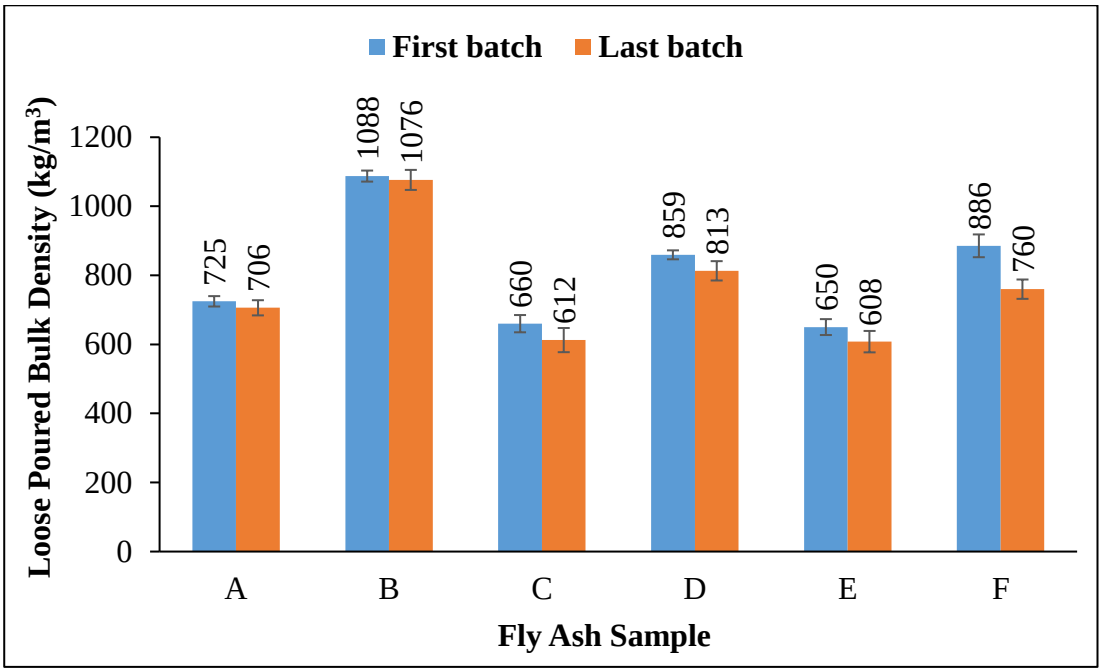

Figure 5.6: Comparison of loose poured bulk densities of ash between first and last batch (sifting segregation)

Figures 5.7 and 5.8 show the comparison of the fineness of powders and their loose poured bulk densities between the top and bottom batches in case of fluidisation segregation. The results show that the top batches for all the fly ash samples (A to F) had higher fines than the bottom batches. Also, it can be seen that the top samples were heavier (represented by higher loose poured bulk density values) than the bottom samples. This further confirms the occurrence of fluidisation segregation in which the fine powders moved upwards to occupy the spaces between the coarse particles. These results indicate that in cases of fluidising of powders in practical hoppers (e.g. for hopper aeration), the bulk powders would get segregated with the top layer having more fines (but will be heavy) as compared to the bottom lot of bulk powders which would be coarser (but lighter). Such segregated powder layers (caused by fluidisation segregation) could result in differences in subsequent powder conveying or flow behaviour.

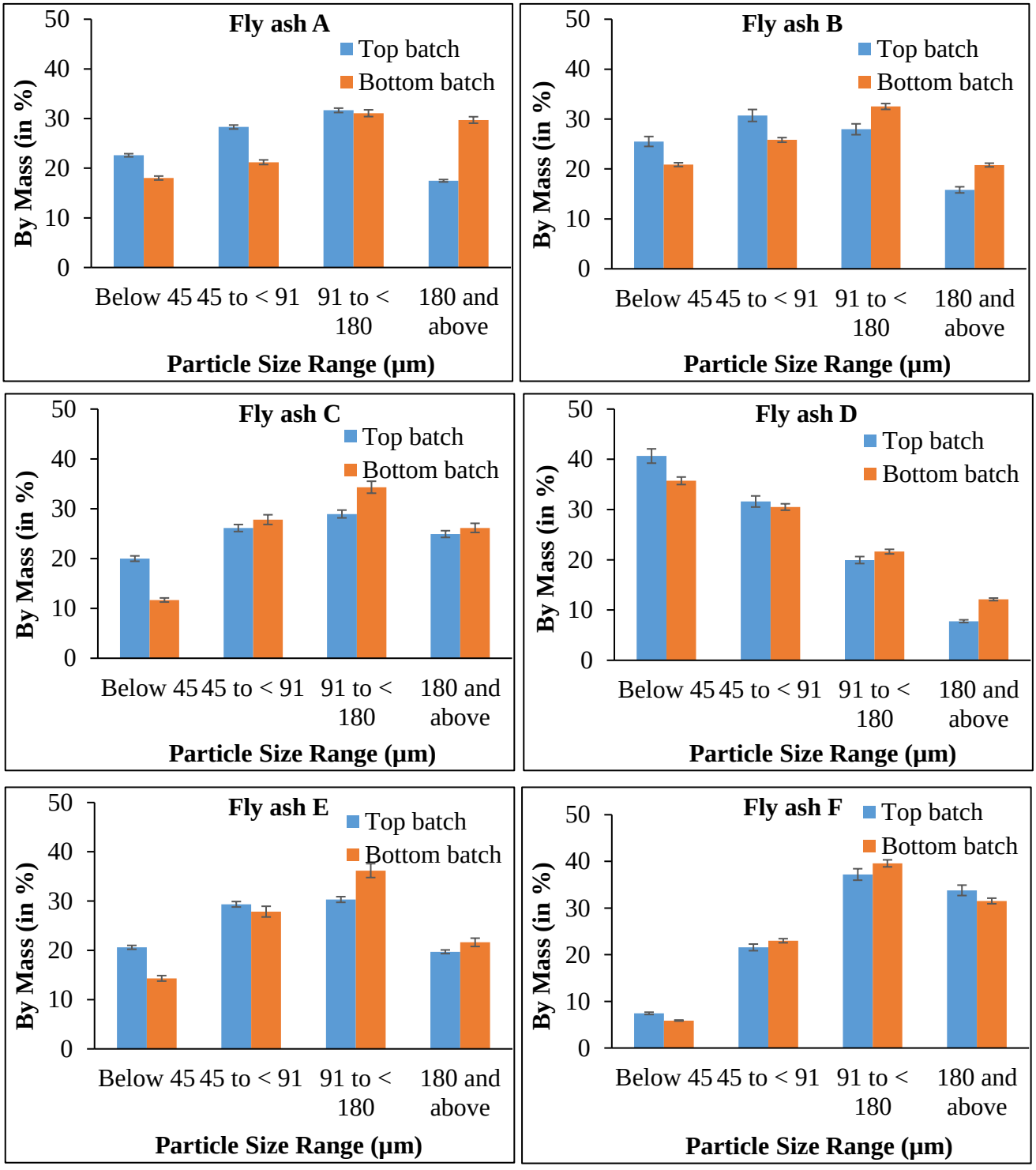

Figure 5.7: Comparison of fineness of ash between the top and bottom batch (fluidisation segregation)

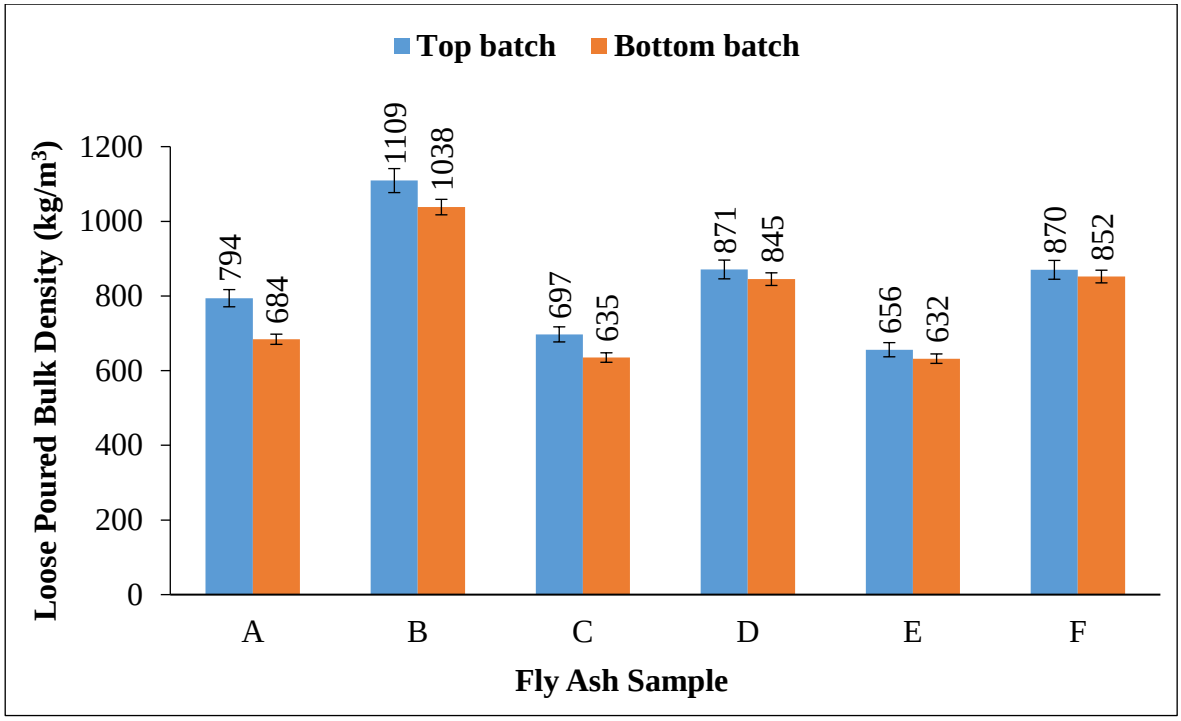

Figure 5.8: Comparison of loose poured bulk densities of ash between top and bottom batch (fluidisation segregation)

5.4 Segregation index

The sifting segregation index, $I_{SS(k)}$, is defined as the ratio of mass content (%) difference between the first and last batch to the average of mass content (%) in the first and last batch in the particle size range of 'k'. The fluidisation segregation index, $I_{FS(k)}$, is defined as the ratio of the difference of mass content (%) between the top and bottom batch to the average of mass content (%) in the top and bottom batch in the particle size range of 'k' (Deng et al., 2021; Behjani, 2018).

For sifting segregation (based on fineness), the segregation index is defined as:

$$I_{SS(k)} = 2\left(\frac{C_L - C_F}{C_L + C_F}\right)_k \tag{5.1}$$

where C_L and C_F denote the mass content (in %) of the last batch and first batch, respectively, in the particle size range of 'k'.

For fluidisation segregation (based on fineness), the segregation index is defined as:

$$I_{FS(k)} = 2\left(\frac{C_B - C_T}{C_B + C_T}\right)_k \quad (5.2)$$

where C_B and C_T denote the mass content (in %) of the bottom sample and top batch, respectively, in the particle size range of 'k'. The mean segregation Index, $\overline{I_S}$, is defined as the sum of segregation index values for the entire size range.

$$\overline{I_S} = \frac{1}{n}\sum_n | I_{S(k)} | \quad (5.3)$$

In this study, particle size ranges are: below 45, 45 to < 91, 91 to < 180 and 180 and above (in μm). The mean segregation index for sifting and fluidisation segregation index is denoted as $\bar{I}_{SS}$ and $\bar{I}_{FS}$, respectively. The values of the mean segregation index for sifting and fluidisation segregation for the fly ash samples are provided in Table 5.2 for the entire range of sizes as well as for mass percentages up to 45 μm range. The (-) sign in $I_{SS(45)}$ and $I_{FS(45)}$ indicate that in sifting segregation, the finer particles tend to built-up in the centre region of the heap in the hopper of lower assembly, which comes out first. In fluidisation segregation, the (-) sign in $I_{SS(45)}$ and $I_{FS(45)}$ indicate that the finer particles moved upwards and got accumulated on the top layer of a powder bed.

Table 5.2: Sifting and fluidisation segregation index for ash samples

Fly ash sample	**d_{50} (μm)**	**ρ_b (kg/m^3)**	**ρ_p (kg/m^3)**	**V (m/s)**	**$\bar{I}_{SS}$ (%)**	**$\bar{I}_{FS}$ (%)**	**$I_{SS(45)}$ (%)**	**$I_{FS(45)}$ (%)**
A	68	744	1761	0.015	5.03	26.25	-4.80	-22.55
B	85	1096	1750	0.015	9.11	19.9	-15.38	-20.01
C	97	648	1605	0.017	30.74	20.14	-43.36	-52.42
D	102	853	1653	0.018	21.10	17.05	-27.87	-12.90
E	105	643	1523	0.022	31.95	17.04	-46.44	-36.01
F	141	860	1575	0.028	47.24	10.68	-87.53	-23.08

For sifting segregation, the relative movement amongst the powders under gravity has been considered to be a key contributor. The movement of smaller particles through the voids of coarser particles is expected to depend on the relative flowability of particles. Particles which are either cohesive or fibrous or have rough surface texture would not promote free movement and would, therefore, suppress segregation (Fan et al., 2017; Schulze, 2008). On the contrary, naturally free-flowing particles (possibly due to a combination of less cohesion and/or spherical shape) would be

expected to exhibit enhanced segregation tendencies (Lumay et al., 2013; Behjani, 2018). Therefore, powder flowability would be an essential property contributing to sifting segregation tendencies. In view of this, the material flow function (1/ffc) has been included in representing sifting segregation in this study. The angle of repose (AOR) has been used in several studies as an indicator of flowability (Han et al., 2013). The lower value of the angle of repose indicates the powders are easy to flow (Beakawi Al-Hashemi et al., 2018; Behjani, 2018). Since better powder flowability would cause enhanced segregation tendencies under gravity and the angle of repose is an indicator of flowability; hence the angle of repose has also been used in this study to represent sifting segregation tendencies.

The leading cause of fluidisation segregation (also called air-induced segregation) is due to the differences in upper and lower particle size (in terms of d_{10} and d_{90}) and/or particle density that can cause the particles to remain suspended in the air for different periods of time while filling a silo/bin from the top, and ultimately, they settle down at different rates causing segregated settlement (Tang et al., 2004; Schulze, 2008). Thus, wide particle size distribution and a higher ratio of w_{fo90} to w_{fo10} (i.e., the ratio of terminal settling velocities for coarse and fine particles) cause a greater chance of powder segregation due to the effect of fluidisation. The steady-state settlement of a particle in still air under gravity is referred to as the particle settling velocity (Kalman, 2022) or the terminal settling velocity, which decreases significantly with decreasing particle size (below 100 µm) and particle density (Schulze, 2008). Therefore, the wfo_{90} to wfo_{10} ratio has been included in this study as a parameter to represent fluidisation segregation. The steady-state settlement of a particle in still air under gravity is referred to as the particle settling velocity (Kalman 2022) or the terminal settling velocity, which decreases significantly with decreasing particle size (below 100 µm) and particle density (Schulze 2008). It has been considered that it would be an oversimplification in the first place to assume that all the particles exist separately (i.e. without agglomeration) and that each of the particles gets individually suspended or entrained when subjected to airflow. Under the actual condition, it is quite likely that the particles would be sticking together due to cohesion and being together, the particles are not subjected to air entrainment and differential rate of settlement (Deng et al., 2010; Jaklič et al., 2015). Thus, cohesion would restrict fluidisation segregation at the first place. Therefore, cohesion (C) has been included in this study as a parameter to represent fluidisation segregation. To predict the surface energy for particles, few researchers (Behjani et al., 2017 (a); Behjani et al., 2017 (b)) have utilised a dimensionless cohesion number (Coh). In order to represent cohesion, a modified dimensionless number based on the ratio of strength required to break the bond between the particles due to cohesion to the dynamic pressure of air has been used in this study and is represented as a modified cohesion number (Coh*).

$$Coh^* = {C}/{\frac{1}{2}\rho V^2} \quad (5.4)$$

Where C, ρ and V are the parameters represented as cohesion, air density, and superficial air velocity, respectively. The superficial air velocity was calculated using the average velocity derived from the high and low flow rates observed during the pilot experiment of the fluidisation segregation test for powder sample A to F.

Table 5.3 provides the values of model parameters for sifting and fluidisation segregation.

Table 5.3: Estimated values of model parameters

Fly ash sample	**AOR (°)**	**1/ffc**	**Coh***	$\mathbf{wfo_{90}/wfo_{10}}$	$\mathbf{d_{90}/d_{10}}$
A	55	0.23	311863	187	12.53
B	51	0.21	298517	70.25	7.97
C	47	0.16	153618	52	7.26
D	46	0.15	99728	64.20	7.94
E	46	0.15	56261	47	7.05
F	38	0.11	35542	23.73	4.81

Figure 5.9 collectively demonstrates the different properties that influence segregation characteristics through sifting and fluidisation mechanisms. In sifting segregation, an increase in the coarse-to-fine ratio (d_{90}/d_{10}) results in a notable decrease in segregation. This is because larger coarse particles reduce the ability of fine particles to percolate through the voids, thereby limiting vertical movement and segregation. Similarly, as the material flow function (1/ffc) increases, indicating poorer flowability, sifting segregation is further suppressed. This occurs because cohesive or poorly flowing materials restrict individual particle motion, reducing the likelihood of separation based on size. In contrast, fluidisation segregation behaves differently. As the course-to-fine ratio (d_{90}/d_{10}) increases, fluidisation segregation also rises due to enhanced differences in terminal velocities, causing larger particles to settle more rapidly than finer ones during fluidisation, thus promoting separation. A similar trend is observed with the modified dimensionless cohesion number (Coh*), where increased cohesion promotes agglomeration. These agglomerates behave differently in a fluidised state, exacerbating segregation. Finally, a higher ratio of particle terminal velocities (wfo_{90}/wfo_{10}) results

in increased segregation, as notable differences in settling velocities contribute to a more distinct stratification of the particles.

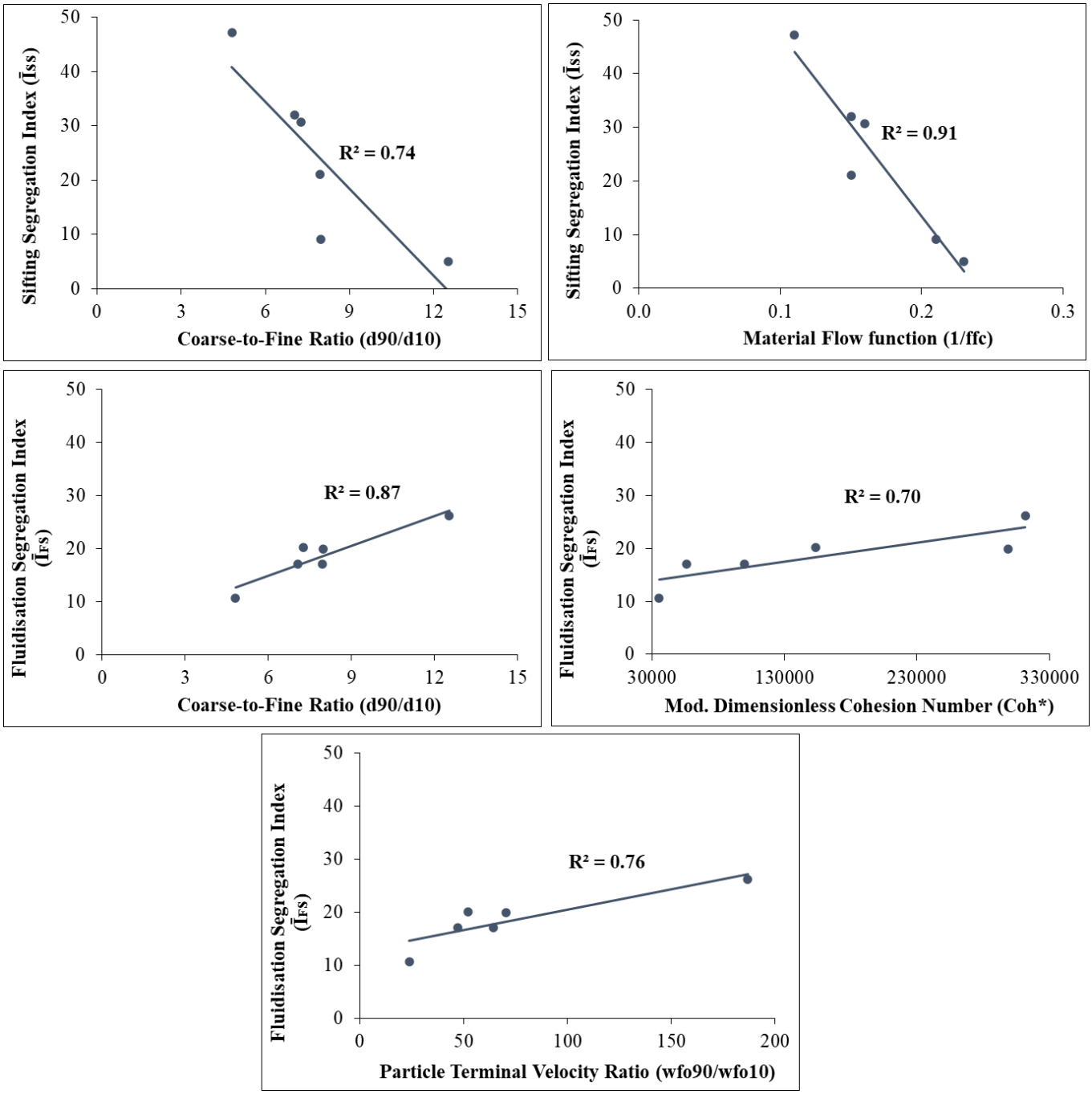

Figure 5.9: Sifting (top plots) and fluidisation (middle & bottom plots) segregation index versus different affecting parameters

The following models have been developed using the above parameters for sifting and fluidisation segregation using the linear regression method.

$$(\bar{I}_{SS})_{Predicted} = 111.3 - 1.17\,(AOR) - 189.9\,(1/ffc) \quad (5.5)$$

$$(\bar{I}_{FS})_{Predicted} = -3.48 + 1.23 \times 10^{-5}(Coh^*) - 0.09\left(\frac{wfo_{90}}{wfo_{10}}\right) + 3.33\,(d_{90}/d_{10}) \quad (5.6)$$

Figures 5.9 and 5.10 show predicted versus experimental results for the segregation index. For both sifting and fluidisation segregation, the correlation values are above 0.9, thus indicating the predicted results are a good fit for the experimental data.

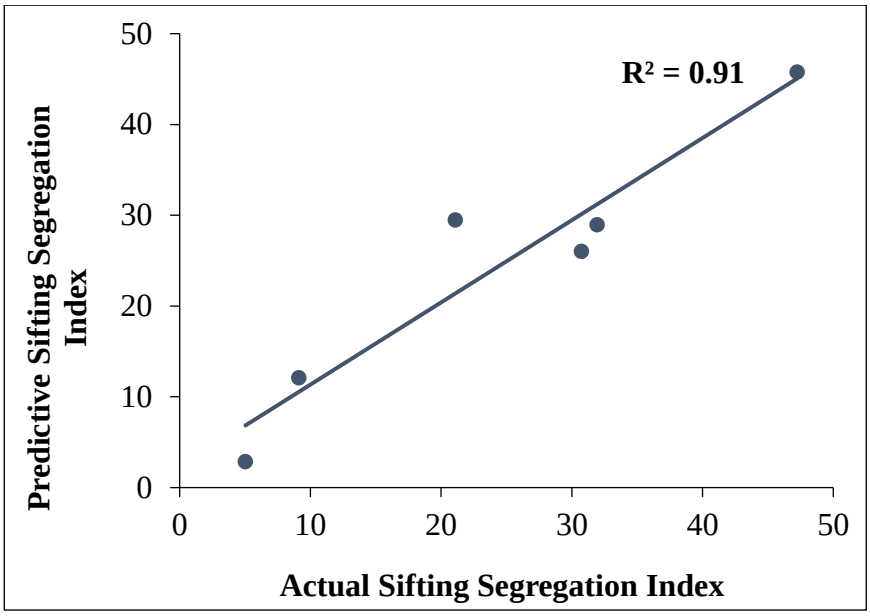

Figure 5.10: Predictive versus actual sifting segregation index

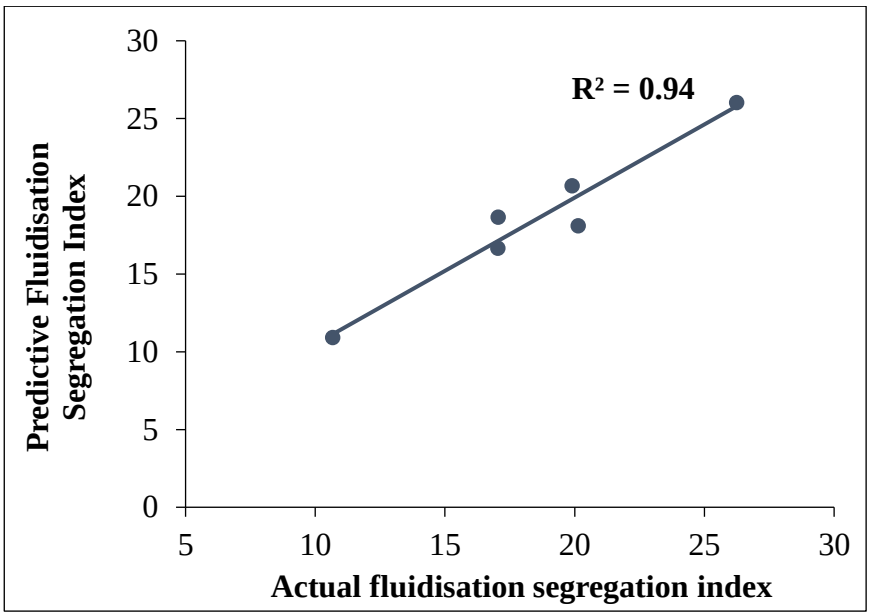

Figure 5.11: Predictive versus actual fluidisation segregation index

5.5 Conclusion

The core objective of this study is to investigate into the interdependency of particle and bulk characteristics, flow properties of fly ash samples to their sifting and fluidisation segregation indexes. By using standard testers, six different fly ash samples (particle size 'd_{50}' ranging from 68 μm to 141 μm) were tested for their morphology, characteristics and flow property test. From SEM images, it is evident that all the fly ash samples have nearly identical-spherical shapes, which could be more prone to segregate under the sifting mechanism. The angle of repose for the fine and coarse ash were 55° and 38°, which indicates poor and good flowability, respectively. The results from their sifting and fluidisation segregation characteristics have shown that with an increase in median particle size, the sifting segregation tendencies have increased and are represented by higher values of segregation indices. The first batches of all fly ash samples A to F have shown higher loose poured bulk density, thus further confirming that fine particles have occupied the interstitial spaces between coarser particles, resulting in higher packing density. The finer ash samples have provided greater fluidisation segregation tendencies than the coarser samples. This has occurred in spite of the higher value of cohesion in finer ash samples. The higher values of the fluidisation segregation index for finer ash show that the difference in particle settling velocities (which promotes segregation) dominates over the particle-particle cohesion (which suppresses segregation). In fluidisation segregation, the upper layer of powders (at the top chamber) has greater packing densities than the bottom layer (at the bottom chamber) due to the upward movement or settlement of fines on the top layer. The angle of repose and material flow function have provided a good correlation (R^2 = 0.91) for the sifting segregation index. In the case of the fluidisation segregation index, cohesion between particles, the ratio of free terminal velocities (coarse to fine) and diameters for coarse to fine particles have provided a good fit (R^2 = 0.94). The proposed model has been tested and validated at an appropriate rate of powder properties. The current study's model can be extended further to other powders, such as limestone, detergent, etc., which may have different shapes.

References

Alkassar, Y., V.K. Agarwal, R.K. Pandey, and N. Behera. 2021. Analysis of Dense Phase Pneumatic Conveying of Fly Ash Using CFD Including Particle Size Distribution. *Particulate Science and Technology* 39, no. 3 (March 4): 322–337.

Antoni, J. Satria, A. Sugiarto, and D. Hardjito. 2017. Effect of Variability of Fly Ash Obtained from the Same Source on the Characteristics of Geopolymer. *MATEC Web of Conferences* 97 (February 1): 1-6.

ASTM Standard, C618-15. 2015. Standard specification for coal fly ash and raw or calcined natural pozzolona for use in concrete, West Conshohocken, PA, USA: ASTM International (www.astm.org).

ASTM Standard, D6941-12. 2012. Standard Practice for Measuring Fluidization Segregation Tendencies of Powders, West Conshohocken, PA, USA: ASTM International (www.astm.org).

ASTM Standard, D6940-10. 2010. Standard Practice for Measuring Sifting Segregation Tendencies of Bulk Solids, West Conshohocken, PA, USA: ASTM International (www.astm.org).

ASTM Standard, D7481-10. 2010. Standard Test Methods for Determining Loose and Tapped Bulk Densities of Powders Using a Graduated Cylinder, West Conshohocken, PA, USA: ASTM International (www.astm.org).

Behjani, M.A. 2018. Numerical Simulation of Segregation of Formulated Powder Mixtures, Thesis, School of Chemical and Process Engineering, The University of Leeds, UK.

Beakawi Al-Hashemi, H.M., and O.S. Baghabra Al-Amoudi. 2018. A Review on the Angle of Repose of Granular Materials. *Powder Technology* 330: 397–417.

Behjani, M.A., A. Hassanpour, M. Ghadiri, and A. Bayly. 2017 (a). Numerical Analysis of the Effect of Particle Shape and Adhesion on the Segregation of Powder Mixtures. Ed. F. Radjai, S. Nezamabadi, S. Luding, and J.Y. Delenne. *EPJ Web of Conferences* 140 (June 30): 06024.

Behjani, M.A., N. Rahmanian, N. Fardina bt Abdul Ghani, and A. Hassanpour. 2017 (b). An Investigation on Process of Seeded Granulation in a Continuous Drum Granulator Using DEM. *Advanced Powder Technology* 28, no. 10 (October): 2456–2464.

Carr, M.J., A.W. Roberts, and C.A. Wheeler. 2019. A Revised Methodology for the Determination of Bulk Material Cohesion and Adhesion. *Advanced Powder Technology* 30, no. 10 (October 1): 2110–2116.

Cho, H.C., and J.K. Kim. 1999. Analysis on the Efficiency of the Air Classification of Fly Ash. *Geosystem Engineering* 2, no. 2: 37–42.

Deng, T., V. Garg, H. Salehi, and M.S.A. Bradley. 2021. Correlations between Segregation Intensity and Material Properties Such as Particle Sizes and Adhesions and Novel Methods for Assessment. *Powder Technology* 387 (July): 215–226.

Devriendt, L., C. Gatumel, and H. Berthiaux. 2013. Experimental Evidence of Mixture Segregation by Particle Size Distribution. *Particulate Science and Technology* 31, no. 6 (November 2): 653–657.

Deng, T., K.A. Paul, M.S.A. Bradley, L. Immins, C. Preston, J.F. Scott, and E.H. Welfare. 2010. Investigations on Air-Induced Segregation of Pharmaceutical Powders and Effect of Material Flow Functions. *Powder Technology* 203, no. 2 (November): 354–358.

Engblom, N., H. Saxén, R. Zevenhoven, H. Nylander, and G.G. Enstad. 2012 (a). Segregation of Powder Mixtures at Filling and Complete Discharge of Silos. *Powder Technology* 215–216 (January): 104–116.

Engblom, N., H. Saxén, R. Zevenhoven, H. Nylander, and G.G. Enstad. 2012 (b). Segregation of Construction Materials in Silos. Part 1: Experimental Findings on Different Scales. *Particulate Science and Technology* 30, no. 2 (March): 145–160.

Engblom, N., H. Saxén, R. Zevenhoven, H. Nylander, and G.G. Enstad. 2012 (c). Segregation of Construction Materials in Silos. Part 2: Identification of Relevant Segregation Mechanisms. *Particulate Science and Technology: An International Journal* 30, no. 2: 161–178.

Engblom, N., H. Saxén, R. Zevenhoven, H. Nylander, and G.G. Enstad. 2012 (d). Effects of Process Parameters and Hopper Angle on Segregation of Cohesive Ternary Powder Mixtures in a Small-Scale Cylindrical Silo. *Advanced Powder Technology* 23, no. 5 (September): 566–579.

Fry, A.M., V. Vidyapati, J.P. Hecht, P.B. Umbanhowar, J.M. Ottino, and R.M. Lueptow. 2020. Measuring Segregation Characteristics of Industrially Relevant Granular Mixtures: Part II – Experimental Application and Validation. *Powder Technology* 368, no. 1 (May): 278–285.

Fan, Y., K. V Jacob, B. Freireich, and R.M. Lueptow. 2017. Segregation of Granular Materials in Bounded Heap Flow: A Review. *Powder Technology* 312 (May): 67–88.

Fernández-Jiménez, A., and A. Palomo. 2003. Characterisation of Fly Ashes. Potential Reactivity as Alkaline Cements. *Fuel* 82, no. 18 (December): 2259–2265.

Gernon, T.M., and M.A. Gilbertson. 2012. Segregation of Particles in a Tapered Fluidized Bed. *Powder Technology* 231 (November): 88–101.

Hastie, D.B. 2015. On the Difficulties of Sampling Bulk Powder Blends in Determining Segregation Propensity — A Case Study. *Powder Technology* 286 (December): 164–171.

Han, X., C. Ghoroi, and R. Davé. 2013. Dry Coating of Micronized API Powders for Improved Dissolution of Directly Compacted Tablets with High Drug Loading. International Journal of Pharmaceutics 442, no. 1–2: 74–85.

He, X., X. Han, N. Ladyzhynsky, and R. Deanne. 2013. Assessing Powder Segregation Potential by near Infrared (NIR) Spectroscopy and Correlating Segregation Tendency to Tabletting Performance. *Powder Technology* 236 (February): 85–99.

Hogg, R. 2009. Mixing and Segregation in Powders: Evaluation, Mechanisms and Processes. *KONA Powder and Particle Journal* 27: 3–17.

Jaklič, M., K. Kočevar, S. Srčič, and R. Dreu. 2015. Particle Size-Based Segregation of Pharmaceutical Powders in a Vertical Chute with a Closed Bottom: An Experimental Evaluation. *Powder Technology* 278 (July): 171–180.

Jha, A.K., and V.M. Puri. 2011. Percolation Segregation in Binary Size Mixtures Under Different Shear and Intensity of Motion. *Particulate Science and Technology* 29, no. 5 (September): 481–492.

Jha, A.K., and V.M. Puri. 2010. Percolation Segregation of Multi-Size and Multi-Component Particulate Materials. *Powder Technology* 197, no. 3 (January): 274–282.

Jha, A.K., J.S. Gill, and V.M. Puri. 2008. Percolation Segregation in Binary Size Mixtures of Spherical and Angular-Shaped Particles of Different Densities. *Particulate Science and Technology* 26, no. 5 (September 29): 482–493.

Kalman, H. 2022. Role of Reynolds and Archimedes Numbers in Particle-Fluid Flows. *Reviews in Chemical Engineering* 38, no. 2 (February 23): 149–165.

Kazys, R., R. Sliteris, L. Mazeika, L. Van den Abeele, P. Nielsen, and R. Snellings. 2021. Ultrasonic Monitoring of Variations in Dust Concentration in a Powder Classifier. *Powder Technology* 381 (March): 392–400.

Ketterhagen, W.R., J.S. Curtis, C.R. Wassgren, A. Kong, P.J. Narayan, and B.C. Hancock. 2007. Granular Segregation in Discharging Cylindrical Hoppers: A Discrete Element and Experimental Study. *Chemical Engineering Science* 62, no. 22 (November): 6423–6439.

Kiattikomol, K., C. Jaturapitakkul, S. Songpiriyakij, and S. Chutubtim. 2001. A Study of Ground Coarse Fly Ashes with Different Finenesses from Various Sources as Pozzolanic Materials. *Cement and Concrete Composites* 23, no. 4–5 (August): 335–343.

Lanzerstorfer, C. 2018. Fly Ash from Coal Combustion: Dependence of the Concentration of Various Elements on the Particle Size. *Fuel* 228, no. March (September): 263–271.

Lumay, G., F. Boschini, R. Cloots, and N. Vandewalle. 2013. Cascade of Granular Flows for Characterizing Segregation. *Powder Technology* 234 (January): 32–36.

Lumay, G., F. Boschini, K. Traina, S. Bontempi, J.-C. Remy, R. Cloots, and N. Vandewalle. 2012. Measuring the Flowing Properties of Powders and Grains. *Powder Technology* 224 (July): 19–27.

Marucci, M., B. Al-saaigh, C. Boissier, M. Wahlgren, and H. Wikström. 2018. Sifting Segregation of Ideal Blends in a Two-Hopper Tester: Segregation pro Files and Segregation Magnitudes. *Powder Technology* 331: 60–67.

Miller, B. G. 2005. CHAPTER 3 - The Effect of Coal Usage on Human Health and the Environment. *in Coal Energy Systems, ed. B. G. Miller (Burlington: Academic Press)*: 77–122.

Oka, S., A. Sahay, W. Meng, and F. Muzzio. 2017. Diminished Segregation in Continuous Powder Mixing. *Powder Technology* 309 (March): 79–88.

Snellings, R., H. Kazemi-Kamyab, P. Nielsen, and L. Van den Abeele. 2021. Classification and Milling Increase Fly Ash Pozzolanic Reactivity. *Frontiers in Built Environment* 7, no. April (April 12): 1–13.

Schulze, D. 2008. Powders and Bulk Solids. *Chemie Ingenieur Technik* 82, no. 4 (April): 553–554.

Shah, K.R., S.I. Farag Badawy, M.M. Szemraj, D.B. Gray, and M.A. Hussain. 2007. Assessment of Segregation Potential of Powder Blends. *Pharmaceutical Development and Technology* 12, no. 5 (January 7): 457–462.

Shinohara, K., and B. Golman. 2002. Segregation Indices of Multi-Sized Particle Mixtures during the Filling of a Two-Dimensional Hopper. *Advanced Powder Technology* 13, no. 1: 93–107.

Stange, K. 1985 (a). Pneumech silo-solution for large-scale and long-term storage of fly ash. *Bulk Solids Handling (Germany, Federal Republic of)* 5(2): 407-416.

Stange, K. 1985 (b). Silo storage of fly ash in power stations and in the cement industry. *Bulk Solids Handling (Germany, Federal Republic of)* 5(5): 997-1006.

Tang, P., and V.M. Puri. 2007. Segregation Quantification of Two-Component Particulate Mixtures: Effect of Particle Size, Density, Shape, and Surface Texture. *Particulate Science and Technology* 25, no. 6 (December 5): 571–588.

Tang, P., and V.M. Puri. 2005. An Innovative Device for Quantification of Percolation and Sieving Segregation Patterns–Single Component and Multiple Size Fractions. *Particulate Science and Technology* 23, no. 4 (October): 335–350.

Tang, P., and V.M. Puri. 2004. Methods for Minimising Segregation: A Review. *Particulate Science and Technology* 22, no. 4 (October): 321–337.

Wang, J., X. Cai, Y. Guo, and L. Jiang. 2022. Problem Analysis and Operation Evaluation of Dry Ash Removal System in Coal-Fired Power Plant. In *2022 2nd International Conference on Bioinformatics and Intelligent Computing*, 285–288. New York, NY, USA: ACM.

Wattimena, O.K., Antoni, and D. Hardjito. 2017. A Review on the Effect of Fly Ash Characteristics and Their Variations on the Synthesis of Fly Ash Based Geopolymer. In *AIP Conference Proceedings*, 1887:1–12.

Xing, Y., F. Guo, M. Xu, X. Gui, H. Li, G. Li, Y. Xia, and H. Han. 2019. Separation of Unburned Carbon from Coal Fly Ash: A Review. *Powder Technology* 353 (July): 372–384.

CHAPTER 6

Modelling Segregation Index of Powders

6.1 Introduction

Powders are essential in many industries, serving pivotal roles in pharmaceuticals, food processing, construction, cosmetics, manufacturing, etc. The effectiveness of these industries relies largely on understanding the intricate behaviours of powders, particularly concerning their segregation and flow characteristics (Zinatlou et al., 2024; Thomas et al., 2024; Liu et al. 2023; Schulze, 2008). Segregation, the separation of components within a particulate mixture due to variations in its physical, fluid and flow attributes, poses a significant challenge throughout the handling, processing, manufacturing, and storage of powdered materials. This phenomenon is driven by forces such as gravity, vibration, and shear and demonstrates as one component migrating away from the other, impacting product quality and process reliability (Schulze, 2008; Tang et al., 2004). Segregation may be desirable in certain separation processes, but it often compromises of the quality of the final product or poses safety risks (Ansari et al., 2023; Johanson et al., 2014). Two primary strategies are often employed to reduce segregation issues: 1) optimising processing equipment and 2) modifying powder materials. The former involves continuous powder material processing using lesser number of handling devices, while the later involves altering the powder properties to diminish segregation (Oka et al., 2017; Lamešić et al., 2022). Addressing or preventing segregation necessitates a comprehensive understanding of several key factors. Firstly, identifying the dominant segregation mechanisms within a process is crucial. Additionally, it is essential to understand how powder segregation tendencies correlate with the process and the properties of the particles and blends involved. Especially the equipment and processes utilised to handle powders are as influential as material properties in determining segregation tendencies. For instance, adjustments during the filling process, such as reducing the size of heap formation, can mitigate sifting segregation tendencies, while controlling free fall height aids in managing fluidisation segregation (Alizadeh et al., 2017; Engblom et al., 2012(a)). Powder segregation deeply impacts product and process quality, so predicting segregation tendencies based on single/multiple properties is highly desirable. Currently, two predominant approaches are employed for this purpose: computational modelling and bench-scale testing. Computational models, categorised into continuum, kinetic theory, and discrete models, offer insights into segregation dynamics but often struggle to simulate real-world complexities (Moakher et al., 2000). Bench scale testers, such as the sifting (ASTM Standard D6941, 2010) and fluidisation segregation (ASTM Standard D6940, 2012) testers, as per ASTM standards, provide practical experimental measures of segregation tendencies. During the filling of a silo from the top, when a bulk powder consists of different particles in size, shape and density, the larger ones tend to migrate towards the base of the heap. In contrast, the smaller particles accumulate predominantly on

its top or upper layer. Consequently, periodic avalanches occur, resulting in the formation of small particle clusters within the large particles (Alizadeh et al., 2017, Poddar et al., 2023(a)). Transport in vertical chutes and pipes is a prominent source of powder segregation, known as fluidisation segregation, driven by air entrapment and particle dispersion (Levin, 2011; Chowhan, 1995). These mechanisms operate at every powder handling and transport stage, further intensified by air escaping through the powder bed. Powder properties, particularly particle size, shape, and density, significantly influence segregation tendencies, affecting particle aerodynamic behaviour (Levy, 2001; Marucci et al., 2018; Ketterhagen et al, 2007; Shah et al., 2007; Deng et al., 2010; He et al., 2013). In the literature, the research attention has been predominantly directed towards studying segregation characteristics in larger particles, typically for Geldart Group B or D type particles (Oka et al., 2017; Devriendt et al., 2013; Shinohara et al., 2002; Fry et al., 2020; Tang et al., 2005; Jha et al., 2008; Tang et al., 2007; Jha et al., 2010; Jha et al., 2011), where segregation has been generally found to exists. On the contrary, the effect of segregation has been found to be significantly less for particles that lie in Geldart Group A particles (Engblom et al., 2012(a); Deng et al., 2010; He et al., 2013; Engblom et al., 2012(b); Engblom et al., 2012(c); Engblom et al., 2012(d); Hastie, 2015; Jaklič et al., 2015). Very little research on the segregation characteristics has been carried out for particles which are in the Geldart Group A to B borderline zone (Devriendt et al., 2013; Shinohara et al., 2002; Fry et al., 2020; Oka et al., 2017; Tang et al., 2005; Jha et al., 2008; Tang et al., 2007; Jha et al., 2010; Jha et al., 2011; Deng et al., 2010; Engblom et al., 2012 (b); Engblom et al., 2012 (d); Engblom et al., 2012 (a); He et al., 2013; Hastie, 2015; Jaklič et al., 2015; Ghoroi et al., 2013). This study aims to the investigation into the segregation characteristics of powder samples, including three detergents, sand, and semolina, which are typically borderline Geldart A to B materials. The novelty of this study lies in development of a sifting segregation model using flow function, morphology, and coarse to fine size ratio and a fluidisation segregation model using minimum fluidisation velocity for single and multicomponent particles and dimensionless cohesion number. The model formats provided in the previous chapter for sifting and fluidization segregation index have been further improved in this chapter by flow function, morphology, and coarse to fine size ratio and minimum fluidisation velocity in the model format.

6.2 Physical and flow properties of powders

Table 6.1 displays the particle size distribution for each powder sample, indicating the median diameter size in volume concentration d(50), representing 50% of particles lying below it, while d(10)

and d(90) signify the points below which 10% and 90% of particles lie, respectively. Median particle sizes range from 191 to 487 μm, with loose poured bulk densities ranging from 728 to 1194 kg/m^3 and particle densities from 1727 to 2363 kg/m^3. The coarse-to-fine ratio, ranging from 3.78 for semolina to 9.22 for detergent_1, varies by a factor of 2.44, which is crucial for assessing segregation behaviour. The angle of repose is notably higher for sand (52.92˚) compared to semolina (36.55˚), as depicted in Figure 6.1, which illustrates actual powder heaps (blue) and software-generated isosceles triangle heaps (red). A larger angle of repose values for sand, detergent_1, and detergent_2, along with non-uniform heaps, possibly suggest poor flowability and higher cohesion (Alizadeh et al., 2017; Poddar et al., 2023(a); levy, 2001; Engblom et al., 2012(b)). Additionally, Figure 6.2 presents SEM images that indicate non-spherical particle shapes with a shape factor that is mostly below "unity," indicating non-perfect circularity. To study the effect of particle shape on segregation and flow characteristics, the shape factor is considered, as presented in Table 6.1.

Table 6.1: Physical properties of powder samples

Powder sample	**Particle size (μm)**			**CFR**	**ρ_{lb} (kg/m^3) with SD**	**ρ_p (kg/m^3) with SD**	**Geldart group**	**AoR (˚) with SD**	**SF with SD**
	d(10)	**d(50)**	**d(90)**						
Sand	76	191	295	3.88	1194±23	2363±52	B borderline	52.92±1.2	0.89±0.02
Detergent_1	92	269	848	9.22	852±16	1944±36	B borderline	49.71±0.85	0.90±0.01
Detergent_2	129	352	971	7.53	728±22	1898±14	B borderline	44.1±0.48	0.84±0.03
Detergent_3	146	369	873	5.98	1045±35	1727±39	B borderline	43.27±1.1	0.89±0.08
Semolina	265	487	895	3.78	696±13	2096±25	B borderline	36.55±0.9	0.77±0.09

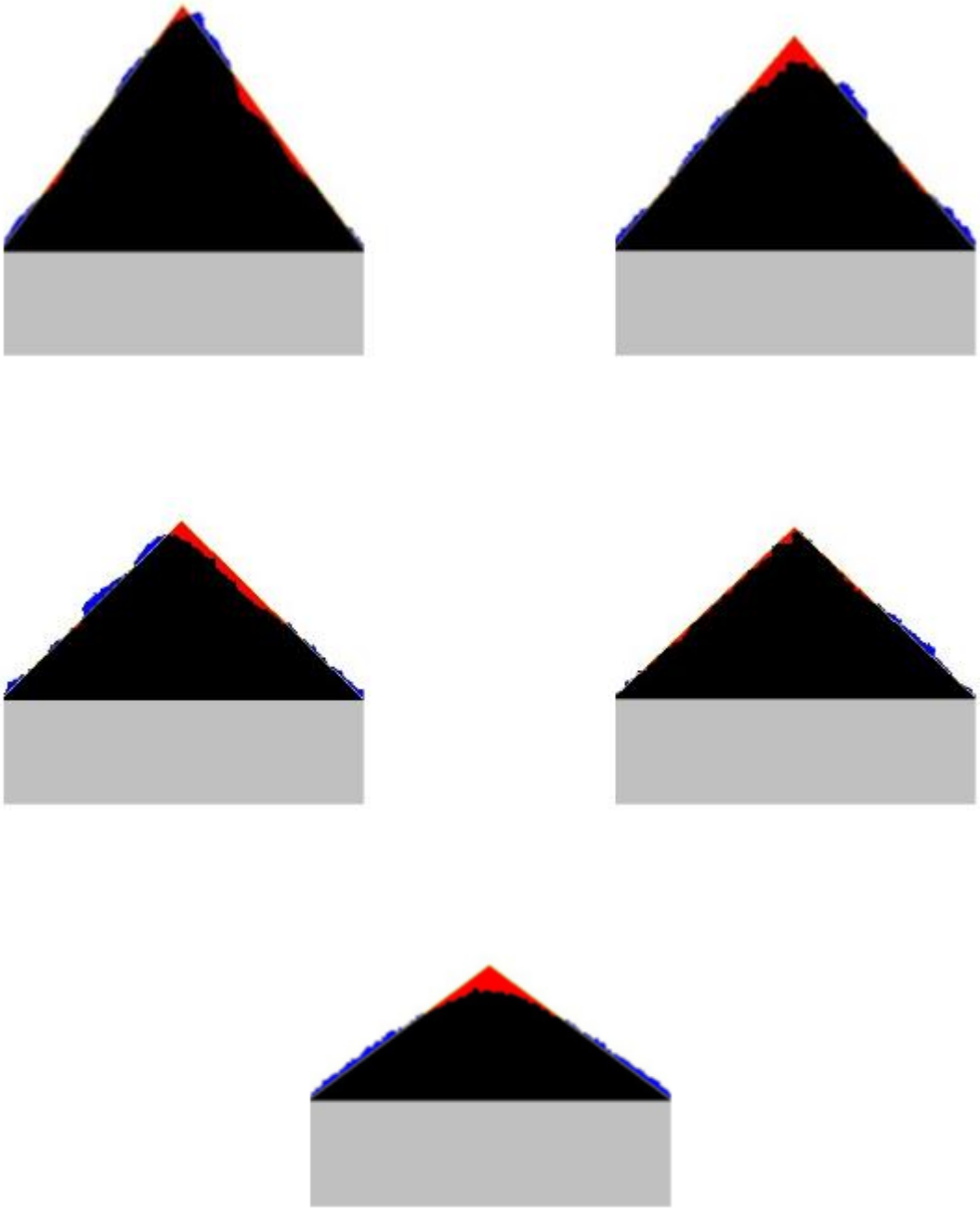

Figure 6.1: Heap images of powder samples

(The top and the left image is of sand; the bottom image is of semolina)

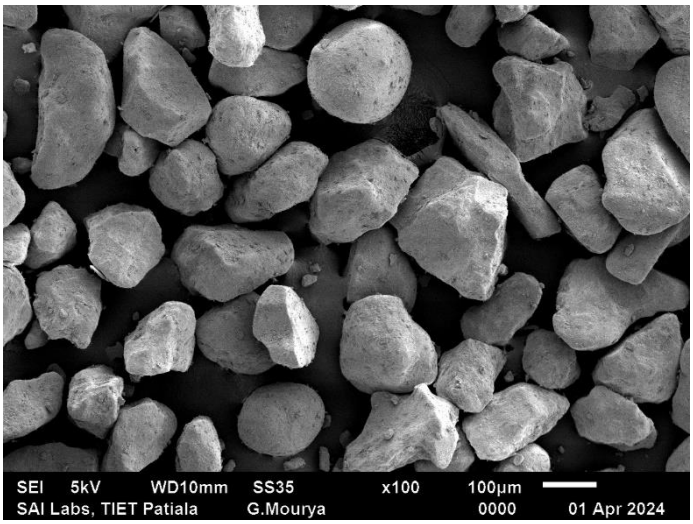

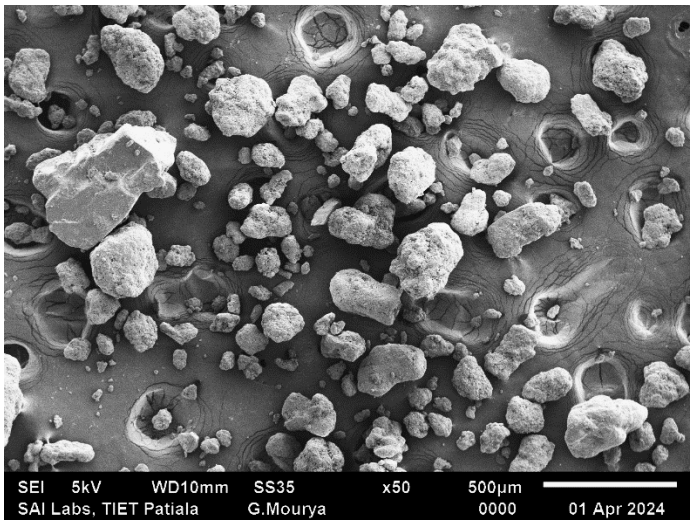

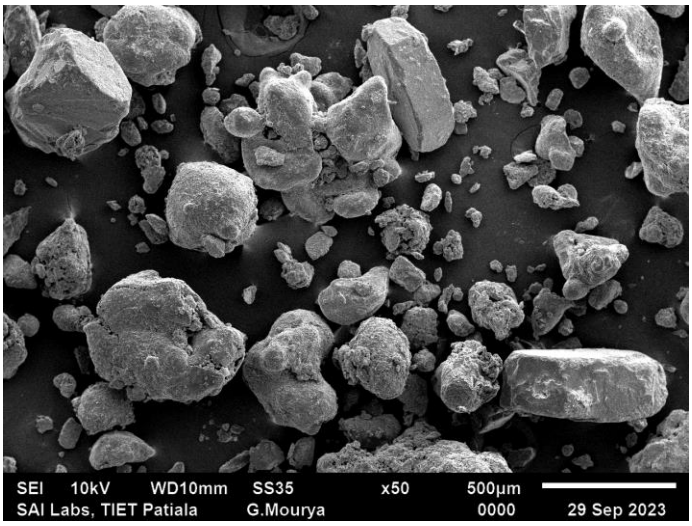

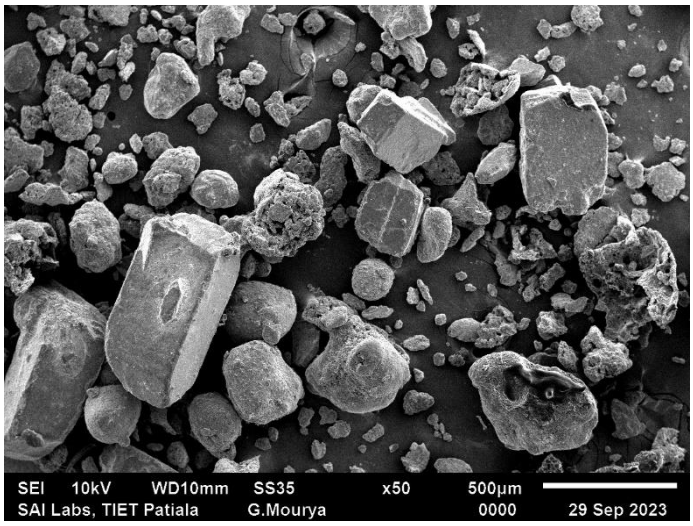

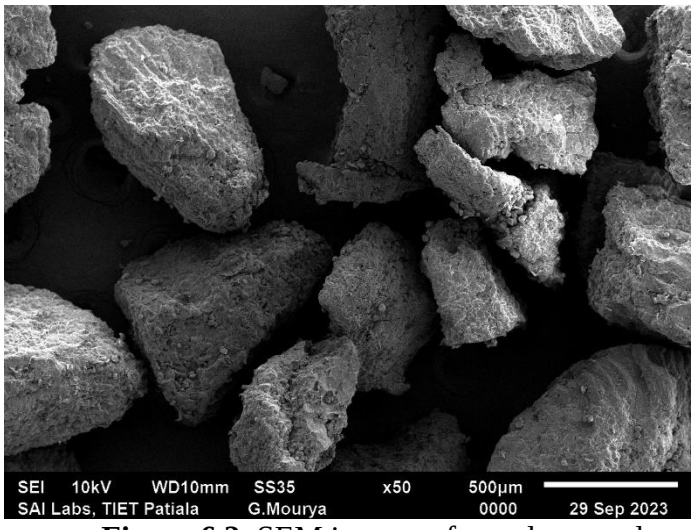

Figure 6.2: SEM images of powder samples

(The top and the left image is of sand; the bottom image is of semolina)

For powder to flow, consolidation stress is a crucial parameter (Schulze, 2008)). For all powder samples, the annular shear tester obtained the yield locus test for different normal consolidated stresses ranging from 1 to 9 kPa at various pre-shear stresses ranging from 0.5 to 5 kPa. The following equation (1) represents the pre-shear stress (τ) as a function of given consolidation stress (σ) and angle of friction (ϕ) with (c) as cohesion value:

$$\tau = \sigma (\tan\phi) + c \qquad (5.1)$$

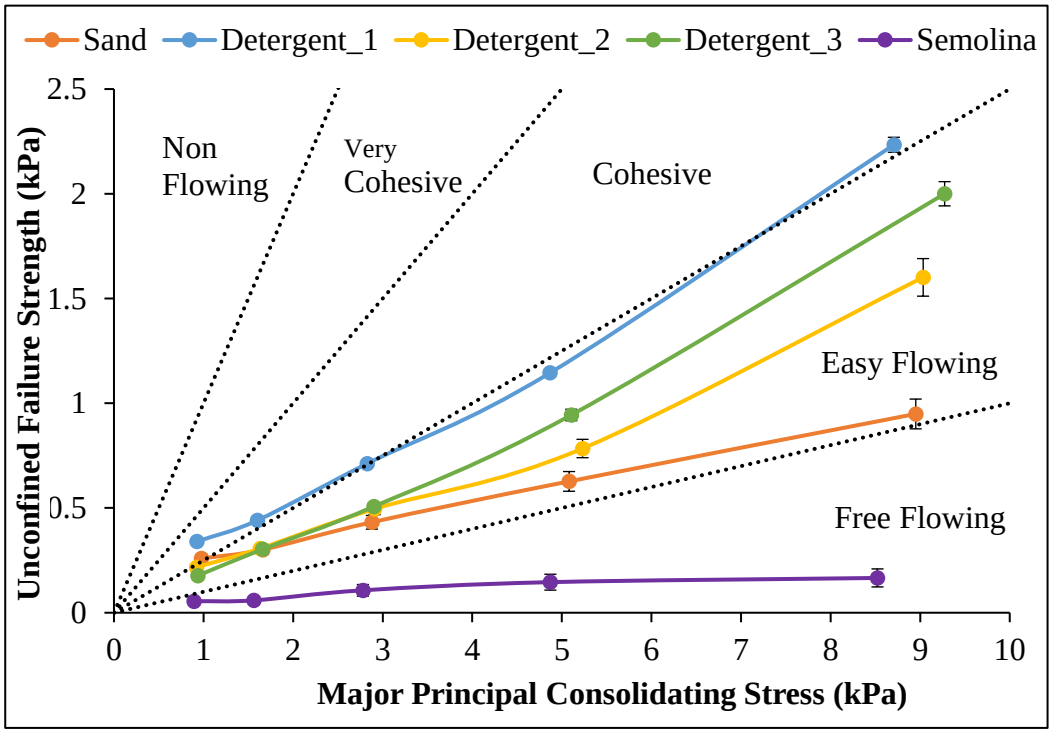

Figure 6.3: Flow function curve for powder samples

As per Jenike's methodology of flow behaviour (Jha et al., 2010), Figure 6.3 is divided into five regimes of flow behaviour: non-flowing (ffc value less than 1), very cohesive (ffc lies between 1 and 2), cohesive (ffc lies between 2 and 4), easy flowing (ffc lies between 4 and 10) and free-flowing (ffc value greater than 10). All the samples were found to be cohesive (borderline) to a free-flowing zone. As consolidating stress increased, particle-to-particle/wall forces such as static friction, cohesion, and adhesion forces increased due to the removal of voids between the particle-to-particle/ wall and more number of particle-to-particle/wall contacts in a given space.

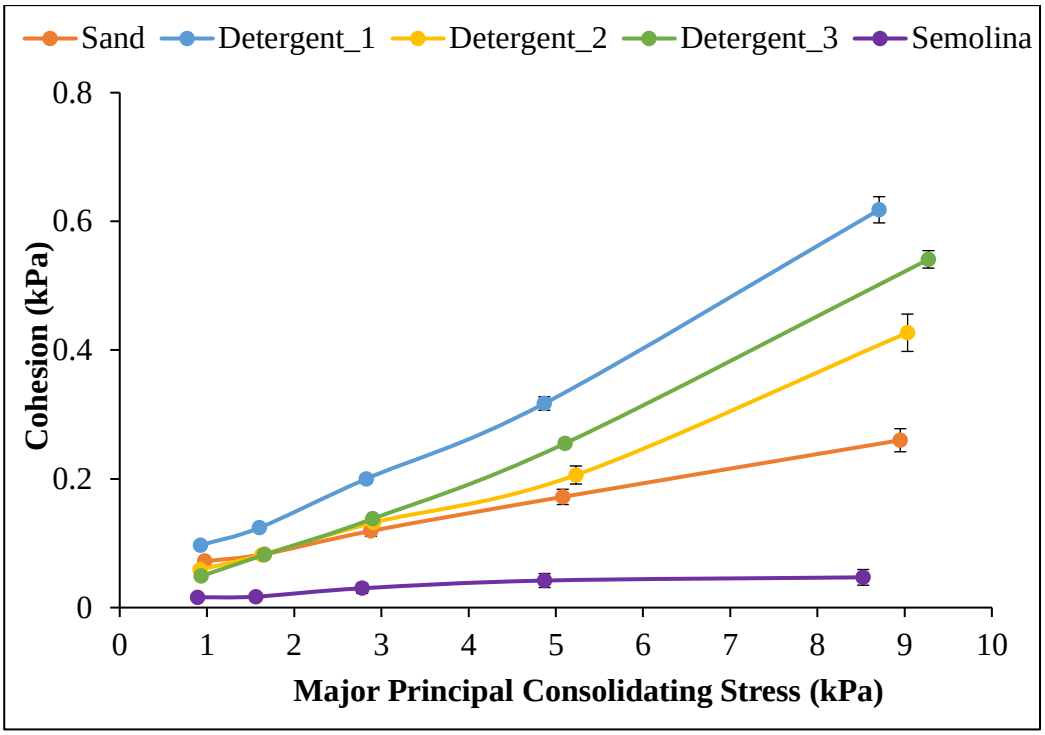

Figure 6.4: Cohesion for powder samples

Figure 6.4 illustrates the effect on cohesion by increasing the major principal consolidation stress for different powder samples by following the Jenike methodology. All detergent samples showed a significant cohesion on increase in major principal consolidating stress, indicating its consolidation under high-stress value. The sand sample exhibits moderate cohesion compared to the detergent samples. In contrast, semolina remains non-cohesive with increasing the major principal consolidating stress, indicating free flow condition under higher stress values. These outcomes show that detergent powder might have some flowability problems under higher stress, while semolina would sustain better flow characteristics.

6.3 Sifting segregation

The segregation index presents the tendency of a powder sample to be segregated while handling or processing, which can be evaluated by comparing the content inhomogeneity (by mass or volume) of the separated samples obtained and it's the virgin sample (Poddar et al., 2023(a); Marucci et al., 2018). Researchers have developed various methods to quantify segregation tendency, including comparing the fine mass or volume fraction of the first and last samples (Marucci et al., 2018; Jaklič et al., 2015), considering the potency range (Shah et al., 2007; Gentzler et al., 2015), examining

chemical characteristics of the segregated samples (Deng et al., 2010; He at al., 2013), and analysing the relative standard deviation (Oka et al, 2017; Ketterhagen et al., 2007). In this study, the segregation index is determined using the segregated samples (first or top and last or bottom batches) obtained from the segregation tests and their virgin sample, as described in the experimental section. Typically, the phenomenon of sifting segregation becomes more noticeable in powder samples containing a lower percentage of smaller particles (Barik et al., 2023; Shinohara et al., 2001). This observation is found to be in line when comparing the powder samples from detergent_1, detergent_2, and detergent_3 to those of sand and semolina, as shown in Figure 6.5 and Table 6.2. Initially, the smaller particles descending along the surface of the heap will interlace within the gaps amongst larger particles. When the initial lot contains fewer smaller particles, it will settle closer to the vessel's centre. Consequently, there arises an opportunity for a subsequent lot of smaller particles to segregate further away from the vessel's centre compared to the first lot. This results in a reduction in the height of the maximum concentration of smaller particle lots, accompanied by an increase in their width. Therefore, the results in Figure 6.5 reveal that the first batches of all powder samples contain a greater proportion of smaller particles than the last batches. This observation serves as additional evidence of sifting segregation due to the download migration of smaller particles to fill the voids amidst larger particles. These outcomes suggest that in practical scenarios of hopper flow, particularly those governed by gravity, upon opening the discharge valve at the hopper's base, the initial powder batch will exhibit a higher concentration of smaller particles relative to the final batch, which will have larger/coarser particles.

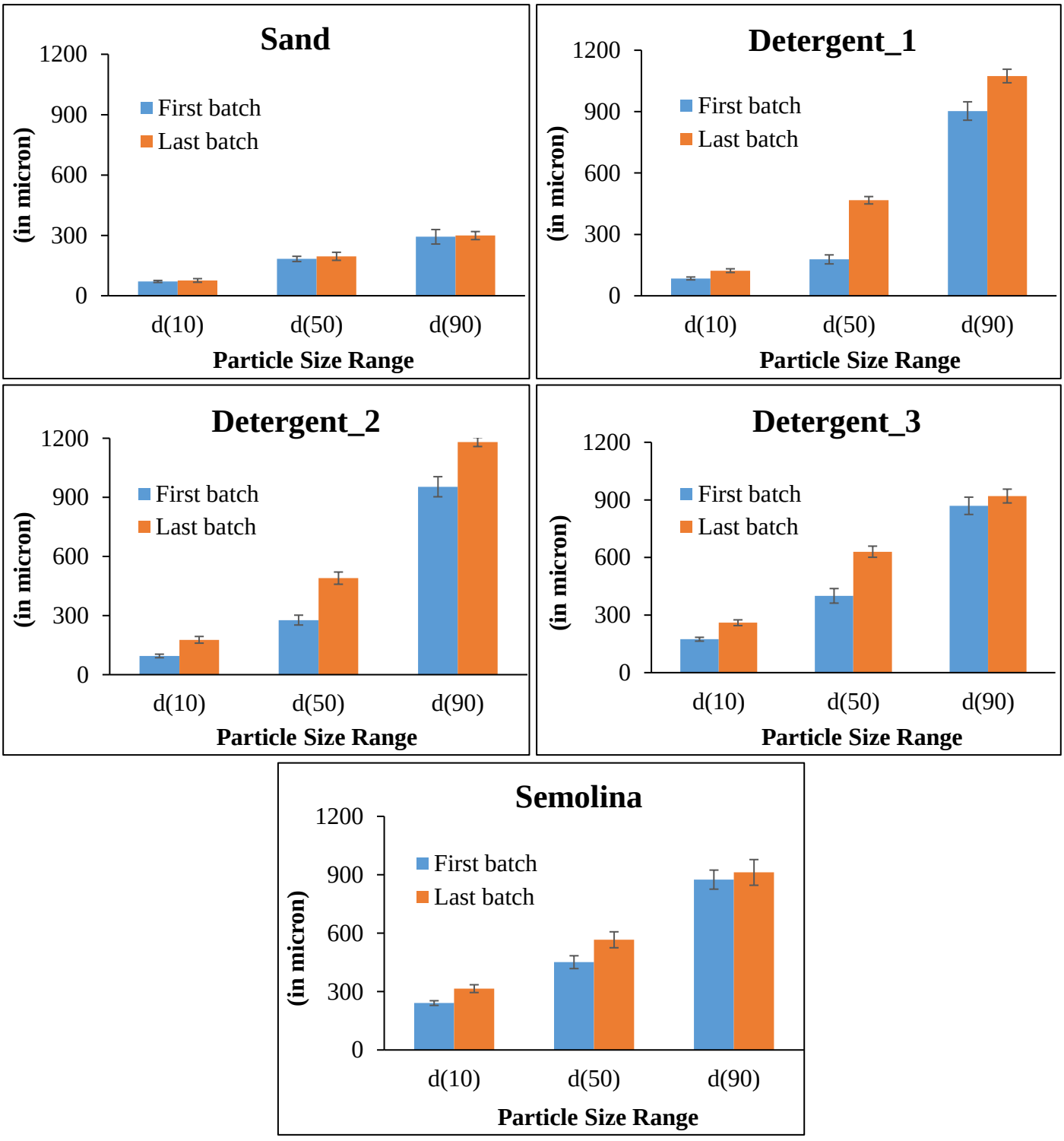

Figure 6.5: Comparison of fineness of powder sample between first and last batch (Sifting segregation)

6.4 Fluidisation segregation

Figure 6.6 shows a schematic representation of the airflow rate plotted against time to test the tendency of fluidisation segregation in five powder samples. The specific trajectory followed by each powder sample aligns with the description outlined in Section 2.5.

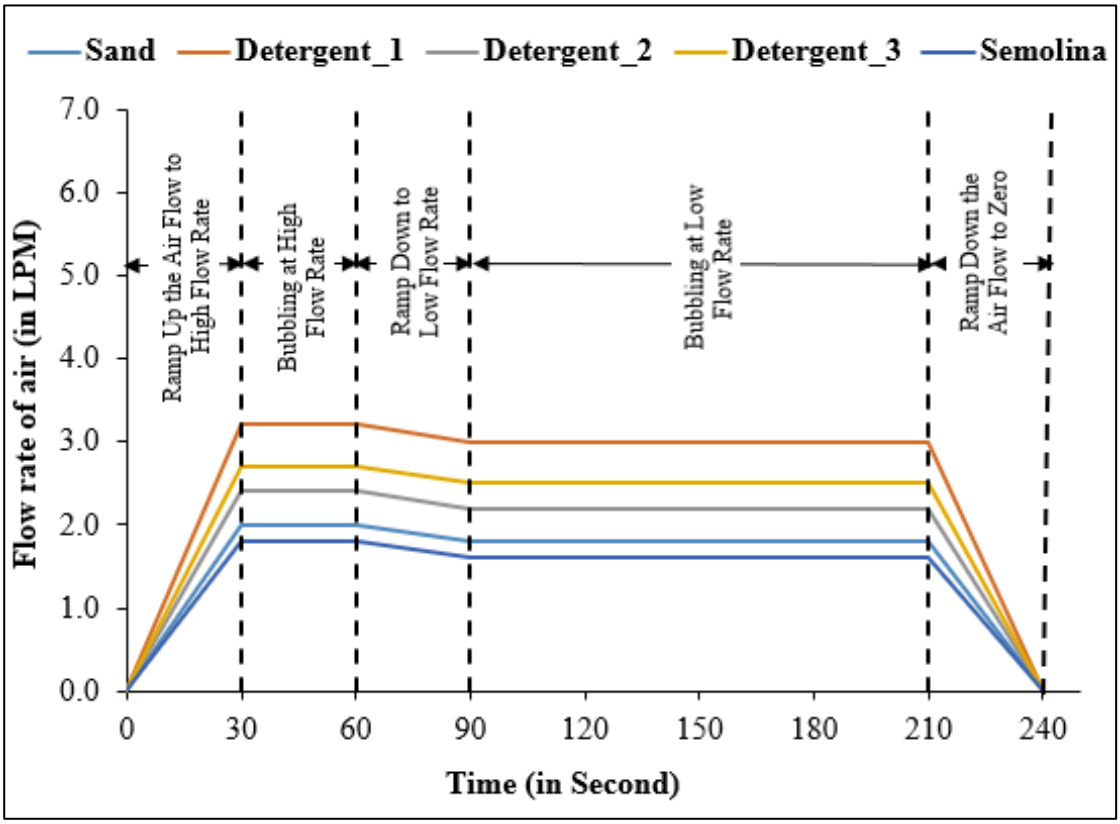

Figure 6.6: Timing Profile of powder samples

In fluidisation segregation, Figure 6.7 compares the powder fineness of the top and bottom batches. The results show that in all powder samples top batches had a higher proportion of smaller particles than the bottom batches because during the fluidisation of the powder sample in the test chamber, smaller particles from the middle and lower cylinders were trapped by the air stream and were directed upward, which led to a higher concentration of smaller particles to be gathered in the top cylinder. In contrast, larger particles of powder sample begin to sink towards the bottom cylinder of the test chamber, resulting in variations in bulk density from bottom to top. Therefore, the top batches exhibited higher values of loose-poured bulk density than the bottom batches. These findings can align with real-world situations where segregation occurs when the powder is fluidised within a

hopper (e.g., hopper with aeration), with the top layer having smaller particles than the bottom layer, which has larger particles.

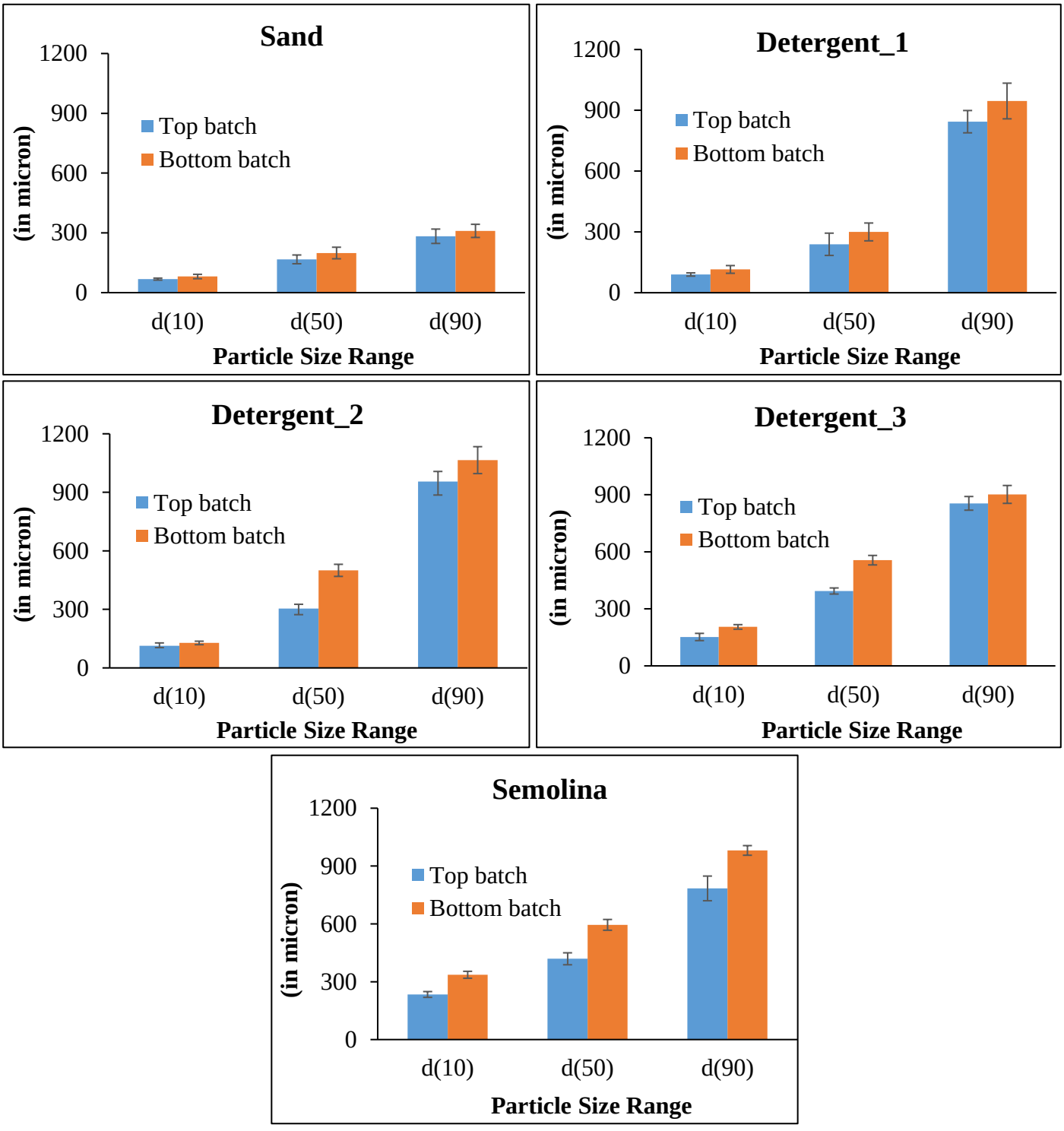

Figure 6.7: Comparison of fineness of powder sample between the top and bottom batch (Fluidisation segregation)

6.5 Modelling sifting and fluidisation segregation indexes

In order to improve the segregation index, $I_{S(k)}$, used in previous Chapter 5 (section 5.4), the comparison between segregated samples with the virgin samples is included and defined as the ratio of the variance of the content of fines between the segregated samples (first/top and last/bottom batches) to the content of fines in their virgin sample at particle size range, *k* (Deng et al., 2021; Behjani, 2018).

$$I_{S(k)} = \left(\frac{C_L - C_F}{C_V}\right)_k \times 100\ \% \tag{6.2}$$

where C_F, C_L, and C_V denote the fines content (by mass or volume) in the first/top, last/bottom, and their virgin sample at the particle size range, *k*.

Then, the mean segregation Index, $\overline{I_S}$, is defined as the segregation tendency of a powder sample throughout the entire size range.

$$\overline{I_S} = \frac{1}{n}\sum_n |\, I_{S(k)} \,| \tag{6.3}$$

where 'n' is the number of particle size range. In this study, particle size ranges are d(10), d(50) and d(90) (in µm). The mean segregation Index, $\overline{I_S}$, as a parameter expressed to assess the segregation tendency for both the sifting and fluidisation mechanism for which segregation occurs, $\bar{I}_{SS}$ and $\bar{I}_{FS}$, respectively, are provided in Table 6.2.

Table 6.2: Sifting and fluidisation segregation index for powder samples

Powder sample	**Particle size d(50) (µm)**	**CFR**	**1/ffc (at 9 kPa)**	**SF**	$\bar{\mathbf{I}}_{\mathbf{SS}}$ **(%)**	$\bar{\mathbf{I}}_{\mathbf{FS}}$ **(%)**
Sand	191	3.88	0.106	0.89	5.14	14.32
Detergent_1	269	9.22	0.257	0.90	56.30	20.63
Detergent_2	352	7.53	0.177	0.84	49.15	26.21
Detergent_3	369	5.98	0.216	0.89	42.36	28.54
Semolina	487	3.78	0.019	0.77	18.56	32.21

Parameters influencing sifting segregation

In previous Chapter 5 (section 5.4), the influencing parameters were considered as flow function (1/ffc) and angle of repose (AOR) as the flow property parameters for modelling the sifting segregation of different fly ash. In order to move a step forward for more fundamental understanding, the AOR as the repeated flow property parameter needs to be replaced; therefore, in this Chapter, the AOR is replaced with the ratio of particle sizes and particle shape as the particle properties.

One of the most prevalent segregation methods is sifting, which occurs with a difference in particle size followed by a difference in particle shape (Tang et al., 2007; Prescott et al., 1994; Duffy et al., 2002; Lawerance et al., 1969; Swaminathan et al., 2002; Vallance et al., 2000; Drahun et al., 1983). Larger particles frequently roll down easily over the steep portion of the heap and manage to get past obstacles and surface imperfections over the slope. They are located at the foot of the heap due to the kinetic energy created by the rolling movement. The interparticle adhesion force is the primary force preventing flow and causing the smaller particles to collect at the top. The powder must have strong interparticle mobility and should be free-flowing for sifting segregation to occur. Segregation would be suppressed by cohesive, fibrous, or rough-textured particles since they would not allow free movement (Fan et al., 2017; Schulze, 2008). Therefore, powder flowability would be an important attribute contributing to sifting segregation tendencies (Marucci et al., 2018; Ketterhagen et al., 2007; Engblom et al, 2012 (b)). Several researchers have used the flow function curve (refer to Figure 6.3) to describe the flow characteristics of powders (Deng et al. 2010; Poddar et al., 2023(b); Engblom et al., 2012(c); Asachi et al., 2018; Jallo et al., 2012). Based on these findings, flow function (1/ffc) as a flow property parameter, course-to-fine ratio (CFR), and shape factor (SF) as particle properties have been included to model the sifting segregation index.

Parameters influencing the fluidisation segregation

In order to have a more fundamental understanding and better results from a new model of fluidisation segregation in existing Chapter 6, a complex parameter related to the ratio of terminal settling velocity for coarse and fine particles (utilised in previous Chapter 5, section 5.4) needs to be replaced. Therefore, a fundamental parameter based on powder bed characteristics is considered as the replacement in the current Chapter 6 to the model of fluidisation segregation index.

In a solid-gas fluidisation system, increasing gas velocity from the bottom (through the distributor plate) of the fixed powder bed in the vertical column would not fluidise the powder bed because of the interparticle forces. At first, the top layers of the power bed got fluidised while the bottom layers remained fixed. Further, with the increase in the gas velocity, the exerted drag force on the particles that break down the interparticle bonds causes the fluidisation of the powder bed. The state at which the whole weight of the powder bed in the column starts to be supported only by the fluidising gas and pressure drop across the powder bed remains constant with an increase in gas velocity is the minimum fluidising state, and the corresponding velocity is the minimum fluidisation velocity (Schulze, 2008; Alghamdi et al., 2021). The particles reached the suspended mode at velocity greater than the minimum fluidisation velocity, and the whole powder bed gets fluidised. In a fluidised bed system, the minimum fluidisation velocity is a significant operating parameter as it helps to measure the flow regime changeover from the fixed to the fluidised state of the powder bed (Wang et al., 2022; Alghamdi et al., 2021). When fluidising the single or multicomponent particles, they tend to get segregated into the top and the bottom layers of the powder bed, depending on the difference in the particle properties. This type of segregation due to the fluidisation of particles could affect the overall performance and stability of the fluidised bed system (Wang et al., 2022; Paudel et al., 2013; Kumoro et al., 2014; Fu et al., 2018; Subramani et al., 2007).

Different correlations of minimum fluidisation velocity for single/multicomponent and their relevance in terms of corelation coefficient with the fluidisation segregation index of powder samples have been carried out in this study. As a typical example, the best fit corelation coefficient between minimum fluidisation velocity and the fluidisation segregation index is presented below (refer to Figure 6.8) using the minimum fluidisation velocity corelation (Rincon et al., 1994), and rest of the correlations are presented in Table 6.3.

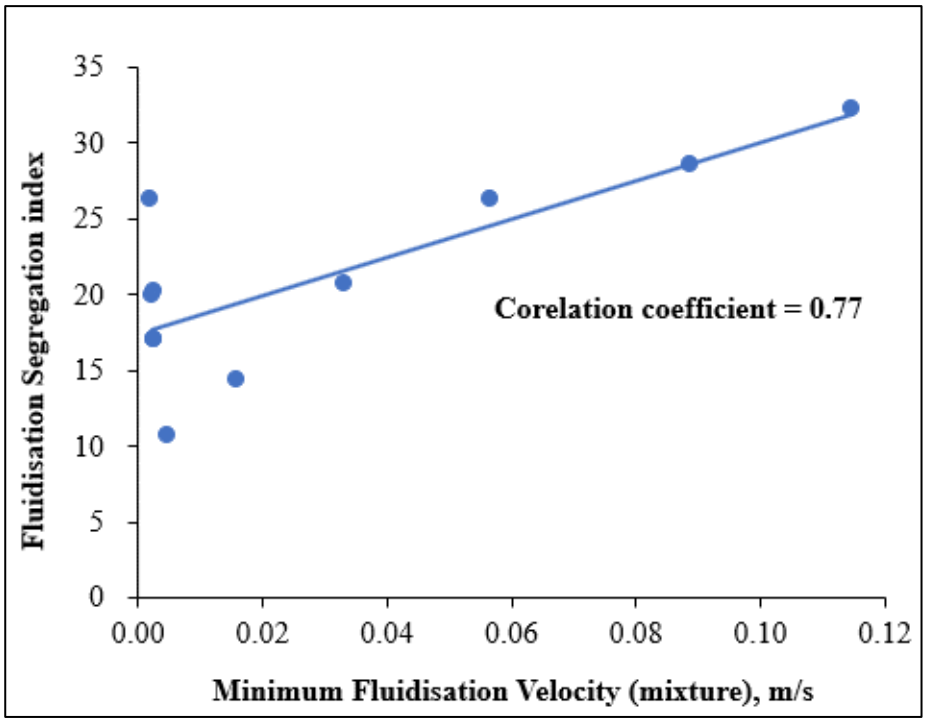

Figure 6.8: The best-fit corelation coefficient between minimum fluidisation velocity (mixture) and the fluidisation segregation index

Table 6.3: Correlations of minimum fluidisation velocity for single and multicomponent/mixture particles, reported in the literature

Reference	Corelation	Experimental conditions	Corelation coefficient
For Single Particle:			
Nakamura et al., 1985	$Ar = 1460\ Re_{mf} + 21.5\ Re_{mf}^2$	Uniformly-sized glass beads (diameter, 0.2 to 4.0 mm) were tested in a vertical fluidised bed (bed diameter, 30 to 50 mm & bed height, 3.4 to 4.7 m) with pressure varied up to 5 Mpa using nitrogen gas as a fluidised medium.	0.73
Xie et al., 1995	Based on Carman-Kozeny $U_{mf} = \frac{\varepsilon_{mf}^3}{1-\varepsilon_{mf}} \frac{(\rho_p - \rho) g d^2}{180\mu}$	FCC powders (diameter, 26 to 137 μm) were used in a vertical fluidised bed (bed diameter, 0.152 m and bed height, 1.4 m) with the gas velocity variation up to 1.5 cm/s, and air, argon, neon, carbon dioxide and Freon-12, as the fluidised medium.	0.64
Bin, 1994	$Ar = 1416 Re_{mf} + 25.926 Re_{mf}^2$	Alumina (aluminium oxide), glass beads, and steel beads (size falls under Geldart B to D) were tested in a vertical fluidised bed with varied bed diameter, 50 mm, 95 mm, 194 mm, 434 mm and bed height, 2.4 m, air-gas velocity was kept between 36 to 46 cm/s.	0.57
Reina et al, 2000	$Re_{mf} = (48^2 + 0.045 Ar)^{1/2} - 48$	Five different scrap-wood particles with diameter 1.14 to 1.69 mm were selected for testing in a vertical fluidised bed (bed diameter, 51 mm and bed height, 1 m) by keeping the air flow rates between 0.4 to 6 m^3/hr.	0.73

Bourgeis et al., 1968	$Re_{mf} = (25.46^2 + 0.03824Ar)^{1/2} - 25.46$	Lucite, glass, lead and tungsten (diameter, 0.086 to 25.1 mm) were used in a vertical 12-inch column with flow rate (distilled water and air) varied from 0.35 to 0.465 m/s.	0.73
Chitester et al., 1984	$Re_{mf} = (28.7^2 + 0.049Ar)^{1/2} - 28.7$	Coal, char and ballotini with diameters, 88 to 361 µm, 157 to 374 µm and 96 to 102 µm, were utilised in a three-dimensional vertical fluidised bed (bed diameter, 10.16 cm and bed height 47 to 53 cm) by reducing the nitrogen gas velocity from 21.3 to 5.49 cm/s.	0.73
Coltters et al., 2004	$U_{mf} = K\left[\frac{d^2(\rho_p - \rho)g}{\mu}\left(\frac{\rho_p}{\rho}\right)^{1.23}\right]^{\alpha}$ For metal category, K = 4.7673 x 10^{-6} ; α = 0.71635 ± 0.02213	Nineteen sets of experimental data of metal powders were utilised (diameter, 3 to 900 µm) with nitrogen gas as the fluidised medium.	0.69 0.68
Baerg et al, 1950	$U_{mf} = \frac{0.361(d\rho_{sb})^{1.23}}{\rho}$	Iron powder, round and foundry sand, silica, scotch lite beads, cracking catalyst, and alumina with particle size 0.000385 to 0.00288 ft. were used in a vertical fluidised bed with bed diameter, 15.5 in. & bed height, 22 in. and the air flow rate of 400 lb/ hr-sq. ft. was supplied.	0.60
Miller et al., 1951	$U_{mf} = \frac{0.00125d^2(\rho_\rho - \rho)^{0.9}\rho^{0.1}\, g}{\mu}$	Silicon carbide, aluminium oxide and sand with varying diameter from 0.0038 to 0.0098 in. were used in a vertical fluidised bed having bed diameter, 2 in. and bed height, 70	0.73

		in. and the different gas mediums used were air, carbon dioxide, and helium.	
Van et al., 1951	$U_{mf} = \frac{0.00123 d^2 \rho_{sb}\, g}{B\mu}$	Different median sizes of carborundum (75 to 240 µm), iron oxide (75 to 800 µm) and coke (75 to 110 µm) were used in a vertical fluidised bed (bed diameter, 6.2 cm & bed height, 3.28 ft.) with the mass velocity of 738 lb/ft^2 h and the gas mediums used were air, argon, carbon dioxide, nitrogen-hydrogen mixtures, town gas and methane.	0.72
Ergun, 1952	$Ar = \frac{150(1-\varepsilon_{mf})}{\varepsilon_{mf}^3 \psi^2} Re_{mf} + \frac{1.75 Re_{mf}^2}{\varepsilon_{mf}^3 \psi}$	Sand and pulverised coke with mesh size 30 to 50 µm were used in a vertical fluidised bed with bed height of 30 cm and the fluidised mediums were CO_2, N_2, CH_4, and H_2.	0.66
Andersson, 1961	$Ar = \frac{36(1-\varepsilon_{mf})}{2(1-\varepsilon_{mf})_{mf}^{4.59} \psi^2} Re_{mf} + \frac{6 C q^3 Re_{mf}^2}{\varepsilon_{mf}^3 \psi}$ where $q = 1.71 \frac{(1-\varepsilon_{mf})^{0.15}}{\varepsilon_{mf}}; C$ $= \begin{Bmatrix} 45/8 \, for\, Re_{mf} < 20 \\ \frac{1}{2 Re_{mf}^{1/3}} \, for\, Re_{mf} > 20 \end{Bmatrix}$	Different sized glass beads (0.186 to 5.692 mm), steel balls (3.165 mm) and lead shots (1.158 to 1.608 mm) were utilised in a large-scale column (diameters 12.0, 8.4 and 6.0 cm) and a small-scale column (diameters of 1.69 and 1.02 cm) with the fluidised mediums as water, water-glycerol mixtures and lubricant oil.	0.62

Narsimhan, 1965	$U_{mf} = \frac{42.9\mu}{d\rho}(0.231log\ +1.417)\left[\left\{1 + \frac{2.12\times10^{-5}}{d0.55}(du_t\rho/\mu)\right\}^{1/2} - 1\right]$	Lead shots, glass beads, 130lexig beads and sea sand in size 0.0029 to 0.0171ft. were used in a vertical column of diameter, 35 mm and height, 51.8 cm with water and air as the fluidised medium.	0.70
Wen et al., 1966	$Re_{mf} = (33.7^2 + 0.0408Ar)^{1/2} - 33.7$ $U_{mf} = \frac{d^2(\rho_p - \rho)g}{1650\mu}$ $U_{mf} = \left(\frac{d^2(\rho_p - \rho)g}{24.5\rho}\right)^{1/2}$	Spherical and non-spherical particles (size of 0.002 to 1.97 inch. And shape factor of 0.385 to 0.935) were used in a vertical fluidised bed (particle diameter to column diameter 0.000807 to 0.25) with the air gas velocity varied from 0.385 to 0.935 cm/s.	0.73 0.73 0.66
Goroshko et al., 1966	$Re_{mf} = \frac{Ar}{\frac{150(1-\varepsilon_{mf})}{\varepsilon_{mf}^3} + \left(\frac{1.75Ar}{\varepsilon_{mf}^3}\right)^{1/2}}$	Sand and pulverised coke having particle size, 833 to 1168 µm were used in a vertical fluidised bed (bed diameter of 30.4 mm and bed height of 300 mm) with the supply of nitrogen gas at 96.5 kPa and the velocity of 0.088 to 0.487 m/s. The other fluidised mediums utilised were CO_2, CH_4 and H_2.	0.66
Kunii, 1969	$U_{mf} = \frac{(\psi d)^2(\rho_p - \rho)g\varepsilon_{mf}^3}{150\mu(1-\varepsilon_{mf})}$ $U_{mf} = \left(\frac{\psi d(\rho_p - \rho)g\varepsilon_{mf}^3}{1.75\rho}\right)^{1/2}$	Sand and pulverised coke having particle size of 833 to 1168 µm were used in a vertical fluidised bed (bed diameter 30.4 mm and bed height 300 mm) with the supply of nitrogen gas at 96.5 kPa and the velocity of 0.088 to 0.487 m/s. The other fluidised mediums utilised were CO_2, CH_4 and H_2.	0.65 0.61

Broadhurst et al., 1975	$Re_{mf}^2 = \frac{Ar^{1.85}}{\left(2.42\ x\ 10^5 \left(\frac{\rho_P}{\rho}\right)^{0.13} + 37.7Ar^{0.85}\right)}$	Glass beads with size 0.1 to 0.481 mm, iron shots of size 0.243 to 0.356 mm, sand of size 0.071 to 0.343 mm, cracking catalyst of size 0.060 mm and clover seed of size 1.09 mm have used in a vertical column having diameters of 10 cm with fluidised mediums of helium, air and Freon-12.	0.72
Riba et al., 1978	$Re_{mf} = 0.0154\ Ar'^{0.66}\ M_v^{0.7}$ $Ar' = d^3\ \rho^2 g/\mu^2$ $M_v = (\rho_P - \rho)/\rho$	Glass bead of 4 mm, plastic beads of 4.91 to 10.36 mm and steel beads of 0.637 to 2.39 mm were used in a vertical column of diameter 94 mm and water was used as a fluidised medium.	0.66
Vaid et al., 1978	$Re_{mf} = (24^2 + 0.0546Ar)^{1/2} - 24$	Coal of size 0.0194 to 0.0472 cm, graphite of size 0.0194 to 0.0472 cm, sand of size 0.0194 to 0.1829 cm, dolomite of size 0.0114 to 0.0947 cm and magnetite of size 0.0367 to 0.1101 cm were used in a vertical fluidised bed of bed diameter, 5 cm and bed height, 90 cm with the supplied air velocity 0.09 cm/s.	0.66
Thonglimp et al., 1984	$Re_{mf} = 0.0034\ Ar^{0.3}\ M_v^{-0.1}$ $Re_{mf} = 0.0279\ Ar^{0.63}$ $Re_{mf} = (19.9^2 + 0.03196Ar)^{1/2} - 19.9$ $M_v = \frac{(\rho_P - \rho)}{\rho}$	Alumina of size 0.045 to 0.085 cm, glass of size 0.0112 to 0.2125 cm, and steel of size 0.0225 to 0.0755 cm were utilised in a vertical cylindrical column with varied bed diameters, 50 mm, 95 mm, 194 mm and 434 mm and bed height of 600 mm with air as the fluidised medium.	0.47 0.65 0.73

Noda et al., 1986	$Re_{mf} = (0.114^2 + 0.0605Ar)^{1/2} - 0.114$ $Re_{mf} = (138.24^2 + 0.0605Ar)^{1/2} - 138.24$	Sand of size 0.454 to 2.8 mm, glass beads of size 0.454 to 1.68 mm, wood chips of size 6.54 mm to 12.5 mm, marten shots of size 0.647 to 0.772 mm, soya beans of size 7.85 mm, small beans of size 5.76 mm and rubber balls of size 2.83 mm were used in a vertical acryl column having bed diameter of 160 mm and bed height of 1700 mm in which fine particles of sands and glass beads were used as a fluidised medium.	0.58 0.73
Lucas et al., 1986	$Re_{mf} = (29.5^2 + 0.0357Ar)^{1/2} - 29.5$ $Re_{mf} = (32.1^2 + 0.0571Ar)^{1/2} - 32.1$ $Re_{mf} = (25.2^2 + 0.0672Ar)^{1/2} - 25.2$	Different sizes of silica sand of size from 177 to 750 µm were used in a vertical stainless-steel column having bed diameters of 70 mm in which air was used as a fluidising medium.	0.73 0.73 0.73
Wu et al., 1991	$Re_{mf} = 7.33 \times 10^{-5}\ 10^{\sqrt{8.24logAr - 8.81}}$	Lime having diameter of 1970 mm was fluidised in a refractory lined reactor (0.48 m x 0.25 m), limestone and sand (diameter, 104 to 939 mm) were fluidised in a metal column (bed diameter of 0.4 m) and the mixture of propane and air were used as a fluidised medium.	0.73
Adánez et al., 1991	$Re_{mf} = (25.18^2 + 0.0373Ar)^{1/2} - 25.18$ $Re_{mf} = (9.88^2 + 0.0297Ar)^{1/2} - 9.88$	Limestone of size 0.4 to 2.5 mm, lime of size 0.4 to 3.2 mm, sulphated lime of size 0.8 mm to 3.2 mm, coal of size 0.63 to 4.0 mm and char of size 0.63 to 4.0 mm were	0.73 0.72

		utilised in a vertical fluidised bed of diameter of 50 mm with air as the fluidised medium.	
Fletcher et al., 1992	$Re_{mf} = \frac{Ar}{1170 + Ar^{1/2}}$	Three simplified Ergun equations were found to be correlated with the 25 Group B sand (average particle size of 0.2 mm) and with published fluidised data and suggested a corelation based on the sphericity of the sand particle.	0.73
Mourad et al., 1994	$Re_{mf} = 0.000552Ar^{1.044}$ $Re_{mf} = 0.00106Ar^{1.040}$	Corn kernels (6.3 to 8.0 mm) and sand particles (0.25 to 0.32 mm) were used in a rectangular steel column (0.340 x 0.122 m and 0.62 m high) with fluidisation air velocity varied from 0.161 and 0.40 m/s.	0.73 0.73
Gautheir et al., 1999	$Re_{mf} = 0.0022Ar^{0.818}$ $Re_{mf} = 0.0052Ar^{0.777}$	Different size river sand of 282.5 µm, 450 µm, 900 µm, 1425 µm & 1800 µm were used in a met acrylate cylindrical column of diameter of 0.14 m and height 1.10 m in which the air flow rate was kept at 0.5 m/s and pressure drop due to the whole distributor was 8.3 kPa.	0.70 0.69
Hartman et al., 2000	$Ar = 1608Re_{mf} + 46.4Re_{mf}^2$ $Ar = 1386Re_{mf} 98.58Re_{mf}^2$	Dolomite and its calcine having average particle size, 0.142 to 0.715 mm used in a glass column of diameter, 80 mm and height 2.5 m with air entrained velocity from 0.4 to 2.0 m/s.	0.73 0.72
Delebarre, 2004	$Ar = 29400\varepsilon_{mf}^3(1 - \varepsilon_{mf})Re_{mf} + 24.5Re_{mf}^2$	An improvement of the Wen and Yu equation [71] was suggested to accurately predict minimum fluidisation	0.70

		velocity by replacing the sphericity with a function of the bed voidage.	
Zhiping et al., 2007	$Re_{mf} = (22.1^2 + 0.0354Ar)^{1/2} - 22.1$	Sand with average particle size of 0.735 to 1.789 mm and glass with average particle size of 0.442 to 0.922 mm were used in a fluidisation column of carbon steel of diameter of 80 mm and height of 600 mm and air as a fluidised medium.	0.73
Subramani et al., 2007	$Re_{mf} = \frac{Ar}{1502}$	Ilmenite having diameters 128 to 50 µm, sand having diameters 134 to 200 µm, limestone having diameters 134 to 200 µm, and quartz magnetite having diameters 163 to 200 µm were used in a fluidised glass column of diameter 2.8 cm and hight of 72 cm with air as a fluidised medium.	0.73
For Multicomponent/mixture Particles:			
Cheung et al., 1974	$U_{mf(\,mixture\,)} = U_{mf(S)}\left(\frac{U_{mf(B)}}{U_{mf(S)}}\right)^{(x_B)^2}$	A total of 16 mixtures were fluidised which were glass powder, sugar balls, bronze particles and ballotine having particle size of 96 to 1305 µm and diameter ratio of 0.15 and 0.85 used in a vertical vessel of diameter 14 cm and filling depth of 10 cm and air as a fluidised medium.	0.68
Rincon et al., 1994	$U_{mf(\,mixture\,)} = \frac{1}{\left(\frac{x_1}{U_{mf1}} + \frac{x_2}{U_{mf2}} + \_\_\_\_\_ + \frac{x_n}{U_{mfn}}\right)}$	Mixtures of glass beads having diameters 1090, 920, 775, 655, 55, 460 µm and density, 2700 kg/m^3 and plastic particles having diameter, 2900 µm, and density of 980	0.77

		kg/m^3 were used in a vertical 135lexigl column of diameter 9 cm and hight of 90 cm with air as a fluidised medium.	
Rao et al., 2001	$U_{mf(\ mixture\ )} = \frac{d^2_{p(\ effective)}\left(\rho_{p(\ mixture\ )} - \rho_f\right)g}{1650\mu_f}$ $\rho_{p(\ mixture\ )} = \sum\left(x_i\rho_{p(i)}\right)$ *and,* $d_{p(\ effective\ )} = kd_{p2}\left[\left(\frac{\rho_{p1}}{\rho_{p2}}\right)\left(\frac{d_{p2}}{d_{p1}}\right)\right]^{w_{2/w_1}}$	Mixtures of biomass having rice husk having of width 2 mm, height of 10 mm, thickness of 1 mm, and sawdust diameter of 1000 µm and groundnut shell powder diameter of 1200 µm and sand having diameters of 355 and 600 µm were used in a vertical stainless steel fluidised bed column of bed diameter, 5 cm and hight of 100 cm with the air as a fluidised medium.	0.34
Si et al., 2008	$U_{mf(\ mixture\ )} = \frac{Re_{(mixture}\,\mu_f}{\rho_f d_{p\ (effective\ )}}$ $d_{p(\ effective\ )} = d_{p1}d_{p2}\left(\frac{x_1\rho_{p2} + x_2\rho_{p1}}{x_1\rho_{p2}d_{p2} + x_2\rho_{p1}d_{p1}}\right)$ $Re_{mf(\ mixture\ )} = \left(C_1^2 + C_2Ar_{(mixture\ )}\right)^{1/2} - C_1$ $Ar_{(\ mixture\ )} = \frac{d^3_{p\ (effective)}\,\rho_f\left(\rho_{p(\ effective)} - \rho_f\right)g}{\mu_f^2}$ $C_1 = 25.65\left(\emptyset_{p1}^{0.25}\emptyset_{p2}^{0.15}\right)$ $C_2 = 0.056\left(\emptyset_{p1}^{-0.045}\emptyset_{p2}^{0.025}\right)$	A mixture of wheat stalk having diameters 800 to 1300 µm, sawdust having diameters 70 to 1200 µm and quartz sand having diameters 255 µm were used in an acoustic bubbling fluidised bed (135lexigl column bed diameter of 53 mm and height of 800 mm) with have frequency ranging from 100-200 Hz.	0.70
Paudel et al., 2013	$U_{mf(\ mixture\ )} = \frac{Re_{(mixture}\,\mu_f}{\rho_f d_{p\ (effective\ )}}$	Experiments were performed with biomass particles (corn cobs of size 1040 µm and walnut shells of size 856 µm), inert particles (sand of size 240 µm, glass of size 383 µm,	0.72

	$Re_{mf} = (30.28^2 + 0.046Ar)^{1/2} - 30.28 \; for \; inert \; particles$ $Ar_{(\,mixture\,)} = \frac{d_{p\,(effective)}^3 \rho_f (\rho_{p(\,effective)} - \rho_f) g}{\mu_f^2}$ $d_{p(\,effective\,)} = \frac{1}{\left(\sum \frac{X_i}{d_{p(i)}}\right)}$	wall nut of size 100 µm and alumina of size 490 µm), and biomass and sand mixtures were used in a cold fluidised bed of acrylic 136lexiglas of diameter 145 mm and height 1000 mm with air as a fluidised medium. The weight percentages of biomass particles (ranging from 0 to 100%) in the mixture of biomass and sand.	
Kumoro et al., 2014	$U_{mf(\,mixture\,)} = \frac{Re_{(mixture}\,\mu_f}{\rho_f d_{p\,(effective\,)}}$ $Ar_{(\,mixture\,)} = 1176(1 - x_2)\emptyset_m^2 Re_{(\,mixture\,)} + 22.432 x_2^{1/2} Re_{(\,mixture\,)}^2$ $Ar_{(\,mixture\,)} = \frac{d_{p\,(effective)}^3 \rho_f (\rho_{p(\,effective)} - \rho_f) g}{\mu_f^2}$ $d_{p(\,effective\,)} = d_{p1} d_{p2} \left(\frac{x_1 \rho_{p2} + x_2 \rho_{p1}}{x_1 \rho_{p2} d_{p2} + x_2 \rho_{p1} d_{p1}}\right)$	Biomass particles (rice husk of size 1560 µm and corn cob of size 1040 µm), inert particles (river sands of size 241 µm and 350 µm), and the mixture of biomass and inert particles were used in a cold fluidisation column of Perspex (bed diameter of 10 cm and height of 100 cm) with air as a fluidised medium. The biomass mass fraction in the biomass and inert particles mixtures was 0 to 1, in range.	0.70
Fu et al., 2019	$U_{mf(\,mixture\,)} = U_{mf(F)} \left(U_{mf(P)} / U_{mf(F)}\right)^{x_p^{1.26 \times \left(d_{d(P)}/d_{p(F)}\right)^{0.53}}}$ $\chi_P = w_P \frac{\rho_{P(\,effective\,)}}{\rho_{p(P)}}$	Fifteen types of mixtures of magnetite having diameters 150 to 300 µm and sand/gangue/coal particles having diameters 150 to 710 µm, and 710 to 850 µm at ten different particle compositions (5 to 95 %, by volume) were used in a vertical gas-solid fluidised bed of bed diameter of 152.4 mm with air as a fluidised medium.	0.67

The above study showed that most of the correlations of minimum fluidisation velocity for single/multicomponent particles depend on particle properties and powder bed characteristics. In these correlations, the effect of forces due to particle-to-particle interaction were not considered, which plays a pivotal role before the fluidisation state (Thomas, 2024; Seville et al., 2000; Xu et al., 2009). The below-mentioned is repeated again as described in the previous Chapter 5 for the sake of completeness.

Air drag on a single particle must be substantial compared to the interparticle forces for the powder to fluidise properly. Particles will remain in contact with one another until the air flow rate becomes exceedingly significant and turbulent if cohesive forces are significant relative to air drag, which is at the most equivalent to the weight of the particle. On the other hand, the lowest fluidisation air may readily flow around particles and extend the bed where interparticle forces are small in relation to particle weight. Consequently, cohesive forces are believed to be the main source of resistance to bed expansion during fluidisation (He et al., 2013; Gentzler et al., 2015; Thomas, 2024). Thus, cohesion, C, has been incorporated as a crucial parameter to describe fluidisation segregation in this study. Some researchers (Behjani et al., 2017(a); Behjani et al., 2017(b)) have used a dimensionless cohesion number (Coh) to predict particles' surface energy. In this study, a novel dimensionless cohesion number (Coh*) has been developed and calculated by dividing the interparticle cohesion to the dynamic pressure of gas which is suppling as the fluidising gas. The term dynamic pressure of the gas is defined as the kinetic energy per unit volume of gas. The significance of dimensionless cohesion number (Coh*) represents the effort required by the dynamic pressure of gas to break the interparticle cohesion bond, during fluidising of a static powder bed.

$$\text{Coh}^* = \frac{\text{Interparticle cohesion}}{\text{Dynamic pressure of air}} = {}^{C}\Big/_{\frac{1}{2}\rho V^2} \tag{6.4}$$

where ρ and V are the gas properties, which are the gas density and superficial gas velocity, respectively.

Minimum fluidisation velocity, $U_{mf\,(mixture)}$, having best corelation coefficient [90] (refer to Table 6.3), as a powder bed characteristic and modified dimensionless cohesion number, Coh*, as an interparticle property to investigate their impact on fluidisation segregation has been included in model. The six additional data points from Poddar et al., 2023(b) have been utilised for validation

purposes. For sifting and fluidisation segregation, Table 6.4 provides the estimated values of model parameters.

Table 6.4: Estimated values of model parameters

Powder sample	**1/ffc (at 9 kPa)**	**SF**	**CFR**	$U_{mf(mixture)}$	**Coh***
Fly ash A	0.114	0.90	12.53	0.00216	311863
Fly ash B	0.096	0.89	7.97	0.00243	298517
Fly ash C	0.112	0.85	7.26	0.00280	153618
Fly ash D	0.099	0.86	7.94	0.00283	99728
Fly ash E	0.102	0.82	7.05	0.00279	56261
Fly ash F	0.084	0.77	4.81	0.00496	35542
Sand	0.106	0.89	3.88	0.01592	22103
Detergent_1	0.257	0.90	9.22	0.03324	11632
Detergent_2	0.177	0.84	7.53	0.05689	12578
Detergent_3	0.216	0.89	5.98	0.08880	8254
Semolina	0.019	0.77	3.78	0.11480	6064

The aforementioned sifting and fluidisation segregation parameters have been used to create the following models.

$$(\bar{I}_{SS})_{predicted} = 299.21 + 331.68\left({}^{1}/_{ffc}\right) - 369.3\,(SF) - 0.4\,(CFR) \quad (6.5)$$

$$(\bar{I}_{FS})_{predicted} = 12.63 + 3.5E-05\,(Coh^{*}) + 179.82\,(U_{mf(mixture)}) \quad (6.6)$$

The below-mentioned scatter plots (refer to Figures 6.9 and 6.10) compare the predicted and actual segregation indexes for sifting and fluidisation segregation mechanisms. As per Figure 6.9, the predicted sifting segregation index showed a strong corelation with the actual index, with an R^2 value of 0.97. Figure 6.10 depicts the predicted fluidisation segregation index versus the actual index value, which has an R^2 value of 0.86, suggesting a good fit correlation.

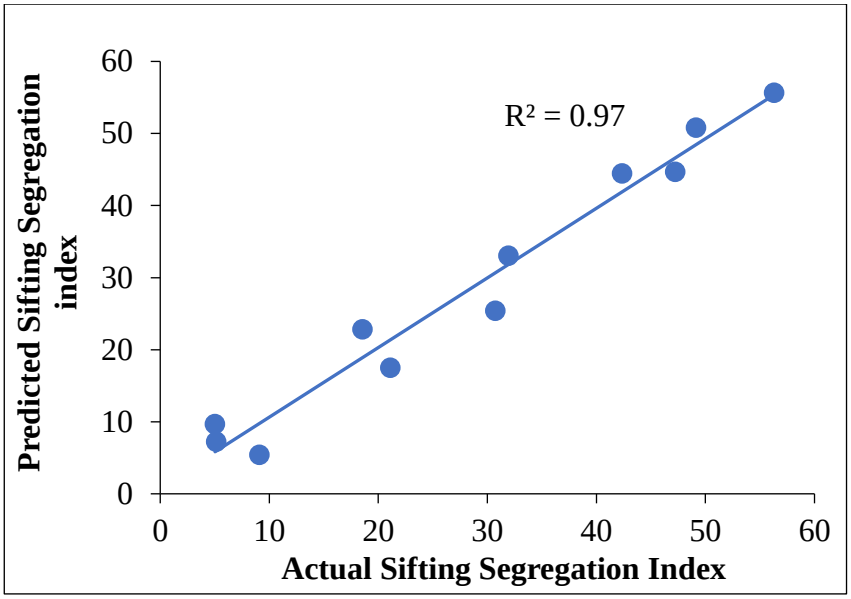

Figure 6.9: Predicted versus actual sifting segregation index

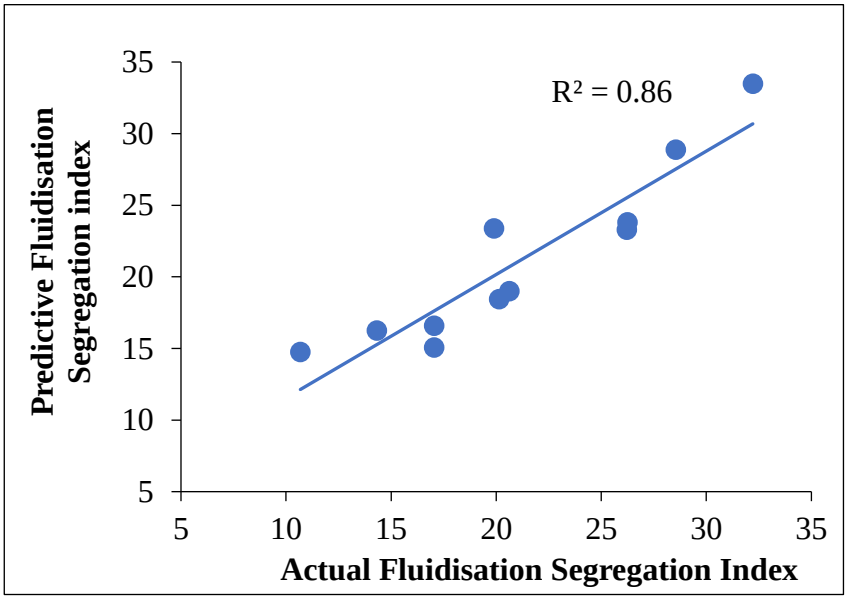

Figure 6.10: Predicted versus actual fluidisation segregation index.

To predict the segregation index based on existing powder data in Chapter 2, Literature review (Table 2.1), the proposed segregation models have been validated for the Geldart A to B borderline powders, and found that the R^2 values range from 71% to 95%. Further, the model proposed in Chapter 4 has been validated against various powders discussed throughout this thesis. The resulting coefficient of determination, R^2, was found to be 83% (refer to Figure 6.11), indicating a good fit between the model and the experimental data.

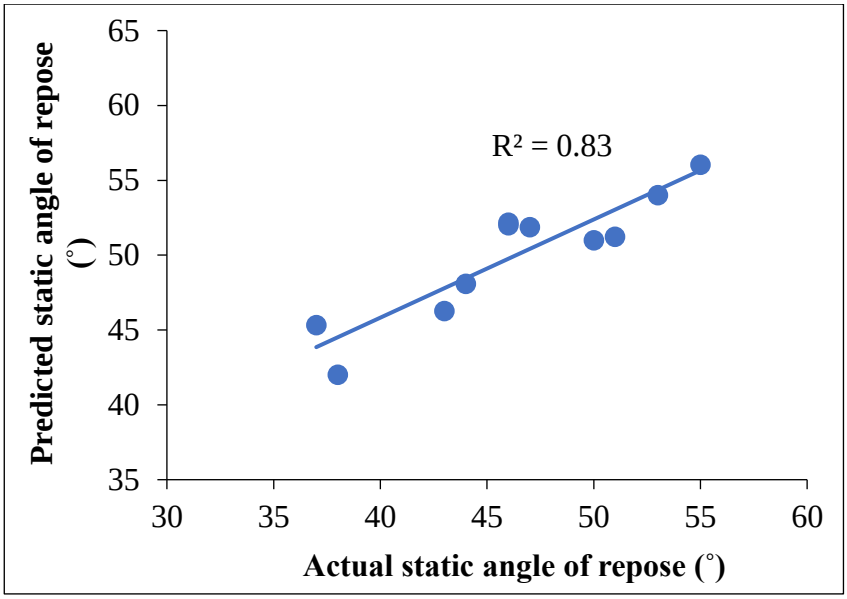

Figure 6.11: Predicted versus actual static angle of repose

6.6 Conclusion

In this study, sifting segregation and fluidisation segregation characteristics of sand, three different brands of detergent, and semolina powders were studied. The findings from the segregation characteristics show a significant difference between the particle size distribution of the first and last samples taken during the sifting segregation test and the top and bottom samples taken during the fluidisation segregation test. In both segregation tests, the first and the top samples consist of larger fine particles than the last and the bottom samples, indicating the change in the bulk properties of Geldart group A to B borderline powders. Due to the wide particle size distribution of three different brands of detergent powders, more particles separated from each other while forming the powder heap, indicating a higher sifting segregation index than those of sand and semolina powder. Sifting segregation was found to be influenced by dimensionless parameters such as powder flow function, course-to-fine ratio and shape factor, whereas a novel dimensionless cohesion number and minimum fluidisation velocity seem to be addressing fluidisation segregation well. The models for the sifting and fluidisation segregation index provided a good fit of 97 % and 86 %, respectively, with the experimental data. The proposed model has been tested and validated at an appropriate rate of powder properties. The future scope of research would include further validating the model against more experimental data and to develop a more fundamental model describing sifting and fluidisation segregation using surface roughness of powders.

References

Ansari, M.I.H., A. Bhateja, and I. Sharma. 2023. Axial Segregation of Granular Mixtures in Laterally Shaken Multi-Trapezium Channels. *Powder Technology* 417, no. August 2022.

Alghamdi, Y.A., Z. Peng, Z. Almutairi, H. Alibrahim, F.M. Al-Alweet, B. Moghtaderi, and E. Doroodchi. 2021. Assessment of Correlations for Minimum Fluidization Velocity of Binary Mixtures of Particles in Gas Fluidized Beds. *Powder Technology* 394: 1231–1239.

Asachi, M., A. Hassanpour, M. Ghadiri, and A. Bayly. 2018. Experimental Evaluation of the Effect of Particle Properties on the Segregation of Ternary Powder Mixtures. *Powder Technology* 336: 240–254.

Alizadeh, M., A. Hassanpour, M. Pasha, M. Ghadiri, and A. Bayly. 2017. The Effect of Particle Shape on Predicted Segregation in Binary Powder Mixtures. *Powder Technology* 319: 313–322.

Adánez, J., J.C. Abanades. 1991. Minimum fluidisation velocities of fluidised-bed coal combustion solids, *Powder Technology* 67 (2), 113–119.

Andersson, K.E.B., 1961. Pressure drop in ideal fluidisation, *Chemical Engineering Science* 15 (3–4), 276–297.

Barik, S.K., V.N. Lad, I. Sreedhar, and C.M. Patel. 2023. Investigation of Mass Discharge Rate, Velocity, and Segregation Behaviour of Microcrystalline Cellulose Powder from a Copley Flow Tester. *Powder Technology* 417, no. September 2022: 118234.

Behjani, M.A. 2018. Numerical Simulation of Segregation of Formulated Powder Mixtures. *Thesis*, School of Chemical Engineering, The University of Leeds, UK.

Behjani, M.A., A. Hassanpour, M. Ghadiri, and A. Bayly. 2017(a). Numerical Analysis of the Effect of Particle Shape and Adhesion on the Segregation of Powder Mixtures. Ed. F. *EPJ Web of Conferences* 140, 06024.

Behjani, M.A., N. Rahmanian, N. Fardina bt Abdul Ghani, and A. Hassanpour. 2017(b). An Investigation on Process of Seeded Granulation in a Continuous Drum Granulator Using DEM. *Advanced Powder Technology* 28, no. 10 (October): 2456–2464.

Bin, A.K. 1994. Prediction of the minimum fluidisation velocity, *Powder Technology* 81 (2), 197–199.

Broadhurst, T.E., H.A. Becker. 1975. Onset of fluidisation and slugging in beds of uniform particles, *AIChE Journal* 21, 238.

Bourgeois, P., and P. Grenier. 1968. The Ratio of Terminal Velocity to Minimum Fluidising Velocity for Spherical Particles. *The Canadian Journal of Chemical Engineering* 46, no. 5: 325–328.

Baerg, J.K., P.E. Gishler. 1950. Heat transfer in a fluidised solids bed, *Canadian Journal of Research* F28, 287.

Ghoroi, C., X. Han, D. To, L. Jallo, L. Gurumurthy, and R.N. Davé. 2013. Dispersion of Fine and Ultrafine Powders through Surface Modification and Rapid Expansion. *Chemical Engineering Science* 85: 11–24.

Coltters, R., A.L. Rivas. 2004. Minimum fluidisation velocity correlations in particulate systems, *Powder Technology* 147, 34–48.

Chowhan, Z.T., 1995. Segregation of particulate solids, part I, *Pharma Technology*, 19, 56–70.

Cheung, L., A.W. Nienow, P.N. Rowe. 1974. Minimum fluidisation velocity of a binary mixture of different sized particles, *Chemical Engineering Science* 29, 1301–1303.

Deng, T., V. Garg, H. Salehi, and M.S.A. Bradley. 2021. An Experimental Study on Free-Surface Rolling Segregation and Correlations with Angle of Repose and Particle Sphericity. *Powder Technology* 379: 307–320.

Devriendt, L., C. Gatumel, and H. Berthiaux. 2013. Experimental Evidence of Mixture Segregation by Particle Size Distribution. *Particulate Science and Technology* 31, no. 6 (November 2): 653–657.

Deng, T., K.A. Paul, M.S.A. Bradley, L. Immins, C. Preston, J.F. Scott, and E.H. Welfare. 2010. Investigations on Air Induced Segregation of Pharmaceutical Powders and Effect of Material Flow Functions. *Powder Technology* 203, no. 2 (November): 354–358.

Delebarre, A. 2004. Revisiting the Wen and Yu equations for minimum fluidisation velocity prediction, *Chemical Engineering Research and Design* 82 (5), 587–590.

Duffy, S.P., and V.M. Puri. 2002. Primar y Segregation Shear Cell for Size-Segregation Analysis of Binary Mixtures, no. 20: 196–207.

Drahun, J. A., J. Bridgwater. 1983. The mechanisms of free surface segregation, *Powder Technology* 36, 39–53.

Engblom, N., H. Saxén, R. Zevenhoven, H. Nylander, and G.G. Enstad. 2012(a). Segregation of Powder Mixtures at Filling and Complete Discharge of Silos. *Powder Technology* 215–216 (January): 104–116.

Engblom, N., H. Saxén, R. Zevenhoven, H. Nylander, and G.G. Enstad. 2012(b). Effects of Process Parameters and Hopper Angle on Segregation of Cohesive Ternary Powder Mixtures in a Small Scale Cylindrical Silo. *Advanced Powder Technology* 23, no. 5 (September): 566–579.

Engblom, N., H. Saxén, R. Zevenhoven, H. Nylander, and G.G. Enstad. 2012(c). Segregation of Construction Materials in Silos. Part 1: Experimental Findings on Different Scales. *Particulate Science and Technology* 30, no. 2 (March): 145–160.

Engblom, N., H. Saxén, R. Zevenhoven, H. Nylander, and G.G. Enstad. 2012(d). Segregation of Construction Materials in Silos. Part 2: Identification of Relevant Segregation Mechanisms. *Particulate Science and Technology* 30, no. 2 (March): 161–178.

Ergun, S. 1952. Fluid flow through packed columns, *Chemical Engineering Progress* 48, 89–94.

Fry, A.M., V. Vidyapati, J.P. Hecht, P.B. Umbanhowar, J.M. Ottino, and R.M. Lueptow. 2020. Measuring Segregation Characteristics of Industrially Relevant Granular Mixtures: Part II – Experimental Application and Validation. *Powder Technology* 368, no. 1 (May): 278–285.

Fu, Z., J. Zhu, S. Barghi, Y. Zhao, Z. Luo, C. Duan. 2019. Minimum fluidization velocity of binary mixtures of medium particles in the air dense medium fluidised bed, *Chemical Engineering Science* 207, 194–201.

Fan, Y., K. V Jacob, B. Freireich, and R.M. Lueptow. 2017. Segregation of Granular Materials in Bounded Heap Flow: A Review. *Powder Technology* 312 (May): 67–88.

Fletcher, J.V., M.D. Deo, F.V. Hanson. 1992. Re-examination of minimum fluidisation velocity correlations applied to Group B sands and coked sands, *Powder Technology* 69 (2), 147–155.

Gentzler, M., J.N. Michaels, and G.I. Tardos. 2015. Quantification of Segregation Potential for Polydisperse, Cohesive, Multi-Component Powders and Prediction of Tablet Die-Filling Performance - A Methodology for Practical Testing, Re-Formulation and Process Design. *Powder Technology* 285: 96–102.

Gauthier, D., S. Zerguerras, G. Flamant. 1999. Influence of the particle size distribution of powders on the velocities of minimum and complete fluidisation, *Chemical Engineering Journal* 74 (3), 181–196.

Goroshko, V.D., R.B. Rozembaum, O.M. Todes, in: S.S. Zabrodsky (Ed.). 1966. Hydrodynamics and Heat Transfer in Fluidized Beds, *MIT press,* Cambridge, Massachusetts, pp. 71–73.

Hastie, D.B. 2015. On the Difficulties of Sampling Bulk Powder Blends in Determining Segregation Propensity — A Case Study. *Powder Technology* 286 (December): 164–171.

He, X., X. Han, N. Ladyzhynsky, and R. Deanne. 2013. Assessing Powder Segregation Potential by near Infrared (NIR) Spectroscopy and Correlating Segregation Tendency to Tabletting Performance. *Powder Technology* 236 (February): 85–99.

Hartman, M., O. Trnka, K. Svoboda. 2000. Fluidization characteristics of dolomite and calcined dolomite particles, *Chemical Engineering Science* 55 (24), 6269–6274.

Jaklič, M., K. Kočevar, S. Srčič, and R. Dreu. 2015. Particle Size-Based Segregation of Pharmaceutical Powders in a Vertical Chute with a Closed Bottom: An Experimental Evaluation. *Powder Technology* 278 (July): 171–180.

Johanson, K. 2014. Review of New Segregation Tester Method by Dr . Kerry Johanson , P . E . *Powder Technology* 257: 1–10.

Jha, A.K., and V.M. Puri. 2011. Percolation Segregation in Binary Size Mixtures Under Different Shear and Intensity of Motion. *Particulate Science and Technology* 29, no. 5 (September): 481–492.

Jallo, L.J., C. Ghoroi, L. Gurumurthy, U. Patel, and R.N. Davé. 2012. Improvement of Flow and Bulk Density of Pharmaceutical Powders Using Surface Modification. International Journal of Pharmaceutics 423, no. 2: 213–225.

Jha, A.K., and V.M. Puri. 2010. Percolation Segregation of Multi-Size and Multi-Component Particulate Materials. *Powder Technology* 197, no. 3 (January): 274–282.

Jha, A.K., J.S. Gill, and V.M. Puri. 2008. Percolation Segregation in Binary Size Mixtures of Spherical and Angular-Shaped Particles of Different Densities. *Particulate Science and Technology* 26, no. 5 (September 29): 482–493.

Kumoro, A., D. Nasution, A. Cifriadi, A. Purbasari, A. Falaah. 2014. A new correlation for the prediction of minimum fluidisation of sand and irregularly shape biomass mixtures in a bubbling fluidised bed, *International Journal of Applied Engineering Research* 9, 21561–21573.

Ketterhagen, W.R., J.S. Curtis, C.R. Wassgren, A. Kong, P.J. Narayan, and B.C. Hancock. 2007. Granular Segregation in Discharging Cylindrical Hoppers: A Discrete Element and Experimental Study. *Chemical Engineering Science* 62, no. 22 (November): 6423–6439.

Kunii, O. Levenspiel. 1969. Fluidization Engineering, *John Wiley*, New York, UK.

Liu, X., Q. Zheng, L. Yang, M. Cai, G. Cheng, and A. Yu. 2023. The Segregation of Cement Clinker Particles in a Mill-Feeding Hopper: PIV Experiment and FEM Modelling. *Powder Technology* 426, no. May: 118656.

Lamešić, D., B. Grilc, R. Roškar, S. Kolokytha, J. Hofmann, A. Malekos, R. Kaufmann, and O. Planinšek. 2022. Spherical Agglomerates of Lactose Reduce Segregation in Powder Blends and Improve Uniformity of Tablet Content at High Drug Loads. *AAPS Pharm Sci Tech* 23, no. 1 (January 10): 17.

Lumay, G., F. Boschini, K. Traina, S. Bontempi, J.-C. Remy, R. Cloots, and N. Vandewalle. 2012. Measuring the Flowing Properties of Powders and Grains. *Powder Technology* 224 (July): 19–27.

Levin (Ed.). M., 2011. Pharmaceutical Process Scale-Up, *Informa Healthcare*, New York, USA

Levy, A., C.J. Kalman, 2001. Handbook of Conveying and Handling of Particulate Solids, *Elsevier*, UK.

Lucas, A., J. Arnaldos, J. Casal, L. Puigjaner. 1986. High temperature incipient fluidisation in mono and poly disperse systems, *Chemical Engineering Communications* 41, 121–132.

Lawrence, L.R., J.K. Beddow. 1969. Powder segregation during die filling, *Powder Technology* 2, 253–259.

Marucci, M., B. Al-saaigh, C. Boissier, M. Wahlgren, and H. Wikström. 2018. Sifting Segregation of Ideal Blends in a Two-Hopper Tester: Segregation pro Files and Segregation Magnitudes. *Powder Technology* 331: 60–67.

Moakher, M., T. Shinbrot, F.J. Muzzio, 2000. Experimental validated computations of flow, mixing, and segregation of non-cohesive grains in 3D tumbling blenders. *Powder Technology* 109, 58–71.

Mourad, M., M. Hemati, C. Laguerie. 1994. Hydrodynamique d'un séchoir a' lit fluidisé a' flottation: détermination des vitesses caractéristiques de fluidisation de mélanges de maïs et de sable, *Powder Technology* 80, 45–54.

Miller, C.O., A.K. Logwinuk. 1951. Fluidization studies of solid particles, *Industrial and Engineering Chemistry* 43, 1220–1226.

Noda, K., S. Uchida, T. Makino, H. Kamo. 1986. Minimum fluidisation velocity of binary mixture of particles with large size ratio, *Powder Technology* 46 (2–3), 149–154.

Nakamura, M., Y. Hamada, S. Toyama, A.E. Fouda, and C.E. Capes. 1985. An Experimental Investigation of Minimum Fluidization Velocity at Elevated Temperatures and Pressures. *The Canadian Journal of Chemical Engineering* 63, no. 1: 8–13.

Narsimhan, G. 1965. On generalised expression for prediction of minimum fluidisation velocity, *AIChE Journal* 11, 550–554.

Oka, S., A. Sahay, W. Meng, and F. Muzzio. 2017. Diminished Segregation in Continuous Powder Mixing. *Powder Technology* 309 (March): 79–88.

Poddar, R., G. Saluja, S.S. Mallick, and L. Kundan. 2023(a). An Investigation into Static Angle of Repose Using Pharmaceutical Powders. *Particulate Science and Technology* 42, no. 3 (April 2): 344–353.

Poddar, R., S.S. Mallick, and L. Kundan. 2023(b). An Experimental Investigation into Sifting and Fluidization Segregation Characteristics for Coal Fly Ash. *Particulate Science and Technology* 42, no. 4 (May 18): 515–526.

Paudel, B., Z.-G. Feng. 2013. Prediction of minimum fluidisation velocity for binary mixture of biomass and inert particles, *Powder Technology* 237, 134–140.

Prescott, J.K., R.J. Hossfeld. 1994. Maintaining product uniformity and uninterrupted flow to direct compression tablet press, 18(6), 99–114.

Rao, T.R., J.V. Ram Bheemarasetti. 2001. Minimum fluidisation velocities of mixtures of biomass and sands, *Energy* 26, 633–644.

Reina, J., E. Velo, L. Puigjaner. 2000. Predicting the minimum fluidisation velocity of polydisperse mixtures of scrap-wood particles, *Powder Technology* 111 (3), 245–251.

Rincon, J., J. Guardiola, A. Romero, G. Ramos. 1994. Predicting the minimum fluidisation velocity of multicomponent systems, *Journal of Chemical Engineering* 27, 177–181.

Riba, J.P., R. Routie, J.P. Couderc. 1978. Minimum conditions for fluidisation by a liquid, *Canadian Journal of Chemical Engineering* 56 (1), 26–30.

Schulze, D. 2008. Powders and Bulk Solids. *Chemie Ingenieur Technik* 82, no. 4 (April): 553–554.

Si, C., Q. Guo. 2008. Fluidization characteristics of binary mixtures of biomass and quartz sand in an acoustic fluidised bed, *Industrial & Engineering Chemical Research* 47, 9773–9782.

Subramani, H.J., M.B.M. Balaiyya, L.R. Miranda. 2007. Minimum fluidisation velocity at elevated temperatures for Geldart's group-B powders, *Experimental Thermal and Fluid Science* 32 (1), 166–173.

Shah, K.R., S.I. Farag Badawy, M.M. Szemraj, D.B. Gray, and M.A. Hussain. 2007. Assessment of Segregation Potential of Powder Blends. *Pharmaceutical Development and Technology* 12, no. 5 (January 7): 457–462.

Shinohara, K., and B. Golman. 2002. Segregation Indices of Multi-Sized Particle Mixtures during the Filling of a Two-Dimensional Hopper. *Advanced Powder Technology* 13, no. 1: 93–107.

Swaminathan, V., D.O. Kildsig. 2002. Polydisperse powder mixtures: effect of particle size and shape on mixture stability, *Drug Development and Industrial Pharmacy* 28 (1), 41–48.

Shinohara, K., B. Golman, and T. Nakata. 2001. Size Segregation of Multicomponent Particles during the Filling of a Hopper. *Advanced Powder Technology* 12, no. 1: 33–43.

Seville, J.P.K., C.D. Willett, P.C. Knight. 2000. Inter-particle forces in fluidisation: a review, *Powder Technology* 113, 261–268.

Tang, P., and V.M. Puri. 2007. Segregation Quantification of Two-Component Particulate Mixtures: Effect of Particle Size, Density, Shape, and Surface Texture. *Particulate Science and Technology* 25, no. 6 (December 5): 571–588.

Tang, P., and V.M. Puri. 2005. An Innovative Device for Quantification of Percolation and Sieving Segregation Patterns–Single Component and Multiple Size Fractions. *Particulate Science and Technology* 23, no. 4 (October): 335–350.

Tang, P., and V.M. Puri. 2004. Methods for Minimizing Segregation: A Review. *Particulate Science and Technology* 22, no. 4 (October): 321–337.

Thomas, A.L. 2024. A Mechanistic Framework for the Characterisation of Cohesive, Frictional and Interlocking Effects on Powder Flow Behaviour. *Particuology* 2, 54-62.

Thonglimp, V., N. Hiquily, C. Laguerie. 1984. Vitesse minimale de fluidization et expansion des couches de Mélanges de particules solides fluidisées par un gaz, *Powder Technology* 39, 223–239.

Vallance, J.W., S.B. Savage. 2000. Particle segregation in granular flows down chutes, in: A.D. Rosato, D.L. Blackmore (Eds.), *IUTAM Symposium on Segregation in Granular Flows*, Kluwer Academic Publishers, Boston, pp. 31–51.

Vaid, R.P., P. Sen Gupta. 1978. Minimum fluidisation velocities in beds of mixtures, *Canadian Journal of Chemical Engineering* 56, 292–296.

Van Heerden, C., A.P.P. Nobel, D.W. van Krevelen. 1951. Studies on fluidisation I — the critical mass velocity, *Chemical Engineering Science* 1 (1), 37–49.

Wang, S., Y. Fu, Y. Zhao, L. Dong, and Z. Chen. 2022. Effect of Bed Density on the Segregation Behavior of Fine Coal Particles (<6 Mm) in a Gas–Solid Separation Fluidized Bed. *Powder Technology* 395 (January): 872–882.

Wu, S.Y., J. Baeyens. 1991. Effect of operating temperature on minimum fluidisation velocity, *Powder Technology* 67 (2), 217–220.

Wen, C.Y., Y.H. Yu. 1966. A generalised method for predicting the minimum fluidisation velocity, *AIChE Journal* 12, 610–612.

Xu, C.C., J. Zhu. 2009. Prediction of minimum fluidisation velocity for fine particles of various degrees of cohesiveness, *Chemical Engineering Communications* 196, 499–517.

Xie, H.Y., and D. Geldart. 1995. Fluidization of FCC Powders in the Bubble-Free Regime: Effect of Types of Gases and Temperature. *Powder Technology* 82, no. 3: 269–277.

Zinatlou, S., D. Sofia, C. Hare, D. Barletta, and M. Poletto. 2024. Experimental Characterisation of the Spreading of Polymeric Powders in Powder Bed Fusion Additive Manufacturing Process at Changing Temperature Conditions. *Advanced Powder Technology* 35, 4, 104412.

Zhiping, Z., N. Yongjie, L. Qinggang. 2007. Effect of pressure on minimum fluidisation velocity, *Journal of Thermal Science* 16 (3), 264–269.

CHAPTER 7

Segregation Behaviour Under Different Moisture Content

7.1 Introduction

Moisture content can significantly impact the static and dynamic behaviour of powders, and hence potentially in may alter powder flowability and segregation characteristics (Emery et al., 2009; Opaliński et al., 2016). There is an inverse relationship between the flowability and moisture content of the powders, i.e., with an increase in the moisture content, the flowability of powders also decreases (Zou et al., 2002; Wang et al., 2010; Xu et al., 2017; Xu et al., 2006; Aviara et al., 2013; Mitra et al., 2017; Jin et al., 2018; Lu et al., 2018; Chinwan et al., 2019) due to the formation of liquid bridges (Zou et al., 2002; Harnby et al., 1996; Fitzpatrick et al., 2004; Plinke et al., 1994). This moisture-absorbing effect and the corresponding change in powder behaviour can significantly affect powders or particles that are hygroscopic in nature. The response of each powder sample towards change in moisture content is diverse (Fitzpatrick et al., 2004; Plinke et al., 1994), but very little work has been done on modelling the effect of moisture on particle segregation. Geldart A to B borderline powders have been considered for study. The aim of this study is to model the change in the sifting and fluidisation segregation behaviour of powders due to the presence of moisture. In the literature, the research attention has been predominantly directed towards studying segregation characteristics of larger particles, typically for Geldart Group B or D type particles (Kalman et al., 2023; Emery et al., 2009; Opaliński et al., 2016; Zou et al., 2002; Wang et al., 2010; Xu et al., 2017; Xu et al., 2006), where segregation has been generally found to exist. On the contrary, the effect of segregation has been found to be significantly less for particles that lie in Geldart Group A particles (Amagliani et al., 2016; Hastie, 2015; Marucci et al., 2018; Aviara et al., 2013; Mitra et al., 2017; Jin et al., 2018; Lu et al., 2018; Chinwan et al., 2019; Harnby et al., 1996). Very little research has been carried out on the segregation characteristics of particles in the Geldart Group A to B borderline zone. The novelty of this chapter is that it investigates into the effect of moisture on the segregation index of powders, and the study deals with the less explored Geldert Group A to B borderline zone.

7.2 Physical and flow properties

To understand the physical properties of different powder samples (as received), the results are presented in Table 7.1. This table provides the physical characteristics of various powder samples, including sand, three detergent powders (detergent_1, detergent_2, and detergent_3), and semolina. The size is represented by three values: d(10), in which 10% of the sample's mass is comprised of smaller particles; d(50), the median particle diameter, meaning 50% of the sample's mass is

comprised of smaller particles and d(90), in which 90% of the sample's mass is comprised of smaller particles. The particle size and course-to-fine ratio (CFR) results showed that the sand and semolina have relatively narrower size distributions than the detergents, with detergent_1 and detergent_2 having broader distributions. Figure 7.1 displays SEM images at a 500 μm scale, showing that the particles are non-spherical with a sphericity factor (SF) generally below unity, indicating that they are not perfectly circular. The shape factor has been considered in this study. The powders with a shape factor of 0.85 and above indicates more spherical in shape except semolina having a shape factor of 0.78, which may promote the particles to segregate but also depend on other powder properties. Density measurements indicate that sand has the highest bulk density of 1203 kg/m³, tapped density of 1622 kg/m³, and particle density of 2363 kg/m³. Semolina has the lowest bulk and tapped density of 694 kg/m³ and 806 kg/m³, respectively, while detergent_3 has the lowest particle density of 1723 kg/m³.

Table 7.1: Physical properties of different powder samples (as received)

Powder sample	**Particle size (μm)**			**CFR**	**SF**	**ρ_{lb} (kg/m^3)**	**ρ_t (kg/m^3)**	**ρ_p (kg/m^3)**	**Geldart group**
	d_{10}	**d_{50}**	**d_{90}**						
Sand	73	201	306	4.19	0.88±0.03	1203±36	1622±42	2366±44	B borderline
Detergent_1	98	274	856	8.73	0.91±0.06	859±24	1059±61	1945±29	B borderline
Detergent_2	127	362	983	7.74	0.85±0.04	731±28	929±24	1909±38	B borderline
Detergent_3	154	370	866	5.62	0.89±0.02	1055±44	1217±55	1723±42	B borderline
Semolina	260	477	902	3.47	0.78±0.08	694±14	806±39	2110±38	B borderline

Table 7.2 presents various powder samples' physical and flow properties (sand, three detergent powders labelled detergent_1, detergent_2, detergent_3, and semolina) at different moisture contents. The properties analysed include bulk density (ρ_{lb}), tapped density (ρ_t), repose angle (α_r), flow function coefficient inverse (1/ffc) at consolidation stress of 9 kPa, and cohesion. The increased capacity to retain moisture was attributed to the uneven and coarse surface texture, which allows for greater moisture adhesion to the particle surface (Kalman et al., 2021; Emery et al., 2009). As moisture content increases, the sand, detergent_1, and semolina powders exhibit decreased bulk and tapped densities. Increasing moisture from 0% to 1.4% for sand reduces loose poured bulk density from 1307

to 1106 kg/m³, and tapped density decreases from 1633 to 1579 kg/m³. Figure 7.2 illustrates the angle of repose of actual powder heaps (blue) and software-generated isosceles triangle heaps (red). With increasing the moisture content from 0 to 1.4 %, the angle of repose for sand increases from 41˚ to 55˚, which may indicate the loss of flowability. The cohesion also rose sharply from 0.105 kPa to 0.339 kPa with adding moisture. Detergent_1 shows a decrease in loose poured bulk density from 922 to 845 kg/m³ and a decrease in tapped density from 1084 to 1043 kg/m³ as moisture increases from 0% to 2.4%. Its angle of repose increases from 43˚ to 50˚, and cohesion more than doubles from 0.328 kPa to 0.738 kPa, reflecting decreased flowability and increased stickiness. Detergent_2 has loose poured densities with 690 kg/m³ at 0% moisture, maximum value at 728 kg/m³ at 2.2%, then 673 kg/m³ at 4.4%. Its angle of repose shows slight variation, while cohesion increases significantly from 0.534 kPa to 1.066 kPa, indicating higher adhesion. Detergent_3's bulk density initially increases at 0.75% moisture before dropping at 1.5%, with tapped density showing similar trends. Its angle of repose rises from 43˚ to 51˚, and cohesion increases from 0.437 kPa to 1.000 kPa. Semolina remains relatively stable in density, angle of repose, and cohesion across moisture levels, indicating minimal changes in flow properties. This stability makes semolina less sensitive to moisture changes than other powders, which experience decreased flowability and increased cohesion with higher moisture content. Kalman et al., 2021, found that for non-porous particles (like sand and glass beads), there is a sharp increase in AOR with an initial increase in moisture content from 0 to 1.5 % and then starts declining with a further increase in moisture content. In contrast, porous particles (like zeolite, bakelite and round rice) exhibit change in AOR with an increase of moisture content of 0 to 27 % and then sharply rise after a further increase in moisture content.

Table 7.2: Physical and flow properties of different powder samples at different moisture content

Powder sample	**Moisture content (%)**	**ρ_{lb} (kg/m^3)**	**ρ_t (kg/m^3)**	**AoR (˚)**	**1/ffc (at 9 kPa)**	**Cohesion (kPa)**
Sand	0	1307	1633	41	0.05	0.019
	0.7	1194	1635	53	0.11	0.072
	1.4	1106	1579	55	0.14	0.072
Detergent_1	0	922	1084	43	0.14	0.044
	1.2	852	1065	50	0.26	0.097
	2.4	845	1043	50	0.31	0.088
Detergent_2	0	690	863	47	0.13	0.049
	2.2	728	921	44	0.18	0.059
	4.4	673	891	47	0.41	0.093
Detergent_3	0	899	1123	43	0.14	0.034
	0.75	1045	1201	43	0.22	0.049
	1.5	773	1045	51	0.38	0.129
Semolina	0	699	812	38	0.02	0.012
	7	696	800	37	0.02	0.016
	14	685	805	39	0.03	0.033

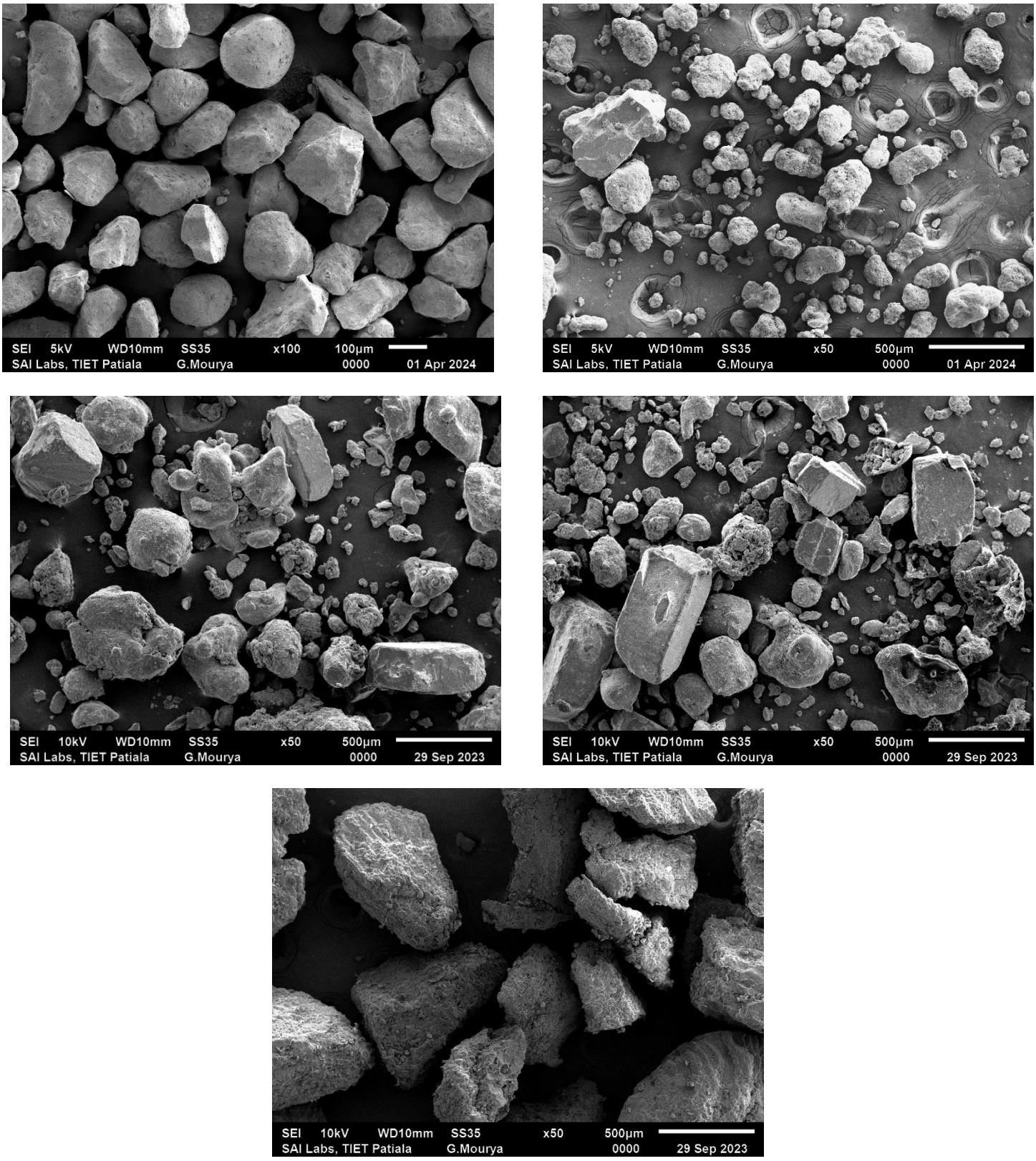

Figure 7.1: SEM images of different powder samples

(The top and the left image is of sand; the bottom image is of semolina)

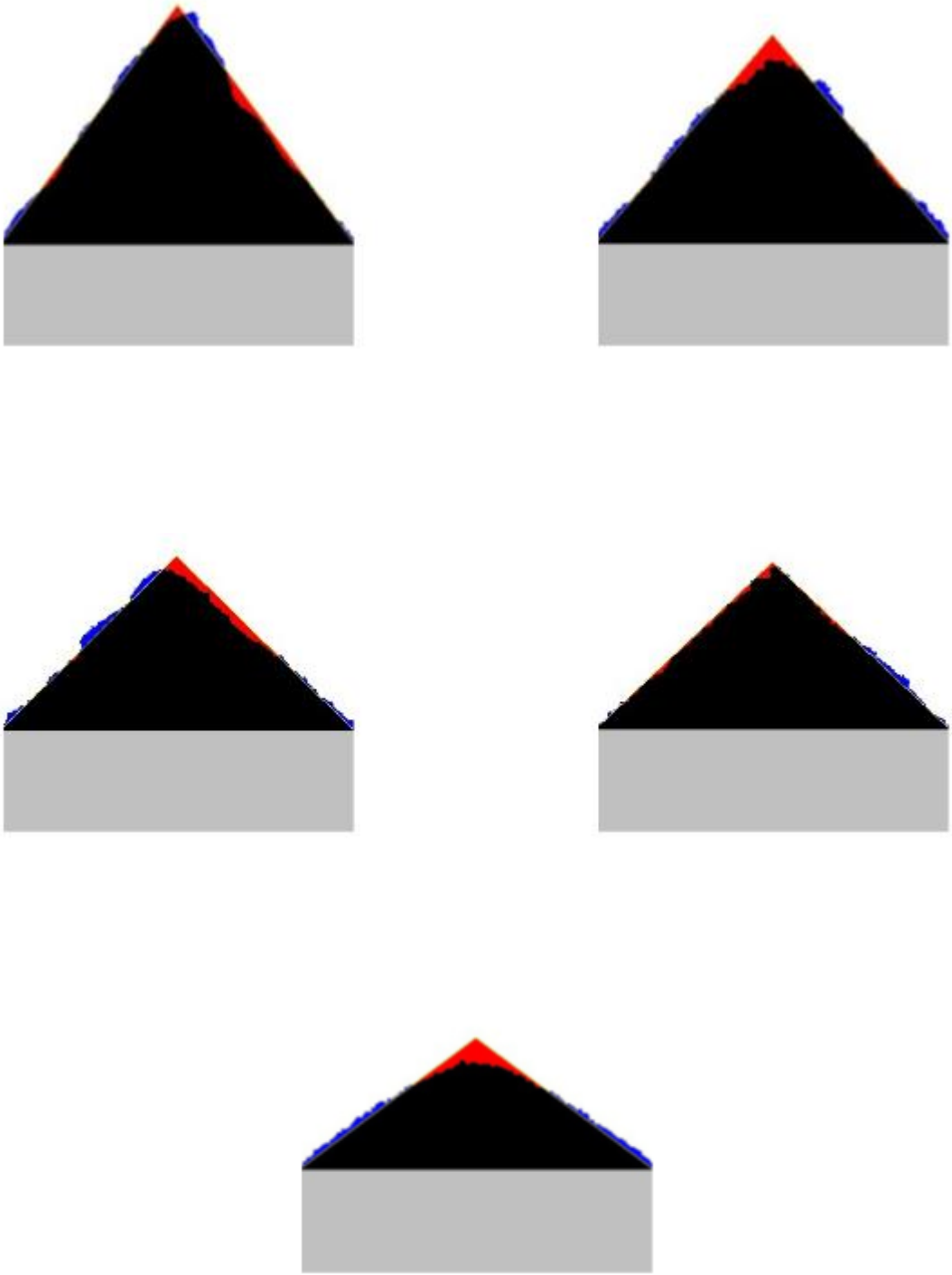

Figure 7.2: Heap images and angle of repose of different powder samples at a middle value of moisture content (The top and the left image is of sand; the bottom image is of semolina)

The powder flow behaviour under consolidation stress is presented by the flow function curve, which conducted the yield locus test with normal consolidated stress ranging from 1 to 9 kPa, while pre-shear stress ranged from 0.5 to 5 kPa. According to Jenike's methodology for assessing flow behaviour, Figure 7.3 (flow function graph) is categorised into five distinct flow regimes based on

the flow function coefficient (ffc) values. Powder with an ffc value of less than 1 is classified as non-flowing, and an ffc value between 1 and 2 is considered very cohesive. Cohesive powder has an ffc value between 2 and 4. Powder that is easy to flow has an ffc value between 4 and 10; an ffc value greater than ten is classified as free-flowing. The tendency of powder to flow is often reduced as its moisture content increases because the liquid layer at the particle surface strengthens the liquid bridges that develop between the particles (Emery et al., 2009; Opaliński et al., 2016; Mitra et al., 2017). Figure 7.3 has shown the flow function curve and cohesion for sand at different moisture content, indicating sand typically remains in a "free-flowing regime" at 0 % MC and further shifts in an "easy-flowing regime" with MC of 1.4 % due to an increase in cohesion. The result in Figure 7.3 (top-right) has shown a % increase in unconfined failure strength (σ_c) by 5.1 % with increasing the major principal consolidating stress (σ_1) from 5 to 9 kPa when moisture content is increased from 0 to 1.4 %. From 0 to 0.7 % increase in moisture content, the % increase in σ_c was found to be 3.3 % by increasing the σ_1 from 5 to 9 kPa. With an increase in moisture content, the % increase in σ_c from 3.3 % to 5.1 % and the % increase in cohesion from 5.9 % to 9.2 % represents the strengthening of the liquid bridge between the particles. Similarly, the effect of increasing MC and σ_1, on % increase in σ_c and cohesion for three different brands of detergent and semolina are presented in Figures 7.4 to 7.7. The results of three detergent powders (detergent_1, detergent_2, and detergent_3) and semolina powders have shown poor flowability and high cohesion with increased moisture content. The above observations are in line with the study suggested by the researchers that the moisture content remains on the surface of the sand particles due to no surface pores, which strengthens the liquid bridges, causing poor flowability. In contrast, the moisture content is distributed internally through pores and on the surface for detergents and semolina [8, 47-54]. I. Opaliński et al., 2016, has also found the same observation that the moisture content of up to 15 % was distributed by the food powders (semolina and course wheat flour) into the cores as well as the surface of their particles, which may change the particle surface properties.

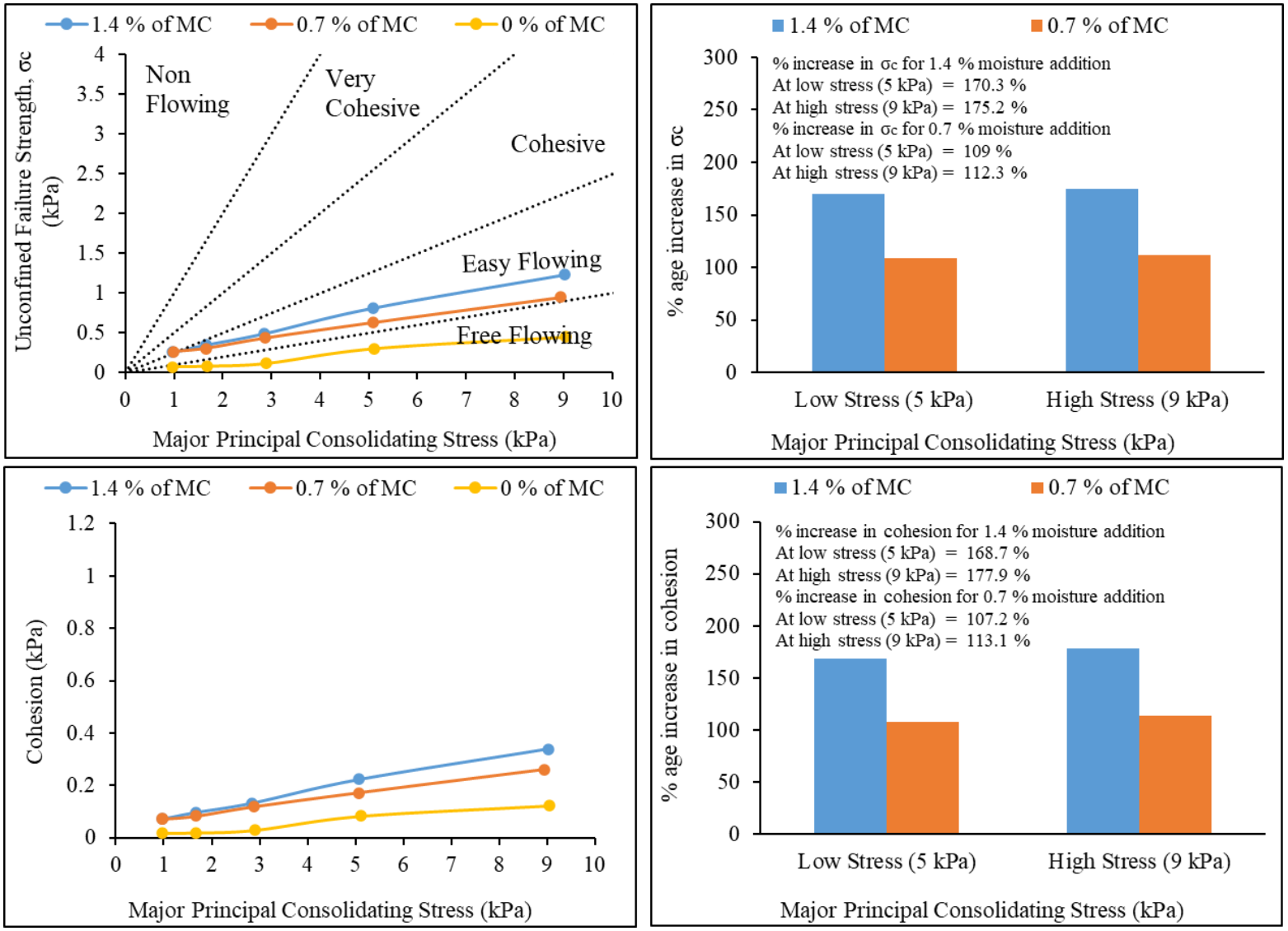

Figure 7.3: Results of flow function curve and cohesion for sand at different moisture content

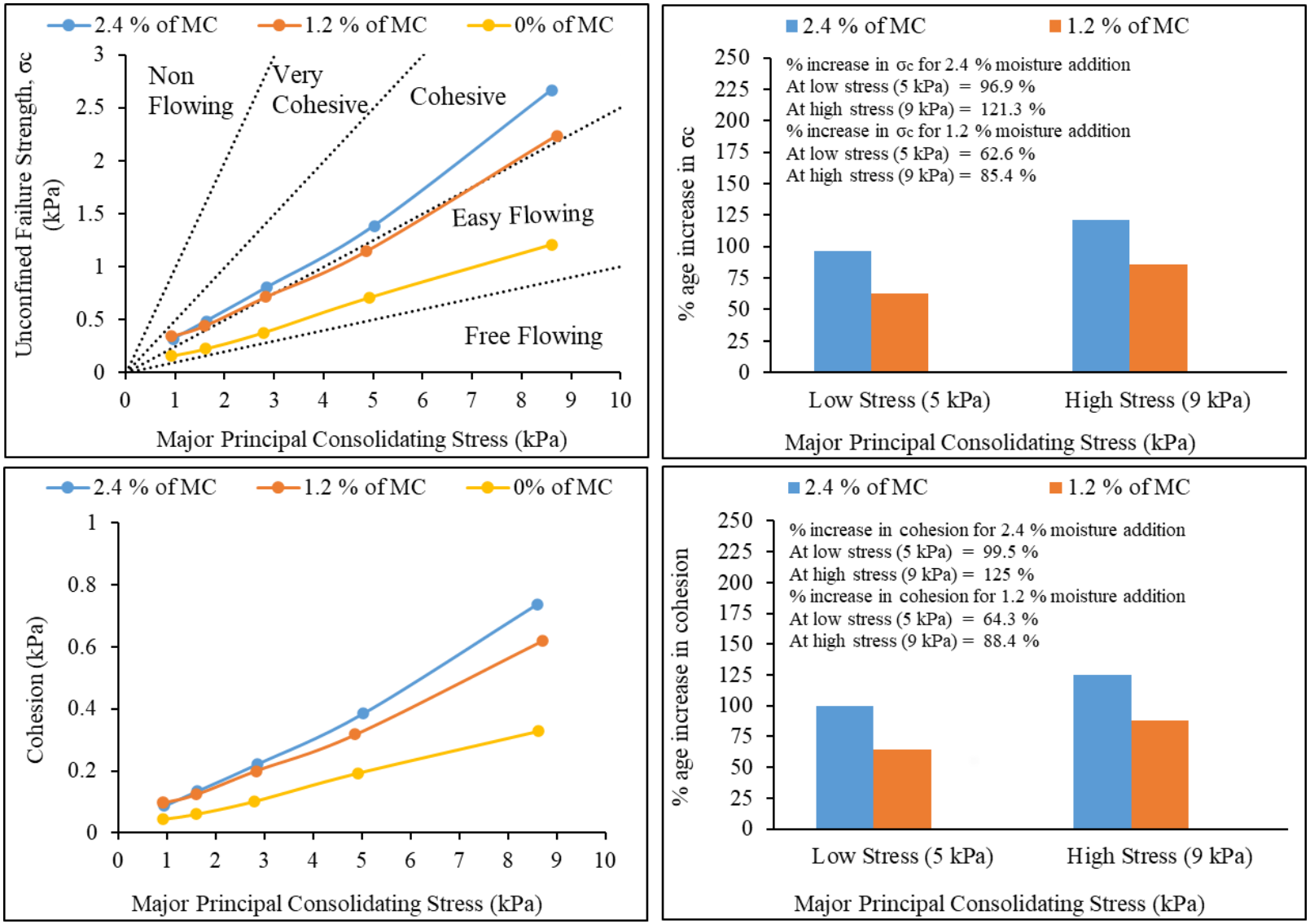

Figure 7.4: Results of flow function curve and cohesion for detergent_ 1 at different moisture content

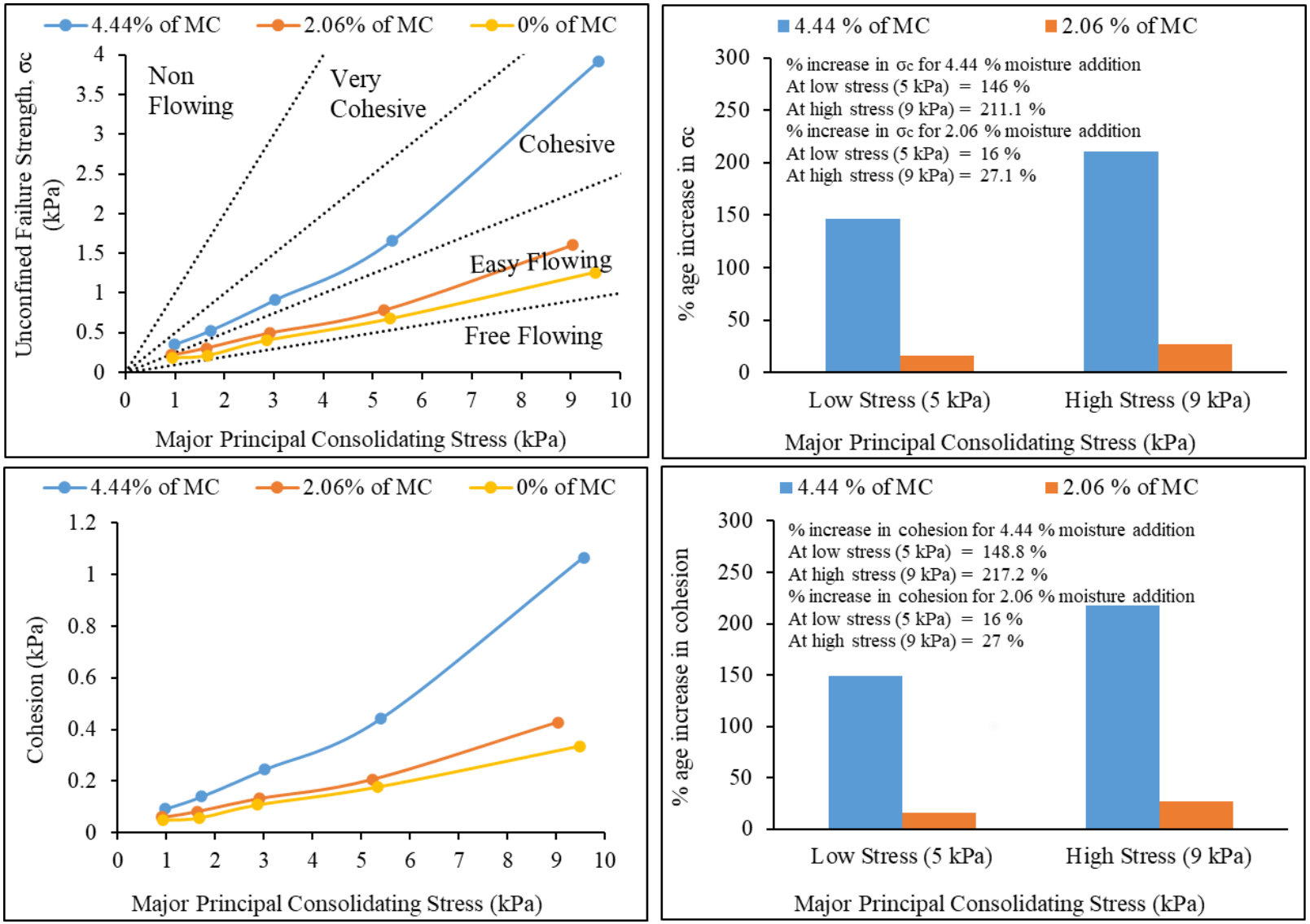

Figure 7.5: Results of flow function curve and cohesion for detergent_ 2 at different moisture content

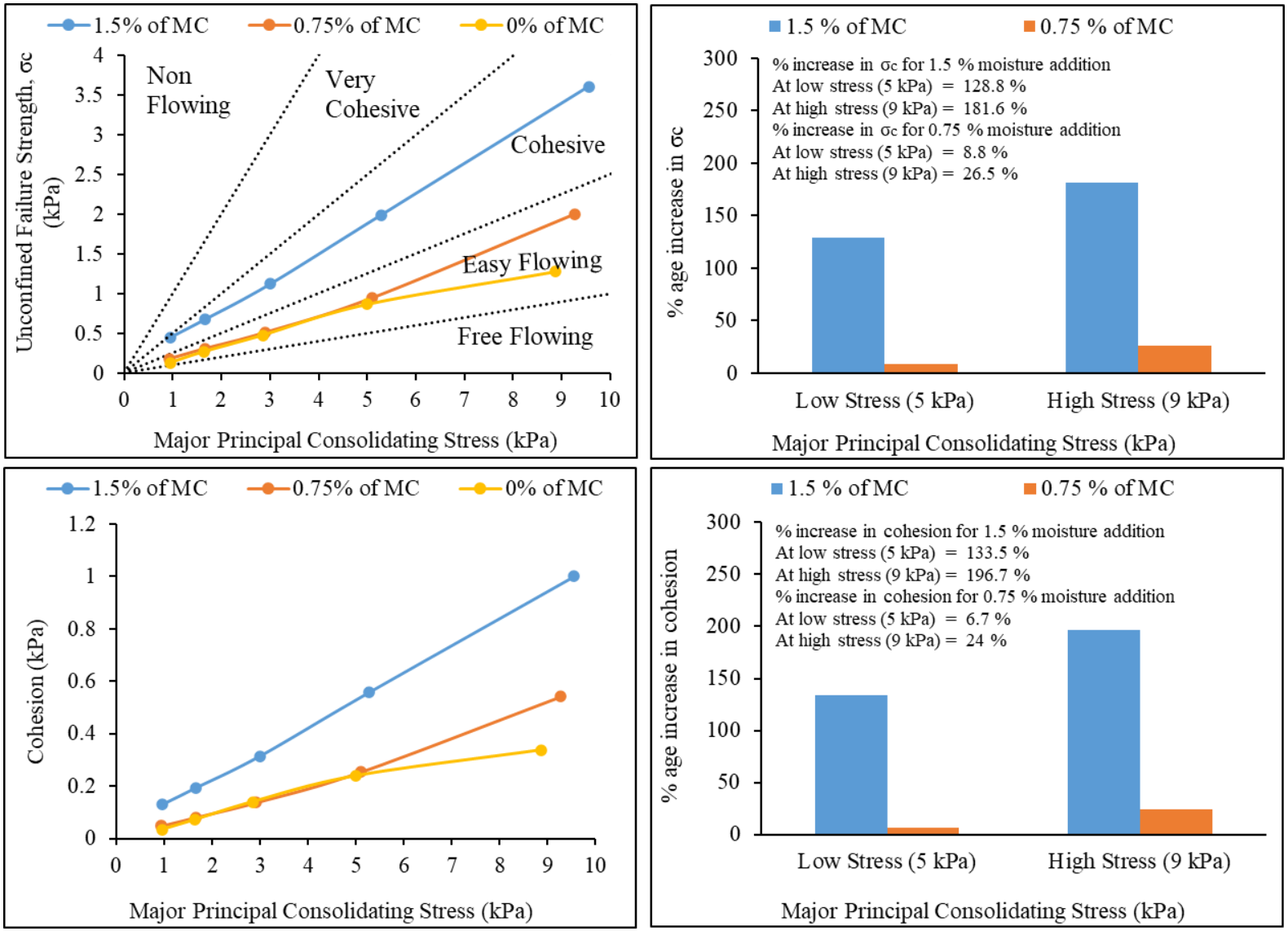

Figure 7.6: Results of flow function curve and cohesion for detergent_ 3 at different moisture content

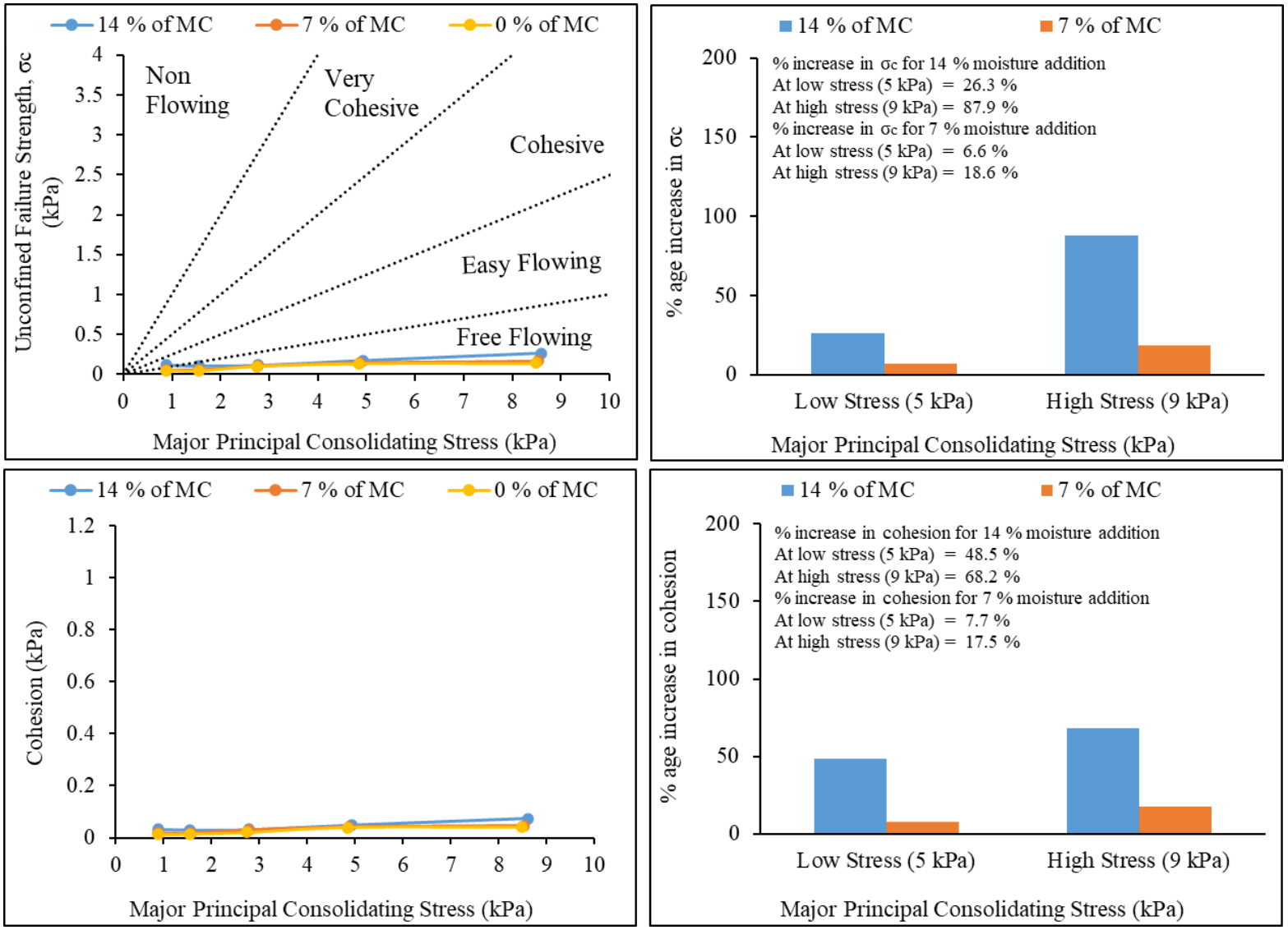

Figure 7.7: Results of flow function curve and cohesion for semolina at different moisture content

Figures 7.8 and 7.9 illustrate the effects of segregation on the particle-size distribution of powder samples analysed under different moisture content levels. These figures highlight two types of segregation mechanisms: sifting and fluidisation.

7.3 Sifting segregation

Figure 7.8 shows the results of sifting segregation, the particle-size distribution is presented for powder samples from the first and last batch at various moisture content levels. The data are color-coded for clarity: green for zero value, red for average value, and blue for maximum value. The particle-size distribution graphically represents the proportion of different-sized particles within a sample. In sifting segregation, the distribution changes as smaller particles accumulate in certain areas and larger particles dominate others. By comparing each powder sample, the green colour-coded zero moisture content significantly impacts this process compared to the average and at zero moisture content. Higher moisture levels increase particle cohesion, causing them to clump together and reducing their tendency to segregate. Jha et al., 2008, found that segregated fines mass and segregation rate values decreased significantly when relative humidity changed from 40 % to 60 %. It is also observed from Figure 7.8 that the difference in particle size distribution between the first and the last sample is wide for detergents: detergent_1, detergent_2, and detergent_3 compared to the sand and semolina at different moisture content levels, which promotes segregation od particles.

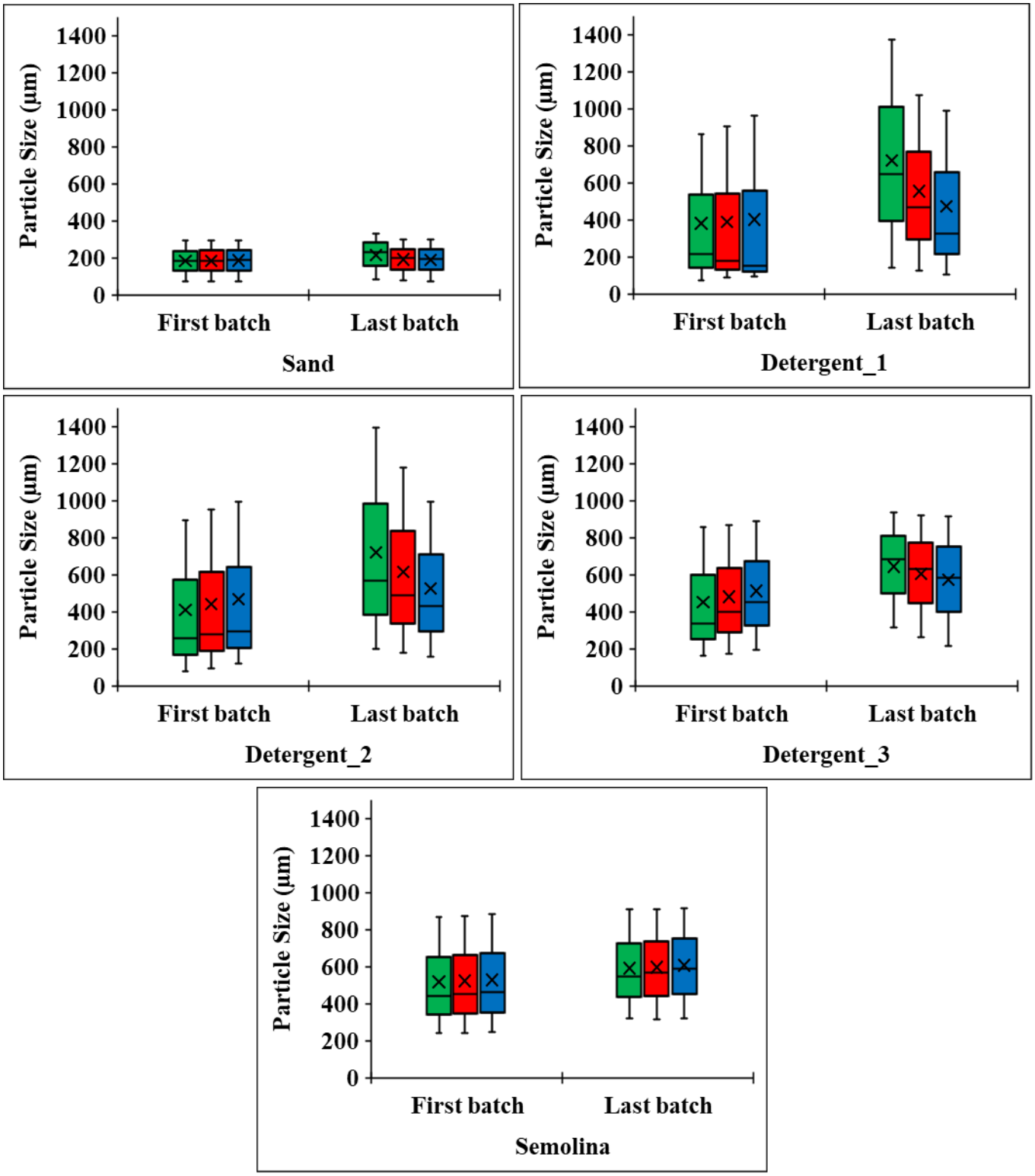

Figure 7.8: Results of sifting segregation: the particle-size distribution of powder samples (first and last batch) at different moisture content levels

7.4 Fluidisation segregation

Figure 7.9 presents the results of fluidisation segregation, which occurs when powders are suspended in an air stream. The figure displays the particle-size distribution for powder samples from the top and bottom batches at different moisture levels, using the colour coding: green for zero value, red for average value, and blue for maximum value. Due to the upward air steam in the test chamber, more moist particles interact with each other, causing particles to form agglomerates, which behave differently compared to individual particles in a fluidised state. Further, these agglomerates were segregated and settled down in the lower of the test chamber. In contrast, fine particles were carried out with the air stream in the upper section of the test chamber. Yang, 2003, observed that the agglomerates formed due to liquid contents segregated along the axial direction during a fluidised state. By comparing the results from Figure 7.9, the difference in particle size distribution is dominant for the blue colour-coded maximum value of moisture content (indicating higher tendency of powder segregation) compared to the green and red colour-coded, zero and average value of moisture content.

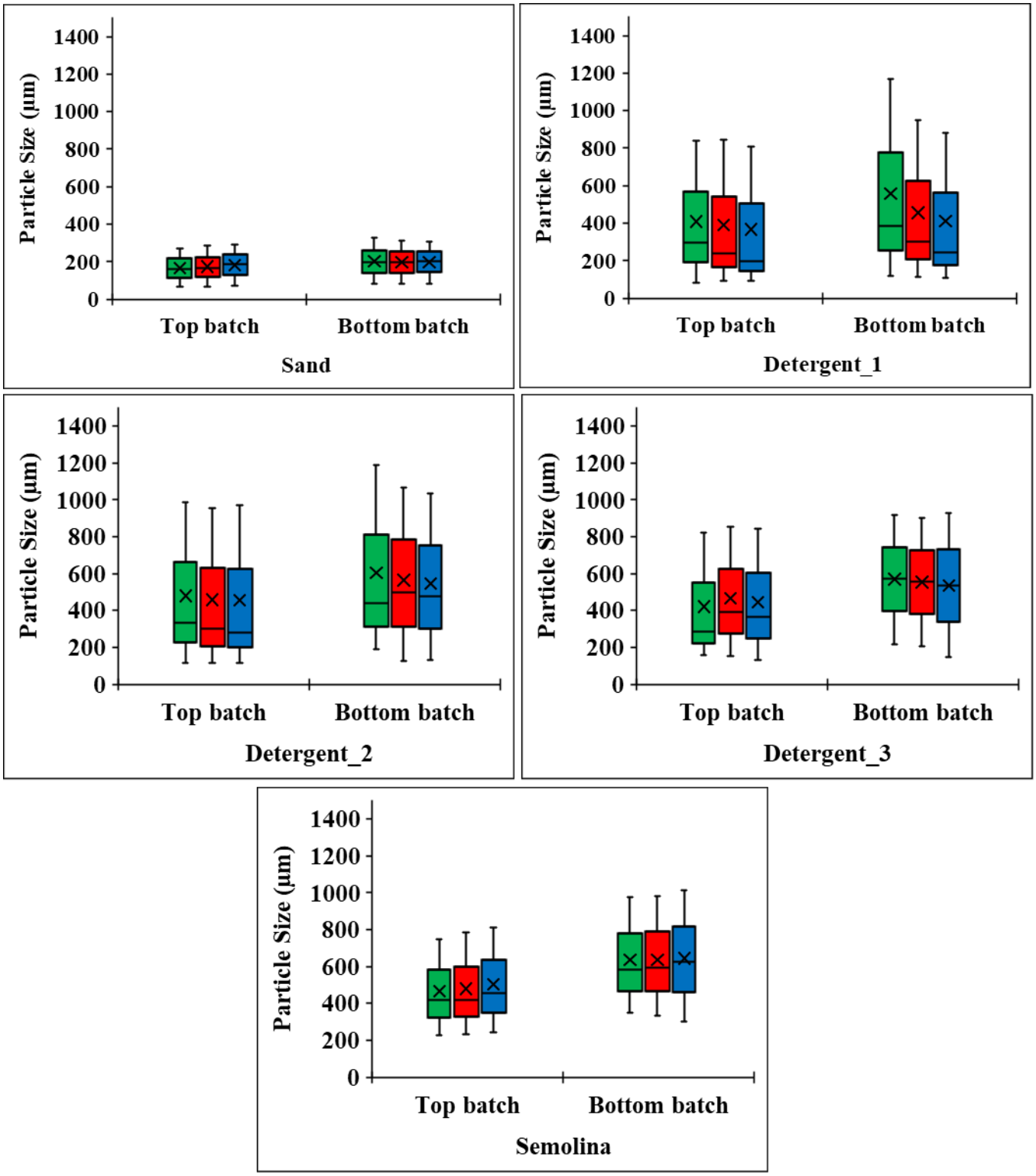

Figure 7.9: Results of fluidisation segregation: the particle-size distribution of powder samples (top and bottom batch) at different moisture content levels

In Figures 7.8 & 7.9, the Sand sample shows consistent particle size distributions with minimal variation, indicating excellent homogeneity across all batch positions. For Detergent_1 and Detergent_2, notable differences are observed between the first and last batches (sifting segregation) as well as between the top and bottom batches (fluidisation segregation). Specifically, the last and bottom batches tend to have higher median particle sizes and wider distributions, suggesting that coarser particles have either settled downward or segregated over time, indicating poor mixing or flow characteristics. Detergent_3 shows more consistent behaviour, with relatively uniform distributions across both comparisons, implying better homogeneity and resistance to segregation. Semolina also shows minor differences between batches, with slightly larger particles appearing in the last and bottom batches, but overall displays relatively consistent particle distributions. In summary, Figure 7.8 depicts temporal changes (start vs. end of processing), and the second image reflects longitudinal stratification (top vs. bottom of bulk material). Materials like Sand and Semolina show stability in both cases, whereas Detergent_1 and Detergent_2 exhibit clear signs of segregation, more pronounced in the bottom and last batch, due to differences in particle properties or flow behaviour.

7.5 Modelling sifting and fluidisation segregation indexes

The tendency of a powder sample to be segregated is known to be measured with the segregation index ($I_{S(k)}$), can be defined as the ratio of the difference of fine contents between segregated samples to the fine contents in their fresh/virgin sample at particle size range, k (Deng et al., 2021; Behiani, 2018). The mean segregation index ($\bar{I}_S$), demarcates certainty of powder segregation over the entire size range. To represent the mean segregation index for two different segregation mechanisms, i.e., sifting and fluidisation, the abbreviation is used, $\bar{I}_{SS}$ and $\bar{I}_{FS}$, respectively, as provided in Table 7.3.

$$I_{S(k)} = \left(\frac{C_L - C_F}{C_V}\right)_k \times 100\ \% \tag{7.1}$$

$$\bar{I}_S = \frac{1}{n}\sum_n |\, I_{S(k)} \,| \tag{7.2}$$

Where the parameters C_F, C_L, and C_V represent the fine content (by mass or volume) in the first/top, last/bottom and virgin sample at the particle size range (k). The particle size ranges are d(10), d(50) and d(90) (in µm), and n is the number of the particle size range.

Table 7.3: Sifting and fluidisation segregation index for powders at different moisture content

Powder sample	**Moisture content (%)**	**Particle size d(50) (μm)**	**CFR**	**ρ_P (kg/m^3)**	**SF**	**$\bar{I}_{SS}$ (%)**	**$\bar{I}_{FS}$ (%)**
Sand	0	199	3.82	2349	0.87	16.03	19.50
	0.7	191	3.88	2363	0.89	5.14	14.34
	1.4	195	3.97	2374	0.9	1.80	9.31
Detergent_1	0	368	9.95	1869	0.88	77.40	29.64
	1.2	269	9.22	1944	0.9	56.30	20.63
	2.4	215	8.63	1993	0.9	32.01	15.40
Detergent_2	0	371	8.44	1826	0.81	72.39	33.65
	2.2	352	7.53	1898	0.84	49.15	26.21
	4.4	389	8.61	1958	0.85	21.16	21.98
Detergent_3	0	354	5.76	1681	0.85	69.53	43.68
	0.75	369	5.98	1727	0.89	42.36	28.83
	1.5	380	6.30	1789	0.9	17.58	22.14
Semolina	0	482	3.36	2039	0.73	19.17	35.07
	7	487	3.38	2096	0.77	18.56	32.21
	14	524	3.32	2155	0.77	18.41	25.23

Figure 7.10 shows that the sifting segregation index decreases for all powders as the moisture content increases. At zero moisture content, Detergent_1 exhibits the highest segregation index (77.40), indicating significant separation, whereas Sand and Semolina have much lower values (16.03 and 15.37, respectively). The sifting segregation index for the powders was reduced as the moisture content reached an average level, showing that Detergent_1 was reduced to 56.30 and that sand reached the value of 5.14. With further increases in moisture content, the trend of the segregation index also goes down, with Detergent_1 dropping to 32.01 and sand to 1.80. Similarly, the sifting segregation index for Semolina showed a decreased value with increasing moisture content. The introduction of moisture significantly influences the cohesion and flow properties of powders. As moisture content increases, the segregation index declines, indicating that moisture acts as a binder, reducing the tendency of particles to separate. This effect is particularly pronounced in detergent powder samples (detergent_1, detergent_2, and detergent_3), which exhibit greater cohesion

compared to sand and semolina powders. Increased moisture creates liquid bridges between particles, enhancing cohesion but hindering flow. As moisture content (MC) increases, the moisture at each contact point also rises, leading to an increase in the filling angle of the liquid bridge. This mechanism increases the available surface area for liquid bridging, especially when combined with a wide particle size distribution. Consequently, the likelihood of different components separating diminishes, leading to a more homogeneous and stable mixture. The rough and irregular surface shapes of particles facilitate greater moisture adhesion, while the material's nature and structure also play a role in its moisture retention capabilities. The fluidisation segregation index (refer to Figure 7.11) shows a decrease in the segregation index with rising moisture content for most powders. At zero moisture content, Detergent_3 has the highest segregation index (43.68), indicating considerable separation under fluidisation, while Sand and Detergent_1 have the lowest indices (19.50 and 29.64, respectively). When moisture content reaches average levels, the segregation indices exhibit varying amounts of changes, with Detergent_3 dropping to 28.83, indicating even lesser separation. At maximum moisture content, the indexes continue to decrease for all powders, with Detergent_3 reaching 22.14. Increasing the moisture content in powder samples significantly impacts fluidisation segregation by enhancing particle cohesion through the formation of liquid bridges. These liquid bridges create attractive forces between particles, which help to keep them together during fluidisation, thereby preventing separation. Additionally, higher moisture levels increase the mass of fine particles, making them less susceptible to being lifted by airflow and reducing the likelihood of airborne particles—a common issue in fluidisation processes. Furthermore, moisture can promote the agglomeration of smaller particles, leading to a more uniform particle size distribution, which minimises segregation.

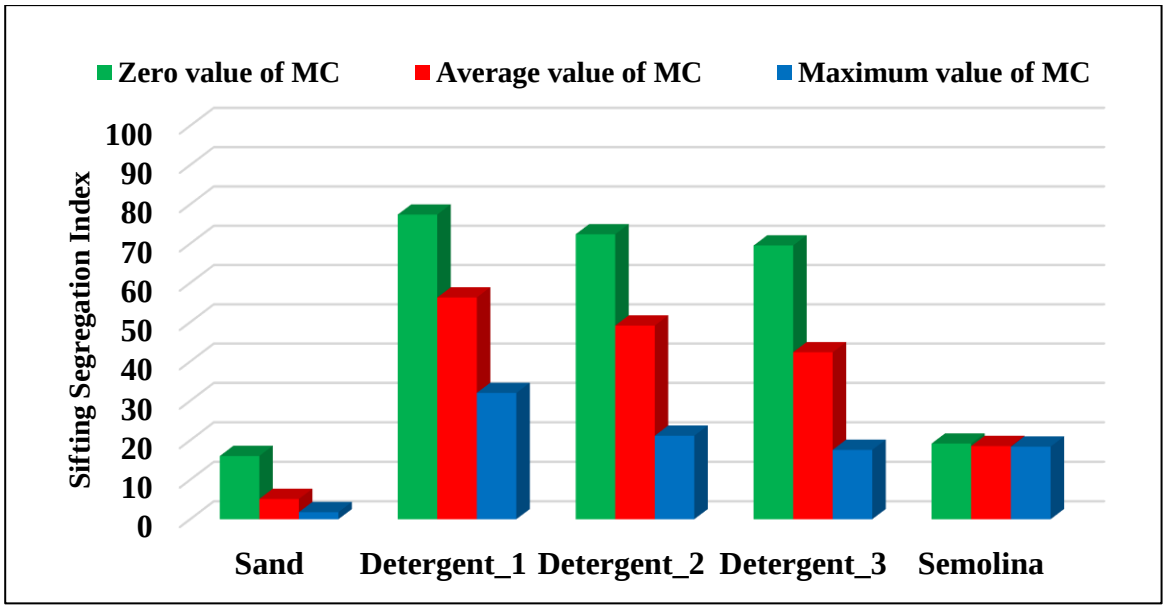

Figure 7.10: Sifting segregation index of powder samples at different moisture content

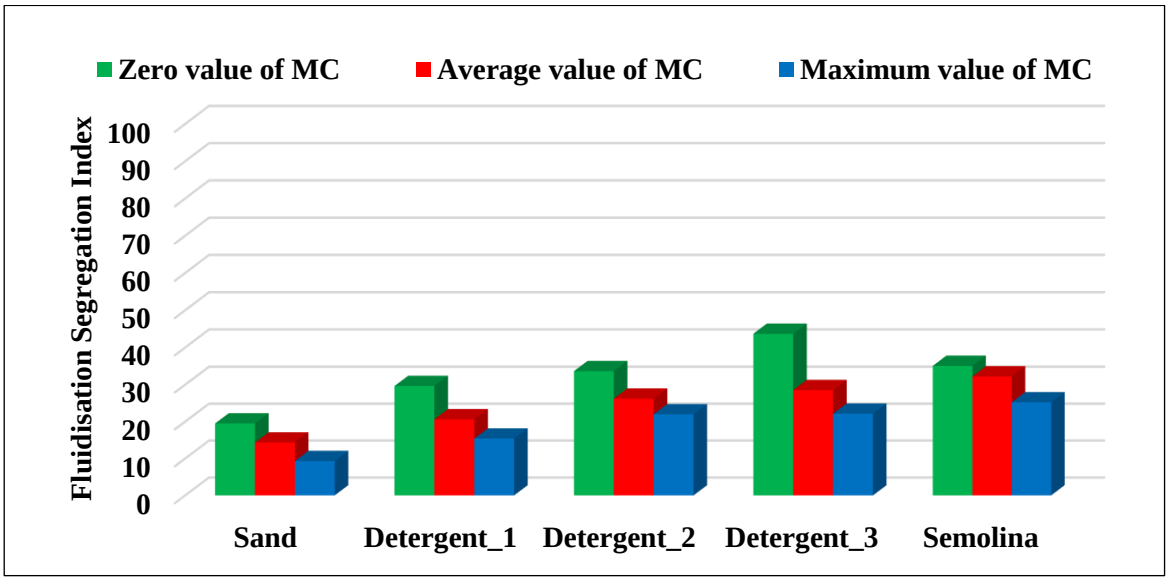

Figure 7.11: Fluidisation segregation index of powder samples at different moisture content

Parameters influencing sifting segregation

For the sake of completeness, the below-mentioned parameters have been repeated again as in the previous section. The particle properties influencing the sifting segregation are particle size ratio and particle shape (Tang et al., 2007; Prescott et al., 1994; Duffy et al, 2002; Lawerance, et al., 1969; Swaminathan et al., 2002; Vallence et al., 2000; Drahun et al., 1983). During hopper flow, the big

particles roll down due to their momentum from the top of the slope of the powder heap by passing the obstacles and reaching up to the bottom of the heap. The adhesion force between the particles has prevented the flow and allowed it to collect at the top of the heap. In this way, fine particles were collected at the top, and big particles gathered at the bottom of the heap, near the hopper wall. For sifting to happen, the powder should be free-flowing and cohesive powders are less prone to segregate due to fibrous and rough-textured particles, which restrict their free movement (Schulze, 2008; Fan et al., 207). Hence, the powder flowability also contributes to the sifting of powders during segregation (Marucci et al., 2018; Ketterhagen et al., 2007; Engblom et al., 2012), and several researchers utilised the flow function test to obtain the flow function (ffc) for describing the flow character of the powders (Behjani, 2018; Engblom et al., 2012; Deng et al., 2010; Asachi et al., 2018). Based on these conclusions, flow function as flow property, coarse-to-fine ratio, and shape factor have been considered to model the sifting segregation index.

Parameters influencing the fluidisation segregation

For the sake of completeness, the below-mentioned parameters have been repeated again as in the previous section. With the increase in gas velocity, the drag force on the particles starts to break the interparticle bond, and the powder bed gets fluidised. After this, a condition when the weight of the powder bed was balanced by the fluidising gas velocity and pressure drop across the powder bed remained fixed with an increase in the gas velocity. Then, this condition is known as the minimum fluidisation condition, and the corresponding velocity is the minimum fluidisation velocity (Schulze, 2008; Poddar et al., 2023(b); Hastie, 2015; Marucci et al., 2018). Beyond this minimum fluidisation velocity, the particles were suspended in the vertical column, and the powder bed was fully fluidised. The minimum fluidisation velocity is found to be a crucial parameter to measure the shift from a fixed state to a fluidised state of the powder bed in the vertical fluidising column (Wang et al., 2022; Alghamdi et al., 2021). While fluidising a powder bed, the fine and coarse particles may get segregated from each other, and fines collected in the upper portion while coarse settle down in the bottom, depending on their particle properties (Poddar et al., 2023(a); Tang et al., 2007). Different correlations of minimum fluidisation velocity for multicomponent particles are considered in this study to evaluate its relevance with the fluidisation segregation index in terms of coefficient corelation. Using the corelation of minimum fluidisation velocity as a typical example (Rincon et al., 1994), a best-fit correlation between minimum fluidisation velocity and fluidisation segregation index is considered.

The air drag required for a particle to remain in the air should equal its weight force. Additionally, while testing through the fluidisation test, it was observed that the gas flow rate required to raise or expend the powder bed depends on interparticle cohesion, which is the powder property (Wang et al., 2022; He et al., 2013; Gentzler et al., 2015; Thomas, 2024; Carr et al., 2019). Therefore, cohesion (C) has also been considered in the present study as a crucial parameter for studying the fluidisation segregation characteristics. Some researchers (Behjani et al., 2017 (a); Behjani et al., 2017 (b)) have used a dimensionless cohesion number (Coh) to predict particles' surface energy. In the current study, cohesion is utilised as a modified dimensionless cohesion number (Coh*), determined by having the ratio of required strength to overcome the interparticle cohesion to the dynamic pressure of gas supplied as a fluidising gas. The dynamic pressure of a gas meant by in this study is the kinetic energy per unit volume of gas supplied. This dimensionless cohesion number's importance is to represent the strength or effort involved of the dynamic pressure of gas supplied to overcome the interparticle cohesion by breaking it during the fluidising of a powder bed.

$$\text{Coh}^* = \frac{\text{Interparticle cohesion}}{\text{Dynamic pressure of air}} = \frac{C}{\frac{1}{2}\rho V^2} \tag{7.3}$$

The parameters ρ and V are the gas properties, gas density and superficial gas velocity, respectively. The best-fit correlation of minimum fluidisation velocity, $U_{mf\ (mixture)}$ (Rincon et al., 1994)) as a powder bed characteristic and the dimensionless cohesion number (Coh*) as an interparticle property are considered to model the fluidisation segregation index. The values of the parametric model are provided in Table 7.4, and Table 7.5 presents the percentage change in the parametric model for change in MC from zero to maximum value.

Table 7.4: Estimated values of the parametric model for sifting and fluidisation segregation

Powder sample	**Moisture content (%)**	**1/ffc (at 9 kPa)**	**SF**	**CFR**	**Coh***	$U_{mf(mixture)}$
Sand	0	0.05	0.87	3.82	7201	0.01486
	0.7	0.11	0.89	3.88	22103	0.01592
	1.4	0.14	0.9	3.97	16713	0.01679
Det_1	0	0.14	0.88	9.95	6003	0.03264
	1.2	0.26	0.9	9.22	11632	0.03324
	2.4	0.31	0.9	8.63	9348	0.03455
Det_2	0	0.13	0.81	8.44	12432	0.05601
	2.2	0.18	0.84	7.53	12578	0.05689
	4.4	0.41	0.85	8.61	16893	0.05792
Det_3	0	0.14	0.85	5.76	6680	0.0776
	0.75	0.22	0.89	5.98	8254	0.0888
	1.5	0.38	0.9	6.3	20205	0.1011
Semolina	0	0.02	0.73	3.36	6549	0.1063
	7	0.02	0.77	3.38	6064	0.1148
	14	0.03	0.77	3.32	10130	0.1266

To model the change in sifting and fluidisation segregation index with change in moisture content, it appears logic to utilise the same parameters as in the previous Chapter 6. Therefore, Table 7.5 represents the percentage change in the parameters influencing sifting and fluidisation segregation index with change in moisture content.

Table 7.5: Percentage change in estimated values of the parametric model for MC from zero to maximum value

Powder sample	**ΔMC (%)**	**Δ(1/ffc) at 9 kPa (%)**	**Δ(SF) (%)**	**Δ(CFR) (%)**	**Δ(Coh*) (%)**	**$\Delta U_{mf(mixture)}$ (%)**	**$\overline{\Delta I}_{SS}$ (%)**	**$\overline{\Delta I}_{FS}$ (%)**
Sand	1.4 %	180	3	4	132	12.99	89	52
Detergent_1	2.4 %	121	2	13	56	5.85	59	48
Detergent_2	4.4 %	215	5	2	36	3.41	71	35
Detergent_3	1.5 %	171	6	9	202	30.28	75	49
Semolina	14 %	50	5	1	55	19.10	4	28

The above-mentioned parametric models were utilised for the following models:

$$(\Delta\bar{I}_{SS})_{predicted} = 0.87 + 0.45\,\Delta\left({}^{1}/_{ffc}\right) - 3.63\,\Delta(SF) + 1.32\,\Delta(CFR) \quad (7.4)$$

$$(\Delta\bar{I}_{FS})_{predicted} = 35.49 + 0.23\,\Delta(Coh^{*}) - 1.07\,\Delta(U_{mf(mixture)}) \quad (7.5)$$

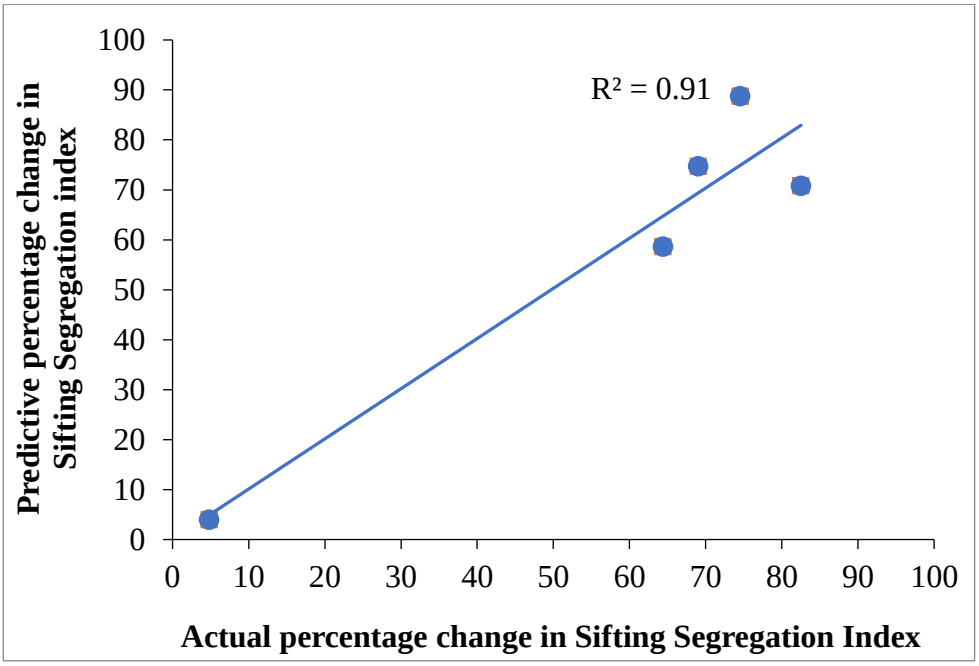

Figure 7.12: Predictive percentage change versus actual percentage change in sifting segregation index

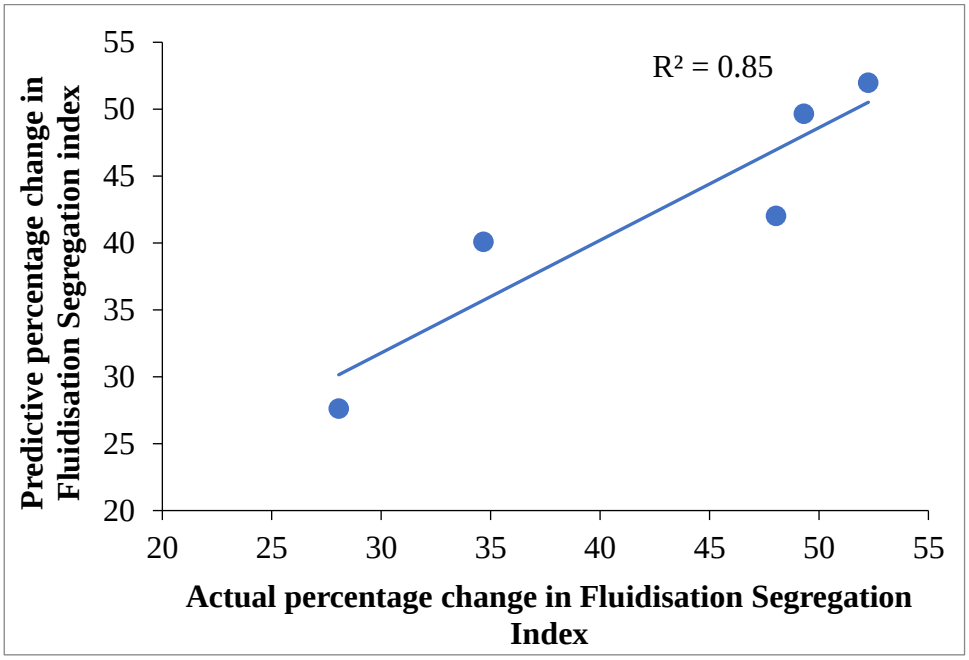

Figure 7.13: Predictive percentage change versus actual percentage change in fluidisation segregation index

The plots shown in Figures 7.12 and 7.13 compared the predicted percentage change and actual percentage change in segregation indexes for sifting and fluidisation segregation mechanisms. The results showed that the predicted percentage change in the sifting segregation index was 91 % accurate with the experimental data. The predicted percentage change in the fluidisation segregation index versus the experimental data, which has 85 % accuracy, suggests a good fit correlation.

7.6 Conclusion

The sifting and fluidisation segregation index is decreased with increasing the moisture content from zero to maximum for Geldart group A to B borderline powders considered in this study. It is observed that the sifting segregation characteristics is influenced by flow function as flow property, course-to-fine ratio and shape factor as the particle property. Based on these dimensionless parameters, a model has been developed for the sifting segregation index that provides a good fit of 91 % accuracy with the experimental data. For modelling the fluidisation segregation index, seven different correlations of minimum fluidisation velocity were evaluated, and a best-fit correlation of minimum fluidisation velocity has been considered along with a novel dimensionless cohesion number based on interparticle cohesion. The model of the fluidisation segregation index suggested a good fit of 85 % accuracy with the experimental data. The proposed model has been tested and validated at an appropriate rate of powder properties. In the future, a wide range of hygroscopic and non-hygroscopic powders with varying physical characteristics may be studied for further insight into the effect of moisture on segregation characteristics at a more fundamental level.

References

Ansari, M.I.H., A. Bhateja, and I. Sharma. 2023. Axial Segregation of Granular Mixtures in Laterally Shaken Multi-Trapezium Channels. *Powder Technology* 417, no. August 2022.

Alghamdi, Y.A., Z. Peng, Z. Almutairi, H. Alibrahim, F.M. Al-Alweet, B. Moghtaderi, and E. Doroodchi. 2021. Assessment of Correlations for Minimum Fluidization Velocity of Binary Mixtures of Particles in Gas Fluidized Beds. *Powder Technology* 394: 1231–1239.

Asachi, M., A. Hassanpour, M. Ghadiri, and A. Bayly. 2018. Experimental Evaluation of the Effect of Particle Properties on the Segregation of Ternary Powder Mixtures. *Powder Technology* 336: 240–254.

Alizadeh, M., A. Hassanpour, M. Pasha, M. Ghadiri, and A. Bayly. 2017. The Effect of Particle Shape on Predicted Segregation in Binary Powder Mixtures. *Powder Technology* 319: 313–322.

Amagliani, L., J.O. Regan, A.L. Kelly, and J.A.O. Mahony. 2016. Physical and Flow Properties of Rice Protein Powders. *Journal of Food Engineering* 190: 1–9.

Aviara, N.A., P.P. Power, T. Abbas. 2013. Moisture-dependent physical properties of Moringa oleifera seed relevant in bulk handling and mechanical processing, *Industrial Corporative Production* 42, 96–104.

Abou-Chakra, H., U. Tüzün. 2000. Microstructural blending of coal to enhance flowability, *Powder Technology* 111, 200–209.

Behjani, M.A. 2018. Numerical Simulation of Segregation of Formulated Powder Mixtures. *Thesis*, School of Chemical Engineering, The University of Leeds, UK.

Behjani, M.A., A. Hassanpour, M. Ghadiri, and A. Bayly. 2017(a). Numerical Analysis of the Effect of Particle Shape and Adhesion on the Segregation of Powder Mixtures. Ed. F. *EPJ Web of Conferences* 140, 06024.

Behjani, M.A., N. Rahmanian, N. Fardina bt Abdul Ghani, and A. Hassanpour. 2017(b). An Investigation on Process of Seeded Granulation in a Continuous Drum Granulator Using DEM. *Advanced Powder Technology* 28, no. 10 (October): 2456–2464.

Bourgeois, P., and P. Grenier. 1968. The Ratio of Terminal Velocity to Minimum Fluidising Velocity for Spherical Particles. *The Canadian Journal of Chemical Engineering* 46, no. 5: 325–328.

Chinwan, D., M.E. Castell-Perez. 2019. Effect of conditioner and moisture content on flowability of yellow cornmeal, *Food Science and Nutrition* 7, 3261–3272.

Coltters, R., A.L. Rivas. 2004. Minimum fluidisation velocity correlations in particulate systems, *Powder Technology* 147, 34–48.

Cheung, L., A.W. Nienow, P.N. Rowe. 1974. Minimum fluidisation velocity of a binary mixture of different sized particles, *Chemical Engineering Science* 29, 1301–1303.

Deng, T., V. Garg, H. Salehi, and M.S.A. Bradley. 2021. An Experimental Study on Free-Surface Rolling Segregation and Correlations with Angle of Repose and Particle Sphericity. *Powder Technology* 379: 307–320.

Devriendt, L., C. Gatumel, and H. Berthiaux. 2013. Experimental Evidence of Mixture Segregation by Particle Size Distribution. *Particulate Science and Technology* 31, no. 6 (November 2): 653–657.

Deng, T., K.A. Paul, M.S.A. Bradley, L. Immins, C. Preston, J.F. Scott, and E.H. Welfare. 2010. Investigations on Air Induced Segregation of Pharmaceutical Powders and Effect of Material Flow Functions. *Powder Technology* 203, no. 2 (November): 354–358.

Delebarre, A. 2004. Revisiting the Wen and Yu equations for minimum fluidisation velocity prediction, *Chemical Engineering Research and Design* 82 (5), 587–590.

Duffy, S.P., and V.M. Puri. 2002. Primary Segregation Shear Cell for Size-Segregation Analysis of Binary Mixtures, no. 20: 196–207.

Drahun, J. A., J. Bridgwater. 1983. The mechanisms of free surface segregation, *Powder Technology* 36, 39–53.

Drahun, J.A., J. Bridgwater. 1983. The mechanisms of free surface segregation, *Powder Technology* 36, 39–53.

Engblom, N., H. Saxén, R. Zevenhoven, H. Nylander, and G.G. Enstad. 2012(a). Segregation of Powder Mixtures at Filling and Complete Discharge of Silos. *Powder Technology* 215–216 (January): 104–116.

Engblom, N., H. Saxén, R. Zevenhoven, H. Nylander, and G.G. Enstad. 2012(b). Effects of Process Parameters and Hopper Angle on Segregation of Cohesive Ternary Powder Mixtures in a Small Scale Cylindrical Silo. *Advanced Powder Technology* 23, no. 5 (September): 566–579.

Engblom, N., H. Saxén, R. Zevenhoven, H. Nylander, and G.G. Enstad. 2012(c). Segregation of Construction Materials in Silos. Part 1: Experimental Findings on Different Scales. *Particulate Science and Technology* 30, no. 2 (March): 145–160.

Engblom, N., H. Saxén, R. Zevenhoven, H. Nylander, and G.G. Enstad. 2012(d). Segregation of Construction Materials in Silos. Part 2: Identification of Relevant Segregation Mechanisms. *Particulate Science and Technology* 30, no. 2 (March): 161–178.

Emery, E., J. Oliver, T. Pugsley, J. Sharma, and J. Zhou. 2009. Flowability of Moist Pharmaceutical Powders. *Powder Technology* 189, no. 3: 409–415.

Fry, A.M., V. Vidyapati, J.P. Hecht, P.B. Umbanhowar, J.M. Ottino, and R.M. Lueptow. 2020. Measuring Segregation Characteristics of Industrially Relevant Granular Mixtures: Part II – Experimental Application and Validation. *Powder Technology* 368, no. 1 (May): 278–285.

Fu, Z., J. Zhu, S. Barghi, Y. Zhao, Z. Luo, C. Duan. 2019. Minimum fluidization velocity of binary mixtures of medium particles in the air dense medium fluidised bed, *Chemical Engineering Science* 207, 194–201.

Fan, Y., K. V Jacob, B. Freireich, and R.M. Lueptow. 2017. Segregation of Granular Materials in Bounded Heap Flow: A Review. *Powder Technology* 312 (May): 67–88.

Fitzpatrick, J., S.A. Barringer, T. Iqbal. 2004. Flow property measurements of food powders and sensitivity of Jenike's hopper design methodology to the measured values, *Journal of Food Engineering* 61, 399–405.

Fletcher, J.V., M.D. Deo, F.V. Hanson. 1992. Re-examination of minimum fluidisation velocity correlations applied to Group B sands and coked sands, *Powder Technology* 69 (2), 147–155.

Garcia, M.C., H.J. Feise, S. Strege, and A. Kwade. 2015. Segregation in Heaps and Silos : Comparison between Experiment , Simulation and Continuum Model. *Powder Technology*.

Gentzler, M., J.N. Michaels, and G.I. Tardos. 2015. Quantification of Segregation Potential for Polydisperse, Cohesive, Multi-Component Powders and Prediction of Tablet Die-Filling Performance - A Methodology for Practical Testing, Re-Formulation and Process Design. *Powder Technology* 285: 96–102.

Gauthier, D., S. Zerguerras, G. Flamant. 1999. Influence of the particle size distribution of powders on the velocities of minimum and complete fluidisation, *Chemical Engineering Journal* 74 (3), 181–196.

Hastie, D.B. 2015. On the Difficulties of Sampling Bulk Powder Blends in Determining Segregation Propensity — A Case Study. *Powder Technology* 286 (December): 164–171.

He, X., X. Han, N. Ladyzhynsky, and R. Deanne. 2013. Assessing Powder Segregation Potential by near Infrared (NIR) Spectroscopy and Correlating Segregation Tendency to Tabletting Performance. *Powder Technology* 236 (February): 85–99.

Hartman, M., O. Trnka, K. Svoboda. 2000. Fluidization characteristics of dolomite and calcined dolomite particles, *Chemical Engineering Science* 55 (24), 6269–6274.

Harnby, N., A.E. Hawkins, I. Opaliński. 1996. Measurement of the adhesional force between individual particles with moisture present. Part 2. A novel experimental technique, *Chemical Engineering Research and Design* 74, 616–626 (Part A).

Jin, Y., H. Lu, X. Guo, X. Gong. 2018. Effect of water addition on flow properties of lignite particles, *Chemical Engineering Research and Design* 132, 1020–1029.

Jaklič, M., K. Kočevar, S. Srčič, and R. Dreu. 2015. Particle Size-Based Segregation of Pharmaceutical Powders in a Vertical Chute with a Closed Bottom: An Experimental Evaluation. *Powder Technology* 278 (July): 171–180.

Jha, A.K., and V.M. Puri. 2010. Percolation Segregation of Multi-Size and Multi-Component Particulate Materials. *Powder Technology* 197, no. 3 (January): 274–282.

Jha, A.K., and V.M. Puri. 2011. Percolation Segregation in Binary Size Mixtures Under Different Shear and Intensity of Motion. *Particulate Science and Technology* 29, no. 5 (September): 481–492.

Jha, A.K., H. Yi, and V.M. Puri. 2008(a). Percolation Segregation and Flowability Measurement of Urea under Different Relative Humidity Conditions. *KONA Powder and Particle Journal* 26, no. March: 167–177.

Jha, A.K., J.S. Gill, and V.M. Puri. 2008(b). Percolation Segregation in Binary Size Mixtures of Spherical and Angular-Shaped Particles of Different Densities. *Particulate Science and Technology* 26, no. 5 (September 29): 482–493.

Kalman, H. 2021. Effect of Moisture Content on Flowability: Angle of Repose, Tilting Angle, and Hausner Ratio. *Powder Technology* 393: 582–596.

Ketterhagen, W.R., J.S. Curtis, C.R. Wassgren, A. Kong, P.J. Narayan, and B.C. Hancock. 2007. Granular Segregation in Discharging Cylindrical Hoppers: A Discrete Element and Experimental Study. *Chemical Engineering Science* 62, no. 22 (November): 6423–6439.

Liu, P., S. Yang, J. Hu, and H. Wang. 2024. Density-Induced Segregation Property of Solid Phase in a Three-Dimensional Liquid-Solid Fluidized Bed. *Powder Technology* 432, no. October 2023: 119167.

Liu, X., Q. Zheng, L. Yang, M. Cai, G. Cheng, and A. Yu. 2023. The Segregation of Cement Clinker Particles in a Mill-Feeding Hopper: PIV Experiment and FEM Modelling. *Powder Technology* 426, no. May: 118656.

Lumay, G., F. Boschini, K. Traina, S. Bontempi, J.-C. Remy, R. Cloots, and N. Vandewalle. 2012. Measuring the Flowing Properties of Powders and Grains. *Powder Technology* 224 (July): 19–27.

Levin (Ed.). M., 2011. Pharmaceutical Process Scale-Up, *Informa Healthcare*, New York, USA

Levy, A., C.J. Kalman, 2001. Handbook of Conveying and Handling of Particulate Solids, *Elsevier*, UK.

Lucas, A., J. Arnaldos, J. Casal, L. Puigjaner. 1986. High temperature incipient fluidisation in mono and poly disperse systems, *Chemical Engineering Communications* 41, 121–132.

Marucci, M., B. Al-saaigh, C. Boissier, M. Wahlgren, and H. Wikström. 2018. Sifting Segregation of Ideal Blends in a Two-Hopper Tester: Segregation pro Files and Segregation Magnitudes. *Powder Technology* 331: 60–67.

Mitra, H., H.A. Pushpadass, M.E.E. Franklin, R.P.K. Ambrose, C. Ghoroi, S.N. Battula. 2017. Influence of moisture content on the flow properties of basundi mix, *Powder Technology* 312, 133–143.

McGlinchey, D. 2005. *Characterisation of Bulk Solids*. Ed. Don McGlinchey. *Characterisation of Bulk Solids*. Wiley.

Moakher, M., T. Shinbrot, F.J. Muzzio, 2000. Experimental validated computations of flow, mixing, and segregation of non-cohesive grains in 3D tumbling blenders. *Powder Technology* 109, 58–71.

Mourad, M., M. Hemati, C. Laguerie. 1994. Hydrodynamique d'un séchoir a' lit fluidisé a' flottation: détermination des vitesses caractéristiques de fluidisation de mélanges de maïs et de sable, *Powder Technology* 80, 45–54.

Miller, C.O., A.K. Logwinuk. 1951. Fluidization studies of solid particles, *Industrial and Engineering Chemistry* 43, 1220–1226.

Noda, K., S. Uchida, T. Makino, H. Kamo. 1986. Minimum fluidisation velocity of binary mixture of particles with large size ratio, *Powder Technology* 46 (2–3), 149–154.

Nakamura, M., Y. Hamada, S. Toyama, A.E. Fouda, and C.E. Capes. 1985. An Experimental Investigation of Minimum Fluidization Velocity at Elevated Temperatures and Pressures. *The Canadian Journal of Chemical Engineering* 63, no. 1: 8–13.

Narsimhan, G. 1965. On generalised expression for prediction of minimum fluidisation velocity, *AIChE Journal* 11, 550–554.

Oka, S., A. Sahay, W. Meng, and F. Muzzio. 2017. Diminished Segregation in Continuous Powder Mixing. *Powder Technology* 309 (March): 79–88.

Opaliński, I., M. Chutkowski, and A. Hassanpour. 2016. Rheology of Moist Food Powders as Affected by Moisture Content. *Powder Technology* 294 (June): 315–322.

Poddar, R., S.S. Mallick, and L. Kundan. 2023(a). An Experimental Investigation into Sifting and Fluidization Segregation Characteristics for Coal Fly Ash. *Particulate Science and Technology* 42, no. 4 (May 18): 515–526.

Poddar, R., G. Saluja, S.S. Mallick, and L. Kundan. 2023(b). An Investigation into Static Angle of Repose Using Pharmaceutical Powders. *Particulate Science and Technology* 42, no. 3 (April 2): 344–353.

Plinke, M.E., D. Leitch, F. Loffler. 1994. Cohesion in granular materials, *Bulk Solids Handling* 14, 101–106.

Prescott, J.K., R.J. Hossfeld. 1994. Maintaining product uniformity and uninterrupted flow to direct compression tablet press, 18(6), 99–114.

Reina, J., E. Velo, L. Puigjaner. 2000. Predicting the minimum fluidisation velocity of polydisperse mixtures of scrap-wood particles, *Powder Technology* 111 (3), 245–251.

Rincon, J., J. Guardiola, A. Romero, G. Ramos. 1994. Predicting the minimum fluidisation velocity of multicomponent systems, *Journal of Chemical Engineering* 27, 177–181.

Riba, J.P., R. Routie, J.P. Couderc. 1978. Minimum conditions for fluidisation by a liquid, *Canadian Journal of Chemical Engineering* 56 (1), 26–30.

Salehi, H., J.G. Timmerfors, H. Hajmohammadi, V. Garg, R.J. Berry, D. Barletta, M. Poletto, L.J. Jönsson, M.S.A. Bradley, and S.H. Larsson. 2024. The Role of Particle Size and Other Properties on Silo Discharge Behaviour of Chipped Wood Biomass. *Powder Technology* 432, no. August 2023.

Schulze, D. 2008. Powders and Bulk Solids. *Chemie Ingenieur Technik* 82, no. 4 (April): 553–554.

Si, C., Q. Guo. 2008. Fluidization characteristics of binary mixtures of biomass and quartz sand in an acoustic fluidised bed, *Industrial & Engineering Chemical Research* 47, 9773–9782.

Subramani, H.J., M.B.M. Balaiyya, L.R. Miranda. 2007. Minimum fluidisation velocity at elevated temperatures for Geldart's group-B powders, *Experimental Thermal and Fluid Science* 32 (1), 166–173.

Shah, K.R., S.I. Farag Badawy, M.M. Szemraj, D.B. Gray, and M.A. Hussain. 2007. Assessment of Segregation Potential of Powder Blends. *Pharmaceutical Development and Technology* 12, no. 5 (January 7): 457–462.

Shinohara, K., and B. Golman. 2002. Segregation Indices of Multi-Sized Particle Mixtures during the Filling of a Two-Dimensional Hopper. *Advanced Powder Technology* 13, no. 1: 93–107.

Swaminathan, V., D.O. Kildsig. 2002. Polydisperse powder mixtures: effect of particle size and shape on mixture stability, *Drug Development and Industrial Pharmacy* 28 (1), 41–48.

Shinohara, K., B. Golman, and T. Nakata. 2001. Size Segregation of Multicomponent Particles during the Filling of a Hopper. *Advanced Powder Technology* 12, no. 1: 33–43.

Seville, J.P.K., C.D. Willett, P.C. Knight. 2000. Inter-particle forces in fluidisation: a review, *Powder Technology* 113, 261–268.

Thomas, A.L. 2024. A Mechanistic Framework for the Characterisation of Cohesive, Frictional and Interlocking Effects on Powder Flow Behaviour. *Particuology* 2, 54-62.

Tang, P., and V.M. Puri. 2007. Segregation Quantification of Two-Component Particulate Mixtures: Effect of Particle Size, Density, Shape, and Surface Texture. *Particulate Science and Technology* 25, no. 6 (December 5): 571–588.

Tang, P., and V.M. Puri. 2005. An Innovative Device for Quantification of Percolation and Sieving Segregation Patterns–Single Component and Multiple Size Fractions. *Particulate Science and Technology* 23, no. 4 (October): 335–350.

Tang, P., and V.M. Puri. 2004. Methods for Minimizing Segregation: A Review. *Particulate Science and Technology* 22, no. 4 (October): 321–337.

Vallance, J.W., S.B. Savage. 2000. Particle segregation in granular flows down chutes, in: A.D. Rosato, D.L. Blackmore (Eds.), *IUTAM Symposium on Segregation in Granular Flows*, Kluwer Academic Publishers, Boston, pp. 31–51.

Wang, S., Y. Fu, Y. Zhao, L. Dong, and Z. Chen. 2022. Effect of Bed Density on the Segregation Behavior of Fine Coal Particles (<6 Mm) in a Gas–Solid Separation Fluidized Bed. *Powder Technology* 395 (January): 872–882.

Wang, W., J. Zhang, S. Yang, H. Zhang, H. Yang, G. Yue. 2010. Experimental study on the angle of repose of pulverised coal, *Particuology* 8, 482–485.

Wu, S.Y., J. Baeyens. 1991. Effect of operating temperature on minimum fluidisation velocity, *Powder Technology* 67 (2), 217–220.

Wen, C.Y., Y.H. Yu. 1966. A generalised method for predicting the minimum fluidisation velocity, *AIChE Journal* 12, 610–612.

Xu, G., X. Chen, C. Liang, P. Xu, C. Zhao. 2017. Experimental investigation on the flowability properties of cohesive carbonaceous powders, *Particulate Science and Technology* 35, 322–329.

Xu, C.C., J. Zhu. 2009. Prediction of minimum fluidisation velocity for fine particles of various degrees of cohesiveness, *Chemical Engineering Communications* 196, 499–517.

Xu, J.Q., R.P. Zou, A.B. Yu. 2006. Quantification of the mechanisms governing the packing of iron ore fines, *Powder Technology* 169, 99–107.

Xie, H.Y., and D. Geldart. 1995. Fluidization of FCC Powders in the Bubble-Free Regime: Effect of Types of Gases and Temperature. *Powder Technology* 82, no. 3: 269–277.

Zou, Y., G.H. Brusewitz. 2002. Flowability of uncompacted marigold powder as affected by moisture content, Journal of Food Engineering. 55, 165–171.

CHAPTER 8

Conveying of Segregated Powders

8.1 Introduction

The purpose of this chapter is to illustrate the effects of the potential difficulties of handling powders with a narrower size distribution compared to a wider size distribution w.r.t pneumatic conveying. Narrower size distribution may occur as a result of segregation, where the larger particles tend to get separated from the finer components. While fully removal of segregation may not be practically possible, methods could be adopted in the design stage and during operation to limit the extent of segregation as much as possible. This chapter provides a threshold limiting criteria for segregation which would compromise the fluidised dense-phase conveyability of powders. Fly ash has been chosen as a material for study in this chapter. The main reason for the selection of fly ash is it is a bulk solid which has a large significance in India as the Indian power stations being most coal-based and Indian ash has high ash content (typically 35-45%). At the same time, fly ash is a rather unpredictable material to be handled due to its Group A to B borderline characteristics (Setia, 2016(a); Pan, 1992; Desai, 1992; Wypych, 1989).

Coal-fired thermal power plants are the major source of power generation in India and worldwide (Srinivasan et al., 2021; Liu et al., 2021; Howladar et al., 2016; Wang et al., 2022). Indian coal used in thermal power plants suffers from high ash content (generally 35 to 45% by weight of coal) (Xing et al., 2019; Sahoo et al., 2011). The large amount of ash that is produced every day needs to be transported reliably, economically, and in an environmental- friendly manner. Out of the total amount of ash that is generated, a major portion (80%) is in the form of fly ash and is collected in different fields of Electrostatic Precipitator (ESP) hoppers and a minor quantity is collected in Air Preheater Hoppers (APH) (Ohenoja et al., 2018; Rani et al., 2019; Fuller et al., 2018). Commonly, the fly ash collected in ESP hoppers is conveyed pneumatically to a nearby buffer using a vacuum system or pressure conveying system. Subsequently, the ash is transported to remote silos using a pressure conveying system. Some reasons for the use of a pneumatic conveying system to transport fly ash include: totally enclosed conveying, dry handling, environmentally friendly mode of transport, relatively low capital and maintenance costs (for a well-designed system), layout flexibility, ash reuse and ease of automation and installation (Bhatia, 2019; Jones et al., 2008; James et al., 2012; Mills et al., 2016; Woodcock et al., 1987). The traditional pneumatic transport mode is called the dilute phase (or suspension flow), where the carrier gas velocity is sufficiently high to entrain and suspend all the particles along the pipeline (Jones et al., 2008; Klinzing et al., 2010; Yang et al., 2003). Due to the dispersed and suspended nature of the flow, the researchers/designers have enjoyed good success in modelling the relevant particle interactions and mechanisms (e.g. friction, impact, drag, slip velocity,

etc.) for dilute-phase systems (Jones et al., 2008; Mallick, 2009; Setia et al., 2016; Cenna et al., 2014). The fluidised dense-phase (FDP) mode of conveying for fine powders (typically Geldart Group A powders, such as fly ash) is gaining more popularity due to the high achievable solids-to-gas mass flow ratio (Sharma et al., 2019). This high concentration results in reduced capital and operating cost of the compressor, smaller pipe and fitting sizes, and lower conveying velocity, resulting in reduced rate of product and pipeline damage and smaller size of filtration equipment requirement (Bhatia, 219; Alkassar et al., 2021). Fluidised dense-phase pneumatic transport takes benefits from the air-retention properties of bulk material. The non-suspension method of conveying, also known as dense-phase flow, can be achieved by reducing the conveying velocity relative to the bulk powder's saltation velocity. However, insufficient airflow or a drop in gas flow rate above the optimal "steady state" dense-phase domain would result in unstable dunes with substantial pressure variations. Additional decreases in gas velocity could happen in deposits of powder building up in the pipeline, causing the system to be unable to achieve a steady-state conveying condition (i.e. the pressure indication would progressively build over time). Rapid pressure rise would signify a flow blockage caused by a further decrease in gas flow rate. The limitation of the fluidised dense-phase system is there is an upper permissible limit of particle size and loose poured bulk density (Saluja et al., 2023(a); Saluja et al., 2023(b); Pan, 1999), i.e. for coarse and/or heavy powders, the fluidised dense-phase mode of conveying is not feasible, and the only method of achieving stable conveying is a dilute-phase mode for such powders.

One of the challenges faced by thermal power plants is to reliably convey fly ash. A recent extensive study (Saluja et al., 2023(a); Saluja et al., 2023(b)) carried out which is based on fly ash collected from 5 different power plants have shown that the median size and loose poured bulk density of APH ash vary from 96 to 192 μm and 801 to 986 kg/m^3, respectively, whereas the same for ESP first field ash varies from 84 to 190 μm and 785 to 1031 kg/m^3, respectively, and for ESP second field ash these vary from 11 to 63 μm and 667 to 784 kg/m^3, respectively (Saluja et al., 2023(b)). Generally, each source hopper of ash is separately conveyed to the same buffer hopper or intermediate surge hopper using a pneumatic vacuum conveying system. From this surge hopper, the mixed ash is transported using a pressure conveying system to the remote silo. APH ash is generally coarse/gritty with a "sand-like" appearance, and only dilute-phase conveying is feasible for this ash (Saluja et al., 2023(b)). ESP first field ash can be conveyed in both dilute and dense-phase (Saluja et al., 2023(b)). However, ESP second-field ash is a good fluidised dense-phase medium (Sharma et al., 2021). It is difficult to predict the likely mode of conveying for ESP first field ash (which is about 75% of total fly ash) at the design

stage as the actual properties of ash during the running condition of the plant will depend on the source of coal, boiler load, mill condition etc.

Because the ash evacuation in a vacuum system occurs sequentially from starting from the APH hopper (largest particle size) to ESP first field hopper (moderate particle size) to ESP second field hopper (smallest particle size) (Saluja et al., 2023(b)), it is expected that in the buffer hopper, the ash would be present in layers (a layer of coarse particles, followed by a layer of fine particles). Hence, the feed to the pneumatic pressure conveying system is likely to be in the segregated group of powders. The segregation tendency could be further enhanced due to the funnel flow design of the buffer hoppers (Marucci et al., 2018). As a result, the pneumatic pressure conveying system could end up handling a segregated flow of powders. In some conveying cycles, where the feed is "dense-phase" material, the conveying would occur with abundant air, causing additional or non-optimized power consumption, and excessive air velocity would cause pipeline wear (Cenna et al., 2014; Sharma et al., 2023). On the contrary, if the actual ash in some conveying cycles comes as a "dilute-phase" material (coarse/gritty), this would cause pipeline blockage and or significant reduction in achievable conveying capacity (Saluja et al., 2023(a); Poddar et al., 2024). Thus, material segregation would naturally cause the installed pneumatic conveying system to be operating in a non-optimized manner. Therefore, there is a need to change the operation of the plant, such as sequence of evacuation of ash, so that there is a proper mixture of ash in the buffer hopper. This may include evacuation of APH ash, followed by ash from ESP field 2 to 10 fields, followed further by the ESP first field ash. This chapter aims to develope a criteria for the physical properties of the mixed ash which can be optimally conveyed in fluidised dense-phase. To determine the above, fine ash was progressively mixed with coarse ash and were conveyed till from a non-conveying state (requiring pure dilute-phase conveying) to fluidised dense-phase conveying was achieved.

8.2 Experimental work

Powder characterisation

Two fly ash samples, termed as 'A' and 'B', were in this study; these samples were collected from the air preheater hopper (APH) and the third field of the Electro Static Precipitator (ESP) hopper, respectively, of a coal-fired thermal power plant. Eight blends of fly ash samples were prepared by

mixing (by weight) different portions of fly ash sample ‘A’ (coarse ash) with fly ash sample ‘B’ (fine ash). Particle and bulk characteristics, such as particle size distribution (d_{10}, $d_{50,}$ and d_{90}), particle, loose poured and tapped bulk densities for the two samples of fly ash (‘A’ and ‘B’) and the eight different blends of fly ash samples are presented in Table 8.1. Figure 8.1 shows the static angle of repose (S-AOR) of fly ash (‘A’ and ‘B’). The results are provided in Table 8.1. Powder flowability and S-AOR generally have an inverse correlation, which indicates that the higher the S-AOR, the lesser the powder flowability (Saluja et al., 2023(b); Lumay et al., 2012; Poddar et al., 2023). A customised edge recognition software was used to locate the powder/air interface in each captured image, as shown in Figure 8.1. The dynamic repose (D-AOR) angle at each rotational speed was determined from the derived parameters. The results are provided in Table 8.1. Flow information from ‘Blockage’ to ‘Reliable conveying’ is also mentioned in Table 8.1.

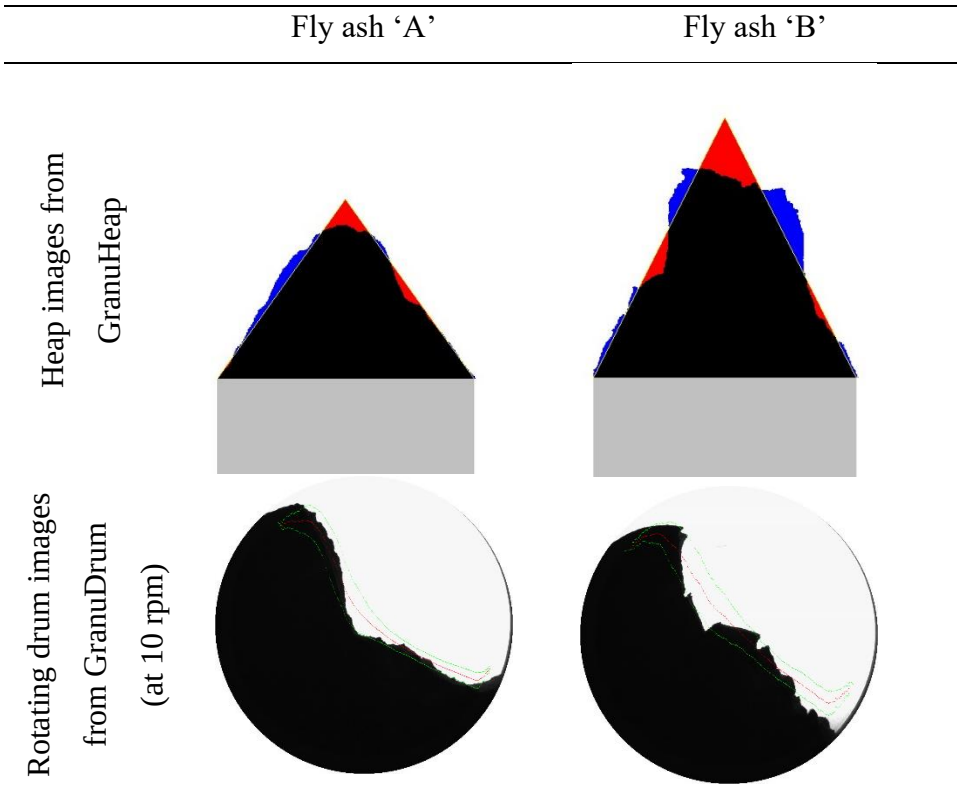

Figure 8.1: Heap and rotating drum images of coarse and fine fly ash

Pneumatic pressure conveying pilot plant

The pneumatic conveying test facility included a multistage screw compressor (equipped with an air receiver and dryer) with a maximum output pressure of about 700 kPa-g and a capacity of 605 m^3/hr (Free Air Delivery). As shown in Figure 8.2, a bottom-discharge type blow-tank (A) with a 0.8 m^3 empty capacity fed the product into the conveying pipeline. A receiver bin (B) with an insertable pulse jet dust filter and a volume of 2 m^3 was placed on top of the blow tank. The conveying pipeline had 128 m length, a pipeline bore of 105 mm, 12 nos. of 90^o bends with 1 m radius of curvature, and a 5 m vertical lift. The test rig has several static pressure transmitters, and for this study, P1 was used to monitor the total pipeline pressure drop. The specifications for the static pressure transducers (manufactured by Wika with model S-20 type) are 0-2.5 bar-g pressure range and 4–20 mA current pulse. The pressure-reducing valve, non-return valve, flow-control valve, and other required instruments were all mounted in their respective positions (Sharma, 2020(a); Sharma, 2020(b)). The receiver bin and blow tanks were supported on load cells (shear beam type) to determine the solid mass flow rates. A flow control valve was used to change the air mass flow rate to achieve a wide range of airflow rates. The electrical output impulses from the load cells, static pressure sensor, and airflow meters were recorded using a portable computer-compatible data recorder (Data Taker 80 and CEM20 channel expansion module). A toughened borosilicate sight glass was fitted in the pipeline for flow observation. The fly ash samples were conveyed through the test set-up at variable solids and airflow rates. The pressure conveying pilot plant's process and Instrumentation Diagram (P&ID) is shown in Figure 8.3. Flow information from 'Blockage' to 'Reliable conveying' is mentioned in Table 8.1.

A	Blow Tank
B	Receiver Bin
C	Bag Filter
D	Compressed Air
P1-P6	Pressure Transducers

No. of Bends	12
Bend Radius	1 m
Pipe Diameter	105 mm
Loop Length	128 m
All dimensions shown here are in meters	

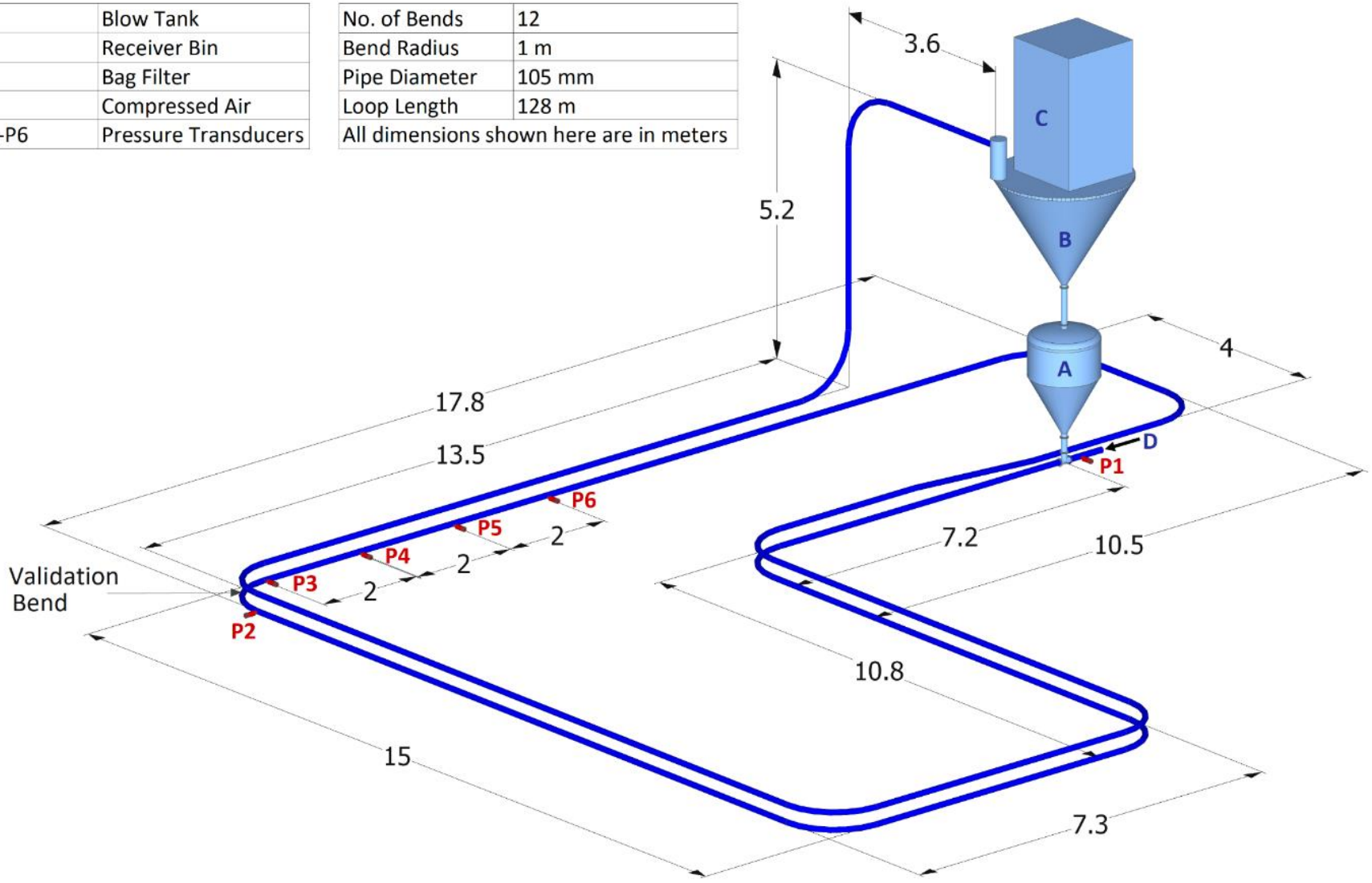

Figure 8.2: Schematic layout of pneumatic pressure conveying pilot plant at TIET, 105 mm ID × 128 m length

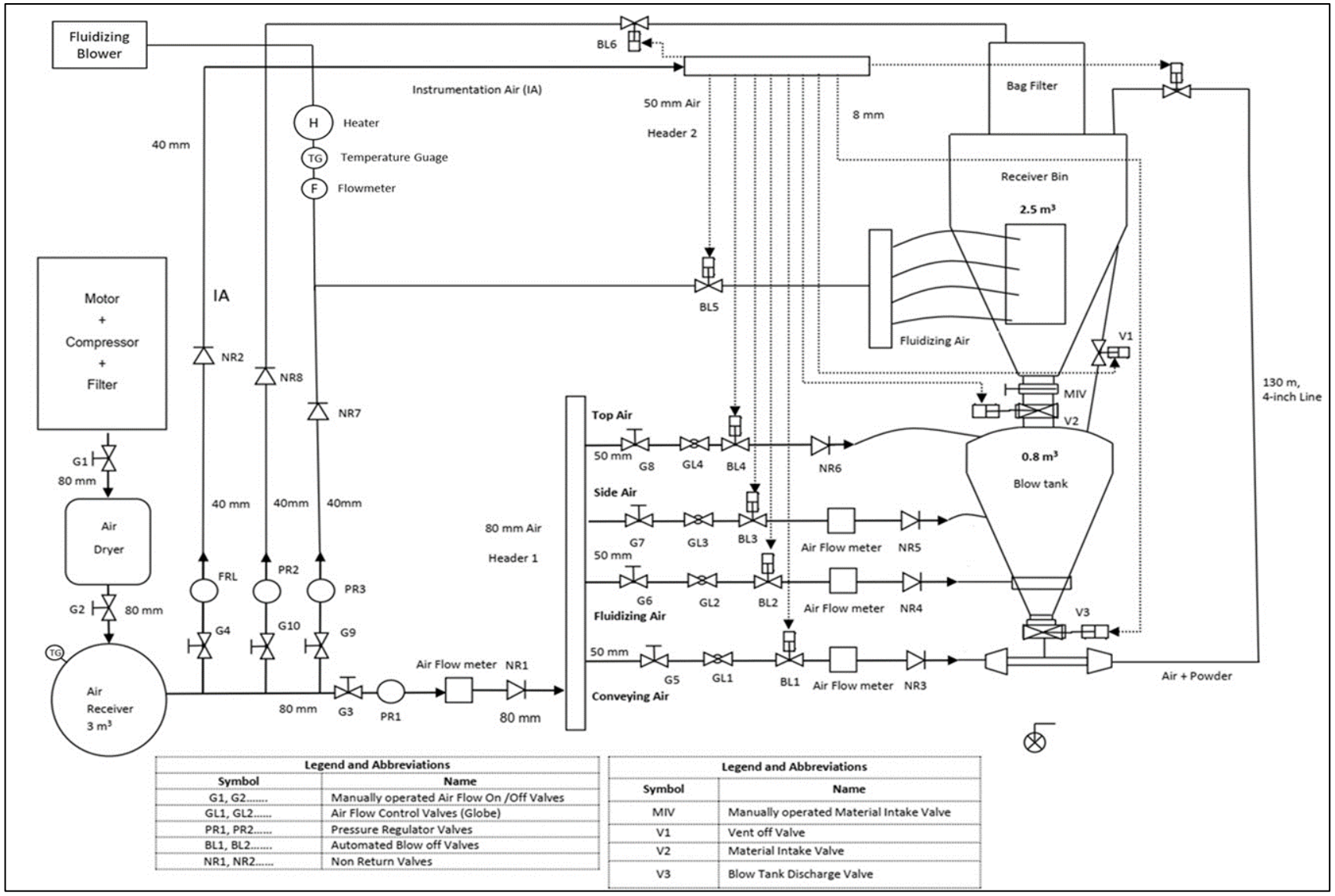

Legend and Abbreviations	
Symbol	Name
G1, G2.....	Manually operated Air Flow On /Off Valves
GL1, GL2.....	Air Flow Control Valves (Globe)
PR1, PR2.....	Pressure Regulator Valves
BL1, BL2.....	Automated Blow off Valves
NR1, NR2.....	Non Return Valves

Legend and Abbreviations	
Symbol	Name
MIV	Manually operated Material Intake Valve
V1	Vent off Valve
V2	Material Intake Valve
V3	Blow Tank Discharge Valve

Figure 8.3: P&ID for the newly developed pneumatic conveying pilot plant

Table 8.1: Physical properties and pneumatic conveyability of fly ash

Fly ash	**d_{10} (µm)**	**d_{50} (µm)**	**d_{90} (µm)**	**CFR**	**ρ_p (kg/m^3)**	**ρ_{lb} (kg/m^3)**	**ρ_t (kg/m^3)**	**HR**	**S-AoR (°)**	**D-AoR at 10 rpm (°)**	**Pneumatic conveyability**
A: B (100%: 0%)	30	133	226	7.5	1358	920	1332	1.45	57.0	38.7	Pipeline blockage in first cycle.
A: B (95%: 5%)	27	130	220	8.1	1362	918	1330	1.45	57.1	47.4	
A: B (90%: 10%)	25	126	214	8.6	1378	915	1331	1.45	57.2	52.4	
A: B (85%: 15%)	23	120	208	9.0	1396	904	1329	1.47	58.6	59.9	Conveying happened for 1-2 cycles with pipeline vibrations and then blockage occurred.
A: B (80%: 20%)	21	114	200	9.5	1413	899	1320	1.47	58.8	49.8	
A: B (75%: 25%)	19	109	195	10.3	1441	884	1322	1.50	59.2	44.7	Conveying occurred over several cycles without blockage; however high back pressure was persistent (40 to 50 kPa).
A: B (70%: 30%)	18	102	188	10.4	1449	876	1319	1.51	60.2	52.6	
A: B (65%: 35%)	16	98	181	11.3	1451	869	1316	1.51	60.7	48.3	Reliable conveying was achieved without blockage, however moderate back pressure was persistent (20 to 30 kPa).
A: B (60%: 40%)	15	93	175	11.7	1463	862	1317	1.53	61.2	49.1	
A: B (0%: 100%)	11	62	150	13.6	1475	855	1315	1.54	65.6	43.5	

Annular shear testing

Using a powder flow tester-PFT (Brookfield, Middleboro, USA) based on Jenike's approach, the flow characteristics of fly ash samples were assessed. The fly ash sample was poured into the sample trough of an annular shear cell (PFT-400: 6") after being filtered through 850 microns. A top lid (PFT-500: 6", 304 S.S. vane profiles) was placed to gradually increase the consolidation stress over the sample powder for flow function testing. A trough rotating at one rotation per hour was used to shear the fly ash sample. The induced normal stresses were in the 0.2 to 4.8 kPa range. The PFT technology was combined with Powder Flow Pro software for data processing, which provided instantaneous yield location and unconfined failure strength as functions of the major principal consolidation stress. Figure 8.4 shows the flow function curves for different fly ash blends.

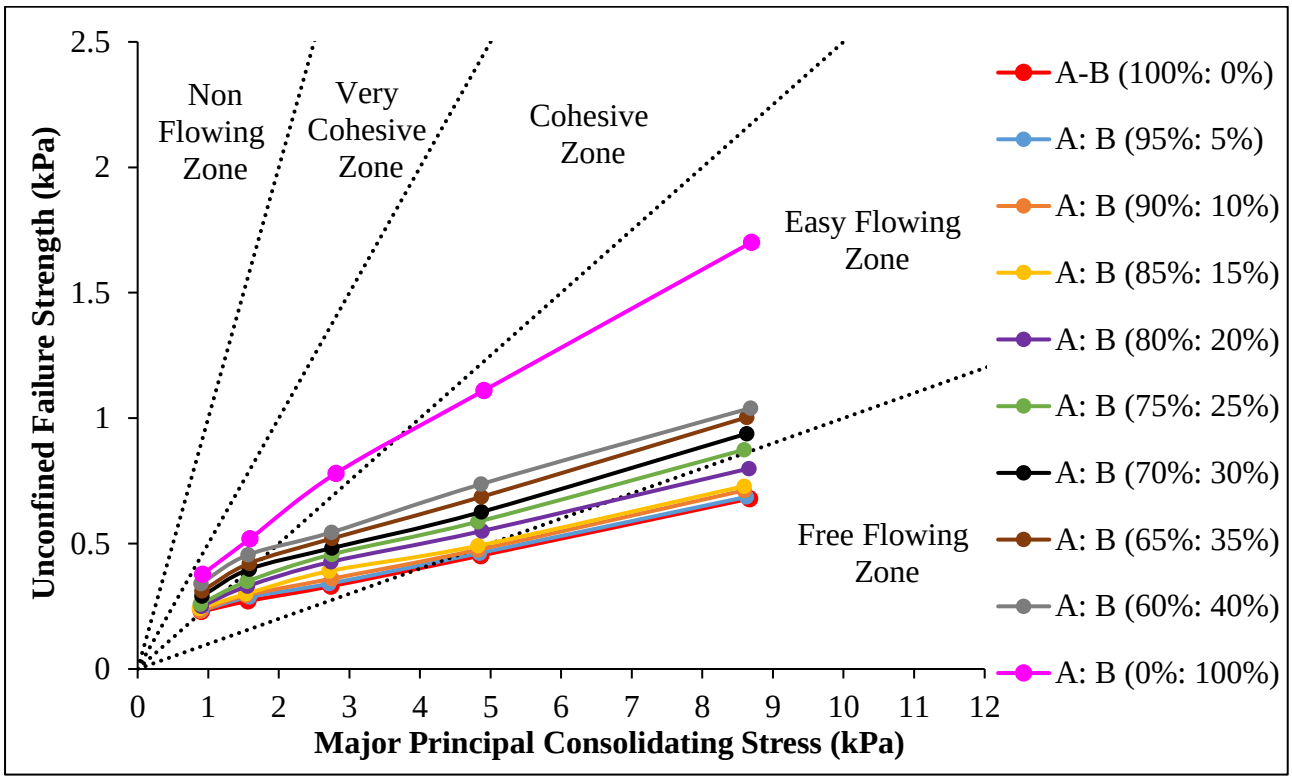

Figure 8.4: Flow function curves for different fly ash blends

It can be seen that with the addition of fines, the ash samples have become more easy flowing from free-flowing. From a pneumatic conveying perspective, the addition of fines would therefore, restrict extremely free-flowing ash from flooding the pneumatic conveying pipeline once the material discharge valve is opened to feed ash into the conveying line. Flooding of ash due to excessive free flow under gravity may choke the pipeline at the feed point.

8.3 Results from experimental data

Whereas fly ash ‘A’ (coarse/gritty ash obtained from APH) could not be conveyed in fluidised dense-phase, fly ash ‘B’ (fine fly ash obtained from the third field of the ESP) was able to be conveyed in fluidised dense-phase. When the ash discharge outlet valve of the blow tank was opened, "sand-like" fly ash ‘A’ flooded the pipeline due to its free-flowing nature. Figure 8.5 shows a typical pressure versus time diagram for ‘A’ type ash. In the initial 10 seconds of conveying, the line pressure slowly increased to 15 kPa, followed by a rise to 130 kPa with an accelerated rate. Subsequently, there was a sharp rise in pipeline pressure; pressure surged to about 170 kPa in the next 5 seconds, leading to pipeline blockage. A similar nature of unsuccessful conveying was experienced for A: B values of 95%: 5% and 90%: 10%.

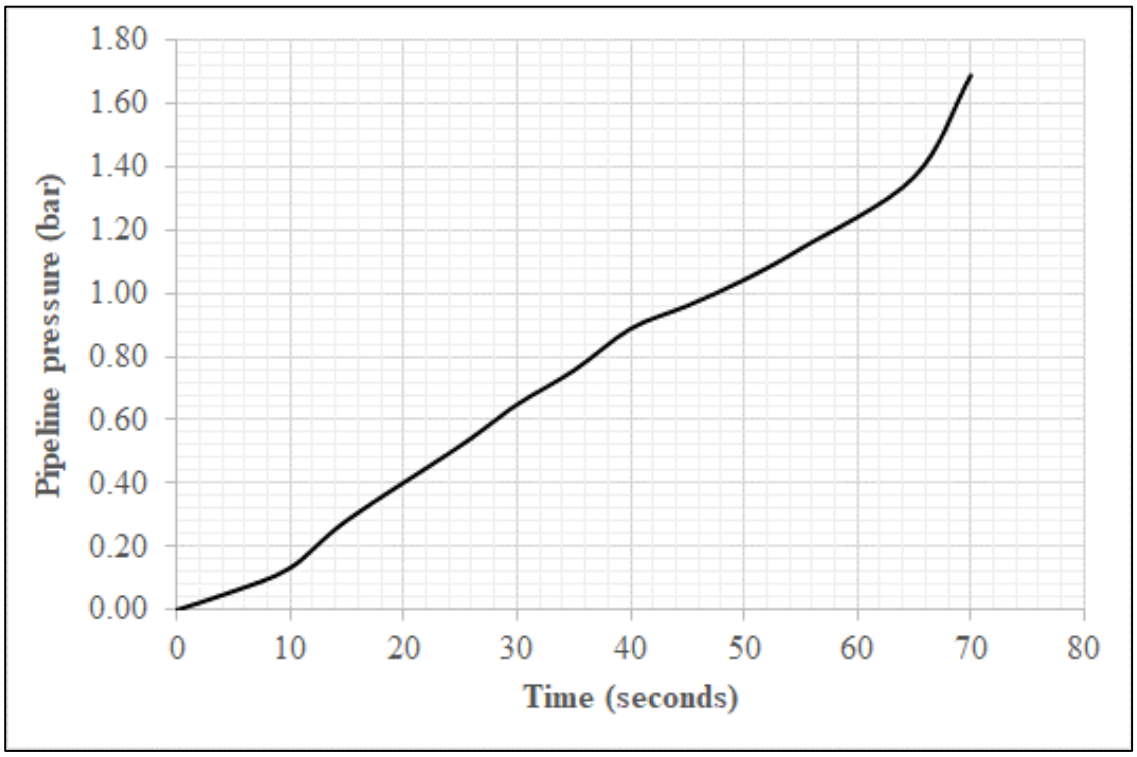

Figure 8.5: Pressure versus time diagram for conveying for ‘A’ type fly ash

When the fly ash blends with A: B of 85%: 15% and 80%: 20% were fed into the conveying line, unstable conveying occurred with moving grating noise, slug-like irregular movement of powders and some pipeline vibration could be felt. This mode of conveyance seems to have been described as weak asymmetric slug flow (Jones et al., 2008), which is an unstable mode that necessitates extremely high transporting velocities to move the materials in "dilute phase". With these fly ash blends, there was no immediate pipeline blockage when the powders were fed into the line, and the slug-like

movement (accompanied by pipeline vibrations) could only be felt during the final phase of the conveying cycle (after a majority of the ash has been pushed into the line). The grating noise with slug movement and line shaking persisted for an extra 5 to 10 seconds even after the conveying air and ash feeding in the line was halted, indicating the possible presence of high-pressure air pockets trapped between the slugs. There were 1 or 2 unstable conveying trials (without pipeline blockage); however, subsequent attempts for conveying resulted in pipeline blockage, indicating possible saltation and powder built up in line during initial conveying cycles. Interestingly, even after the pipeline was blocked, conveying could be resumed within 30 to 60 seconds by supplying a burst of air pulses until the obstruction was removed.

Subsequently, when the fly ash blends with A: B of 75%: 25% and 70%: 30% were fed into the conveying line, stable conveying was achieved without pipeline blockage. However, the line pressure at the end of a conveying cycle took a long time to get reduced to the usual air-only pressure drop (generally about 10 kPa in the given test rig). For example, normally for good fluidised dense-phase flow, it takes 15 to 20 seconds for a steady state/peak conveying pressure of 110 kPa to get reduced to 10 kPa (air-only pressure drop associated with clean pipe). However, for these blends of fly ash (A: B of 75%: 25% and 70%: 30%), it took about 150 seconds for the air-only pressures to be reduced to about 40 kPa. Unfortunately, it took an impractical amount of time for the line pressure to be reduced further to 10 kPa; therefore, the cycle was stopped. Figure 8.6 shows a typical pressure versus time diagram for such types of ash blends (A: B of 75%: 25% and 70%: 30%).

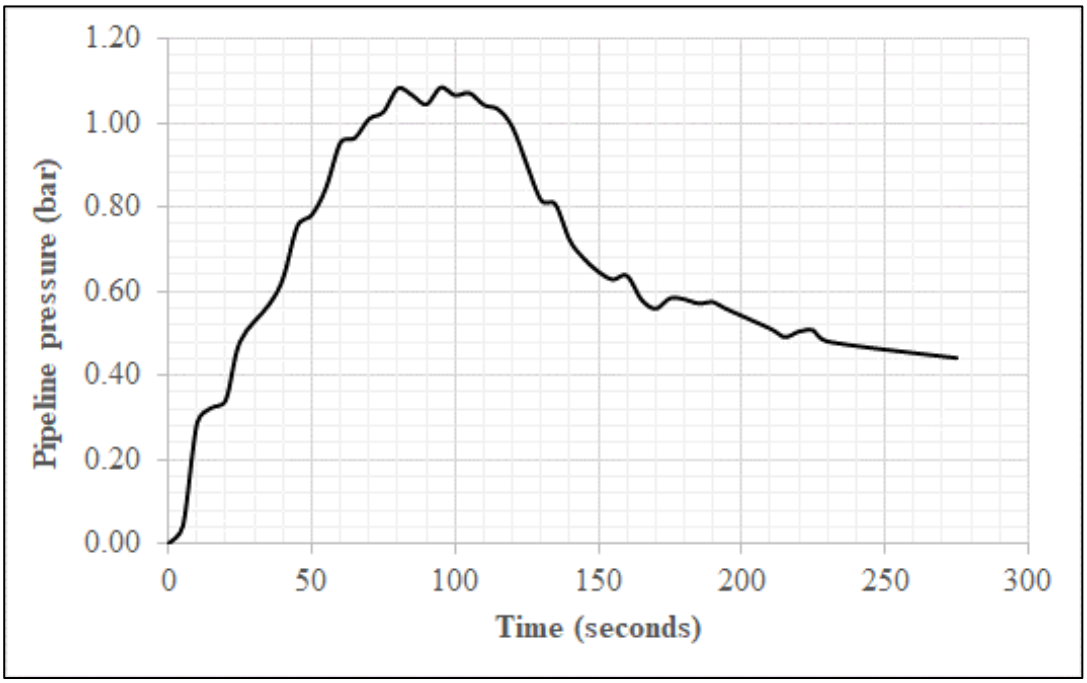

Figure 8.6: Pressure versus time diagram for conveying for A: B of 75%: 25% fly ash

With further increase of fines, i.e. when the fly ash blends having A: B of 65%: 35% and 60%: 40% were fed into the line, stable conveying with good fluidised dense-phase flow could be achieved with stable pipeline pressure and without persisting high line back pressure. However, the back pressure at the end of the conveying cycle still could not be reduced to 10 kPa (the usual clear line/air-only line pressure), and an elevated back pressure was observed (about 25 kPa). Figure 8.7 shows a typical pressure versus time diagram for such types of ash blends (A: B of 65%: 35% and 60%: 40%). The cycle was stopped due to the long time that being taken for the line pressure to be reduced to 10 kPa.

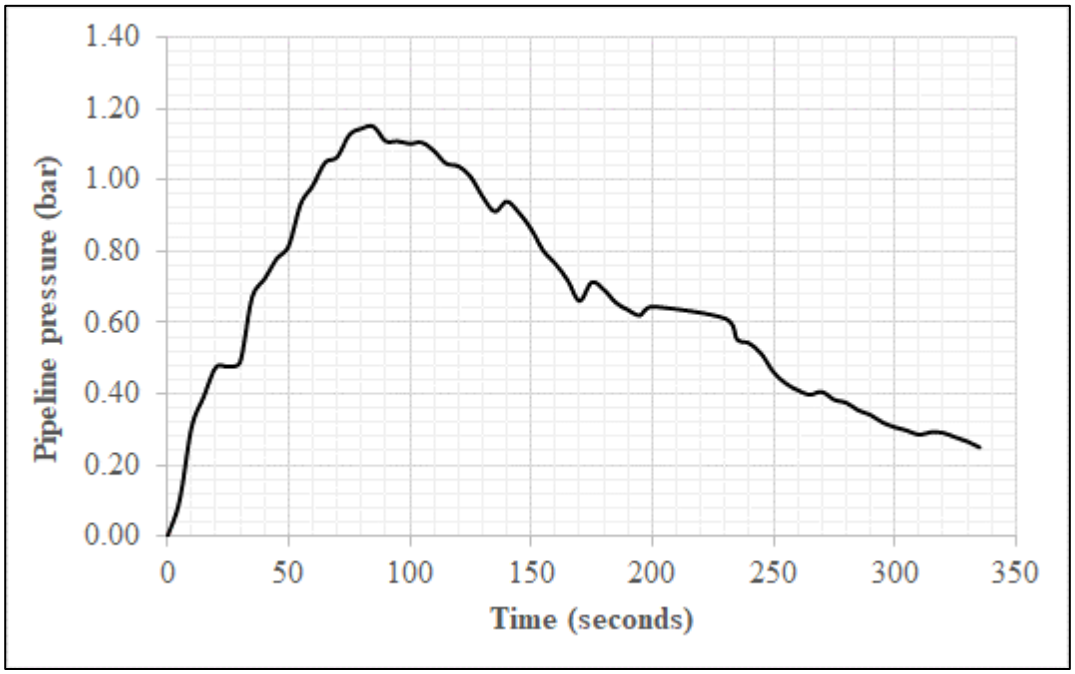

Figure 8.7: Pressure versus time diagram for conveying for A: B of 65%: 35% fly ash

The practical significance of such high or elevated persisting back pressure is if in a conveying installation (in a plant) the operating logic is based on pipeline back pressure, it would take a long time for a cycle to be completed, thus reducing the effective conveying rate. This is because in a practical installation, normally two (or more) blow tanks operate in tandem, i.e. when one blow tank is in filling mode, the other blow tank remains in discharge mode. The operating logic to close the material outlet valve, purge, and open the material discharge valve of the next blow tank in a queue is often based on pipeline back pressure. Therefore, even after one blow tank has completed its discharge, if the line back pressure does not come down to the set pressure (corresponding to clean / air-only line pressure) in a reasonably short time, it would only increase the "idle time" of the cycle, ultimately resulting in decreasing the time-averaged material conveying rate (t/h). The possible reason for elevated line back pressure is the presence of coarse particles (high d_{90}). It is believed that

the coarse particles tend to slide along the bottom of the pipeline; they move slowly as the air stream cannot pick up these particles. As a result, the pipe takes a long time to clear, hence the elevated back pressure. It is interesting to note that while the "fines" dictate reliable transport boundary and conveyability (Saluja et al., 2023(a); Saluja et al., 2023(b); Sharma et al., 2021; Kalman et al., 2023), it is the presence of "coarse" particles which govern the cycle time. Therefore, for a practical installation where conveying mode, reliable conveying and increasing number of cycles per hour are all of interest to achieve the performance guarantee, the presence of both fines and coarse (d(10) and d(90)) in a powder sample are important.

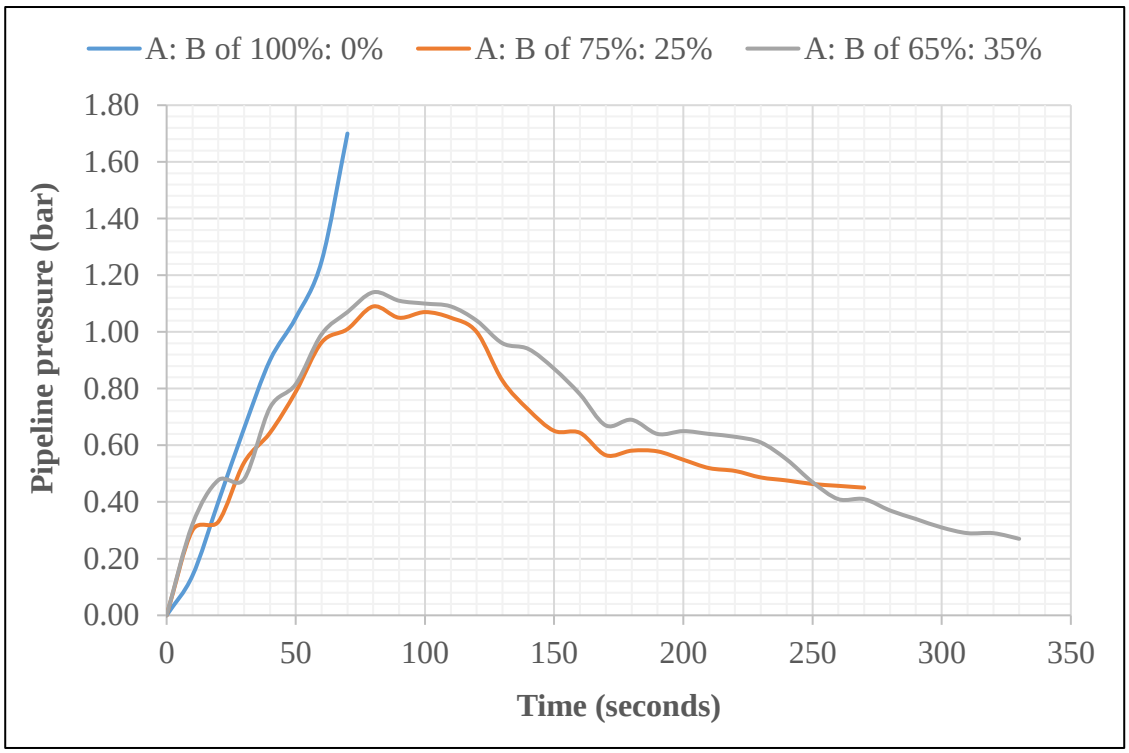

Figure 8.8: Comparison of pressure versus time diagram for conveying for A: B of 100%: 0%, 75%: 25%, and 65%: 35% fly ash

In Figure 8.8, the curve of 100% coarse ash (A) shows a rapid pressure escalation from approximately 15 kPa to 170 kPa within a short duration, indicating immediate pipeline choking due to the free-flowing, sand-like nature of the coarse particles. The lack of fines prevents cohesive fluidisation, resulting in uncontrolled flooding, saltation, and dense slug formation that ultimately blocks the line. In contrast, the 75%:25% blend ratio demonstrates a more stable pressure rise, reaching a steady conveying pressure near 110 kPa; however, the pressure decay exhibits a long tail, taking nearly 150 seconds to approach air-only pressure levels. This behaviour reflects partial fluidised dense-phase conveying, where the presence of some fines improves stability compared to pure coarse ash but

cannot fully eliminate coarse particle sliding along the pipeline bottom, leading to elevated residual back pressure and prolonged cycle times. For the 65%:35% blend, the pressure profile indicates smooth, stable conveying with reduced fluctuations characteristic of good fluidised dense-phase transport. The higher proportion of fines enhances particle suspension and reduces friction, thereby preventing choking; however, the pressure decay still fails to rapidly reach the clean air-only baseline of 10 kPa, instead stabilising around 25 kPa due to residual coarse particle movement and incomplete line clearance.

Figure 8.9 is the modified Dixon slugging diagram (Jones et al., 2008) with fly ash properties superimposed. Figure 8.9 shows that the fly ash sample ‘B’ lies in the regime "no slugging", indicating that this ash sample is expected to be conveyed in a fluidised dense phase. This matches the pilot plant conveying experience (described before). On the other hand, the fly ash sample ‘A’ is located in the regime “weak asymmetric slugs” that is supposed to be challenging to convey in fluidised dense-phase, which also matches the experimental observation. The blends were found to be lying on the borderline between "no slugging" to “weak asymmetric slugs”.

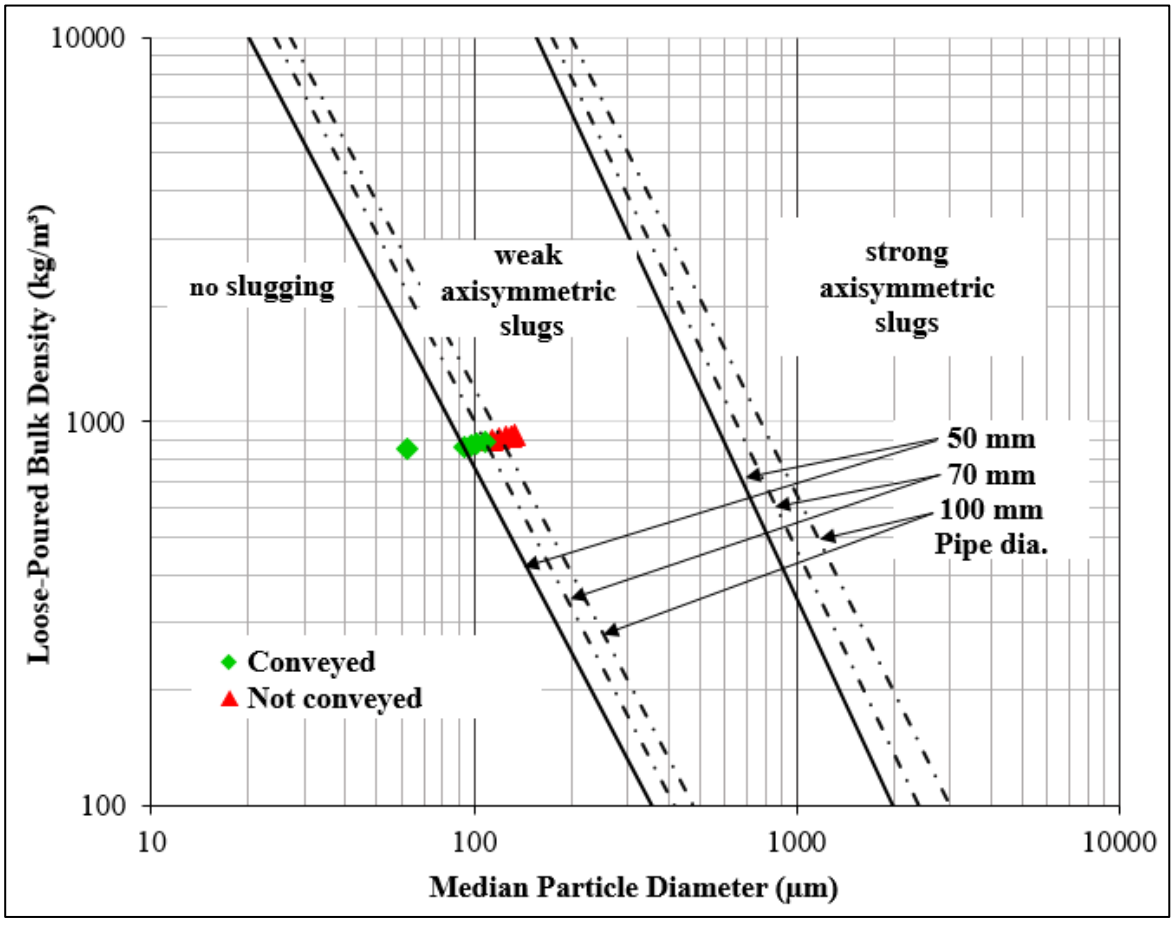

Figure 8.9: Pneumatic conveying flow modes of fly ash (modified Dixon slugging diagram)

Table 8.1 and Figure 8.10 show that the median particle size and loose poured bulk density consistently decreased from' A' to' B'. However, the coarse-to-fine ratio (CFR), Hausner ratio (HR) and static angle of repose (S-AoR) consistently increased from ‘A’ to ‘B’. These findings are in agreement with Saluja et al., 2023(b). The consistent increase of S-AoR and HR with the reduction of median particle size suggests that the mixture is more cohesive as the fly ash's fineness increases (Saluja et al., 2023(b); Poddar et al., 2023). The flow zone/mode has been discovered to be influenced by a combination of particle size and size distribution, as well as loosely poured bulk density. Powders with a larger particle size distribution (particularly those with a higher proportion of fines) support more non-suspension flow (dense phase). Powders with a median size of less than 100 µm are considered "good" dense-phase materials, while bigger particles can only be conveyed in dilute or medium phases. Fine particles are more effective at retaining air than coarser particles, which have a higher permeability. Powders with good air retention are more likely to sustain dense phases (Saluja et al., 2023(b)). When a fine powder with a high inter-particle cohesion is poured loosely, the tiny particles are prevented from flowing easily and form a steeper heap (Kalman et al., 2023; Schulze, 2008). In fine particles, the interparticle cohesive forces dominate over the gravitational force (Schulze, 2008) and thus form large voids when such particles are loosely poured into a container. A greater loose-poured bulk density might lead to a "worse" situation (blockage condition) from a pneumatic conveying aspect due to the need to convey a relatively heavy bulk solid, which would involve higher pressure and airflow. In pneumatic conveying, the Hausner ratio and angle of repose are significantly more reliable and directly measured for providing a quick assessment of the conveyability and flowability of fly ash than particle size and size distribution. The difference might be because, whereas particle size and size distribution are primarily "particle" characteristics, the Hausner ratio and angle of repose are "bulk" qualities (i.e., they incorporate a variety of particle characteristics). Because of the intrinsic bulk nature of the flow, it is possible to argue that a "bulk" characteristic would be better demonstrating medium to dense-phase pneumatic conveying and hopper flow of powders. So, the static angle of repose is an important parameter that can be chosen to predict the probable mode of zone/flow, as shown in Figure 8.10.

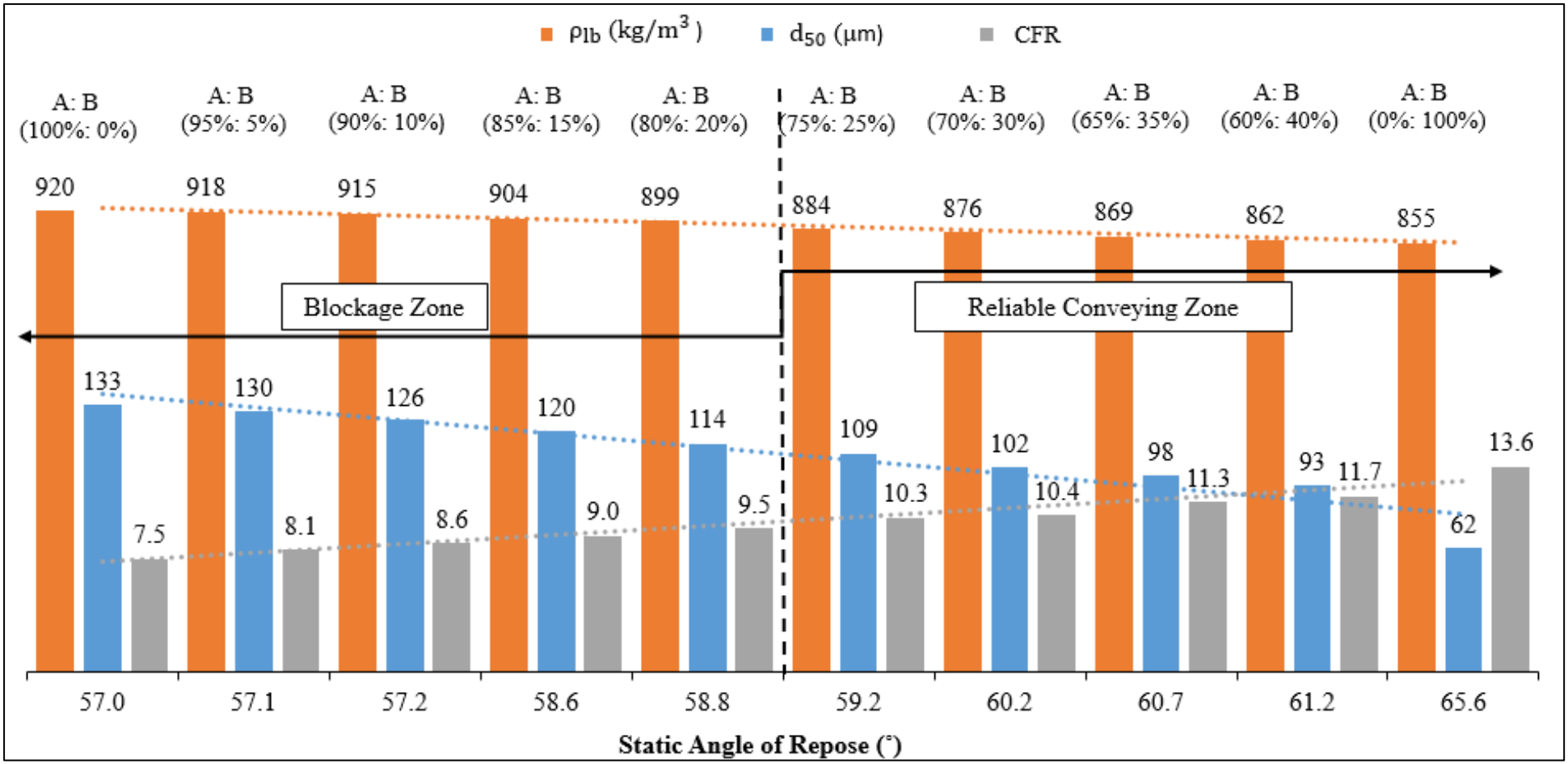

Figure 8.10: Plot of static angle of repose comparing with physical properties of fly ash

Figure 8.9 shows that the conveyability of powders (ash) depends on both loose-poured bulk density and median particle diameter. In order to combine the effects of median particle diameter and loose poured bulk density, a recently developed novel Froude number term (Saluja et al., 2023(a)) has been used in this paper. This novel bulk powder Froude number (Fr_{lb}) is based on bulk powder free settling velocity, where the conventional free settling velocity term (which uses particle density, ρ_p) has been replaced by loose poured bulk density (ρ_{lb}). As the loose-poured bulk density of powders is generally many orders higher than gas density (ρ_f), the gas density term in equation (8.2) can be neglected for all practical calculations.

$$Fr_{lb} = \frac{w_{folb}}{\sqrt{g d_{50}}} \tag{8.1}$$

$$w_{folb} = g\left(\rho_{lb} - \rho_f\right) d_{50}^2 \tag{8.2}$$

Saluja et al., 2023(a), used the bulk powder Froude number term to represent the minimum transport boundary of powders. In the experience of the authors and literature data (Mallick, 2009; Wypych, 1989; Pan, 1992; Setia, 2016; Desai, 1992; Williams, 2008), the powders that are heavier and/or have larger particle sizes require larger conveying air velocities. The bulk powder Froude number term has been chosen to represent conveyability criteria in this paper. The range of Froude number based on loose-poured bulk density and course-to-fine ratio required to ensure reliable dense-phase conveying are shown in Figure 8.11. To achieve reliable dense-phase conveying of fly ash, both the following criteria are to be satisfied:

$$Fr_{lb} < 10 \tag{8.3}$$

$$CFR > 10 \tag{8.4}$$

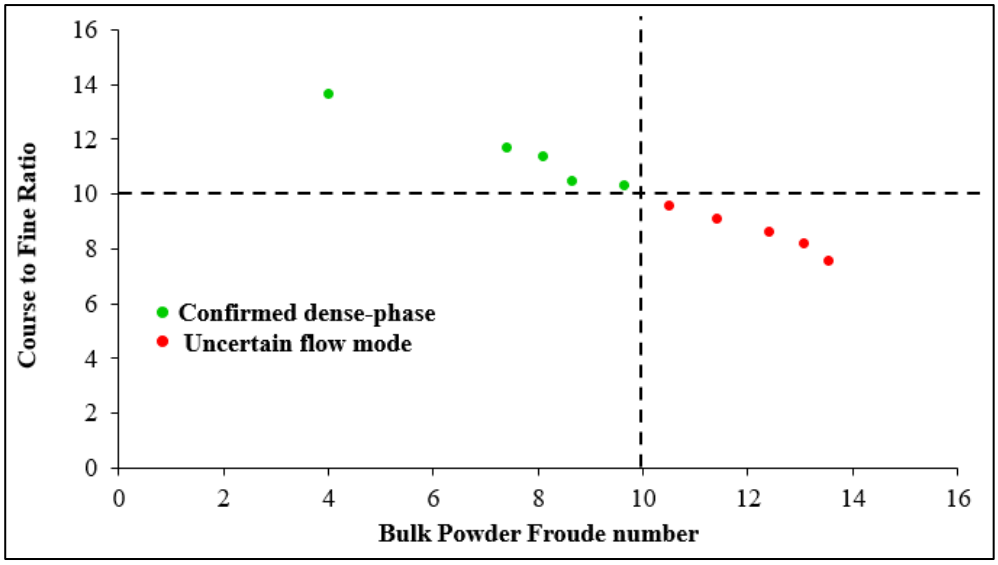

Figure 8.11: Plot of coarse-to-fine ratio versus Froude number based on loose-poured bulk density

Experimental data from 23 samples were taken from the study conducted by author Saluja et al., 2023(b), to validate the existing criteria for reliable dense-phase conveying mentioned in equations 8.3 and 8.4. As shown in Figure 8.12, the samples depicted in green represent a confirmed dense-phase mode of flow in pneumatic conveying, while the rest of the samples, depicted in red, exhibit an uncertain flow mode. This experimental data also confirms the reliability of existing criteria for dense-phase conveying.

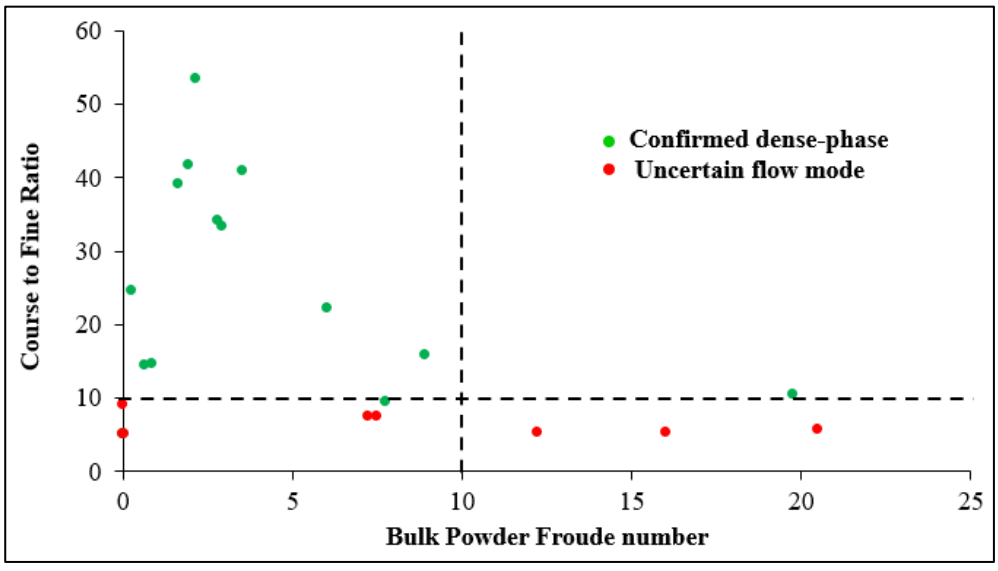

Figure 8.12: Plot of coarse-to-fine ratio versus Froude number based on loose-poured bulk density (experimental data taken from the study conducted by the author Saluja et al., 2023(b), for the validation of existing criteria for reliable dense-phase conveying)

The relation between the dynamic angle of repose (D-AoR) and the shear rate applied (by increasing the drum rotational speed) is depicted in Figure 8.13. This relationship enables the assessment of the rheological characteristics of the fly ash blends, such as shear thickening or shear thinning. D-AoR is influenced by several factors, including particle shape, and cohesive and frictional interactions between particles (Boschini et al., 2015; Janssen et al., 2021; Shi et al., 2020; Yablokova et al., 2015). For the fly ash blends with A: B of 100%: 0% to 80%: 20%, Figure 8.11 shows the trend of D-AoR with an increase in drum rotating speed, which is an increment in D-AoR initially (with an increase in drum rotating speed) and then reaching maxima (which could not be conveyed in the dense phase) are exhibits shear thickening behaviour due to increased cohesiveness at higher stresses, which is related with a decrease of flowability. The above said fly ash blends that are evaluated show shear thickening behaviour. This indicates that cohesiveness increases with rotational speed, which specifies the "worst" fly ash blends for a dynamic process such as pneumatic conveying. The D-AoR decreases with the increase in drum rotating speed for the fly ash blends, with A: B of 75% 25% to 0%: 100%. It can be seen that the said fly ash blends, which could be conveyed in a dense phase, had reached the maxima at low drum speed (within 15 rpm). As a result, flowability improves as the shear rate increases, indicating shear-thinning behaviour that certainly corresponds to an aeration process during flow. The shear thinning behaviour may be explained by the aeration of the aforementioned fly ash blends at higher rotating speeds, which increases particle distance and consequently lowers cohesive surface interaction. This behaviour is completely opposite compared to shear thickening.

.

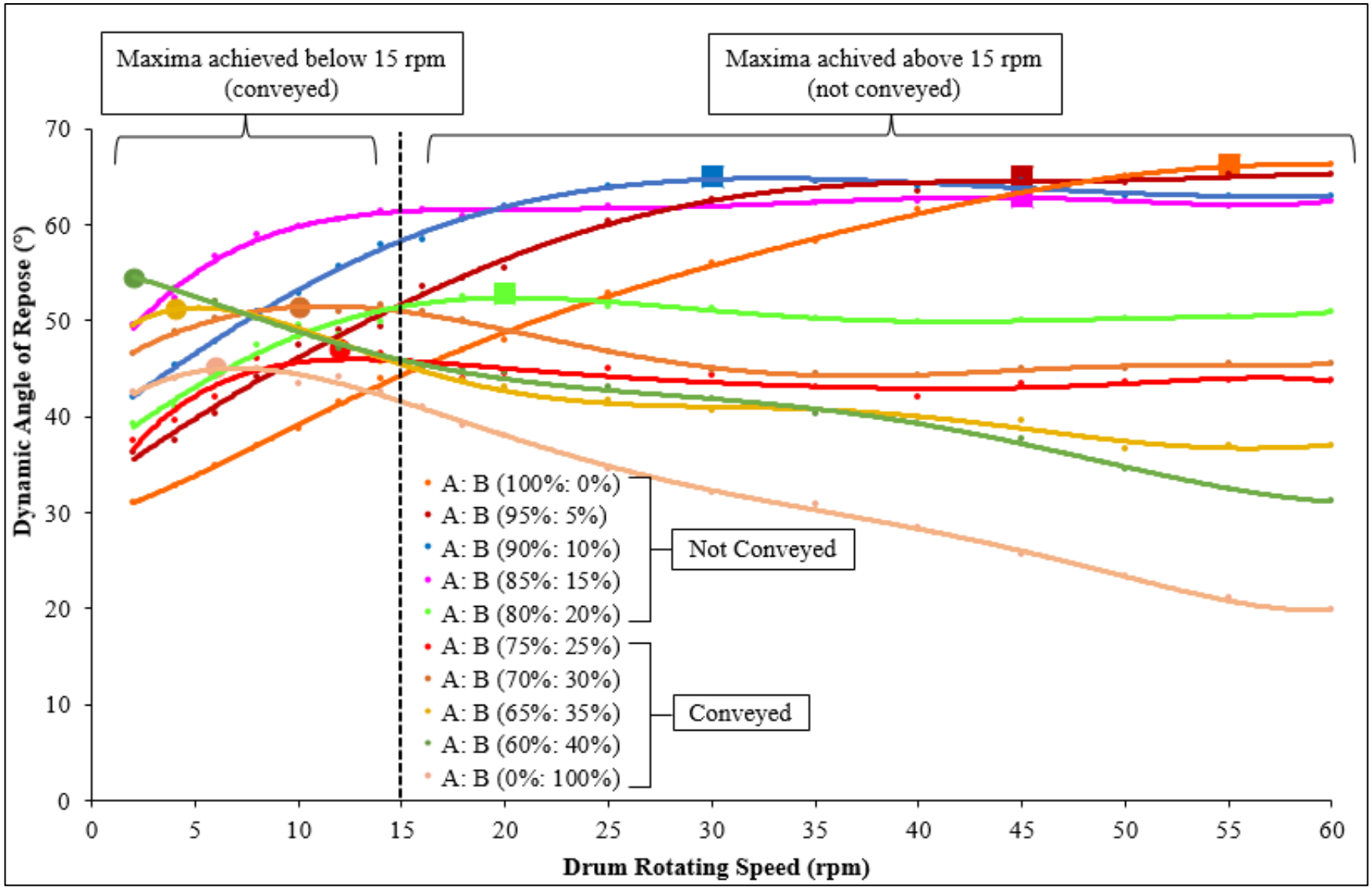

Figure 8.13: D-AOR versus drum rotating speed for fly ash samples

8.4 Conclusion

The characteristics of fly ash collected in ESP and APH hoppers of a thermal power plant can be unpredictable because this ash can be either a dense or dilute-phase material. The conveying trials carried out with several blends of fly ash (by mixing the coarse ash with fine ash) have shown that successful conveying is possible by conveying a blend of 75% coarse ash mixed with 25% fine ash. In a power plant scenario, this implies simultaneous discharge of ash from ESP first field or APH hopper (having coarse ash) and ESP 2^{nd} to 10^{th} field hopper (having fine ash of appropriate amount). This can certainly be made possible in a power plant with minimum hardware changes by fine-tuning the ash evacuation sequence in vacuum mode in such a way that the ash is well mixed in buffer hopper. For dense-phase conveying to be possible, the ash mixture should have a Froude number value (based on loose poured bulk density) less than 10 and a coarse-to-fine ratio above 10. The number of hoppers to be discharged simultaneously and the selection of the same can optimised based on the criteria as mentioned earlier. The control logic for blow tank operation needs to be amended by having an elevated back pressure as the criteria for selecting the blow tank discharge sequence. With training, operators can effectively manage this new conveying strategy, allowing for dynamic adjustments to airflow and pressure settings. Additionally, upgrading monitoring systems will support the performance of the new conveying method, ensuring that the operation consistently meets reliability standards. Emphasising real-time data collection and analysis will empower the team to adapt to evolving material properties and operational conditions effectively. The resulting system has the potential to be a reliable, energy-efficient, and economical dry ash-conveying solution in thermal power plants.

References

Alkassar, Y., V.K. Agarwal, R.K. Pandey, and N. Behera. 2021. Analysis of Dense Phase Pneumatic Conveying of Fly Ash Using CFD Including Particle Size Distribution. *Particulate Science and Technology* 39, no. 3, 322–337.

Bhatia, A. 2019. Pneumatic Conveying Systems. Chemical Engineering (New York). Continuing Education and Development, Inc: 1-57.

Boschini, F., V. Delaval, K. Traina, N. Vandewalle, and G. Lumay. 2015. Linking Flowability and Granulometry of Lactose Powders. *International Journal of Pharmaceutics* 494, no. 1, 312–320.

Cenna, A. A., K. C. Williams, M.G. Jones, and W. Robinson. 2014. Analysis of Wear Mechanisms in Pneumatic Conveying Pipelines of Fly Ash. *Engineering Asset Management* 2011, 539–547.

Desai, M.K. 1992. Flow Assessment of Powders in Pneumatic Conveying: A Bench Top Assessment. *PhD. Dissertation*, University of Wollongong, Australia.

Fuller, A., J. Maier, E. Karampinis, J. Kalivodova, P. Grammelis, E. Kakaras, and G. Scheffknecht. 2018. Fly Ash Formation and Characteristics from (Co-)Combustion of an Herbaceous Biomass and a Greek Lignite (Low-Rank Coal) in a Pulverized Fuel Pilot-Scale Test Facility. *Energies* 11, no. 6, 1581.

Howladar, M.F., and M.R. Islam. 2016. A Study on Physico-Chemical Properties and Uses of Coal Ash of Barapukuria Coal Fired Thermal Power Plant, Dinajpur, for Environmental Sustainability. *Energy, Ecology and Environment* 1, no. 4, 233–247.

Janssen, P.H.M., S. Depaifve, A. Neveu, F. Francqui, and B.H.J. Dickhoff. 2021. Impact of Powder Properties on the Rheological Behavior of Excipients. *Pharmaceutics* 13, no. 8, 1198.

James, A., R. Thring, S. Helle, and H. Ghuman. 2012. Ash Management Review-Applications of Biomass Bottom Ash. *Energies* 5, no. 10, 3856–3873.

Jones, M.G., and K.C. Williams. 2008. Predicting the Mode of Flow in Pneumatic Conveying Systems—A Review. *Particuology* 6, no. 5, 289–300.

Kalman, H., and D. Portnikov. 2023. Underwater Measurements of Flowability by Angle of Repose, Hausner Ratio and Jenike Shear Cell. *Powder Technology* 429, 118883.

Klinzing, G.E., F. Rizk, R. Marcus, and L.S. Leung. 2010. *Pneumatic Conveying of Solids*. Vol. 8. Particle Technology Series. Dordrecht: Springer Netherlands.

Liu, Z., Q. Li, and J. Zhang. 2021. Effect of Moisture Content on Flow Behavior and Resistance Characteristics of Dense-Phase Pneumatic Conveying. *Powder Technology* 387, 1–8.

Lumay, G., F. Boschini, K. Traina, S. Bontempi, J.-C. Remy, R. Cloots, and N. Vandewalle. 2012. Measuring the Flowing Properties of Powders and Grains. *Powder Technology* 224, 19–27.

Marucci, M., B. Al-saaigh, C. Boissier, M. Wahlgren, and H. Wikström. 2018. Sifting Segregation of Ideal Blends in a Two-Hopper Tester: Segregation pro Files and Segregation Magnitudes. *Powder Technology* 331: 60–67.

Mills, D. 2016. *Pneumatic Conveying Design Guide*. Vol. 21. Elsevier.

Mallick, S.S., 2009. Modelling of fluidised dense-phase pneumatic conveying of powders, *PhD. Dissertation*, University of Wollongong.

Molerus, O. 1996. Overview: Pneumatic Transport of Solids. *Powder Technology* 88, no. 3, 309–321.

Ohenoja, K., M. Körkkö, V. Wigren, J. Österbacka, and M. Illikainen. 2018. Fly Ash Classification Efficiency of Electrostatic Precipitators in Fluidized Bed Combustion of Peat, Wood, and Forest Residues. *Journal of Environmental Management* 206, 607–614.

Poddar, R., S.S. Mallick, and K. Lal. 2024. Reliable Pneumatic Transport of Coarse Ash in Dense-Phase by Optimally Mixing with Fine Ash. *Powder Technology* 442, no. May (June): 119876.

Poddar, R., S.S. Mallick, and L. Kundan. 2023. An Experimental Investigation into Sifting and Fluidization Segregation Characteristics for Coal Fly Ash. *Particulate Science and Technology* 42, no. 4, 515–526.

Pan, R. 1999. Material Properties and Flow Modes in Pneumatic Conveying. *Powder Technology* 104, no. 2, 157–163.

Pan, R. 1992. Improving scale-up procedures for the design of pneumatic conveying systems, *Doctor of Philosophy thesis*, Department of Mechanical Engineering, University of Wollongong, Australia.

Rani, R., M. K. Jain. 2019. Hydraulic transportation of coal combustion products for mine fill, *Particulate Science and Technology*, 37:1, 123-129.

Saluja, G., S.S. Mallick, S. Karmakar. 2023(a). Modeling minimum transport boundary for pneumatic conveying of powders. *Particulate Science and Technology*, *42*(3), 418–426.

Saluja, G., S.S. Mallick, S. Karmakar. 2023(b). Predicting pneumatic conveyability and flowability of fly ash using bulk property characterization. *Particulate Science and Technology*, *42*(3), 482–494.

Sharma, A., R. Poddar, G. Saluja, and S.S. Mallick. 2023. Modeling Pressure Drop in Curvature and Reacceleration Zones in Bends during Pneumatic Conveying of Fine Powders. *Particulate Science and Technology* 0, no. 0: 1–16. https://doi.org/10.1080/02726351.2023.2255865.

Sharma, K., S.S. Mallick, and A. Mittal. 2021. An Evaluation of Testing and Modeling Procedure for Solids Friction Factor for Fluidized Dense-Phase Pneumatic Conveying of Fine Powders. *Particulate Science and Technology* 39, no. 1, 62–73.

Srinivasan, P., and A. Shekhar. 2021. Internalizing the External Cost of Gaseous and Particulate Matter Emissions from the Coal-Based Thermal Power Plants in India. *Particulate Science and Technology* 39, no. 5, 632–640.

Sharma, A. 2020(a). An Investigation on Pressure Drop for Gas-Solids Flow through Bends. *PhD Dissertation*, Thapar Institute, India.

Sharma, K. 2020(b). Studies towards Development of Improved Modelling and Scale-Up Procedures for Dense-Phase Pneumatic Conveying of Fine Powders. *PhD Dissertation*, Thapar Institute, India.

Shi, H., G. Lumay, and S. Luding. 2020. Stretching the Limits of Dynamic and Quasi-Static Flow Testing on Cohesive Limestone Powders. *Powder Technology* 367, 183–191.

Sharma, A., and S.S. Mallick. 2019. Modelling Pressure Drop in Bends for Pneumatic Conveying of Fine Powders. *Powder Technology* 356, 273–283.

Setia, G. 2016(a). Improving Scale Up Procedures for Solids Friction and Minimum Transport Boundary for Fluidized Dense Phase Pneumatic Conveying Systems. *PhD Dissertation*, Thapar Institute, India.

Setia, G., S.S. Mallick, R. Pan, and P.W. Wypych. 2016(b). Modeling Solids Friction Factor for Fluidized Dense-Phase Pneumatic Transport of Powders Using Two Layer Flow Theory. *Powder Technology* 294, 80–92.

Sahoo, B.K., S. De, and B.C. Meikap. 2011. Improvement of Grinding Characteristics of Indian Coal by Microwave Pre-Treatment. *Fuel Processing Technology* 92, no. 10, 1920–1928.

Schulze, D. 2010. Powders and Bulk Solids, *Chemie Ingenieur Technik*. 82, 553–554.

Wang, J., X. Cai, Y. Guo, and L. Jiang. 2022. Problem Analysis and Operation Evaluation of Dry Ash Removal System in Coal-Fired Power Plant. In *2022 2nd International Conference on Bioinformatics and Intelligent Computing*, 285–288. New York, NY, USA: ACM.

Williams, K.C. 2008. Dense Phase Pneumatic Conveying of Powders: Design Aspects and Phenomena. *PhD. Dissertation*, University of Newcastle, Australia.

Wypych, P.W. 1989. Pneumatic conveying of bulk solids, *Doctor of Philosophy thesis*, Department of Mechanical Engineering, University of Wollongong, Australia.

Woodcock, C.R., and J.S. Mason. 1987. Components of Pneumatic Conveying Systems. In *Bulk Solids Handling*, 408–437. Dordrecht: Springer Netherlands.

Xing, Y., F. Guo, M. Xu, X. Gui, H. Li, G. Li, Y. Xia, and H. Han. 2019. Separation of Unburned Carbon from Coal Fly Ash: A Review. *Powder Technology* 353, 372–384.

Yablokova, G., M. Speirs, J. Van Humbeeck, J.-P. Kruth, J. Schrooten, R. Cloots, F. Boschini, G. Lumay, and J. Luyten. 2015. Rheological Behavior of β-Ti and NiTi Powders Produced by Atomization for SLM Production of Open Porous Orthopedic Implants. *Powder Technology* 283, 199–209.

Yang, W.-C., (Ed.). 2003. Handbook of Fluidization and Fluid-Particle Systems (1st ed.). *CRC Press.*

CHAPTER 9

Conclusion and Future Scope of Work

9.1 Conclusion

Based on the physical and flow property test data of eight pharmaceutical powder samples, they have shown that the static angle of repose is not strictly correlated to the cohesive index; comparatively, cohesion stress values seem to have a stronger relationship with the static angle of repose. A relationship to represent the static angle of repose has been developed using a bulk powder Froude number based on loose poured bulk density and fine size d(10). The experimental results for eight pharmaceutical powders have shown that the value of the static angle of repose decreases with an increase in the modified particle Froude number, increase in particle shape factor and decrease in the median to fine ratio. Out of all the dimensionless parameter groupings, the particle shape factor seems to have the strongest influence on the static angle of repose, as indicated by its larger absolute exponent value. Based on the six different fly ash samples (particle size d(50) ranging from 68 μm to 141 μm) that were tested for their morphology, characteristics and flow property test. The results from their sifting and fluidisation segregation characteristics have shown that with an increase in median particle size, the sifting segregation tendencies have increased and are represented by higher values of segregation indices. The finer ash samples have provided greater fluidisation segregation tendencies than the coarser samples. This has occurred in spite of the higher value of cohesion in finer ash samples. The higher values of the fluidisation segregation index for finer ash show that the difference in particle settling velocities (which promotes segregation) dominates over the particle-particle cohesion (which suppresses segregation). Based on the investigation into the sifting segregation and fluidisation segregation characteristics of sand, three different brands of detergent and semolina powders have been found that the sifting segregation was found to be influenced by dimensionless parameters such as powder flow function, course-to-fine ratio and shape factor, whereas a novel dimensionless cohesion number and minimum fluidisation velocity seem to be addressing fluidisation segregation well. The models for the sifting and fluidisation segregation index provided a good fit of 97 % and 86 %, respectively, with the experimental data. These models are valid for Geldart group A to B borderline powders having a median particle size range of 50 to 500 μm, particle density range of 1500 to 2400 kg/m^3 and loose poured bulk density range of l600 to 1200 kg/m^3. Based on the other study, the change in sifting and fluidisation segregation index affecting with the change in moisture content for Geldart group A to B borderline powders was considered. It is observed that the change in sifting segregation characteristics is influenced by a change in flow function as flow property, a change in course-to-fine ratio and a change in shape factor as the particle properties. Based on these dimensionless parameters, a model has been developed for the change in the sifting segregation index that provides a good fit of 91 % accuracy with the experimental data.

For modelling the change in fluidisation segregation index, seven different correlations of minimum fluidisation velocity were evaluated, and a best-fit correlation of minimum fluidisation velocity has been considered along with a novel dimensionless cohesion number based on interparticle cohesion. The model of the change in fluidisation segregation index suggested a good fit of 85 % accuracy with the experimental data. These models are valid for Geldart group A to B borderline powders having a median particle size range of 50 to 500 μm, particle density range of 1500 to 2400 kg/m^3 and loose poured bulk density range of l600 to 1200 kg/m^3. The lack of pneumatic conveyability in fluidised dense-phase mode with segregated powder samples having narrower particle size distribution has been illustrated for a pneumatic conveying system. Based on a pilot plant study of conveying different blends of ash, a new bulk powder Froude number term (based on loose poured bulk density) and coarse-to-fine ratio have been used to represent reliable conveying criteria. For reliable dense-phase conveying, the ash mixture should have a bulk powder Froude number < 10 and a coarse-to-fine ratio > 10. The proposed models have been tested and validated at an appropriate rate of powder properties.

The thesis makes a significant contribution to powder technology by developing experimentally validated models that link flow behaviour, segregation mechanisms, and conveying criteria for fine and borderline Geldart A to B powders across diverse materials such as pharmaceuticals, fly ash, sand, detergents, and semolina. It establishes that the static angle of repose is more strongly correlated with cohesion stress than with cohesive index and proposes a relationship using a bulk powder Froude number based on loose poured bulk density and fine particle size. The research highlights the dominant influence of particle shape factor, size distribution, and modified Froude number on flowability while providing novel dimensionless models for sifting and fluidisation segregation, achieving predictive accuracies of 97 % and 86 % respectively. A new dimensionless cohesion number and moisture-dependent models further extend the predictive capability for segregation indices, and the work introduces reliable dense-phase conveying criteria using a modified bulk powder Froude number and coarse-to-fine ratio validated in pilot plant studies. By integrating multi-parameter effects such as particle shape, cohesion, and moisture content into a comprehensive predictive framework, the study offers practical industrial relevance for construction, power generation, and food processing, while bridging laboratory findings to pilot-scale systems. Overall, the research advances powder technology by introducing new dimensionless parameters, scalable models, and robust design correlations that enhance the prediction, control, and optimisation of powder flow, segregation, and conveying behaviour under varied operational conditions.

9.2. Future scope of work

Future scope of work includes:

- **Extending Models to Diverse Bulk Solids:** Validating the developed segregation and flow models across a broader range of powders and bulk materials to ensure wider applicability.
- **Surface Roughness Influence:** Measuring powder surface roughness and studying its effect on flowability and segregation behaviour.
- **Wall and Tube Interaction:** Investigating how wall or tube roughness and different wall materials affect sifting and fluidisation segregation characteristics.
- **Temperature Effects:** Exploring the impact of temperature variations on powder properties, segregation tendencies, and flow behaviour.
- **Wider Data Validation:** Collecting and comparing data from different industrial powders to test the robustness of the models under various operational conditions.
- **Design of Advanced Equipment:** By utilising the outcomes from the thesis, developing high-class powder handling and processing equipment that integrates the new predictive models for improved industrial performance.

ANNEXURE A1

Industry Feedback

Industry survey: powder segregation and flow challenges industry

In the initial part of the thesis, in addition to the literature review, the student approached the industry to learn about the powder handling challenges being faced with respect to segregation. Considering the practical nature of the subject, industry feedbacks were invited to carry out a proper need analysis; i.e. identification of the need and formulation of the problem statement was not just restricted to academic research papers. Industries were approached through the following ways:

- Circulating Google form to industry experts
- Circulating messages through LinkedIn to industry experts
- Visit reputed industry exhibitions
- Carrying out in-person (online) interviews of industry experts
- Organizing symposia to understand power flow challenges from expert lectures

Initially the plan was to include a larger number of pharmaceutical and food powders and to visit these industries. However, due to Covid19 pandemic, visits to pharmaceutical and food industries could not be carried out as such industries apparently maintained a stringent visitor criteria. However, the student managed to visit power plants. This thesis, therefore, contains experimental data of pharmaceutical, detergent, food and fly ash samples.

Several industry personnel were connected/approached. Feedbacks were received from about 45 respondents. Tables A.1 and A.2 provide consolidated information on the challenges faced by the industry, the need for solutions and the powders that are causing the majority of the flowability and segregation-related difficulties.

Table A.1: Powder flowability and segregation challenges faced in pharmaceutical and food industries

Problem faced by the industry (based on survey)	**Requirement/need**
Segregation/ poor flow/rat hole phenomenon/ dust generation/compaction of powder blend in hopper	Tool for segregation/ poor flow/rat hole phenomenon/ dust generation/compaction of powder blend in the hopper
Electrostatic charges after micronisation; poor flow of micronised powders	A flow measurement system that also provides information on the strength of cohesive/adhesive interactions.
Segregation and Arching	To understand how the bulk powder flow properties, such as cohesion and friction, are impacted at higher strain rates.
Agglomeration and flowability	Packing density instrument, which should be independent of wall effect for a wide range of particle size.
Sometimes powders are of a sticky nature, amorphous and hygroscopic. Handling of these powders became difficult.	Particle size machine for solid powders
Critical impacts on product quality like cross-contamination, non-uniform drug in finished dosage form or loss in potency etc.,	Tablet or Powder Porosity, similar but cost-effective powder rheometer like FT4 etc., tablet hardness tester with quartz crystal microbalance or similar, tool to measure dry disintegration
Flow issues with slight change in B.D., PSD	Which predicts PSD and B.D. relationship with flow

Table A.2: List of powders with flowability and segregation challenges in pharmaceutical and food industries

Food powder	Pharmaceutical powder
Skim milk Powder	Lactose, Mannitol, Starch, HPMC
Ultra-fine besan	Magnesium stearate, carbopol, micronised glucose
Horlicks	Microcrystalline cellulose, talc, disintegrates, lubricants
Bournvita	Colloidal Silicon Dioxide, hygroscopic Sodium hydroxide
Ensure	Lyophilised powder, antacids Pantoprazole, Esomeprazole, Rabeprazole
Complain	Maltodextrin, guar gum, gum acacia, xanthan gum
Phthalates, Sugar	Aerosol
Maize starch	PPI powder granules
Tapioca starch	Calcium stearate
Caramel, curcumin or fruit/ vegetable powders	Acetaminophen
Coffee	Hypromellose
cocoa	Titanium Dioxide, Calcium Silicate
Bran	Sorbitol, Beta Cyclodextrin, Povidone, PVP-K30
Icing Sugar	Paracetamol, Ibuprofen, detergent powders

Industrial feedback through Google form

Introductory note:

Pharmaceutical industry feedback form

Dear Sir/Madam,

I am Rachit Poddar, PhD Student of Dr. S.S. Mallick and Dr. Kundan Lal, Powder Flow Laboratory, Department of Mechanical Engineering, Thapar Institute of Engineering & Technology, Patiala.

Through my PhD, I would like to develop (design/fabricate/commercialise) a new machine or powder tester useful for reliable characterisation and/or to handle powders in the pharmaceutical industry. For carrying out the "Need Analysis", I am hereby reaching out to researchers and professionals in the field of the Pharmaceutical Industry.

Please fill up this Google Form provided in the following link by 3rd February 2021 - it would hardly take 10 minutes. Your feedback will greatly help me to decide the exact machine/tester that I should build to support our pharmaceutical industry.

Google Form Link:

https://docs.google.com/forms/d/1zUTL_RI4lpZBicS0ql4sV9NjbzYWyTs3lCfGnjvsz_c/edit

Sincerely

Rachit Poddar/ (C/O, Dr. S.S.Mallick, Dr. Kundan Lal)

Google form questionnaire: (for the Pharmaceutical Industry)

Q1: What type of pharmaceutical powders do you handle in your industry?

A1: 1) API

2) Excipients

3) Both API (or) Excipients

4) Any other……..

Q2: What is the typical particle size range of the pharmaceutical powders that you use in your industry?

Q3: What are the handling or flowability challenges that you face with pharmaceutical powders in your industry?

Q4: How do you typically tackle or intervene into the handling or flowability challenges of pharmaceutical powder in such difficult cases?

Q5: What are the methods or powder testers do you use in your industry to characterize of pharmaceutical powders?

Q6: Could you please suggest any new powder property tester or characterization tool that I can develop (design/fabricate) through my PhD (as a Product/Tester/Machine Development) that will be valuable to pharmaceutical industry for improved powder characterization or better powder handling device.

Industry feedback is provided in Table A.3.

Table A.3: Industry feedback via Google Form

Feedback no.	**Problem faced by the pharmaceutical sector**	**Requirement/need**
1	*"Segregation/ poor flow/rat hole phenomenon/ dust generation/compaction of powder blend in the hopper"*	*"Looking forward to seeing an instrument that can predict all the challenges which are Segregation/ poor flow/rat hole phenomenon/ dust generation/compaction of powder blend in the hopper."*
2	*"Electrostatic charges after micronisation; the poor flow of micronised powders"*	*"Flow measurement system that also provides information on the strength of cohesive/adhesive interactions".*
3	*"Segregation and Arching"*	*"It would be very interesting to understand how the bulk powder flow properties, such as cohesion and friction, are impacted at higher strain rates. All the current state-of-the-art measurement systems work in a quasi-static regime. There is FT4 device which does give directional guidance in terms of powder properties in dynamic scenarios; however, relating it to an actual process and utilising that data for equipment design is not very clear".*
4	*"Agglomeration and flowability"*	*"Packing density instrument, which should be independent of wall effect for a wide range of particle size".*
5	*"Sometimes powders are of sticky nature, amorphous and hygroscopic. Then handling these types of powder became difficult".*	*"Particle size machine for solid powders"*
6	*"Critical impact on product quality like cross-contamination, non-uniform drug in finished dosage form or loss in potency, etc."*	*"**(1).** Tablet or Powder Porosity **(2).** Similar but cost-effective powder rheometer like FT4, etc. (3) tablet hardness tester with quartz crystal microbalance or similar (4) current wet disintegration performed, a tool to measure dry*

		disintegration can be considered innovative. But any approaches will be considered pivotal when the cost-effectiveness approach is performed"
7	*"Flow issues with a slight change in B.D., PSD"*	*"Which predicts PSD and B.D. relationship with the flow"*

Industrial feedback through LinkedIn

Introductory note

Dear Sir/Madam,

I am Rachit Poddar, PhD Student of Dr. S.S.Mallick and Dr. Kundan Lal, Powder Flow Laboratory, Department of Mechanical Engineering, Thapar Institute of Engineering & Technology, Patiala. Our Powder Flow Lab is researching modelling powder segregation, flowability, and moisture ingress effect. We are looking into food and pharmaceutical powders.
Could you please suggest to us the powders that we should use in our experimental work (i.e. powders that show segregation/poor flowability/hygroscopic characteristics)? We will arrange powders accordingly for our lab - it would generate industry-relevant data.
Thanking you
Rachit Poddar

Responses/feedback from different food industries are mentioned below:

Respond/feedback
"Can use Skim Milk powder, ultra-fine besan for your study as these products have very poor flowability".
"Pick up all the Malt Based Health Food Drinks such as Horlicks, and its variants, Bournvita, Ensure, Complan etc.".
"Can use Horlicks powder".
"Go for phthalates".
"Powders like Sugar, Maize starch, tapioca starch are hygroscopic in nature".

Responses/feedback from different pharmaceutical industries are mentioned below:

Respond/feedback
"Generally we use blend of different ingredients. There are different grades of lactose, microcrystalline cellulose. Talc, disintegrants, Lubricants can evaluate".
"You need powder having all characteristics in One or even separate will work; take Colloidal Silicon Dioxide for flowability, Hygroscopic Sodium hydroxide powder form".

"I hope you should focus on Lyophilised powder. Almost all lyophilised powders are hygroscopic in nature. Like simple products like antacids like Pantaprazole, Esomeprazole, Rabeprazole, etc. As you focus on pharmaceutical powder, you shouldn't select any harmful product like oncological, Hormonal, Steroids products, were to handle such products you need at most care and precautions".
"One of the most common powders used in many pharmaceutical formulations is lactose. It is mostly used in the form of lactose monohydrates. Many grades, particle sizes are available. It will cover a large part of pharmaceutical powders".
"Can use mannitol, HPMC, maltodextrin, guar gum, gum acacia, xanthan gum, starch, etc.".
"Take the poor flow where powder having the puff character like aerosol for your experimental work".
"Use the PPI powder granules used for tablets. Dispersible tables containing sugar as well as Powder for Dry syrups, etc.".
"Can try colours such as caramel, curcumin or fruit/ vegetable powders which are also used in pharmaceuticals/Nutraceutical products. These powders are hygroscopic in nature".
"If you are looking for a hygroscopic API, try water-soluble ones like Pregabalin. Segregation and poor flow can be chemical or physical related, meaning powder with mixed shapes of particles or very wide distribution between 1 micron to thousands of microns. Poor flow can be related to micronized powder or needle shape or how much the powder is dry/wet, etc.".
"Like Microcrystalline cellulose, Lactose monohydrate, Magnesium stearate, Talc, Calcium stearate".
"Study on excipients that give you a good idea. As in powder, the major portion is diluent or filler, which give better ideas".
"Magnesium stearate and calcium stearate used as a glidant in tablets manufacturing most of the times results into the poor dissolution of the drug. I hope this can be useful for your study".
"For the pharm, look at how the active ingredient blends with the fillers, time-release powders & so on. Pharm typically uses a P.K. Blender, but it has to be transferred to compactors or to fill capsules. In that instance, particles will segregate if you're not in a mass flow hopper. Even then, you will get segregation. Moisture contents promote agglomeration, which can be more of issue vs segregation!"
"Skim milk powder you can use for it. It contains 0% fat and 3.4 % protein".
"Try different grades of Avicel. Also Acetaminophen they are generic and have varying ranges of cohesion so good for both flow and segregation studies".

"I would suggest a mixture of Sugar, Coffee, Creamer and minor ingredients such as vitamins demonstrate segregation. Cocoa, Bran, Icing Sugar are all materials that are Hygroscopic especially when they are stored for any length of time".
"Titanium Dioxide is a difficult material to handle. Also I think Calcium Silicate".
"Avicel pH 101, which is microcrystalline cellulose, is commonly used excipient in immediate-release formulations and may be a good candidate. Its better flowable grade is 102. For extended-release hypromellose, regular grade from colour kaun should help, and it can be compared against colour cones D.C. great material".
"There are some pharmaceutical diluents, and Active pharmaceutical ingredients will be having flow issues lactose, mannitol, starch, HPMC".
"There are some common powders as magnesium stearate, carbopol, micronized glucose and then you will find even more difficult powders when you will look into the API's, but very often very hard to deal".
"There are so many lactose is a common compound used".
"Sorbitol, Beta Cyclodextrin, Povidone, PVP-K30"
"Drug powders, such as Paracetamol, Ibuprofen etc. are having poor flow".
"We have detergent powders etc. which are very much segregation prone themselves".

ANNEXURE A2

Particle Size Distribution Curve

Particle size distribution curve of fly ash samples

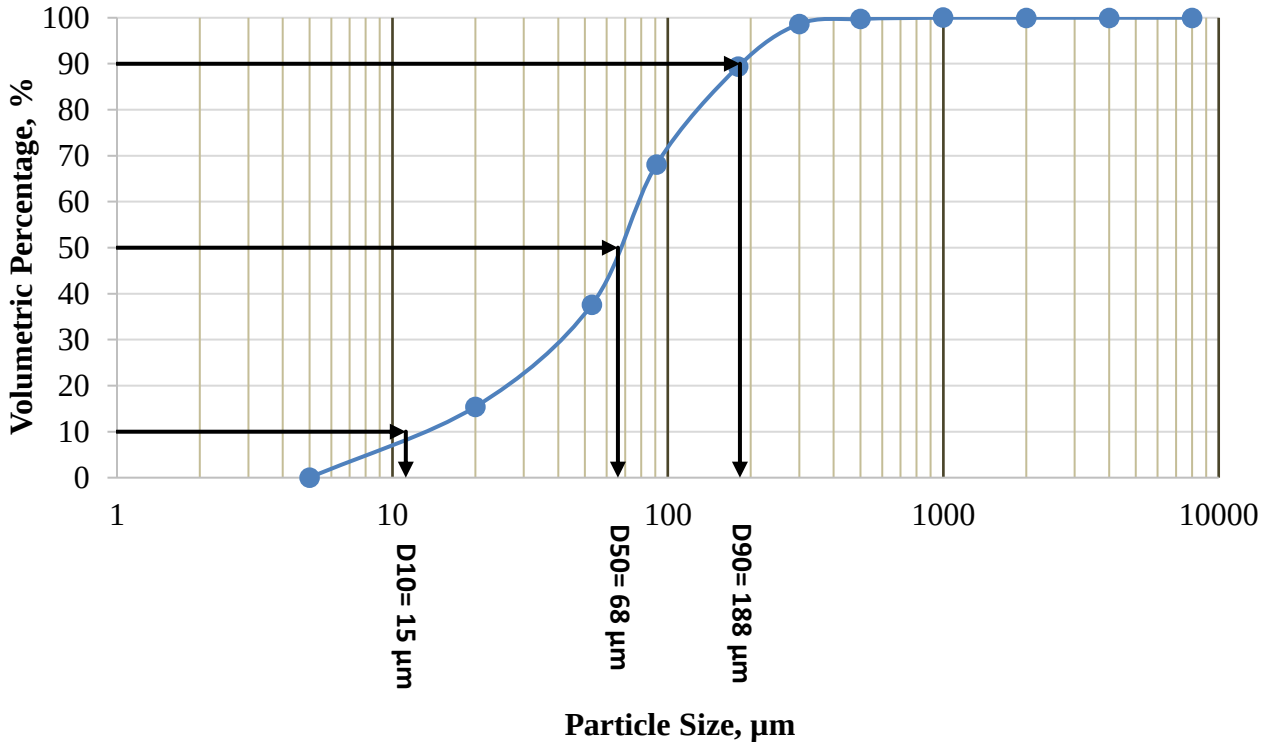

Figure A.1: Particle size distribution curve for fly ash sample A

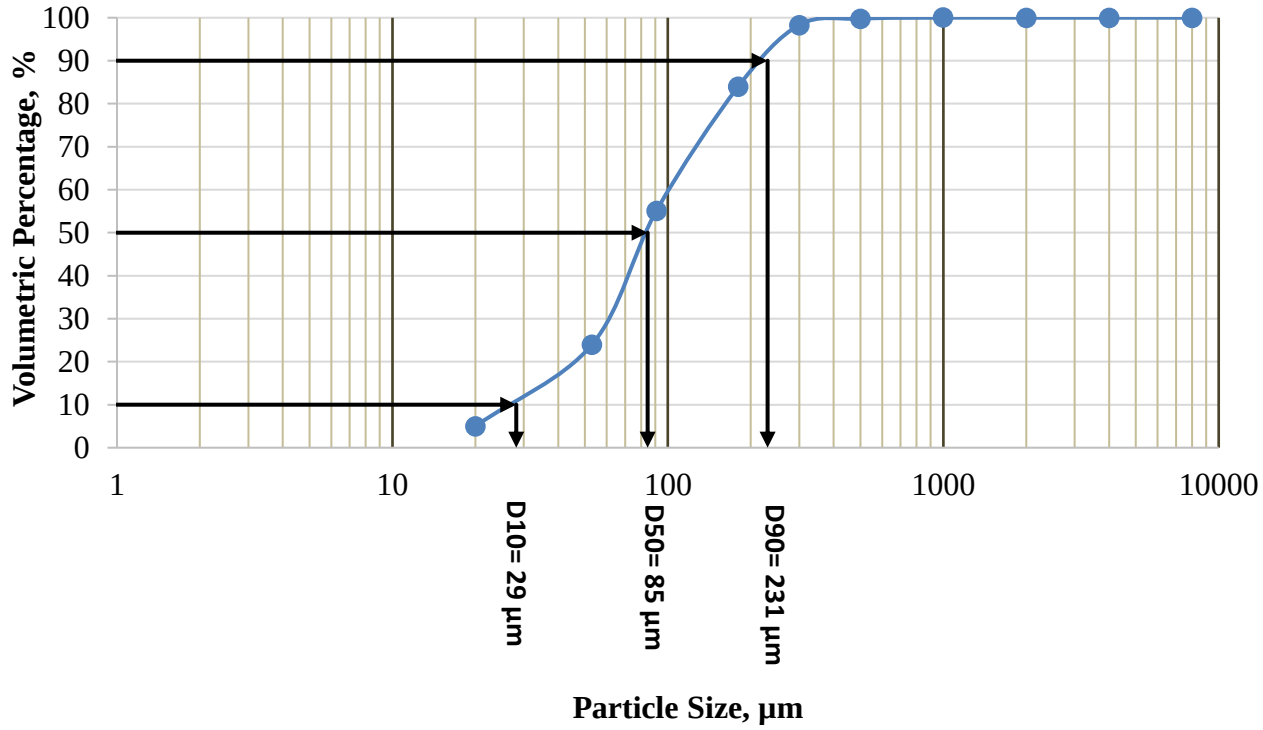

Figure A.2: Particle size distribution curve for fly ash sample B

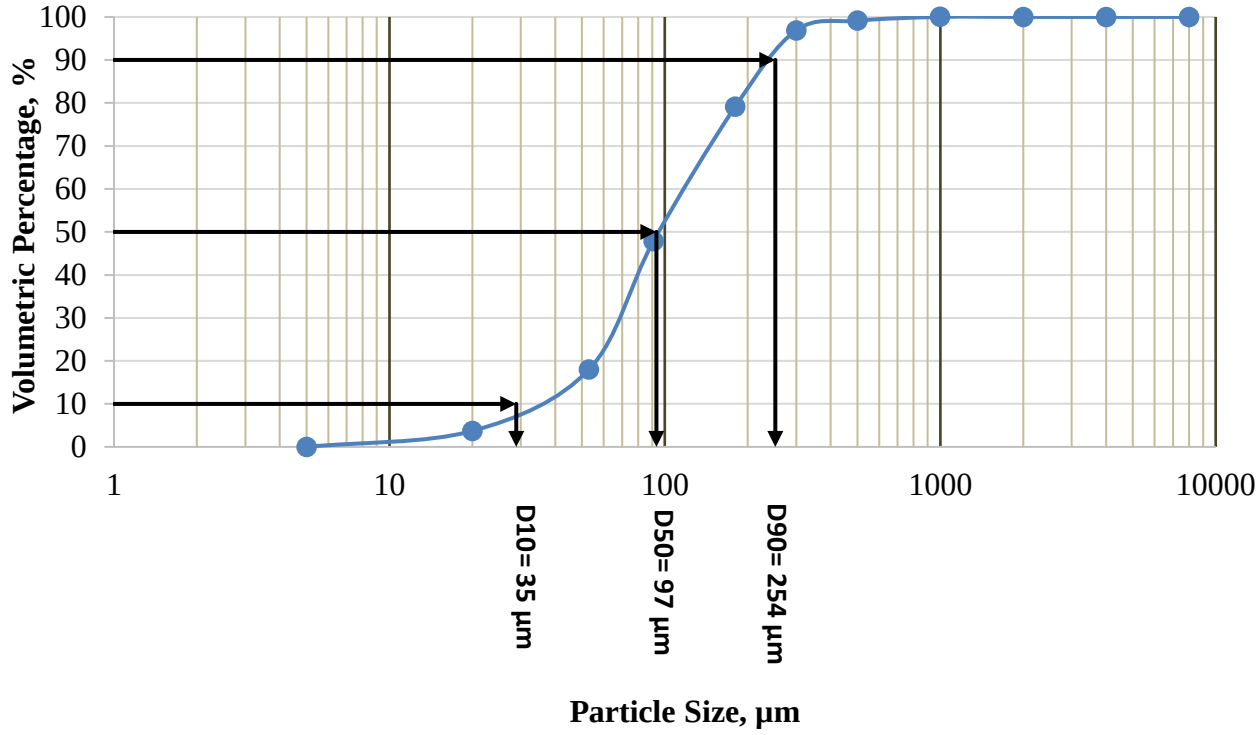

Figure A.3: Particle size distribution curve for fly ash sample C

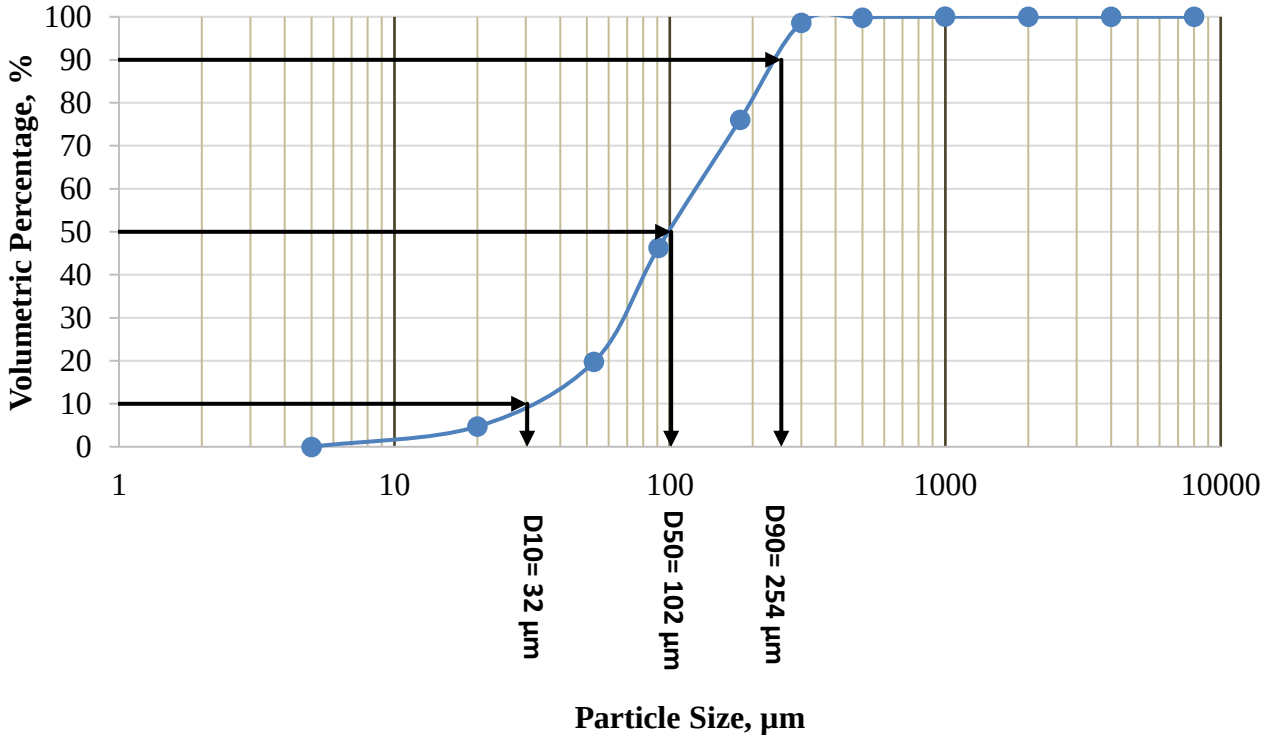

Figure A4: Particle size distribution curve for fly ash sample D

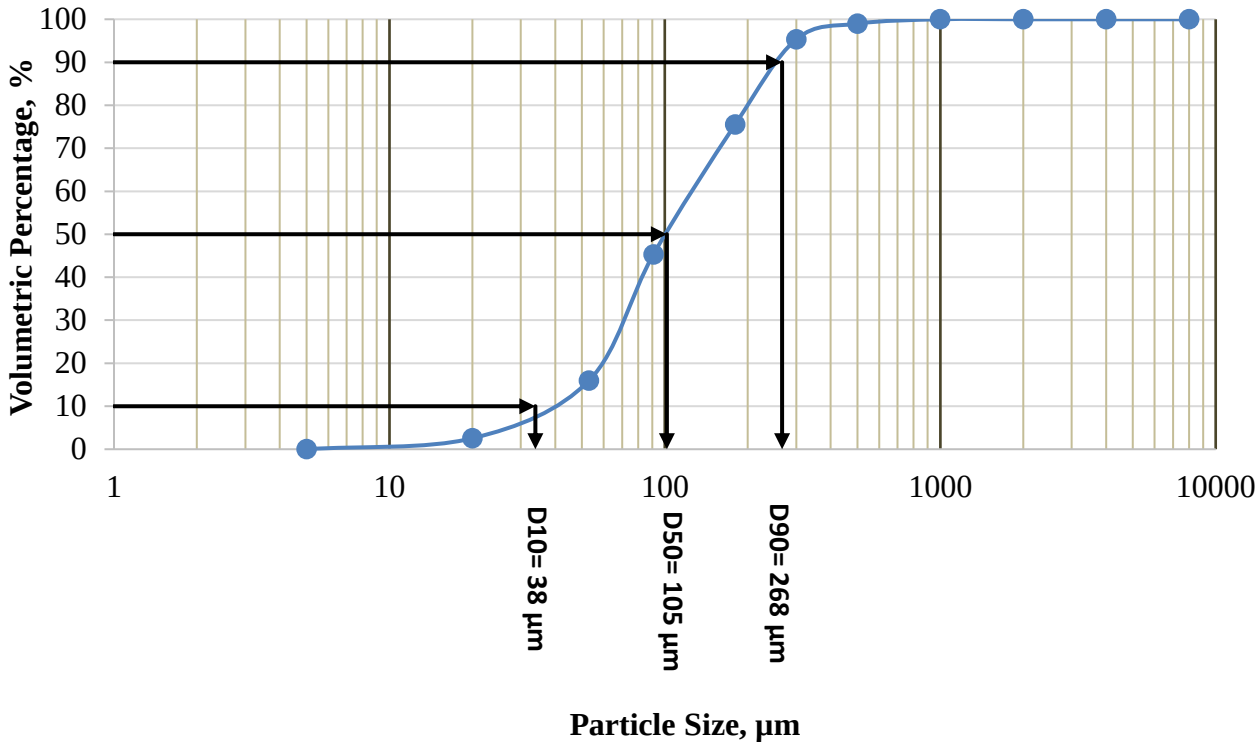

Figure A5: Particle size distribution curve for fly ash sample E

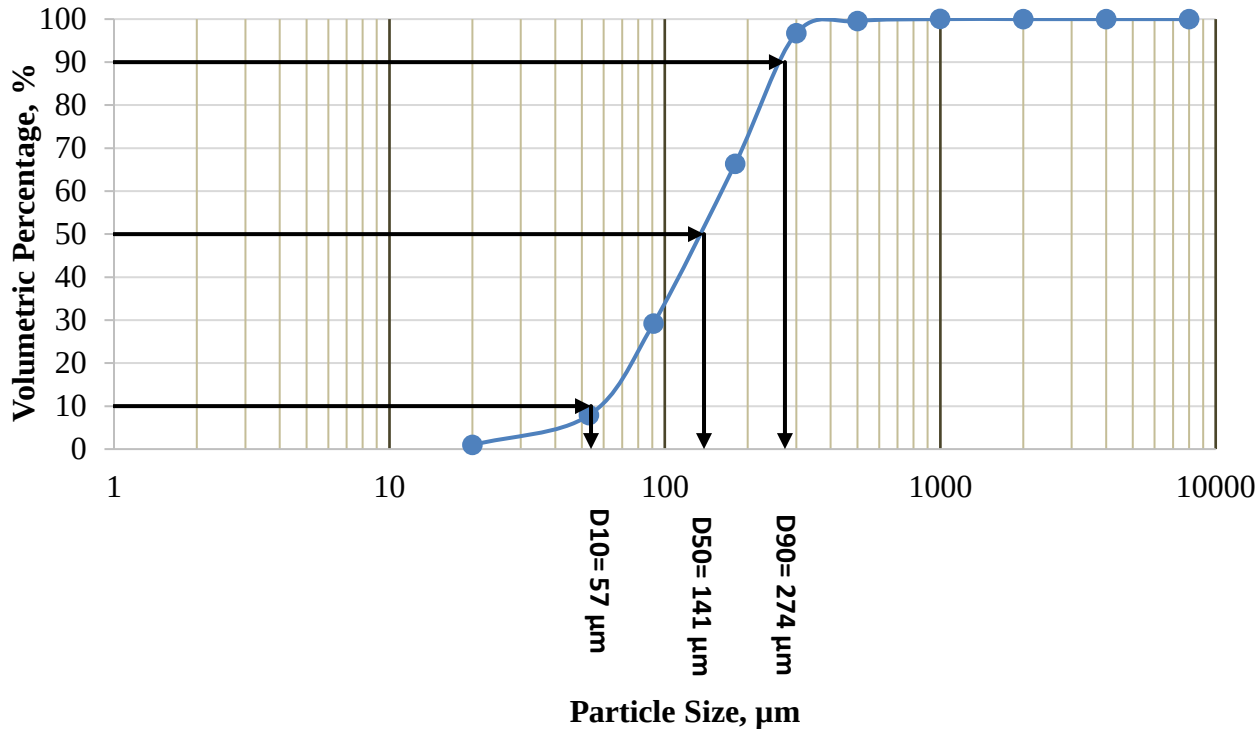

Figure A6: Particle size distribution curve for fly ash sample F

Particle size distribution curve of sand, detergents and semolina

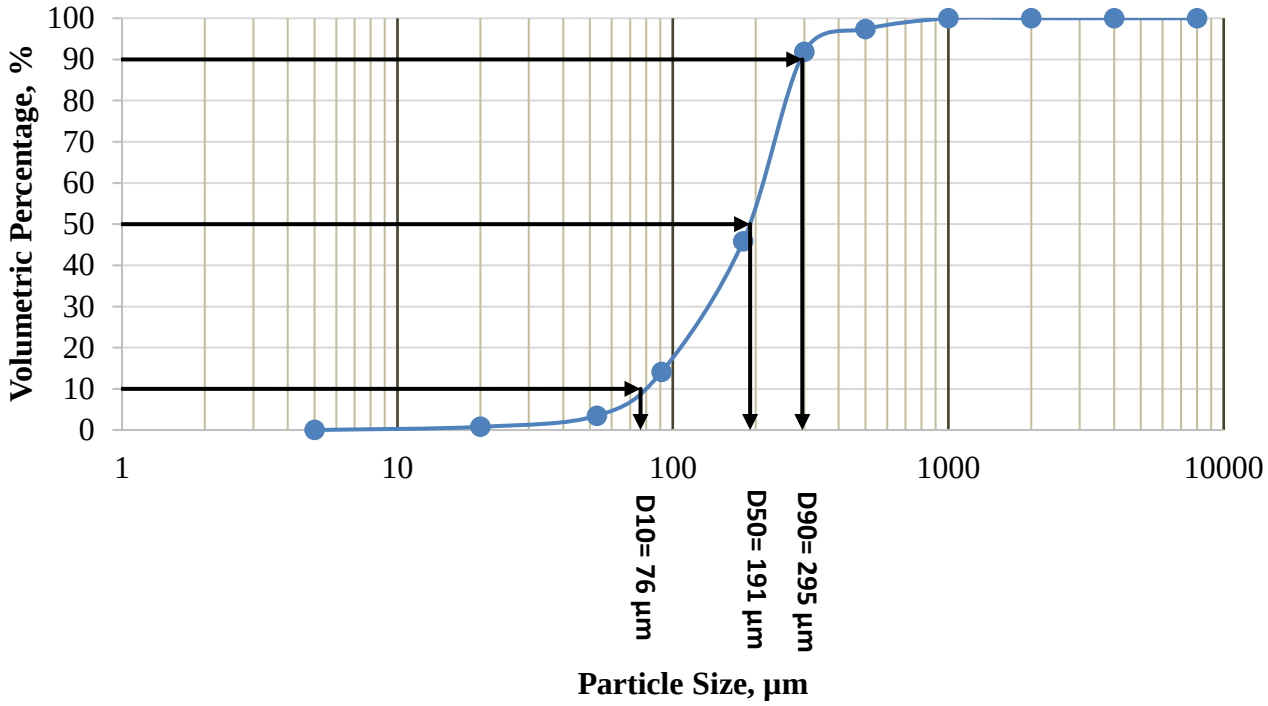

Figure A7: Particle size distribution curve for sand

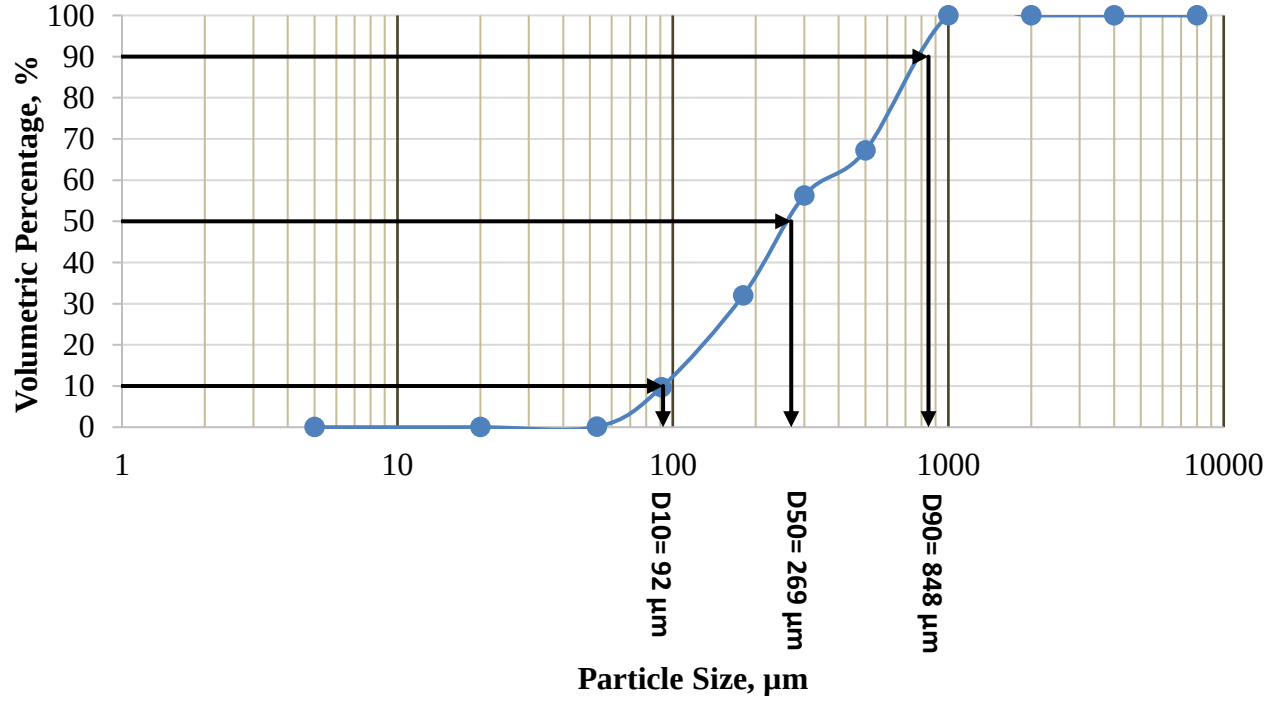

Figure A8: Particle size distribution curve for detergent_1

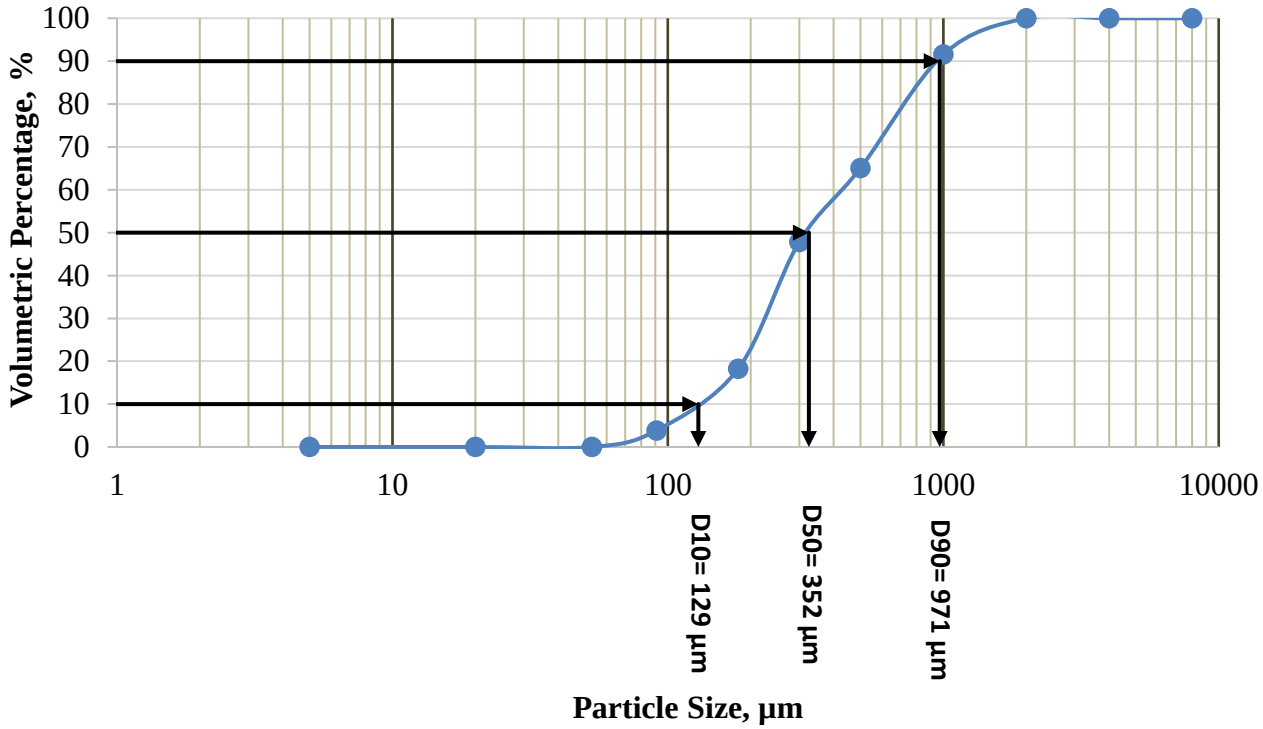

Figure A9: Particle size distribution curve for detergent_2

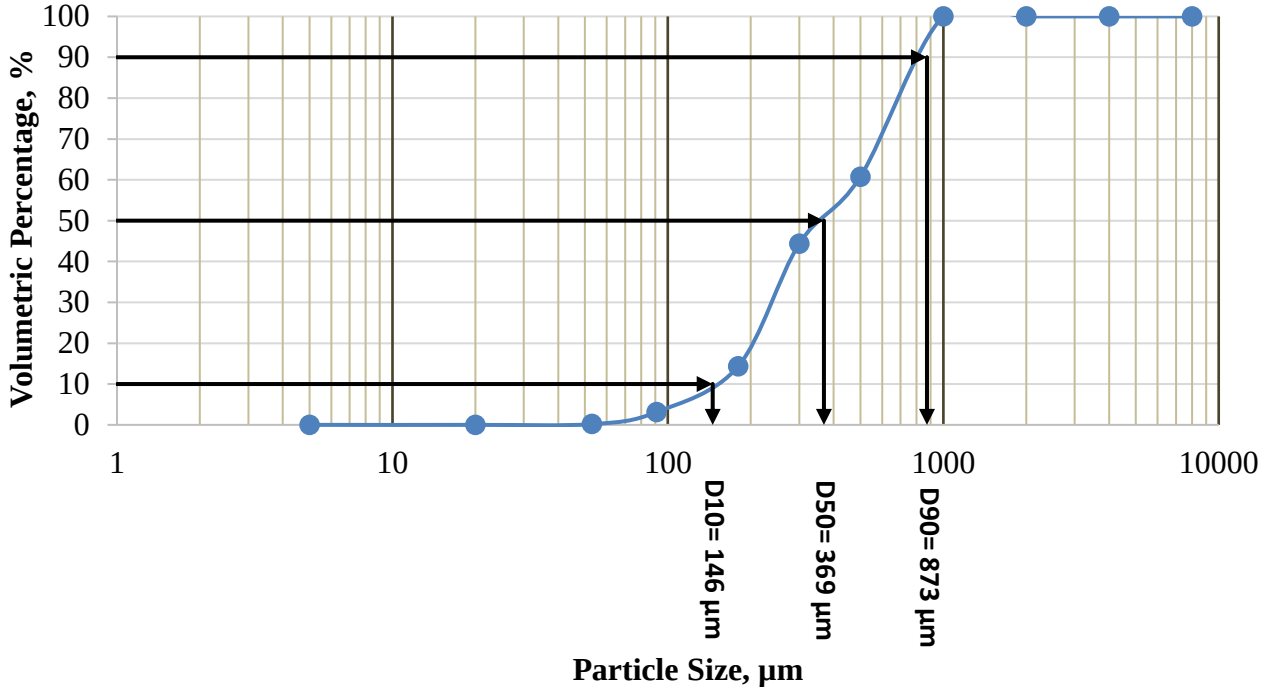

Figure A10: Particle size distribution curve for detergent_3

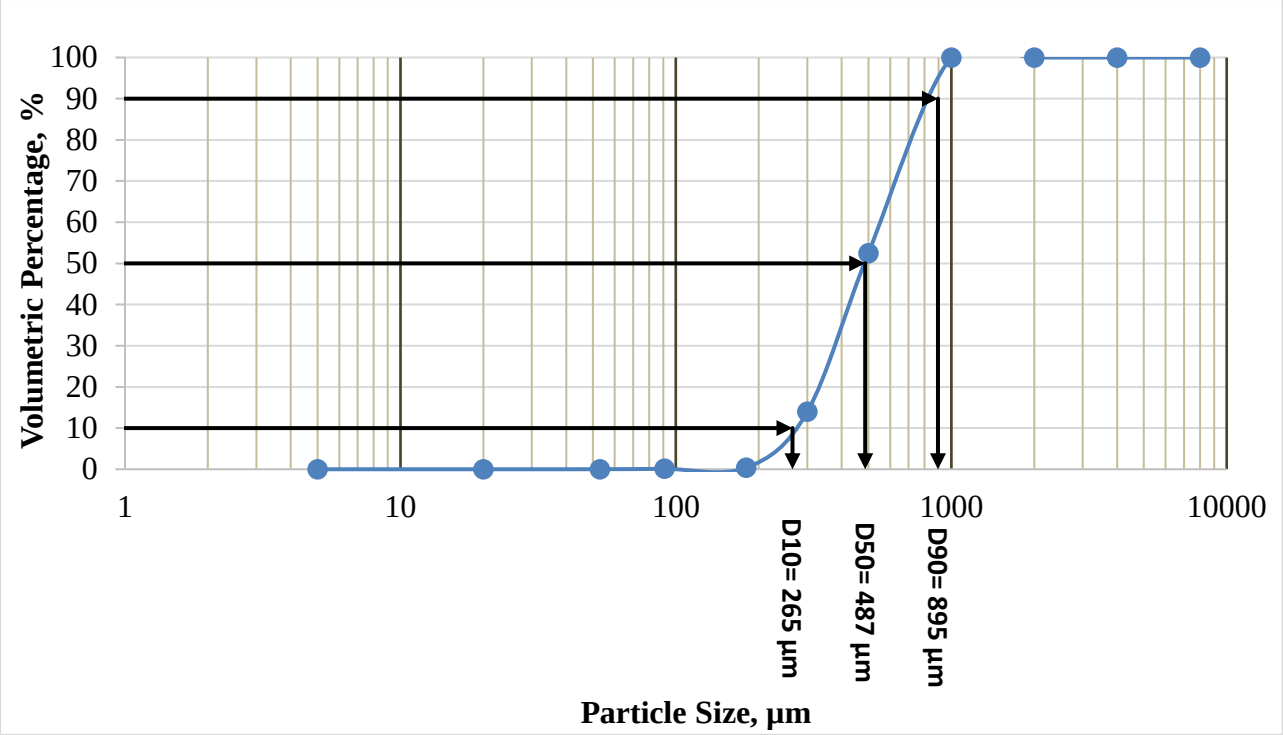

Figure A11: Particle size distribution curve for semolina

List of Publications

SCI Publications

[1] R. Poddar, S.S. Mallick, K. Lal, Reliable pneumatic transport of coarse ash in dense-phase by optimally mixing with fine ash, Powder Technology. 442 (2024) 119876. (IF: 4.5)

[2] R. Poddar, S.S. Mallick, L. Kundan, An experimental investigation into sifting and fluidization segregation characteristics for coal fly ash, Particulate Science and Technology. 42(4) (2023) 515–526. (IF: 2.3)

[3] R. Poddar, G. Saluja, S.S. Mallick, L. Kundan, An investigation into static angle of repose using pharmaceutical powders, Particulate Science and Technology. 42(3) (2023) 344–353. (IF: 2.3)

[4] R. Poddar, S.S. Mallick, K. Lal, Modelling sifting and fluidisation segregation characteristics of powders, Powder Technology. 465 (2025) 121368. (IF: 4.5)

[5] R. Poddar, S.S. Mallick, K. Lal, An investigation into segregation behaviour of powders with different moisture content, Particulate Science and Technology. (Minor comments received) (IF: 2.3)

INTERDEPENDENCE BETWEEN SEGREGATION AND FLOW PROPERTIES OF BULK SOLIDS

by Rachit Poddar

Submission date: 08-Nov-2024 08:09AM (UTC+0530)
Submission ID: 2512243829
File name: Rachit_Poddar_MED_SSMallick.pdf (7.27M)
Word count: 60825
Character count: 309515

INTERDEPENDENCE BETWEEN SEGREGATION AND FLOW PROPERTIES OF BULK SOLIDS

ORIGINALITY REPORT

13%	5%	11%	1%
SIMILARITY INDEX	INTERNET SOURCES	PUBLICATIONS	STUDENT PAPERS

PRIMARY SOURCES

1	citeseerx.ist.psu.edu Internet Source	<1%
2	Allenspach, Carl. "Directly Compressible Hydroxypropyl Methylcellulose (HPMC) to Support Continuous Manufacturing.", Rutgers The State University of New Jersey, School of Graduate Studies, 2021 Publication	<1%
3	Hamzah M. Beakawi Al-Hashemi, Omar S. Baghabra Al-Amoudi. "A review on the angle of repose of granular materials", Powder Technology, 2018 Publication	<1%
4	Submitted to Georgia Institute of Technology Student Paper	<1%
5	M. Combarros, H.J. Feise, H. Zetzener, A. Kwade. "Segregation of particulate solids: Experiments and DEM simulations", Particuology, 2014 Publication	<1%

6	"Proceedings of the 7th International Conference on Discrete Element Methods", Springer Science and Business Media LLC, 2017 Publication	<1 %
7	Iman Rostamsowlat, Babak Akbari, Brian Evans. "Analysis of rock cutting process with a blunt PDC cutter under different wear flat inclination angles", Journal of Petroleum Science and Engineering, 2018 Publication	<1 %
8	Tong Deng, Kirsty A. Paul, Michael S.A. Bradley, Lee Immins, Chris Preston, Jerry F. Scott, Eloise H. Welfare. "Investigations on air induced segregation of pharmaceutical powders and effect of material flow functions", Powder Technology, 2010 Publication	<1 %
9	S. S. Mallick, Lokesh Rohilla, Vivek Garg, Gautam Setia. "Modeling flow properties of fine dry powders using particle morphological properties and its effects on geometry of fly ash evacuation hoppers", Particulate Science and Technology, 2018 Publication	<1 %
10	opus.bath.ac.uk Internet Source	<1 %

11	Pauline H. M. Janssen, Sébastien Depaifve, Aurélien Neveu, Filip Francqui, Bastiaan H. J. Dickhoff. "Impact of Powder Properties on the Rheological Behavior of Excipients", Pharmaceutics, 2021 Publication	<1 %
12	Chun-Chung Liao, Shih-Fu Ou, Shan-Lung Chen, Yu-Ru Chen. "Influences of fine powder on dynamic properties and density segregation in a rotating drum", Advanced Powder Technology, 2020 Publication	<1 %
13	Submitted to University of Pretoria Student Paper	<1 %
14	ndl.ethernet.edu.et Internet Source	<1 %
15	www.researchgate.net Internet Source	<1 %
16	Amalia L. Thomas. "A mechanistic framework for the characterisation of cohesive, frictional and interlocking effects on powder flow behaviour", Particuology, 2024 Publication	<1 %
17	R Pan. "Material properties and flow modes in pneumatic conveying", Powder Technology, 1999 Publication	<1 %